

BUCKLING BEHAVIOUR  
OF WOODEN POLES

by

Jasna Savić

A Thesis  
presented to the University of Manitoba  
in Partial Fulfillment of the  
Requirements for the Degree of

Master of Science

in the Department of Civil Engineering

Winnipeg, Manitoba

April, 1991



National Library  
of Canada

Bibliothèque nationale  
du Canada

Canadian Theses Service    Service des thèses canadiennes

Ottawa, Canada  
K1A 0N4

The author has granted an irrevocable non-exclusive licence allowing the National Library of Canada to reproduce, loan, distribute or sell copies of his/her thesis by any means and in any form or format, making this thesis available to interested persons.

The author retains ownership of the copyright in his/her thesis. Neither the thesis nor substantial extracts from it may be printed or otherwise reproduced without his/her permission.

L'auteur a accordé une licence irrévocable et non exclusive permettant à la Bibliothèque nationale du Canada de reproduire, prêter, distribuer ou vendre des copies de sa thèse de quelque manière et sous quelque forme que ce soit pour mettre des exemplaires de cette thèse à la disposition des personnes intéressées.

L'auteur conserve la propriété du droit d'auteur qui protège sa thèse. Ni la thèse ni des extraits substantiels de celle-ci ne doivent être imprimés ou autrement reproduits sans son autorisation.

ISBN 0-315-76949-1

Canada

BUCKLING BEHAVIOUR OF WOODEN POLES

BY

JASNA SAVIC

A thesis submitted to the Faculty of Graduate Studies of  
the University of Manitoba in partial fulfillment of the requirements  
of the degree of

MASTER OF SCIENCE

© 1991

Permission has been granted to the LIBRARY OF THE UNIVERSITY OF MANITOBA to lend or sell copies of this thesis. to the NATIONAL LIBRARY OF CANADA to microfilm this thesis and to lend or sell copies of the film, and UNIVERSITY MICROFILMS to publish an abstract of this thesis.

The author reserves other publication rights, and neither the thesis nor extensive extracts from it may be printed or otherwise reproduced without the author's written permission.

### ABSTRACT

The research project, sponsored by Manitoba Hydro, was undertaken at the University of Manitoba to determine the buckling behaviour and the axial load-carrying capacity of the wooden poles. Two different species of wood were selected for this project: Lodgepole Pine and Western Red Cedar, the most commonly used by Manitoba Hydro. Poles were randomly chosen from the Manitoba Hydro Yard, representing the most commonly used pole dimensions. Sixty-one specimens, produced from ten wooden poles were tested in axial compression, lying horizontally in the testing frame.

Test results indicated that the compression capacity of the pole is very much influenced by the pole's out-of-straightness.

Predicted nominal compression capacity of the column was compared to measured buckling capacity of the tested poles utilizing the Southwell plot for the measured load-deflection data. The models for combined axial load and bending moment, were also evaluated with regard to account for self-weight and out-of-straightness effect.

Canadian Code CAN/CSA-086.1-M89 predicts the ultimate compression capacity of the column well, using measured

material properties and taking into account the pole's initial out-of-straightness. However, specified material properties are significantly lower than the measured values. The Code also does not make any provisions for the existing crookedness of the pole.

In order to more accurately predict the ultimate capacity of the wooden poles, specified material properties should be based on full-size specimens cut from wooden poles. Based on the limited number of poles considered in this program, calculations taking into account initial out-of-straightness of the poles and material properties for the two species are recommended. The prediction should include both recommended material strength and out-of-straightness.

### ACKNOWLEDGEMENTS

This research project was carried out under the direct supervision of Dr. S.H. Rizkalla. The author wishes to express her sincere gratitude to Dr. Rizkalla for his valuable advice, and for his continued guidance, encouragement and support throughout the investigation.

The author also wishes to express her gratefulness to Mr. C.K. Wong for his help and constructive comments during the realization of this project. The help of Dr. R. Han and Dr. D. Polyzois is greatly appreciated.

Financial support provided by Manitoba Hydro and the Department of Civil Engineering of University of Manitoba is gratefully acknowledged.

For their assistance during the testing procedure, the author thanks Messrs. Moray McVey, Ed Lemke, Martin Green, Brian Turnbull and Steve Meyerhoff of the Civil Engineering Department.

Finally, the author wishes to thank her husband, for his support and encouragement throughout her studies.

TABLE OF CONTENTS

	Page
ABSTRACT .....	i
ACKNOWLEDGEMENTS .....	iii
TABLE OF CONTENTS .....	iv
LIST OF TABLES .....	vii
LIST OF FIGURES .....	viii
NOTATION .....	xi
CHAPTER 1: INTRODUCTION .....	1
1.1 General .....	1
1.2 Objective .....	3
1.3 Scope .....	3
CHAPTER 2: LITERATURE REVIEW .....	5
2.1 Ylinen's column formula .....	7
2.2 Zahn's proposal .....	7
2.3 Buchanan's proposal .....	8
2.4. CAN/CSA-086.1-M89 .....	10
2.5 Research done by Research Institute of Colorado .....	13
2.6 Ontario Highway Bridge Design Code .....	14
2.7 Southwell plot .....	15
CHAPTER 3: EXPERIMENTAL PROGRAM .....	17
3.1 Introduction .....	17

	Page
3.2 Test set-up and instrumentation .....	18
3.3 Test procedure .....	22
3.4 Description of the tested poles .....	24
3.5 Material properties tests .....	27
 CHAPTER 4: TEST RESULTS .....	 30
4.1 Introduction .....	30
4.2 Material properties .....	30
4.3 Wooden poles test results .....	32
 CHAPTER 5: ANALYSIS AND DISCUSSION OF TEST RESULTS ...	 34
5.1 Introduction .....	34
5.2 Specimen behaviour .....	34
5.3 Material properties .....	37
5.4 Buckling capacity of wood poles .....	38
5.4.1 Euler .....	40
5.4.2 Ylinen .....	40
5.4.3 Buchanan .....	41
5.4.4 CAN/CSA O86.1-M89 .....	41
5.5. Combined axial load and bending moment ....	43
5.5.1 Buchanan's proposal .....	44
5.5.2 Modified Buchanan's proposal .....	44
5.5.3 Zahn's proposal .....	44
5.5.4. Code equation .....	45

CHAPTER 6: SUMMARY AND CONCLUSIONS .....	47
REFERENCES .....	50
TABLES .....	54
FIGURES .....	73
APPENDIX A .....	119
APPENDIX B .....	207
APPENDIX C .....	238

LIST OF TABLES

## Table

- 1.1. Poles classification
- 3.1. Dimensions of the tested poles
- 4.1. Compression parallel to the grain test results
- 4.2. Bending test results
- 4.3. Tension test results
- 4.4. Pole deflections and ultimate load
- 4.5. Measured and nominal pole dimensions
- 4.6. Moisture content and specific gravity of the  
tested poles
- 4.7. Material properties
- 5.1. Coefficient  $c$
- 5.2. Pole's out-of-straightness
- C.1. Moments and deflections due to self-weight, out-of-  
straightness
- C.2. Predicted buckling load
- C.3. Predicted buckling load

LIST OF FIGURES

## Figure

- 1.1. Wooden pole in service
- 2.1. Southwell plot
- 3.1. to 3.5. Pole circumference compared to code requirements
- 3.6. End support, equipped with hydraulic jacks to apply the load
- 3.7. End support
- 3.8. Test set-up
- 3.9. Set of rulers for deflection measuring
- 3.10. Initial out-of-straightness measuring
- 3.11. Modified testing frame
- 3.12. End fittings of the modified testing frame
- 3.13. Test specimen before and after the test
- 3.14. Two scars of the pole #3
- 3.15. Pole #8
- 3.16. Hollow heart of the pole #9
- 3.17. Split near the butt of the pole #9
- 3.18. Compression parallel to the grain test setup
- 3.19. Bending test setup
- 4.1. Height-diameter ratio for all compression test specimens
- 4.2. Stress-strain relationship for compression tests for Lodgepole Pine
- 4.3. Stress-strain relationship for compression tests for Western Red Cedar

- 4.4. Stress-deflection relationship for bending tests
- 4.5. Tension test results
- 4.6. Typical load-deflection relationship and deflected shape of the pole 7/1
- 4.7. Effect of out-of-straightness on the buckling capacity of the pole
- 4.8. Typical load-deflection relationship of the test specimens originated from the same pole
- 4.9. Typical load-relative deflections relationship for the specimens originated from the same pole
- 5.1. Imperfect circular cross-section of the pole #2
- 5.2. Two types of buckling behaviour
- 5.3. Pole before applying the load and at ultimate load
- 5.4. Typical Southwell plot
- 5.5. Critical load evaluated by Southwell plot compared to prediction of the Euler's formula
- 5.6. Critical load evaluated by Southwell plot compared to prediction of the Ylinen's column formula
- 5.7. Critical load evaluated by Southwell plot compared to prediction of the Buchanan's formula
- 5.8. Critical load evaluated by Southwell plot compared to prediction of the Code equation
- 5.9. Influence of the coefficient  $c$  on predicted compression strength of the column by Ylinen's formula
- 5.10. Ratio between pole's length and pole's out-of-straightness

- 5.11. Typical pole shape at various loading stages
- 5.12. Predicted load by Buchanan's model compared to measured buckling load
- 5.13. Predicted load by modified Buchanan's model compared to measured buckling
- 5.14. Predicted load by Zahn's model compared to measured buckling load
- 5.15. Predicted load by the Code model compared to measured buckling load
- A1.1. to A1.5 Stress-strain relationship for compression tests
- A2.1. to A2.62. Load-deflection relationships and deflected shape of the pole
- A3.1. to A3.10. Load-deflection relationship of the test specimens originated from the same pole
- A4.1. to A4.10. Load-relative deflections relationship of the test specimens originated from the same pole
- B1.1. to B1.30. Southwell plot

NOTATION

$e_b$	initial out-of-straightness
$e$	deflection at the mid-height of the column
$C_c$	slenderness ratio
$E$	modulus of elasticity
$F$	moment magnification factor proposed by Buchanan
$F'$	moment magnification factor
$f_b$	specified bending strength parallel to grain
$F_b$	bending strength
$f_c$	specified compression strength parallel to grain
$F_c$	compression strength
$F_t$	tension strength
$I$	moment of inertia
$K_c$	slenderness factor
$K_D$	load duration factor
$K_H$	system factor
$K_{Sc}$	service condition factor for compression parallel to the grain
$K_{SE}$	service condition factor for modulus of elasticity
$K_T$	treatment factor
$K_{Zc}$	size effect factor for compression for sawn lumber
$L_e$	effective length
$M_n$	nominal bending moment resistance
$M_r$	nominal moment resistance in case of combined axial load and bending

$P_c$	axial compression strength of the columns cross-section
$P_e$	Euler's elastic buckling load
$P_n$	nominal compression load
$P_r$	nominal moment resistance in case of combined axial load and bending
$r$	radius of gyration
$S$	section modulus

## CHAPTER 1.

### INTRODUCTION

#### **1.1 General**

Wooden poles, shown in Figure 1.1, are popular structural elements currently used by Manitoba Hydro for distribution lines and transmission towers. Wooden poles are considered to be a favourable material for transmission lines because of their availability, low cost, high strength-to-weight ratio, and better aesthetic acceptance. If treated properly, they can provide many years of service with little deterioration. Long-term cost of the transmission lines can be further reduced by reuse of the poles from up-graded or replaced lines.

Wooden poles are designed as free-standing structures, to withstand self-weight, ice build-up, wind and other loads acting on the pole. In recent years, a considerable number of such poles have failed due to heavy ice build-up on the lines, such as YM31 line, La Verendrye-Morden and Y511, La Verendrye-U.S. border. These failures may be attributed to the accuracy or reliability of the design methods and design loads, and/or a lack of understanding and adequate information about their buckling strength.

Requirements of CAN/CSA-086.1-M89 for wooden poles are essentially unchanged from CSA-086-M80. Poles are designed according to provisions given for sawn lumber. Specified strengths for wooden poles bear the same ratio to specified strengths of sawn lumber established and adopted in 1953 (De Grace, 1986). However, in the 1989 edition of the Code, requirements for sawn lumber were changed following the research on in-grade beams under combined axial load and bending moments. Instead of three classes of columns (short, intermediate and long), considered in CAN3-086.1-M84, one equation is given in CAN/CSA-086.1-M89 for the whole range of slenderness ratios, and the resistance factor is the same for all slenderness ratios.

In recent years experimental investigation was conducted to determine the flexural behaviour of wooden poles (Goodman, 1983). While many tests have been conducted to determine flexural capacity of shorter poles, only limited data is available on the strength of longer poles. In addition, there is no research reported regarding testing of wooden poles subjected to axial load to determine the compression capacity of such members. Therefore, this research project, sponsored by Manitoba Hydro, was undertaken at the University of Manitoba to determine the buckling behaviour of the wooden poles.

## 1.2 Objective

The primary objective of this research is to determine the buckling behaviour and the axial load-carrying capacity of the wooden poles currently in use by Manitoba Hydro.

The work attempts to examine the accuracy and the prediction capability of the available models, including the current codes, with regard to the measured load-carrying capacity of the poles. The evaluation of the models will include the effects of out-of-straightness, tapered shape, and measured material properties.

Predictions of the various models will be compared to the measured values to determine the reliability of each model. Based on this investigation, a design procedure for this type of wooden pole will be introduced.

## 1.3. Scope

The scope of the project included testing of sixty one specimens produced out of ten wooden poles. Two different species of wood were selected for this project, Lodgepole Pine and Western Red Cedar, since they are most commonly used by Manitoba Hydro. Poles were randomly chosen from the Manitoba Hydro Yard, representing the most commonly used pole

dimensions. The nominal length, class, and species of the ten poles considered in this study are given in Table 1.1. Material characteristics including modulus of elasticity, compressive strength parallel to the grain, bending strength, moisture content, and specific gravity of the given poles were determined for each species.

## CHAPTER 2.

### LITERATURE REVIEW

The buckling capacity of slender columns was first determined by Euler in 1744 (Chajes, 1974). This initial study included an ideal column, prismatic and perfectly elastic, perfectly straight and compressed by concentrically applied load. The Euler buckling load,  $P_e$ , was determined as the load under which the column of effective length  $L_e$ , is in equilibrium both in the straight and slightly bent configuration:

$$P_e = \frac{\pi^2 EI}{L_e^2} \quad (2.1)$$

where,  $E$  is modulus of elasticity, and  $I$  is moment of inertia about the weak axis of the cross section.

With the increase in load, an ideal column deforms axially, in the direction of the applied load. When the applied load approaches buckling load, a sudden sideways deflection will occur due to stability loss of the column. In practice, perfect columns do not exist in typical engineering structures. This is specially so for wooden members. Wood is non-homogeneous material, and normally contains natural imperfections, such as knots, checks, hollow hearts, etc. In addition to considerable natural imperfections, wooden poles

also have an initial out-of-straightness, and therefore, the load could not be applied concentrically. Due to these conditions, wooden poles start to deflect laterally as the load is applied. Initially, the deflection rate is mainly low and constant; however, it increases rapidly as the applied load approaches the buckling load. As a result, the carrying capacity of wooden poles is always smaller than the value predicted by Euler.

For short columns, failure load is mainly dependant on the material's compression strength parallel to the grain. The compression capacity of the short column will be given as:

$$P_c = F_c \cdot A \quad (2.2)$$

where  $F_c$  is the compression strength parallel to the grain, and  $A$  is cross-sectional area. Since Euler's formula is developed for linearly elastic columns, the prediction is valid only up to the proportional limit of the material. In the case of wood, it is consequently valid only for slender columns. If the induced axial stresses in the column exceed the proportional limit of the material, failure load is always less than Euler's prediction. Behaviour and failure of these columns could be explained by using the tangent modulus theory and/or other inelastic buckling theories (Bleich, 1952).

## 2.1 Ylinen's column formula

For non-linear elastic material, the nominal compression capacity,  $P_n$ , of the column can be determined using the tangent modulus theory (Ylinen, 1956):

$$P_n = \frac{P_c + P_e}{2c} - \sqrt{\left(\frac{P_c + P_e}{2c}\right)^2 - \frac{P_c P_e}{c}} \quad (2.3)$$

where  $c$  is an adjustable constant which can be determined from any given stress-strain diagram,  $f$ - $\epsilon$ , of the material used for the column. An average value of  $c$  can be obtained using various levels of stress,  $f$ , and strain,  $\epsilon$ , as follows:

$$c = \frac{\epsilon \cdot E + F_c \cdot \ln\left(1 - \frac{f}{F_c}\right)}{f + F_c \cdot \ln\left(1 - \frac{f}{F_c}\right)} \quad (2.4)$$

## 2.2 Zahn's proposal

Behaviour of a column, under combined axial load and bending, was proposed by Zahn (1986). The proposed model for combined uniaxial bending and eccentric axial compression load is given as:

$$\left(\frac{P_I}{P_n}\right)^2 + \frac{M_I}{M_n} \leq 1.0 \quad (2.5)$$

where  $P_r$  and  $M_r$  are the combined nominal axial load and bending moment resistance of the column. Nominal bending moment resistance, under the combined load,  $M_r$ , is given as:

$$M_r = \frac{M + e \cdot P_r (1.234 - 0.234\theta)}{\theta} \quad (2.6)$$

where  $M$  is the moment determined by first order analysis,

$$\theta = 1 - \frac{P_r}{P_e} \quad (2.7)$$

$e$  is the total initial eccentricity, including end eccentricity,  $e_l$  and out-of-straightness of the column,  $e_b$ . Ylinen's column formula, given in Equation 2.3, was used to determine the nominal compression capacity of the column,  $P_n$ . The nominal bending moment resistance,  $M_n$ , is determined as  $M_n = S \cdot F_b$ , where  $S$  is section modulus and  $F_b$  is bending strength. It should be noted that Zahn's model was compared only to test results of sawn lumber.

### 2.3 Buchanan's proposal

Extensive research has been done at the University of British Columbia on the behaviour of sawn lumber subjected to combined bending and axial load (Buchanan, 1984, 1985, 1986). An approximate design methodology was recommended to predict the nominal compression capacity,  $P_n$ , of a column. The design equation, proposed for members with rectangular cross-section, is given as:

$$P_n = \frac{P_c}{1 + \frac{F_c}{E} \frac{C_c^3}{40}} \quad (2.8)$$

where  $C_c$  is slenderness ratio, given as:

$$C_c = \frac{L_e}{d} \quad (2.9)$$

where  $L_e$  and  $d$  are effective length and width of the column.

The proposed interaction equation for a member subjected to combined axial load and bending is:

$$\frac{P_r}{P_n} + \frac{M_r}{M_n} \leq 1.0 \quad (2.10)$$

where  $M_r$  is given as:

$$M_r = \frac{F \cdot M}{B} \quad (2.11)$$

where  $F$  is a moment magnification factor given by:

$$F = \frac{1 + \frac{P_r}{P_e}}{1 - \frac{P_r}{P_e}} \quad (2.12)$$

$B$  is a dimensionless factor given by Buchanan as:

$$B = 1.35 \frac{F_c}{F_t} \quad (2.13)$$

where  $F_t$  is the tension strength of the wood.

The research study at the University of British Columbia also considered the size effects on material properties for in-grade lumber (Madsen, 1986, 1990a, 1990b, Buchanan, 1984, 1985, 1986). Effects of moisture content on material properties were examined by Madsen (1982). Equations to evaluate size and moisture content effects on material properties were given, based on tests of the specimens made of sawn lumber up to 5 m long.

#### 2.4. CAN/CSA-086.1-M89

According to Clause 12 of the Canadian Standard CAN/CSA-086.1-M89, a wooden pole should be designed according to appropriate provisions of Clause 5 for Sawn Lumber. Since the poles are tapered members, the effective diameter,  $d_e$ , given in Clause 12.5.2.5. is:

$$d_e = d_{\min} + 0.45 (d_{\max} - d_{\min}) \quad (2.14)$$

where  $d_{\max}$  and  $d_{\min}$  are maximum and minimum diameters of the pole. The factored compression capacity of wood poles,  $P_n$ , is given in the Standard in Clause 5.5.6.2.2. as:

$$P_n = \phi F_c A K_{z_c} K_C \quad (2.15)$$

where  $\phi$  is resistance factor equal to 0.8, and  $F_c$  is the compression strength of wood, given as:

$$F_c = f_c (K_D K_H K_{SC} K_T) \quad (2.16)$$

where  $f_c$  is the specified compression strength parallel to grain,  $K_D$  load duration factor,  $K_H$  system factor,  $K_{SC}$  service condition factor for compression parallel to the grain, and  $K_T$  treatment factor;  $K_{Zc}$  is size effect factor for compression for sawn lumber which is given as:

$$K_{Zc} = 6.3 (d_e L_e)^{-0.13} \leq 1.3 \quad (2.17)$$

$K_C$  is slenderness factor given by the Clause 5.5.6.2.3. as:

$$K_C = \left[ 1.0 + \frac{F_c K_{Zc} C_c^3}{35 E K_{SE} K_T} \right]^{-1} \quad (2.18)$$

where  $K_{SE}$  is service condition factor for modulus of elasticity, and  $C_c$  slenderness ratio. Slenderness ratio,  $C_c$ , for poles is given by the Clause 12.5.2.4.:

$$C_c = \frac{L_e}{r\sqrt{12}} \quad (2.19)$$

where  $L_e$  is effective length, and  $r$  radius of gyration of the cross-section of the member.

The factored bending moment resistance is given in Clause 5.5.4.1 as:

$$M_n = \phi F_b S K_{zb} K_L \quad (2.20)$$

where  $\phi$  is resistance factor equal to 0.9, and  $F_b$  bending strength given as:

$$F_b = f_b (K_D K_H K_{sb} K_T) \quad (2.21)$$

where  $f_b$  and  $K_{sb}$  are specified bending strength and service condition factor for bending consequently;  $K_{zb}$  is size factor for bending, and  $K_L$  lateral stability factor. According to the Clause 12.5.3., the factored bending moment resistance of circular section shall be taken as that of a square section having the same cross-sectional area.

According to Clause 5.5.10. members subjected to combined bending and axial load shall be designed to satisfy:

$$\frac{P_r}{P_n} + \frac{M_r}{M_n} \leq 1.0 \quad (2.22)$$

where  $P_r$  is nominal compressive axial load,  $M_r$  corresponding nominal bending moment, taking into account the magnified moment due to the presence of axial compression loads.

It should be mentioned that the design equations used for design of poles, are based on research conducted at the University of British Columbia (Wood Design Manual-Commentary, 1990) for sawn lumber. The ratio between specified strengths for wooden poles and sawn lumber, is the same as in the 1984 edition of the Code. This ratio was adopted as conservative in

1953 (De Grace 1986).

The load factors given in CAN/CSA-C22.3 No.1-M87. are higher than the ones given for steel structures to account for "varying strength of an individual pole and its deterioration with age" (CAN/CSA-C22.3 No.1-M87. Commentary).

## **2.5 Research done by Research Institute of Colorado**

More reliable design of wooden poles can be achieved by using material properties obtained from tests on full-size pole specimens. An extensive research has been conducted at the Research Institute of Colorado (Goodman, 1983), dealing with reliability-based design of wood transmission line structures. As part of the research, results of pole bending tests were collected and organized into a data bank. However, only a few of the tested poles were longer than 40 ft. The study indicated that for very large Douglas Fir poles, the reduction of strength and stiffness due to pole length (size) was insignificant. However, the sample size was small, and therefore more tests are required for a complete statistical analysis. The tests were also done to evaluate the influence of the pole's age on bending strength. Destructive tests were conducted on 139 poles of various species, removed from service. Test results indicated that the strength of the poles decreased considerably with age. The mean bending strength of

35 Western Red Cedar poles, removed from service after 57 years, and tested by Manitoba Hydro (Munro, 1989) complied with CSA average bending strength for new poles of the same species. Nevertheless, both test samples were limited, and more research is needed to determine the effect of years in service on material properties of wooden poles.

## 2.6. Ontario Highway Bridge Design Code

Ontario Highway Bridge Design Code (OHBDC-1983) also proposes the straight-line strength criterion for member under combined uniaxial bending and compression load as given in Equation 2.20. The Code also requires use of a minimum eccentricity of the applied load,  $e_1$ , of five percent of the lateral dimension of the compression member, if the resulting moment is larger than existing end moments in the structure. All compression members should also be analyzed for the load effect due to a minimum eccentricity at the mid-height of the unsupported column,  $e_b$ , due to the lateral out-of-straightness:

$$e_b = \frac{L_e}{500} \quad (2.23)$$

where  $L_e$  is the effective length of a column.

Ontario Highway Bridge Design Code does not give any specific provisions for the design of wooden poles. Pole bending test data were used to determine specified bending strength and modulus of elasticity for timber piles (OHBDC-Commentary 1983). Consequently, the Code could provide more reliable values in terms of material properties. The Code specifies the same value for compression strength of piles as for the bending strength, since no data is available regarding compression capacity of the wooden poles.

### 2.7. Southwell plot

The nominal compression capacity of an imperfect column,  $P_n$ , can be determined from load-deflection data of a column failing within the elastic region using the Southwell plot method (Timoshenko, 1961). In this case, as the load approaches the buckling load, the total deflection at the mid-height of the column,  $e$ , at various stages of loading,  $P$ , could be determined with sufficient accuracy as:

$$e = \left( e_b + \frac{4e_L}{\pi} \right) \frac{1}{\frac{P_n}{P} - 1} \quad (2.24)$$

where  $e_b$  is the initial out-of-straightness, and  $e_L$  is the eccentricity of the applied load. It should be noted that in this approach, the initial shape of the column axis and the consequent deflected shape, is assumed to be in the form of a sine curve with maximum value at mid-height. Equation 2.2 could be rearranged as:

$$\frac{e}{P} P_n - e = e_b + \frac{4e_L}{\pi} \quad (2.25)$$

which shows that the relation of the ratio  $e/P$  and the measured magnified deflection,  $e$ , is a straight line, with intersection value with the horizontal axis ( $e/P = 0$ ) of  $e_b + \frac{4e_L}{\pi}$ . The inverse slope of the line could be also used to

determine the buckling load,  $P_n$ , as shown in Figure 2.1.

## CHAPTER 3.

### EXPERIMENTAL PROGRAM

#### 3.1 Introduction

A total of 10 wooden poles were selected, with the approval of Manitoba Hydro, to provide sixty-one specimens for this research project. Two species commonly used by Manitoba Hydro were investigated: Lodgepole Pine and Western Red Cedar. Poles were also representative of typical classes and lengths used for transmission lines. Length of the specimens was limited to a maximum of 18.288 m (60 ft), based on space available in the Structures Laboratory of the University of Manitoba. Test specimens were selected randomly from the Manitoba Hydro supply Yard.

Total length, class and species of the poles considered in this investigation are shown in Table 1.1. The measured circumference and the values specified by the CAN3-015-M83 code are shown in Figures 3.1 to 3.5, which clearly indicate that all actual dimensions of the poles exceed the values recommended by the code. In these figures, measured dimensions are also compared to uniform taper from top to the butt of the pole. Length, dimensions (including minimum and maximum diameter), and diameters at quarter height of the pole, for

the sixty-one test specimens, are given in the Table 3.1.

### 3.2 Test set-up and instrumentation

The poles were tested in a horizontal position, using a modified testing frame specially designed and built at the University of Manitoba for the first phase of this research program (Pincheira, 1987). Modifications of the testing frame included:

- (i) large bearing plates to accommodate larger poles diameters
- (ii) stiffeners of the supporting system to provide stability of the end plate under higher load levels.
- (iii) load cell to provide accurate load measuring

The testing frame consisted of two end supports which were connected by four Dywidag bars. One of the end supports, shown on Figure 3.6, included two identical 445 kN (100,000 lb) hydraulic jacks that were used to apply a load up to 890 kN (200,000 lbs). The two jacks were attached to a 90 mm thick plate supported by a bracing system, resting on the floor. The bracing system was used to prevent tipping of the plate at higher loading conditions. The hydraulic jacks were connected to a load cell through a 57 mm thick steel plate to provide more accurate measurements of the applied load. A round steel plate was used to transfer the load to the pole end. The round

plate was supported by a roller system which allowed the plate to move in the axial direction of the pole only. The end of the pole was supported by a 38 mm thick square steel plate which was pin-connected to the round plate, allowing rotation about the horizontal axis only. At the other end of the testing frame, shown in Figure 3.7, the pole was supported by a 38 mm thick square plate which was directly pin-connected to a 90 mm thick steel plate supported by the bracing system. At this end, the rotation was also allowed about the horizontal axis only. This end plate was enlarged to accommodate larger diameters of the poles. The pole was connected to the end plates by a system of three braces. Both end fittings were equipped with chain hoists which were used to position the pole in the testing frame, to hold it in place until the beginning of the test, and to remove the tested pole from the testing frame.

Dywidag bars connecting the end fittings consisted of two or three pieces (depending on the sample length) spliced by high strength couplers. The end two meter section of each bar was utilized as a load cell to measure the applied load using a strain gage attached to the bar. Each of these bars was tested in tension to determine their calibration factors. These bars were also used to balance the applied load to be concentric with the pole. An Linear Variable Differential Transducer, LVDT, was attached to the testing frame to measure

the end plate movement known by the stroke. The complete test set-up is shown in Figure 3.8.

Strain gauge, LVDT and load cell readings were recorded using a 16 channel Techmar Lab Master Data Acquisition System, connected to an IBM-PC computer. Due to the large relative deflections of the pole, a two ruler system was used to measure the deflection, as shown on Figure 3.9. A vertical ruler was attached to the stationary post, while a horizontal ruler was connected to the pole. Deflections of the pole were recorded at one-quarter, one-half and three quarters of the specimen's length.

Initial out-of-straightness of the pole was also measured before application of the load. As can be seen on Figure 3.10, the distance of the top point of the pole from the floor was measured. The pole's diameter was determined by the measured circumference, assuming a circular cross-section. The position of the centerline from the floor was determined by subtracting half of the pole's diameter ( $D/2$ ) from the measured distance of the top point from the floor. Eccentricity was determined as the difference between the measured distance of the centerline from the floor and the height of the applied load,  $h$ . Load was applied at the height of 40.5 cm, except for the pole #10, for which the load was applied at the height of 58.3 cm.

During the test, the load-stroke relationship was plotted using an x-y plotter. The curve obtained by this method clearly indicated when the pole reached its buckling load.

After the completion of the fifty-seven tests, the testing frame was again modified to accommodate specimens with a small slenderness ratio. Modified testing frame is shown in Figure 3.11. Modifications were done mainly to provide better stability of the testing frame, and to allow for higher load levels. The load cell was removed from this setup, since the expected loads were higher than its capacity, and also to provide more stability to the end fitting under higher load levels. To prevent torsion of the end plate, six 445 kN (100,000 lb) hydraulic jacks were used. The jacks were directly connected to the round steel plate on rollers. The end fittings of the modified test frame are shown in Figure 3.12. To accommodate higher loads, and to provide more stability to the testing frame, ten Dywidag bars were used to connect the end supports. Each bar was made of two sections, spliced by high strength couplers. The end section of each bar was equipped with two strain gauges on opposite sides of the bar, utilized to measure the applied load. Calibration factors for all bars were determined from the tension tests. Due to safety reasons, the deflections were measured using a transit, for these test specimens. For this phase of the testing program, strain gauges and LVDT's were connected to an HP-3490

voltmeter/multiplexer data acquisition system, connected to an IBM-PC computer via GPIB parallel interface.

### 3.3 Test procedure

Before testing, the length of the test specimen was measured. The circumference of the test specimen was measured at one quarter, one half and three quarters of the pole length, and at the specimens ends. Each test specimen was marked by two numbers,  $i$  and  $j$ . The first number,  $i$ , indicated the mark of the pole from which the specimen originated, and the second number,  $j$ , indicated the number of the specimen provided from the same pole. Bags filled with plaster were used to provide a uniform contact surface to transfer the load between the two end plates of the testing frame to the test specimen. After the test specimen was in place, initial readings were taken, and the distance of the top of the pole from the floor was measured. Before the test, steel chains were wrapped around the Dywidag bars and the pole, to prevent any possible accident.

The poles were placed in the horizontal position in the testing frame with their maximum natural curvature lying in a vertical plane (upwards where possible). This orientation ensured that buckling would occur in the vertical plane without interference from the Dywidag bars, and about the

hinged end connections. It was observed in some cases that the pole deflected sideways, due to initial out-of-straightness in horizontal direction and/or natural imperfections of the pole. In this case, the test was stopped and the pole rotated and retested.

At the beginning of each test an initial load of 50 to 100 kN was applied and the load in the Dywidag bars was adjusted to ensure that the difference between the forces in the bars was within ten percent. This procedure was used to apply concentric load to the tested pole.

The load was applied in increments which were adjusted according to the response of each pole. For each load level, deformations at the specified locations were measured and recorded. The test was terminated when large deformations occurred without a corresponding increase in the load-carrying capacity. In some cases, the test had to be stopped before the pole reached its ultimate capacity. This was the case when the pole reached the lab floor, the end plates reached its ultimate rotational freedom, or the upward deflections were extremely large, and it was therefore unsafe to proceed any further.

After the completion of the test, the load was released, and a set of deflection readings was recorded. These readings

were compared to the initial readings before the test. In all case, the difference between initial and final readings were within the range of accuracy of the instrument used, showing that the buckling took place within the elastic range. Some residual deflections were recorded after the tests on samples 7/7 and 10/8, indicating that the material reached inelastic range. However, these were the last tests of the given poles. Repeated tests on some of the specimens also confirmed the elastic behaviour of the poles, since the same buckling load was reached in both tests.

Because the buckling capacity of the test specimen was within the elastic range, after completion of the test the specimen was shortened by 5 feet to produce a new test specimen with a different slenderness ratio. The test specimen before the test is compared to the test specimen after the test is completed, as shown on Figure 3.13.

#### 3.4 Description of the tested poles

POLE #1: LODGEPOLE PINE CLASS 3/40 ft

The initial length of the pole was 12.068 m (39'-7.125"). The Pole had large checks, a significant number of knots and spiral grain, one spiral with the full twist through the pole length. The pole also had holes drilled at 8.9 and 29.2 cm from the top.

POLE #2: LODGEPOLE PINE CLASS 4/40 ft

The initial length of the pole was 12.179 m (39'-11.5"). The checks, knots and spiral grain were similar to Pole #1. The drilled holes were located at 10, 30, and 122.5 cm from the top. Holes at 10, and 30 cm were drilled in the same direction, and the hole at 122.5 cm was drilled at a 90 degrees angle from the other two.

POLE #3: LODGEPOLE PINE CLASS 4/45 ft

The initial length of the pole was 13.770 m (45'-2.125"). The pole had large checks, knots, and spiral grain with one full twist through the pole length. The pole also had two large scars, as shown on Figure 3.14, and a cut 2.3 cm deep 31 cm from the butt. The pole had drilled holes drilled at 91.44, 143.5, 203.2, 355.6, and 391.6 cm from the top.

POLE #4: LODGEPOLE PINE CLASS 3/45 ft

The initial length of the pole was 13.748 m (45'-1.25"). Pole had large checks, extensive knots, surrounded with deteriorated wood, and spiral grain. The pole had holes drilled at 92.1, 143.2, 203.2, 355.9 and 391.2 cm from the top.

POLE #5: WESTERN RED CEDAR CLASS 2/45 ft

The initial length of the pole was 13.745 m (45'-1.125"). The pole had large checks, small knots, and the small cracks

across the fibre at 5.2 m from the butt. It also had small holes near the butt and two holes 3.8 cm deep on the opposite sides of the pole 27.9 cm from the butt, probably made by the machine that was lifting the pole. The pole had holes drilled at 90.2, 143.2, 203.5, 355.6 318.8 cm from the top.

POLE #6: WESTERN RED CEDAR CLASS 2/50 ft

The initial length of the pole was 15.221 m (49' 11.25"). Defects of the pole included a large check which reached the poles heart, small knots, and some hollow heart at approximately 4.5 m from the butt. The pole had holes drilled at 94, 113, 202, 355 and 390.5 cm from the top.

POLE #7: WESTERN RED CEDAR CLASS 2/55 ft

The initial length of the pole was 16.688 m (54'-9"). Defects of the pole included a some checks, small knots, small holes near the large end and some cuts due to transportation.

POLE #8: WESTERN RED CEDAR CLASS 2/50 ft

The initial length of the pole was 15.189 m (49'-10"). The pole had very large initial out-of-straightness in one direction, and it had a notable S shape in the other, as shown in Figure 3.15. It also had small holes near the butt, and small knots. Drilled holes were positioned at 93.2, 143.5, 203.5, 357 and 390.5 from the top of the pole.

**POLE #9:** WESTERN RED CEDAR CLASS 1/60 ft

The initial length of the pole was 18.218 m (59'-9.25"). Pole had knots and checks, some hollow heart, as seen on Figure 3.16, which extended approximately 3 m (10 ft) from the butt. Pole also had a split near the butt, as shown on Figure 3.17.

**POLE #10:** WESTERN RED CEDAR CLASS 1/60 ft

The initial length of the pole was 18.234 m (59'-9.875"). The pole did not have any significant defects, but had small knots evenly distributed throughout the pole and very small checks.

### **3.5 Material properties tests**

Material properties for each pole were measured according to ASTM Standards. Moisture content was determined according to ASTM D-2016, using the oven-drying method. Specific gravity was determined according to ASTM D-2395, using the water immersion method to determine sample's volume.

To estimate the modulus of elasticity and compression parallel to grain, ASTM Standard D-198 was used. Test samples were representative of the full cross-sectional area of the pole. For each specimen, height was measured and recorded. The circumference was measured at the top, bottom and points at a

quarter of the sample's height. Diameters of the sample were estimated assuming a circular cross-section of the sample. Cross-sectional area was based on diameter determined as an average of the diameters of three middle points.

The samples were tested in a 600,000 lbs Satec universal testing machine. To provide uniform transfer of the load, bags filled with plaster were used at the both ends of the specimen. Application of the load was adjusted so that the tests lasted approximately the same time as the pole tests. This was done to exclude the effects of duration of load on the material properties. For the first group of specimens, deformations were measured using two dial gauges, positioned at opposite sides of the specimen. The readings for the load and deformation were taken manually. Deformations of the second group of specimens were measured using two LVDT's positioned at opposite sides of the specimen. Readings were taken electronically using the HP-3490 voltmeter/multiplexer data acquisition system, connected to an IBM-PC computer via a GPIB parallel interface. In addition to load and deflection readings, the stroke of the machine was recorded using LVDT's. Test set-up for measuring modulus of elasticity and compression parallel to grain is shown on Figure 3.18.

In order to determine ultimate bending stress, a series of bending tests were done on the remaining portions of the

poles. Tests were done using the 600.000 lbs Satec universal testing machine that was applying point load on the beam. Test setup is shown in Figure 3.19. The pole was supported by two hinged supports, resting on the rigid beam. The test span was 3.2 m. Deflections of the pole were measured at mid-span using LVDT's. Data was recorded using the HP-3490 voltmeter-multiplexer data acquisition system, connected to an IBM-PC computer via a GPIB parallel interface.

All Lodgepole Pine poles were tested in bending. Only two Western Red Cedar poles were tested in bending. A series of tension tests on small clear samples was done for Western Red Cedar poles. Ultimate bending strength for Western Red Cedar poles was evaluated based on the ratio between bending and compression tests and the ratio between tension and bending tests.

CHAPTER 4.  
TEST RESULTS

#### 4.1. Introduction

In this chapter, the measured data for all sixty one poles tested in this research program are presented in tabular and/or graphical form.

The data include the specimen material properties, buckling capacity of wooden poles, and deflection measurements.

#### 4.2 Material properties

Measured compression strength parallel to the grain, for full size specimens, and the corresponding modulus of elasticity are presented in the Table 4.1. In the same table diameter, height, weight, moisture content and specific gravity for each tested specimen are also given. The height-diameter ratios for all tested samples used for compression tests are given in Figure 4.1. The measured stress-strain curves for the compression tests for the Lodgepole Pine and Western Red Cedar samples are presented on Figures 4.2 and 4.3, respectively. These figures indicate that the ultimate compression strength and the elastic modulus for Lodgepole

Pine could vary between 14.92 to 32.01 MPa, and 7,706 to 14,985 MPa respectively, excluding test 1-1. Similarly, the ultimate compression strength and modulus of elasticity for Western Red Cedar could vary between 17.52 to 28.81 MPa, and 7,110 to 11,038, respectively. The same test results are presented for the each pole in Figures A1.1 to A1.5 in Appendix A.

Bending test results are given in Table 4.2. In the same table, the sizes of the tested specimens are also presented. Measured bending stress deflection relationships for the Lodgepole Pine and Western Red Cedar poles are presented in Figure 4.4.

Tension test results for small clear Western Red Cedar specimens are presented in Table 4.3. All tested samples were approximately 30 cm long, having reduced cross-section in the middle of the sample, as given in Table 4.3. The same results are presented in Figure 4.5. In the same figure, the mean value of the tension strength for each pole is presented. The measured values indicate that tension strength of clear wood samples for Western Red Cedar could vary between 48.46 to 66.87 MPa.

### 4.3 Wooden poles test results

The dimensions of the tested specimens are given in Table 3.1. Measured initial out-of-straightness, maximum deflection during the test, and measured buckling load are presented in Table 4.4. In Table 4.5 measured length, effective diameter ( $d_e$ ) and length-diameter ratios ( $l/d_e$ ) are compared to nominal values determined from the pole dimensions based on the Canadian Standard CAN3-015-M83.

Moisture content and specific gravity of the test samples are given in Table 4.6. In Table 4.7 compression strength parallel to the grain, bending strength, and modulus of elasticity for each pole are compared to the specified strengths given by the Code CAN/CSA-086.1-M89. In the same table classification stress and modulus of elasticity given by CAN3-015-M83 and material properties for wooden piles given by OHBDC-83 are also presented.

The typical load-deflection relationship and deflected shape of the pole at load increments of approximately one quarter of the buckling load are shown in Figure 4.6 for the pole 7/1. Load-deflection relationships and deflected shape of each pole are given in Appendix A in Figures A2.1 to A2.62.

The effect of out-of-straightness on the buckling capacity of the poles is shown on Figure 4.7. It represents comparison between two tests administered on the pole 2/1 in two different positions. Pole 2/1 was tested, turned 180 degrees, and then retested.

The typical load-deflection relationship for test specimens originated from the same pole is given in Figure 4.8. In this figure initial out-of-straightness of the test specimen was included. The same relationship is presented for all tested poles in Appendix A in Figures A3.1 to A3.10. Figure 4.9 presents the typical load-relative deflections with respect to the initial deflected shape of the pole relationship for the specimens originated from the same pole. The load-relative deflection relationship for specimens originated from the same pole, for each pole, is shown in Figures A4.1 to A4.10. in Appendix A.

## CHAPTER 5.

### ANALYSIS AND DISCUSSION OF TEST RESULTS

#### **5.1. Introduction**

The behaviour of wooden poles subjected to axial compression load, and tested in this program, is discussed in this Chapter. The various factors that influence the buckling load of the specimen are presented. The measured material properties and pole dimensions, presented in Chapter four, were used to compute the ultimate load-carrying capacity of the wooden poles. The axial load-carrying capacity was compared to predicted critical load for a straight column, using the Southwell plot and measured results, as explained in Chapter two. Capacity of the wooden pole under combined axial load and bending moment, due to out-of-straightness, was also evaluated and compared to measured values, excluding the self-weight effect due to the horizontal orientation during testing.

#### **5.2 Specimen behaviour**

Specimen behaviour during the testing was influenced by its initial out-of-straightness in the vertical and horizontal planes. For each test, an attempt was made to position the

pole to ensure that the maximum out-of-straightness was lying upwards in the vertical plane. The behaviour of the tested pole was also influenced by the effect of the gravity load.

In some cases, poles would start to deflect laterally. This behaviour could be caused by larger out-of-straightness in the horizontal plane than in the vertical plane, and/or due to natural imperfections of the wood (such as knots, checks etc.), or differences in the material properties (material strength and modulus of elasticity) within the pole. Lateral movement of the pole was normally followed by a sudden loss of stability in the vertical plane when the pole reached its buckling load. In the cases when the lateral movement of the test specimen was large under the substantial axial load, the test was stopped and the pole rotated and retested.

Specimens with small initial out-of-straightness normally exhibited a small increase in deflection during the test, followed by a sudden loss of stability as they reached their buckling load level. It was also noticed that the load-deflection curve was steeper for the specimens with smaller initial out-of-straightness than the one for the specimens with larger initial eccentricity. In general, the specimen behaviour was closer to the behaviour described by Euler for slender columns.

Specimens with large initial out-of-straightness started to deflect significantly as the load was applied. For most of these poles, the test had to be stopped before the pole reached its ultimate buckling capacity. This was the case when the pole touched the floor of the testing bed, the end plates reached their ultimate rotational freedom, or the upward deflections were extremely large, and it was therefore unsafe to proceed any further. The measured load for these poles was smaller than the buckling load of the specimen with a larger slenderness ratio originated from the same pole by shortening the pole by 1.5 m (5 feet) from the larger end.

Most of the tested specimens had small deflections at early stages of loading. Normally, the deflection rate started to increase when the load was approximately one half of the buckling load. When the load reached the buckling capacity of the specimen, small increases in the applied load would induce large deflections of the pole. Except for the cases where initial out-of-straightness was very large, test specimens with smaller slenderness ratios exhibited higher buckling load-carrying capacity.

The influence of the out-of-straightness on the buckling behaviour of the specimen can be seen in Figure 4.7. This figure presents the load-deflection relationship of two tests conducted on the same specimen, 2/1, with different

orientations of the pole with respect to the testing frame. Smaller initial out-of-straightness of the specimen in the second test led to a larger buckling load. The different behaviour could be also attributed to the difference in modulus of elasticity, due to the anisotropic nature of the material and the difference in moment of inertia due to the imperfect circular cross-section of the pole, as shown on Figure 5.1.

Depending on the orientation of the pole's out-of-straightness, two types of buckling behaviour were observed, as shown on Figure 5.2. One of the test specimens buckled upward and the other one downward. Comparison of the pole before applying the load and at ultimate load is shown on the Figure 5.3.

### **5.3 Material properties**

The average material properties given in Table 4.7 indicate that the modulus of elasticity and the compression strength of the wooden poles tested in this program have higher values than the specified strengths recommended by the code CAN/CSA-O86.1-M89. The Code also introduces an additional reduction of the compression strength ranging between eighty to ninety percent due to the size effect factor. Measured bending strengths were considerably higher than the one given

by the CAN/CSA-086.1-M89 code, and OHBDC-83 values for piles. Measured modulus of elasticity and compression strength parallel to grain were also higher than values specified in CAN/CSA-086.1-M89, and OHBDC-83 values for piles. Average bending strength for the poles of 7 to 11 m length is specified as classification strength in CAN3-015-M83. The measured bending strength of Lodgepole Pine poles was higher than the classification stress, and for Western Red Cedar, it was the same as the classification stress for given species.

Sample size, moisture content and specific gravity influenced compression capacity of the short samples. Test results indicated that the presence of natural imperfections has greater influence on the material properties than the effect of sample size, moisture content and specific gravity of the sample. Most of the tested specimens failed in tension parallel to the grain around the knots and other defects. Specimens which failed in pure compression showed much higher compression strength than the specimens which failed due to the presence of natural imperfections.

#### **5.4. Buckling capacity of wooden poles**

The nominal buckling capacity of the column was determined from measured load,  $P$ , and corresponding deflection,  $e$ , utilizing the Southwell plot. For each test,

the ratio of the measured deflection to load,  $e/P$ , was related to the measured deflection,  $e$ . A linear regression analysis was used to provide a straight line relation for the measured data within the large deflection range, as shown in Figure 5.4, for pole 10/2. Southwell plots for other poles are given in Appendix B, in Figures B1.1 to B1.30. The reliability of the Southwell plot method can be estimated by comparing the nominal buckling load estimated for two tests of the pole 2/1. The difference between the predicted buckling loads was within two percent. For poles 9/4, 9/5, and 9/6, which exhibited a sudden loss of stability without any significant deflections prior to stability loss, the measured values of the buckling load were used for this investigation.

Test results were divided in two main categories, according to the type of poles tested. The first category, type A, consists of poles having a single curvature of out-of-straightness. For this category the deflected shape of the pole is assumed to be a sine curve with maximum value at the mid-height. This assumption agreed with the theoretical development of the Southwell plot method. Test results of the poles 9/4, 9/5, and 9/6 were also included in this group due to the nature of their failure. The second category, type B, consisted of poles which had double curvature of out-of-straightness. This category also included all other poles with an irregular out-of-straightness. Since the shape of these

poles does not satisfy the assumptions made in the theoretical development of the Southwell plot, it cannot be used to predict the critical load of these poles.

These modified measured axial capacities of the poles were compared to nominal compression capacities using the various models discussed in Chapter Two and the measured material properties and dimensions.

The various models used in this study to predict the nominal compression capacity include:

**5.4.1 Euler:** the equation is given in Equation 2.1. The Euler formula was used in the 1984 edition of Code CAN3-086.1-M84 to predict the compression capacity of the long columns. Comparison between predicted and modified measured load is given in Figure 5.5. It can be seen that Euler's predictions are reasonably good for the members with smaller buckling load. These results suggest that this model predicts compression capacity well for members with high slenderness ratios, and is unconservative for members with smaller slenderness ratios.

**5.4.2 Ylinen:** The constant  $c$  in the Equation 2.3 was evaluated using the stress-strain relation of the compression tests. Evaluated values of coefficient  $c$  for each pole are

given in Table 5.1. For all Lodgepole Pine poles, the constant  $c$  is assumed to be 0.80, and 0.85 for Western Red Cedar. Critical load evaluated by the Southwell plot is compared to predicted values in Figure 5.6. It can be noticed that Ylinen's column formula predicts the buckling load of the wooden pole quite well.

**5.4.3 Buchanan:** in this analysis the slenderness ratio,  $C_c$ , in Equation 2.8 is assumed to be  $L_e/(r\sqrt{12})$ , for members with circular cross-section. Prediction of the model is evaluated in Figure 5.7. Buchanan's formula gives good prediction of the buckling load for members with large slenderness ratios, and is unconservative for members with low slenderness ratios.

**5.4.4 CAN/CSA 086.1-M89:** all modification factors for compression strength and modulus of elasticity are assumed to be unity:

$$K_{Zc} = K_C = K_D = K_H = K_{Sc} = K_T = K_{SE} = 1$$

The resistance factor,  $\phi$ , was also assumed as unity. Consequently the Code equation to predict the nominal compression capacity,  $P_n$ , in terms of the compression strength,  $F_c$ , and elastic modulus,  $E$ , is:

$$P_n = \frac{P_c}{1 + \frac{F_c}{E} \frac{C_c^3}{35}} \quad (5.1)$$

where  $A$  is cross-sectional area, and  $C_c$  is the slenderness ratio given by Equation 2.19. Prediction of the model is compared to the critical load of the column in Figure 5.8. The code equation gives conservative solutions for a wide range of slenderness ratios.

For all the above models, a linear regression analysis was conducted to determine the best-fit line for measured values as related to the perfect prediction 1:1 line in Figures 5.5 to 5.8. The results indicate that Ylinen's column formula gives the best prediction of the test results. However it would require extensive testing to determine the values for the constant  $c$ . In cases where compression test specimens have brittle failure due to tension parallel to the grain around defects before reaching proportional limit of the material, the coefficient  $c$  is assumed as unity. For slender members the value of coefficient  $c$  does not influence the predicted compression strength significantly, as seen in Figure 5.9. It becomes more significant for members with small slenderness ratios. In Figure 5.9 average values for the compression strength to modulus of elasticity ratio, for given species were used to determine the nominal compression capacity of the column, for this comparison.

The code equation does not give as good prediction of the buckling load as Ylinen's column formula, but it is much easier to use with the given material properties.

#### 5.5. Combined axial load and bending moment

Moments due to self-weight were evaluated for each pole. Self-weight was estimated using specific gravity and assuming uniform taper between the measured diameters at the ends and three quarter lengths. Deflections due to self-weight were determined using the conjugate beam method. Measured initial out-of-straightness, deflection due to self-weight, and the pole's out-of-straightness, calculated by subtracting self-weight deflection from measured initial out-of-straightness, are given in Table 5.2. The ratio between the pole's length and its out-of-straightness is presented on Figure 5.10. Eccentricity between the measured points was estimated assuming parabolic shape of the pole. Typical pole shape at various loading stages is shown on Figure 5.11.

Test results were evaluated using four different models to predict the ultimate capacity of the column under combined bending and axial compression. Models were evaluated using initial moments, taken as moment due to the pole self-weight and moment due to axial compression load and pole's out-of-straightness, excluding the deflection due to self-weight.

Ultimate bending moment resistance was determined using measured material properties and assuming uniform taper shape between the measured diameters. Ultimate moment resistances were determined for circular cross section, and for square cross-section having the same area as circular cross section.

The four models used in this study were:

**5.5.1 Buchanan's proposal:** The interaction relationship between axial load and bending moment is given in Equation 2.10. The value of bending strength is taken as the value of tension strength of the material, to determine the dimensionless constant B. Predicted and measured buckling load are compared in Figure 5.12.

**5.5.2 Modified Buchanan's proposal:** using the same Equations as proposed by Buchanan, and a moment magnification factor as:

$$F' = \frac{1}{1 - \frac{P}{P_e}} \quad (5.2)$$

where  $P_e$  is the Euler buckling load. The predicted buckling load was compared to measured values in Figure 5.13.

**5.5.3 Zahn's proposal:** The buckling load and interaction relationship between axial load and bending moment are given

by Equations 2.3 and 2.5 respectively. Prediction of the model using initial moments is shown in Figure 5.14.

**5.5.4. Code equation:** Resistance factor and all modification factors for bending strength are taken as unity:

$$\phi - K_{zb} - K_L - K_D - K_H - K_{sb} - K_T = 1.0$$

$$M_T = F_b \cdot S \tag{5.3}$$

where  $F_b$  is bending strength and  $S$  is section modulus of equivalent square cross-section. Interaction relationship between axial load and moment is given in Equation 2.22. Prediction of the model was compared to test results in Figure 5.15. The commonly used moment magnification factor, given in Equation 5.2, was used to predict buckling load of the pole.

For the first three models, the sectional modulus of the circular cross-section was used to predict ultimate bending moment resistance of the poles, while the sectional modulus of equivalent square cross section was used to predict ultimate bending resistance for the fourth model.

Buchanan's proposal gives a conservative prediction of compression capacity of the poles for both Lodgepole Pine and Western Red Cedar. Using Buchanan's proposal with the commonly used magnification factor instead of the one proposed by

Buchanan gives better prediction of the compression capacity of the column.

Zahn's proposal gives very good prediction for the Lodgepole Pine poles, but it gives unconservative prediction for some Western Red Cedar Poles. This model uses Ylinen's column formula to determine nominal compression strength of the poles, which requires considerable testing to determine the value of constant  $c$ , as explained above.

Use of the equation proposed by the Code with commonly used magnification factor for the moments gives conservative prediction of the compression capacity for all tested samples.

For all evaluated models the linear regression analysis was used to provide the best-fit line for the test results. The standard deviation of the test results is larger for Western Red Cedar than for Lodgepole Pine poles. Comparing the best-fit line for both Lodgepole Pine and Western Red Cedar samples for all given models, it can be concluded:

1. Zahn's model gives the best prediction of the test results
2. Code equation gives better prediction than Buchanan's proposal using both magnification factor.

## CHAPTER 6.

### SUMMARY AND CONCLUSIONS

The research project, sponsored by Manitoba Hydro, was undertaken at the University of Manitoba to determine the buckling behaviour and the axial load-carrying capacity of the wooden poles. Two different species of wood, Lodgepole Pine and Western Red Cedar, were selected for this project since they are most commonly used by Manitoba Hydro. Poles were randomly chosen from the Manitoba Hydro Yard, representing the most commonly used pole dimensions. Sixty-one specimens, produced out of ten wooden poles, were tested in axial compression, while lying horizontally in the testing frame.

The predicted nominal compression capacity of the column was compared to measured buckling capacity of the tested poles using the Southwell plot for the measured load-deflection data. Predicted nominal compression capacity of wood poles with the presence of bending moment, to account for self-weight and out-of-straightness effect, was also evaluated.

Previous analysis showed that the equation introduced in the new edition of the Code can predict the ultimate buckling capacity of the poles well. However, the buckling behaviour of the poles is very much influenced by the initial out-of-

straightness of the pole. If the effect of the pole's out-of-straightness was not considered, the predicted load would be higher than the measured. Current Code CAN/CSA-086.1-M89, does not take into account the pole's initial crookedness to determine its buckling capacity. However, for design of this type of members, the current safety is achieved by using lower values for the material strengths.

To improve the prediction of the ultimate capacity of the wooden poles, specified material properties should be based on full-sized specimens cut from wooden poles, include the effect of initial out-of-straightness, and include the eccentricity of the applied load. These initial eccentricities were included in OHBDC-83 for design of members subjected to axial compression. The value of the recommended eccentricity should be evaluated based on actual pole crookedness. Based on the limited number of poles considered in this program, a recommended initial out-of-straightness of  $L/500$  and  $L/200$  could be assumed for Lodgepole Pine Western Red Cedar poles, respectively.

The average measured compression strength parallel to the grain of the tested specimens cut from Lodgepole Pine and Western Red Cedar poles was 23.33 MPa and 23.07 MPa, respectively. Average values of the modulus of elasticity were 11156 MPa and 8784 MPa for Lodgepole Pine and Western Red

Cedar poles respectively. Average bending strength was 64.10 MPa for Lodgepole Pine, and 39.52 MPa for Western Red Cedar. A design example using these recommended values for the material properties, measured pole dimensions and out-of-straightness is presented in Appendix C. Predicted compression capacity of the pole was compared to the measured value. A design example using code equations with measured material properties, recommended pole out-of-straightness and nominal pole dimensions was also presented in Appendix C. In Appendix C nominal buckling load predicted by the Code was also given.

This study shows that the compression strength and modulus of elasticity of the short portions, having the full cross-section, could be used to predict compression capacity of the pole. To obtain more reliable values for compression strength parallel to the grain of the poles, compression tests should be conducted using short specimens from the pole.

Research is also needed to determine the behaviour of the poles under combined axial load and bending, for lower levels of axial loads. Load duration and time-in-service effects should also be examined for this type of members.

REFERENCES:

American Society for Testing and Materials (1989) Annual Book of Standards. Section 4 Construction. Volume 04.09 Wood. Philadelphia, PA.

Bleich, F. (1952), Buckling Strength of Metal Structures. McGraw-Hill Book Company, Ltd.

Buchanan, A. H. (1984) Strength Model and Design Method for Bending and Axial Load Interaction in Timber Members. Ph. D. Thesis, Department of Civil Engineering, University of British Columbia, Vancouver, B. C.

Buchanan, A. H. (1986) "Combined Bending and Axial Loading in Lumber", *ASCE Journal of Structural Engineering*, **112**(12), 2592-2609.

Buchanan, A. H., Johns, K. C., Madsen, B. (1985), "Column Design Methods for Timber Engineering", *Canadian Journal of Civil Engineering*, **12**(4), 731-744.

Canadian Standards Association CAN/CSA-C22.3 No.1-M87 Overhead Systems. National Standard of Canada. Rexdale, Ontario.

Canadian Standards Association CAN/CSA-086.1-M89 Engineering Design in Wood (Limit States Design). National Standard of Canada. Rexdale, Ontario.

Canadian Standards Association CAN3-015-M83 Wood Utility Poles and Reinforcing stubs. National Standard of Canada. Rexdale, Ontario.

Canadian Standards Association CAN3-086.1-M84 Engineering Design in Wood (Limit States Design). National Standard of Canada. Rexdale, Ontario.

Canadian Standards Association CAN3-086-M84 Engineering Design in Wood (Working Stress Design). National Standard of Canada. Rexdale, Ontario.

Chajes, A. (1974) Principles of Structural Stability Theory. Prentice-Hall, Inc., Englewood Cliffs, New Jersey.

Goodman, J.R., Vanderbilt, M.D., Criswell, M.E. (1983) "Reliability-Based Design of Wood Transmission Structures". *ASCE Journal of Structural Engineering* 109(3), 690-704

Madsen, B., (1982) "Recommended Moisture Adjustment Factors for Lumber Stresses". *Canadian Journal of Civil Engineering* 9, 602-610.

Madsen, B., (1990a) "Length Effects in 38 mm Spruce-pine-fir Dimension Lumber". *Canadian Journal of Civil Engineering* **12**, 226-237.

Madsen, B., (1990b) "Size Effects in Defect-free Douglas Fir". *Canadian Journal of Civil Engineering* **12**, 238-242.

Madsen, B., Buchanan, A. H. (1986) "Size Effect in Timber Explained by a Modified Weakest Link Theory". *Canadian Journal of Civil Engineering* **13**(2), 218-232.

Munro, W. (1989) An Assessment of the Condition of 1931 Western Red Cedar Poles, report, Manitoba Hydro.

Neubauer, L. W. (1973) "A Realistic and Continuous Wood Column Formula". *Forest Products Journal* **23**(3), 38-45.

O86.1.1-M1986 De Grace, R. F. Commentary on CSA Standard CAN3-086.1-M84 Engineering Design in Wood (Limit States Design). Canadian Standards association. Rexdale, Ontario.

OHBDC, 1983. Ontario Highway Bridge Design code. Section 13. Wood structures, including Commentary. Ministry of Transportation and Communications, Downsview, Ontario.

Pincheira, J.A., Rizkalla, S.H., Polyzois, D. (1987) Buckling Behaviour of Wooden poles, Report, Department of Civil Engineering, University of Manitoba.

Timoshenko, S.P. (1961) Theory of Elastic Stability. McGraw-Hill Book Company, Inc.

Wood Design Manual, (1990) Canadian Wood Council, Ottawa, Ontario, Canada.

Ylinen, A. (1956) A Method of Determining the Buckling Stress and the Required Inelastic Range. Publications of the International Association for Bridge and Structural Engineering Vol. 16, 528-549.

Zahn, J.J. (1986) "Design of Wood Members Under Combined Load". *ASCE Journal of Structural Engineering* 112(9), 2109-2126.

# TABLES

pole	Nominal length		Class	Species group
	[m]	[ft]		
1	12.192	40	3	LPP
2	12.192	40	4	LPP
3	13.716	45	4	LPP
4	13.716	45	3	LPP
5	13.716	45	2	WRC
6	15.240	50	2	WRC
7	16.764	55	2	WRC
8	15.240	50	2	WRC
9	18.288	60	1	WRC
10	18.288	60	1	WRC

LPP - Lodgepole Pine  
WRC - Western Red Cedar

Table 1.1. Poles claccification

pole	test	length [m]	dmin [mm]	d1 [mm]	d2 [mm]	d3 [mm]	dmax [mm]
1	1	11.951	218	251	273	299	344
1	2	10.455	218	247	265	284	313
1	3	9.080	218	245	263	278	299
1	4	7.620	218	245	258	269	282
1	5	6.090	218	237	252	262	274
2	1	12.014	239	257	270	283	305
2	2	10.497	239	255	264	281	296
2	3	9.154	239	251	261	271	283
2	4	7.604	239	249	257	262	276
2	5	6.096	239	247	255	259	269
3	1	13.719	227	261	285	306	326
3	2	12.189	227	255	279	293	315
3	3	10.655	227	254	277	291	310
3	4	9.144	227	249	269	284	294
3	5	7.618	227	242	261	282	287
4	1	13.691	243	273	299	329	356
4	2	12.192	243	272	294	321	346
4	3	10.662	243	267	289	308	331
4	4	9.141	243	263	283	299	321
4	5	7.601	243	262	275	291	306
5	1	13.646	246	279	319	360	424
5	2	12.116	246	278	313	344	386
5	3	10.662	246	274	307	330	365
5	4	9.084	246	273	294	318	344
5	5	7.626	246	265	284	311	324
5	6	6.448	259	273	290	311	320
6	1	15.081	216	287	357	437	515
6	2	14.005	216	281	345	420	493
6	3	12.205	216	275	327	392	459
6	4	10.674	216	267	315	368	424
6	5	9.157	216	258	302	342	392
6	6	7.639	216	249	286	320	356

Table 3.1. Dimensions of the tested poles

pole	test	length [m]	dmin [mm]	d1 [mm]	d2 [mm]	d3 [mm]	dmax [mm]
7	1	15.278	235	304	369	414	466
7	2	13.738	235	301	360	395	441
7	3	12.119	235	297	343	380	424
7	4	10.668	235	288	331	372	400
7	5	9.144	235	279	316	357	378
7	6	7.616	235	278	303	338	367
7	7	6.084	235	265	295	313	338
8	1	15.151	237	281	314	366	402
8	2	13.716	237	277	307	354	395
8	3	12.182	237	271	296	349	375
8	4	10.658	237	267	294	321	357
8	5	9.141	237	263	291	307	348
8	6	7.618	237	260	281	295	314
9	1	18.123	223	319	375	436	480
9	2	16.758	223	312	365	424	471
9	3	15.237	223	305	358	408	444
9	4	13.716	223	297	354	401	437
9	5	12.186	223	290	344	376	419
9	6	10.668	223	282	332	361	406
9	7	9.138	223	273	319	354	377
9	8	7.620	223	263	301	335	362
10	1	18.113	224	309	384	444	506
10	2	16.748	224	303	374	433	487
10	3	15.227	224	296	362	417	461
10	4	13.710	224	289	347	402	444
10	5	12.179	224	280	334	384	421
10	6	10.668	224	272	321	367	407
10	7	9.138	224	265	309	347	385
10	8	7.617	224	256	293	324	357

Table 3.1. (Continued) Dimensions of the tested poles

test	Compression strength [MPa]	Modulus of elasticity [MPa]	Sample diameter [mm]	Sample height [cm]	Sample weight [kg]	Moisture content %	Specific gravity [g/cm <sup>3</sup> ]
1-1	14.26	4981	324	126	53.0	16.45	0.503
1-2	15.69	7706	308	117	44.0	18.66	0.519
1-3	14.92	9335	289	109	36.0	16.38	0.463
1-4	16.12	8675	277	104	31.0	16.15	0.475
1-5	18.24	9065	267	104	29.0	14.50	0.509
2-1	24.78	12395	298	69	28.0	20.49	0.611
2-2	23.35	10690	285	61	23.0	16.79	0.583
2-3	26.42	14115	279	127	45.4	17.40	0.599
2-4	23.27	9769	273	100	33.4	16.33	0.570
2-5	27.85	11873	261	102	31.2	16.85	0.577
3-1	20.24	13929	291	108	34.4	12.39	0.497
3-2	31.60	13073	221	88	16.1	10.26	0.543
3-3	26.45	11338	307	118	40.3	N/A	0.497
3-4	25.40	11768	297	107	35.0	N/A	0.496
4-1	19.42	10877	311	118	45.6	16.07	0.514
4-2	22.19	9344	252	90	22.7	13.53	0.539
4-3	30.54	14985	318	121	46.5	11.33	0.498
4-4	32.01	13201	293	126	41.9	N/A	0.553
5-1	21.52	9902	335	135	43.0	13.24	0.365
5-2	28.81	8820	253	108	21.0	12.92	0.399
5-3	24.55	9605	317	123	34.5	12.07	0.374
5-4	24.64	8105	263	100	20.3	12.71	0.387

Table 4.1. Compression test results

test	Compression strength [MPa]	Modulus of elasticity [MPa]	Sample diameter [mm]	Sample height [cm]	Sample weight [kg]	Moisture content %	Specific gravity [g/cm <sup>3</sup> ]
6-1	18.39	7411	377	132	58.3	17.72	0.444
6-2	22.45	9840	337	120	41.8	15.18	0.449
6-3	20.98	7624	313	120	35.8	15.54	0.425
6-4	23.22	8530	225	89	14.8	12.03	0.446
7-1	24.13	8023	353	120	47.3	12.60	0.417
7-2	22.89	7110	376	124	53.6	10.97	0.403
7-3	21.21	11038	330	124	43.6	13.52	0.437
7-4	25.33	8092	242	90	17.6	13.28	0.436
8-1	25.26	10041	326	120	43.2	13.56	0.442
8-2	26.76	10467	303	109	33.3	13.20	0.428
8-3	26.05	9593	292	121	34.2	12.01	0.391
8-4	23.00	9812	244	91	19.4	13.06	0.505
9-1	23.13	7430	362	129	50.5	15.37	0.394
9-2	23.71	9192	350	122	44.4	14.22	0.397
9-3	25.14	8066	289	120	31.3	13.15	0.412
9-4	27.57	10901	237	91	16.0	11.36	0.403
10-1	18.32	7731	396	147	71.3	11.94	0.396
10-2	17.52	8421	372	130	55.9	14.40	0.413
10-3	20.68	5799	346	129	48.7	12.84	0.421
10-4	25.38	9268	229	90	15.2	10.42	0.440

Table 4.1. (Continued) Compression parallel to the grain test results

pole number	Sample diameters			Ultimate measured load [kN]	Modulus of rupture [MPa]	Modulus of elasticity [MPa]
	dmin [mm]	dmax [mm]	dmidspan [mm]			
1	226	255	239	80.76	47.31	9124
2	234	251	247	138.78	79.30	12932
3	253	273	263	134.27	60.14	10560
4	255	283	271	166.43	69.67	11165
6	234	295	267	92.15	40.58	7443
8	255	287	271	93.71	38.37	7200

Table 4.2. Bending test results

pole	sample	Sample height [mm]	Sample width [mm]	Ultimate measured load [kN]	Ultimate tension stress [MPa]
5	1	16.5	11.2	10.28	55.69
	2	15.6	11.2	9.88	56.47
	3	17.2	10.8	9.45	50.85
	4	17.1	10.8	8.38	45.30
	5	15.9	10.8	9.30	54.25
	6	17.3	11.4	11.57	58.58
	7	17.8	10.9	12.34	63.56
	8	17.8	11.3	9.65	48.25
	9	17.8	11.2	10.32	51.93
	10	17.1	11.2	9.39	48.98
6	1	17.7	11.9	5.74	27.35
	2	18.0	11.5	4.74	22.88
	3	18.2	11.4	8.32	40.25
	4	18.8	11.5	9.30	43.14
	5	17.3	11.4	4.78	24.22
	6	17.1	11.6	6.85	34.57
	7	18.7	11.6	4.89	22.55
	8	17.0	11.8	9.43	46.92
	9	17.5	11.8	12.30	59.42
	10	17.8	11.8	6.18	29.44
	11	15.7	10.9	7.83	45.52
	12	16.8	10.2	8.76	51.45
	13	17.9	11.0	6.25	31.68
	14	15.9	11.3	4.23	23.55
	15	16.8	11.2	10.72	56.96
	16	17.8	10.9	6.23	32.07
	17	17.1	11.3	8.63	44.53
	18	17.0	10.8	8.94	48.44
	19	15.9	11.0	7.18	41.08
	20	16.8	10.7	7.52	42.04

Table 4.3. Tension test results

pole	sample	Sample height [mm]	Sample width [mm]	Ultimate measured load [kN]	Ultimate tension stress [MPa]
7	1	15.5	11.8	11.90	65.30
	2	16.6	11.1	12.41	67.41
	3	16.4	11.4	9.79	52.26
	4	16.6	11.3	10.99	58.43
	5	17.7	11.3	9.85	49.38
	6	14.5	11.5	10.59	63.55
	7	16.6	11.4	10.56	55.81
	8	18.5	11.7	9.88	45.58
	9	15.6	11.2	7.78	44.52
	10	18.4	11.2	8.14	39.55
8	1	17.8	11.3	4.45	22.12
	2	18.3	11.7	4.72	22.05
	3	17.0	11.5	6.67	34.15
	4	18.9	11.4	5.12	23.73
	5	16.8	11.8	11.68	58.97
	6	16.7	12.7	11.43	54.02
	7	16.6	12.6	11.70	55.92
	8	16.8	10.7	10.39	57.90
	9	18.6	10.7	10.36	52.18
	10	17.3	10.8	12.50	67.20
	11	15.7	10.8	10.12	59.39
	12	16.6	10.7	8.90	50.13
	13	17.7	10.7	10.23	54.17
	14	18.2	10.8	11.68	59.56
	15	17.5	10.7	11.74	62.81
	16	17.7	10.4	9.96	54.20
	17	17.3	10.5	9.83	54.00

Table 4.3. (Continued) Tension test results

pole	sample	Sample height [mm]	Sample width [mm]	Ultimate measured load [kN]	Ultimate tension stress [MPa]
9	1	19.8	12.0	10.23	43.07
	2	18.3	11.6	12.81	60.35
	3	18.7	11.9	12.46	56.00
	4	18.3	12.0	14.97	68.18
	5	17.1	11.7	14.19	70.84
	6	20.4	11.8	15.57	64.63
	7	19.5	11.5	14.06	62.98
	8	19.8	11.6	15.03	65.75
	9	19.6	11.6	16.41	72.34
	10	19.0	11.7	14.15	63.36
10	1	16.6	11.8	9.79	49.85
	2	16.1	12.1	9.16	47.14
	3	15.5	11.8	8.50	46.33
	4	17.8	11.8	10.63	50.52
	5	15.7	12.0	8.18	43.51
	6	17.6	11.9	8.81	41.97
	7	17.8	12.1	6.92	32.24
	8	18.2	12.1	8.27	37.52
	9	15.4	11.9	5.87	32.11

Table 4.3. (Continued) Tension test results

pole	test	Measured initial out-of-straightness			Ultimate measured deflection			Ultimate measured load [kN]
		e1 [mm]	e2 [mm]	e3 [mm]	e1 [mm]	e2 [mm]	e3 [mm]	
1	1	36	29	-14	175	194	86	133
1	2	32	35	14	155	185	111	149
1	3	30	41	22	149	192	120	188
1	4	17	34	18	107	138	69	264
1	5	-12	-19	-15	-62	-83	-56	312
2	1	38	36	8	176	208	126	185
		9	30	32	118	176	137	205
2	2	18	20	12	115	144	92	245
2	3	14	41	27	105	163	108	289
2	4	11	24	3	129	172	105	405
2	5	5	14	12	76	109	77	558
3	1	55	0	-24	182	140	56	162
3	2	53	23	-9	176	164	75	176
3	3	48	29	0	175	178	92	205
3	4	41	35	-4	162	181	87	251
3	5	27	37	22	118	156	98	312
4	1	35	51	43	157	208	145	177
4	2	21	34	24	157	210	140	233
4	3	15	13	14	83	108	77	293
4	4	12	12	8	104	136	93	346
4	5	2	12	8	77	115	78	462
5	1	-31	-33	-4	-168	-187	-106	168
5	2	-46	-52	-38	-185	-216	-139	182
5	3	-44	-53	-42	-184	-213	-151	216
5	4	-49	-52	-48	-170	-198	-138	255
5	5	-43	-43	-29	-126	-148	-94	302
5	6	-30	-33	-34	-132	-164	-116	506
6	1	30	-12	-15	141	98	47	163
6	2	85	133	74	170	226	128	100
6	3	60	105	77	171	231	154	140
6	4	0	-18	-36	-118	-153	-119	242
6	5	9	5	-11	96	104	47	287
6	6	9	13	6	82	97	59	338

Table 4.4. Pole deflections and ultimate load

pole	test	Measured initial out-of-straightness			Ultimate measured deflection			Ultimate measured load [kN]
		e1 [mm]	e2 [mm]	e3 [mm]	e1 [mm]	e2 [mm]	e3 [mm]	
7	1	32	20	7	160	157	89	197
7	2	19	2	3	139	131	81	239
7	3	31	60	29	145	189	107	215
7	4	25	39	36	159	193	132	266
7	5	15	19	24	122	145	104	338
7	6	14	4	14	91	99	75	445
7	7	-7	-9	2	-58	-87	-64	567
8	1	2	-36	-73	-103	-169	-161	140
8	2	3	-20	-76	-149	-207	-201	162
8	3	14	6	-39	-106	-176	-139	205
8	4	-29	-10	16	-143	-147	-69	202
8	5	-31	-20	4	-135	-147	-78	234
8	6	-25	-27	-6	-115	-141	-81	294
9	1	79	37	36	185	149	102	123
9	2	60	17	23	179	140	96	151
9	3	32	-5	-10	150	114	60	203
9	4	21	9	-26	-67	-93	-92	235
9	5	17	15	-25	11	3	-38	318
9	6	14	17	-10	69	79	25	327
9	7	15	20	21	123	144	99	338
9	8	0	-20	-16	-80	-117	-76	435
10	1	117	76	39	306	284	151	107
10	2	106	80	35	271	254	138	125
10	3	31	59	42	190	242	148	160
10	4	31	73	46	211	275	171	195
10	5	16	41	32	144	189	124	203
10	6	-4	4	8	-83	-77	-39	308
10	7	-15	-16	-2	-123	-151	-84	329
10	8	-18	-37	-26	-129	-169	-106	381

Table 4.4. (Continued) Pole deflections and ultimate load

pole	test	Measured values			Nominal values		
		length [m]	de [mm]	l/de	length [m]	de [mm]	l/de
1	1	11.951	275	43.9	12.192	250	48.7
1	2	10.455	261	40.5	10.668	243	43.9
1	3	9.080	254	36.1	9.144	234	39.1
1	4	7.620	247	31.3	7.620	225	33.9
1	5	6.090	243	25.5	6.096	215	28.4
2	1	12.014	269	45.1	12.192	230	53.1
2	2	10.497	265	40.1	10.668	223	47.9
2	3	9.154	259	35.8	9.144	214	42.6
2	4	7.604	256	30.2	7.620	205	37.2
2	5	6.096	253	24.6	6.096	196	31.2
3	1	13.719	272	50.9	13.716	237	57.9
3	2	12.189	267	46.1	12.192	230	53.1
3	3	10.655	264	40.7	10.668	223	47.9
3	4	9.144	257	36.0	9.144	214	42.6
3	5	7.618	254	30.4	7.620	205	37.2
4	1	13.691	294	47.0	13.716	257	53.3
4	2	12.192	289	42.5	12.192	250	48.7
4	3	10.662	283	38.1	10.668	243	43.9
4	4	9.141	278	33.3	9.144	234	39.1
4	5	7.601	271	28.4	7.620	225	33.9
5	1	13.646	326	42.2	13.716	289	47.4
5	2	12.116	309	39.6	12.192	282	43.2
5	3	10.662	300	36.0	10.668	273	39.0
5	4	9.084	290	31.7	9.144	264	34.6
5	5	7.626	281	27.5	7.620	254	30.0
5	6	6.448	286	22.5	6.096	261	23.4
6	1	15.081	351	43.3	15.240	296	51.5
6	2	14.005	341	41.4	13.716	289	47.4
6	3	12.205	325	37.2	12.192	282	43.2
6	4	10.674	310	34.8	10.668	273	39.0
6	5	9.157	295	31.4	9.144	264	34.6
6	6	7.639	279	27.8	7.620	254	30.0

Table 4.5. Measured and nominal pole dimensions

pole	test	Measured values			Nominal values		
		length [m]	de [mm]	l/de	length [m]	de [mm]	l/de
7	1	15.278	339	45.4	15.240	296	51.5
7	2	13.738	328	42.3	13.716	289	47.4
7	3	12.119	320	38.2	12.192	282	43.2
7	4	10.668	309	34.9	10.668	273	39.0
7	5	9.144	299	30.9	9.144	264	34.6
7	6	7.616	294	26.2	7.620	254	30.0
7	7	6.084	281	21.6	6.096	242	25.1
8	1	15.151	311	49.0	15.240	296	51.5
8	2	13.716	308	44.9	13.716	289	47.4
8	3	12.182	299	41.1	12.192	282	43.2
8	4	10.658	291	37.0	10.668	273	39.0
8	5	9.141	287	32.2	9.144	264	34.6
8	6	7.618	272	28.4	7.620	254	30.0
9	1	18.123	339	53.8	18.288	330	55.4
9	2	16.758	335	50.4	16.764	324	51.7
9	3	15.237	322	47.6	15.240	317	48.0
9	4	13.716	319	43.3	13.716	311	44.2
9	5	12.186	311	39.5	12.192	302	40.3
9	6	10.668	305	35.3	10.668	294	36.3
9	7	9.138	292	31.6	9.144	284	32.2
9	8	7.620	286	26.7	7.620	261	29.2
10	1	18.113	351	51.9	18.288	330	55.4
10	2	16.748	342	49.2	16.764	324	51.7
10	3	15.227	331	46.4	15.240	317	48.0
10	4	13.710	323	42.8	13.716	311	44.2
10	5	12.179	313	39.3	12.192	302	40.3
10	6	10.668	306	35.2	10.668	294	36.3
10	7	9.138	296	31.2	9.144	284	32.2
10	8	7.617	284	26.8	7.620	261	29.2

Table 4.5. (Continued) Measured and nominal pole dimensions

pole	test	Moisture content %	Specific gravity [g/cm <sup>3</sup> ]
1	1	16.45	0.503
1	2	18.66	0.519
1	3	16.38	0.463
1	4	16.15	0.475
1	5	14.50	0.509
2	1	20.49	0.611
2	2	16.79	0.583
2	3	17.40	0.599
2	4	16.33	0.570
2	5	16.85	0.577
3	1	14.16	0.505
3	2	14.00	0.494
3	3	13.74	0.471
3	4	12.39	0.497
3	5	10.26	0.543
4	1	20.82	0.533
4	2	19.57	0.519
4	3	18.52	0.538
4	4	16.07	0.514
4	5	13.53	0.539
5	1	16.03	0.421
5	2	14.30	0.381
5	3	14.46	0.375
5	4	13.24	0.365
5	5	12.92	0.399
5	6	12.39	0.380
6	1	N/A	0.501
6	2	N/A	0.496
6	3	N/A	0.456
6	4	N/A	0.449
6	5	N/A	0.460
6	6	9.18	0.409
7	1	10.15	0.423
7	2	10.81	0.390
7	3	10.21	0.414
7	4	8.89	0.396
7	5	10.29	0.458
7	6	9.72	0.444
7	7	13.40	0.436
8	1	N/A	N/A
8	2	12.64	0.456
8	3	9.96	0.437
8	4	10.39	0.427
8	5	10.46	0.435
8	6	7.79	0.421
9	1	17.68	0.389
9	2	15.72	0.406
9	3	8.08	0.399
9	4	16.27	0.382
9	5	11.26	0.383
9	6	9.56	0.389
9	7	7.60	0.378
9	8	12.97	0.406
10	1	13.85	0.468
10	2	18.17	0.461
10	3	16.66	0.401
10	4	15.35	0.413
10	5	14.71	0.483
10	6	10.92	0.401
10	7	9.46	0.406
10	8	11.63	0.431

Table 4.6. Moisture content and specific gravity of the tested poles

pole	Compression strength [MPa]	Bending strength [MPa]	Modulus of elasticity [MPa]	CAN/CSA-O86.1-M89	CAN3-O15-M83	OHBDC-83
1	16.24	47.31	8695	Fc = 7.60 MPa Fb = 10.88 MPa mean E = 8 500 MPa E = 6 000 MPa	Classification stress 45 MPa  E = N/A	Fc = 19 MPa Fb = 19 MPa  E = 5 500 MPa
2	25.13	79.30	11768			
3	25.92	60.14	12060			
4	26.04	69.67	12101			
5	24.88	39.69*	9108	Fc = 5.76 MPa Fb = 10.24 MPa mean E = 8 000 MPa E = 5 500 MPa	Classification stress 38 MPa  E = 7 700 MPa	Fc = 18 MPa Fb = 18 MPa  E = 5 000 MPa
6	21.26	40.58	8351			
7	23.39	40.17*	8566			
8	25.27	38.37	9978			
9	23.13	44.19*	8897			
10	20.47	34.11*	7805			

\* Note: Bending strength for these poles was evaluated based on tension and compression test results

Table 4.7. Material properties

pole	Coefficient c
1	0.80
2	0.93
3	0.80
4	0.84
5	0.85
6	0.85
7	0.96
8	0.85
9	0.94
10	0.85

Table 5.1. Coefficient c

pole test		Deflection due to self-weight			Measured initial out-of-straightness			Pole's out-of-straightness		
		point 1	point 2	point 3	point 1	point 2	point 3	point 1	point 2	point 3
1	1	26	34	22	36	29	-14	10	-5	-36
	2	16	21	14	32	35	14	16	14	-0
	3	9	12	8	30	41	22	21	29	14
	4	5	6	4	17	34	18	12	28	14
	5	2	3	2	-12	-19	-15	-14	-22	-17
2	1	23	31	21	9	30	32	-14	-1	11
	2	14	19	13	18	20	12	4	1	-1
	3	8	11	8	14	41	27	6	30	19
	4	4	6	4	11	24	3	7	18	-1
	5	2	2	2	5	14	12	3	12	10
3	1	31	40	26	55	0	-24	24	-40	-50
	2	20	26	18	53	23	-9	33	-3	-27
	3	12	15	10	48	29	0	36	14	-10
	4	7	9	6	41	35	-4	34	26	-10
	5	3	5	3	27	37	22	24	32	19
4	1	29	37	25	35	51	43	6	14	18
	2	19	24	16	21	34	24	2	10	8
	3	11	15	10	15	13	14	4	-2	4
	4	6	8	6	12	12	8	6	4	2
	5	3	4	3	2	12	8	-1	8	5
5	1	26	33	21	-31	-33	-4	-57	-66	-25
	2	17	21	14	-46	-52	-38	-63	-73	-52
	3	10	13	9	-44	-53	-42	-54	-66	-51
	4	6	7	5	-49	-52	-48	-55	-59	-53
	5	3	4	3	-43	-43	-29	-46	-47	-32
	6	1	2	1	-28	-33	-34	-29	-35	-35
6	1	50	57	34	30	-12	-15	-20	-69	-49
	2	38	44	27	85	133	74	47	89	47
	3	23	28	17	60	105	77	37	77	60
	4	14	17	11	0	-18	-36	-14	-35	-47
	5	8	10	6	9	5	-11	1	-5	-17
	6	4	5	3	9	13	6	5	8	3

Table 5.2. Pole's out-of-straightness

pole	test	Deflection due to self-weight			Measured initial out-of-straightness			Pole's out-of-straightness		
		point 1	point 2	point 3	point 1	point 2	point 3	point 1	point 2	point 3
7	1	40	47	30	32	20	7	-8	-27	-23
	2	27	32	21	19	2	3	-8	-30	-18
	3	17	21	13	31	60	29	14	39	16
	4	11	13	9	25	39	36	14	26	27
	5	6	8	5	15	19	24	9	11	19
	6	3	4	3	14	4	14	11	-0	11
	7	1	2	1	-7	-9	2	-8	-11	1
8	1	41	52	33	2	-36	-73	-39	-88	-106
	2	29	36	23	3	-20	-76	-26	-56	-99
	3	19	24	15	14	6	-39	-5	-18	-54
	4	11	14	10	-29	-10	16	-40	-24	6
	5	6	8	5	-31	-20	4	-37	-28	-1
	6	3	4	3	-25	-27	-6	-28	-31	-9
9	1	66	79	49	79	37	36	13	-42	-13
	2	51	60	38	60	17	23	9	-43	-15
	3	36	43	27	32	-5	-10	-4	-48	-37
	4	25	29	19	21	9	-26	-4	-20	-45
	5	16	19	12	17	15	-25	1	-4	-37
	6	10	12	8	14	17	-10	4	5	-18
	7	6	7	5	15	20	21	9	13	16
	8	3	4	2	0	-20	-16	-3	-24	-18
10	1	88	101	62	117	76	39	29	-25	-23
	2	66	77	48	106	80	35	40	3	-13
	3	47	55	35	31	59	42	-16	4	7
	4	33	39	24	31	73	46	-2	34	22
	5	22	26	16	16	41	32	-6	15	16
	6	14	16	10	-4	4	8	-18	-12	-2
	7	8	9	6	-15	-16	-2	-23	-25	-8
	8	4	5	3	-18	-37	-26	-22	-42	-29

Table 5.2. (Continued) Pole's out-of-straightness

# FIGURES

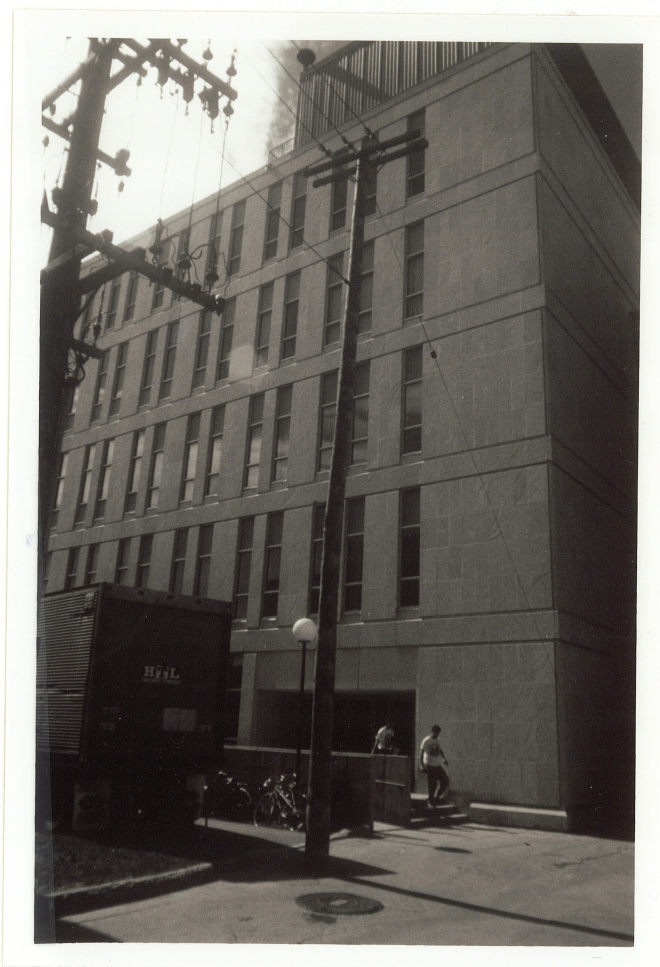


Figure 1.1. Wooden pole in service

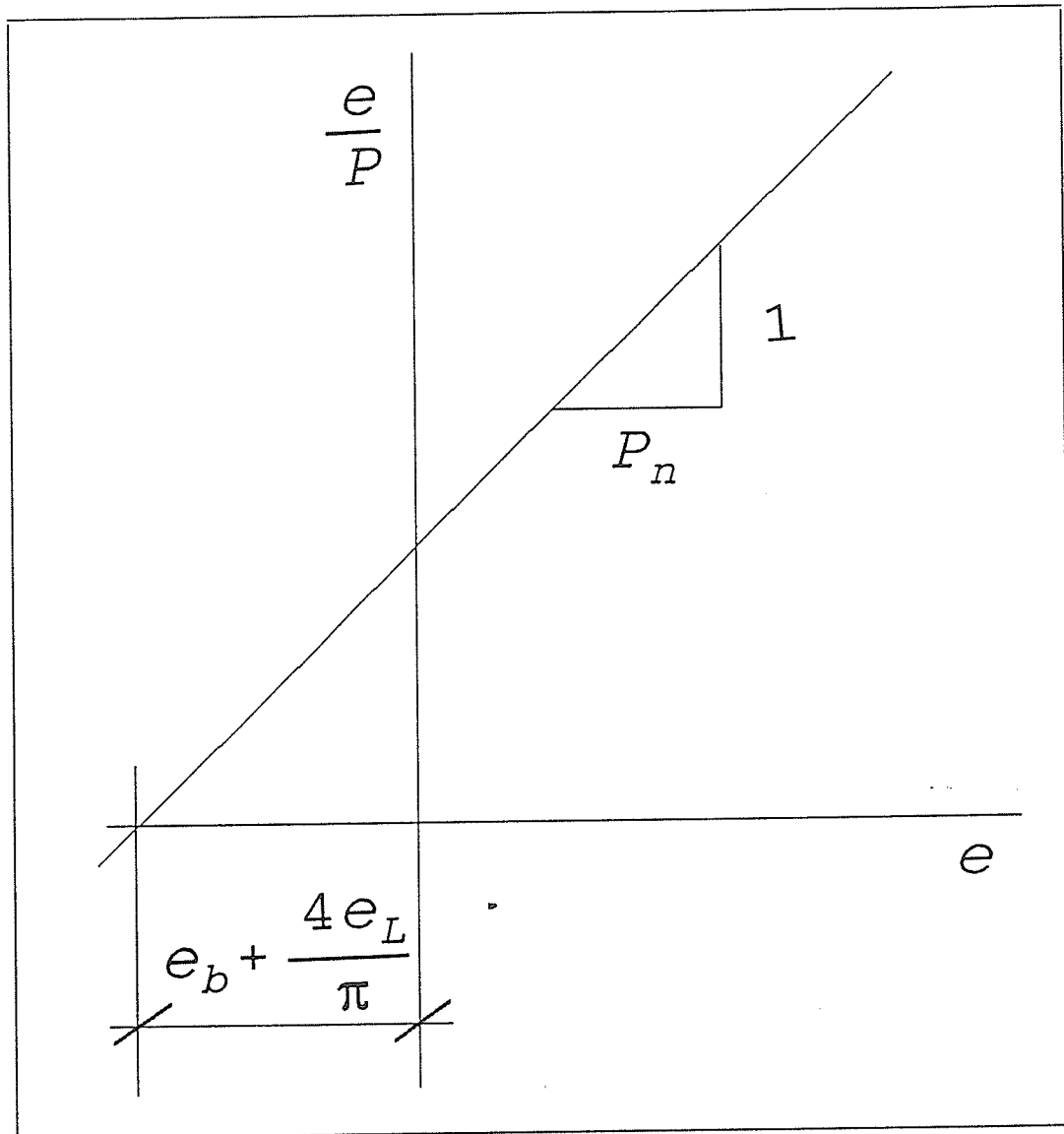
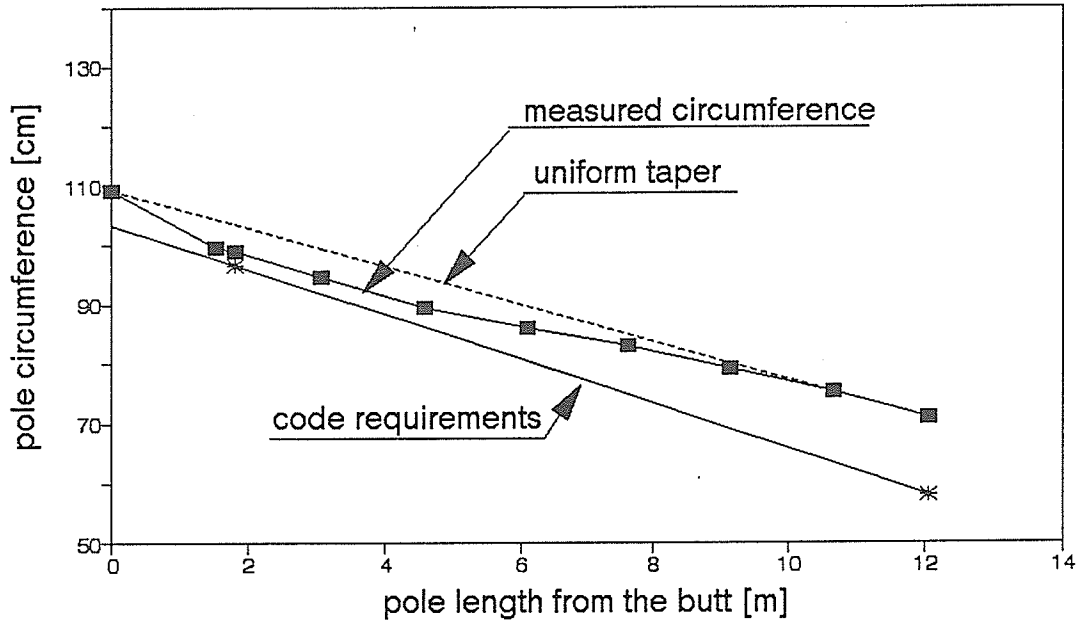


Figure 2.1. Southwell plot

## POLE #1 LODGEPOLE PINE CLASS 3/40 ft



## POLE #2 LODGEPOLE PINE CLASS 4/40 ft

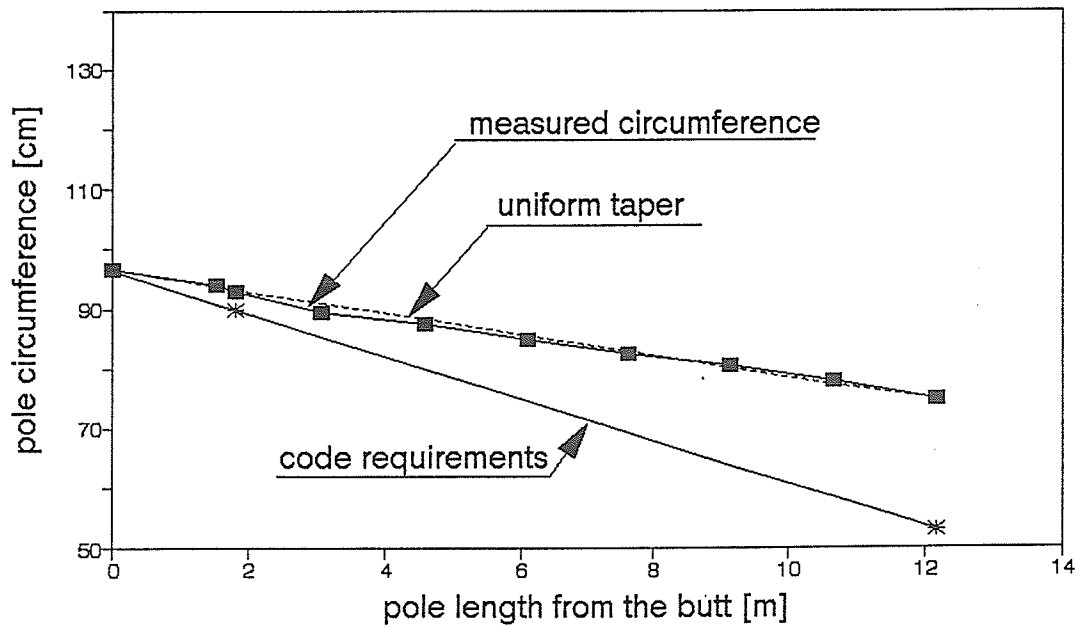
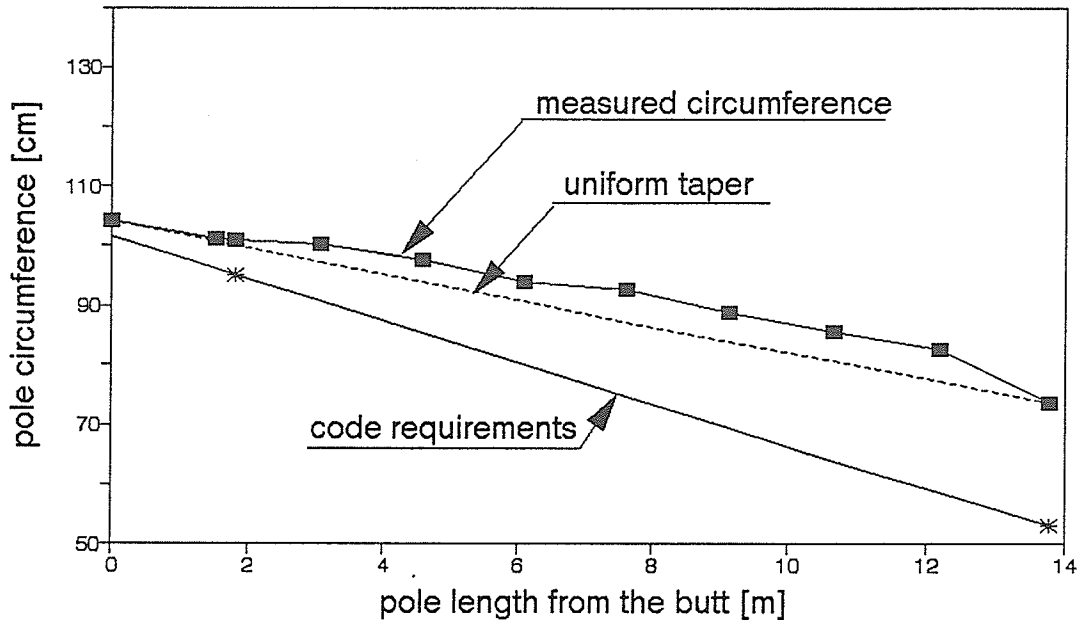


Figure 3.1. Pole circumference compared to Code requirements

## POLE #3 LODGEPOLE PINE CLASS 4/45 ft



## POLE #4 LODGEPOLE PINE CLASS 3/45 ft

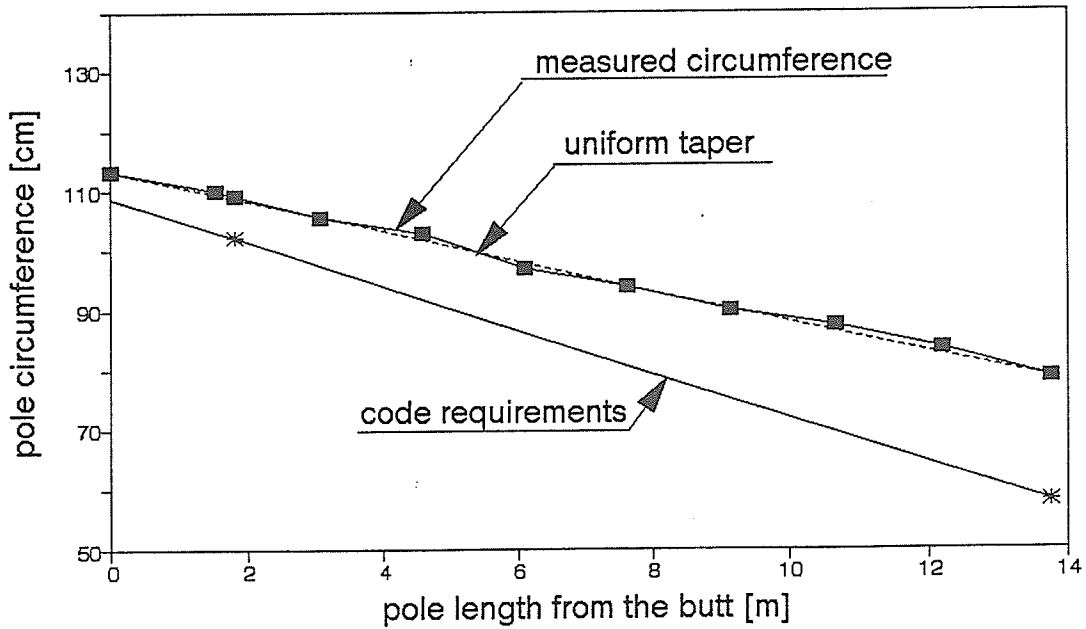
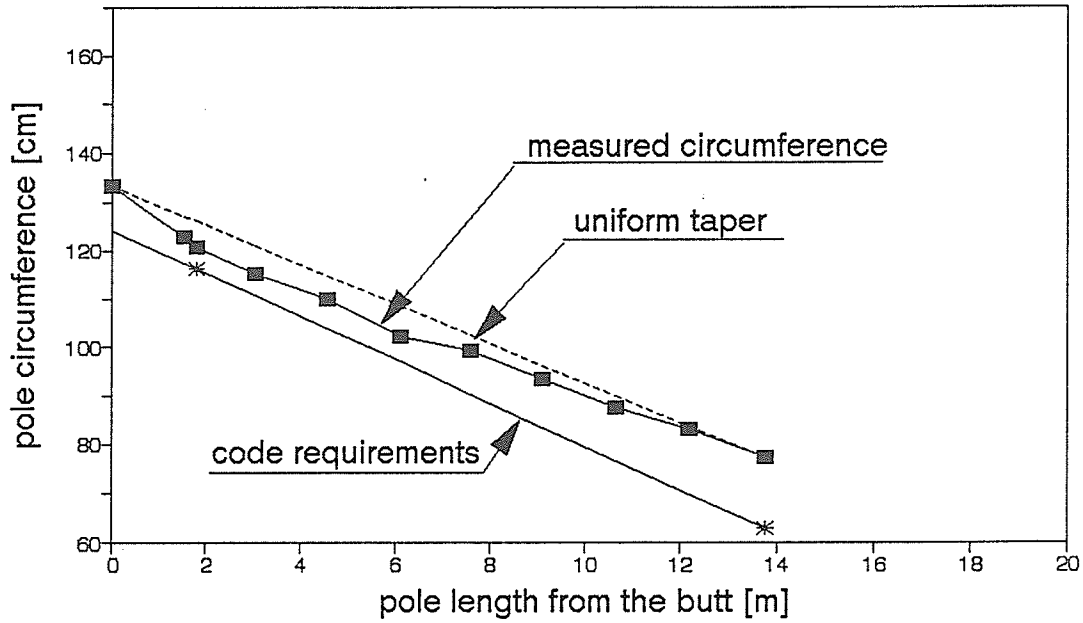


Figure 3.2. Pole circumference compared to Code requirements

## POLE #5 WESTERN RED CEDAR CLASS 2/45 ft



## POLE #6 WESTERN RED CEDAR CLASS 2/50 ft

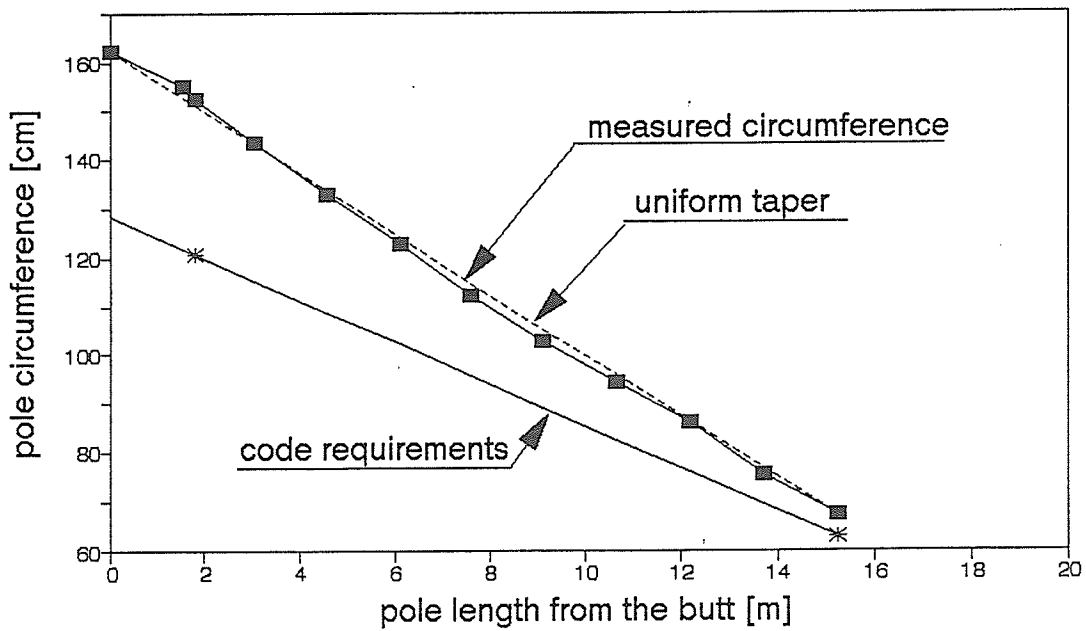
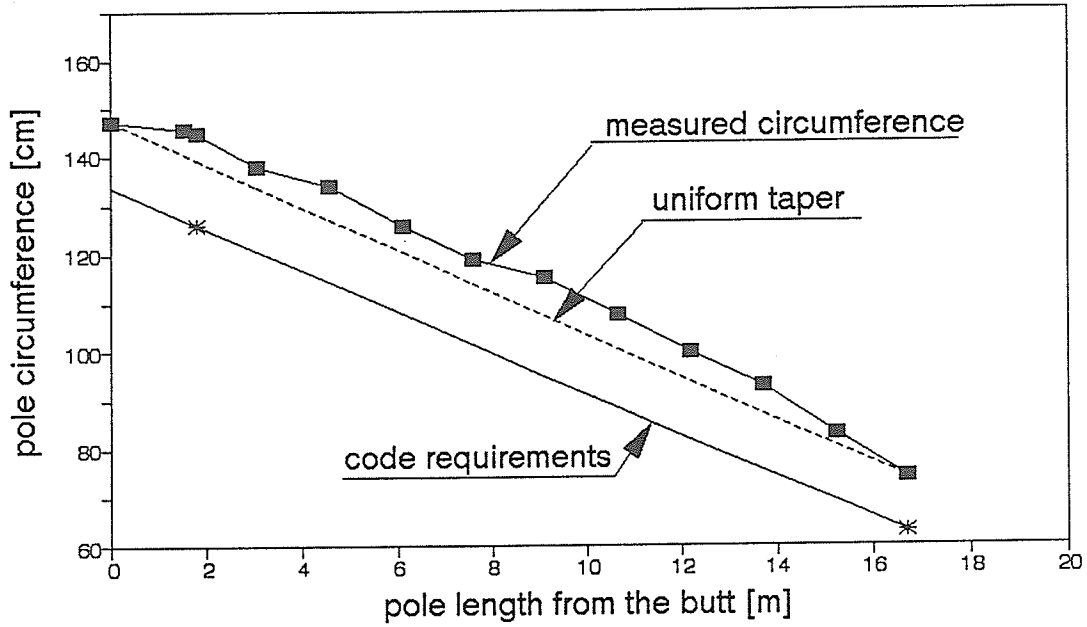


Figure 3.3. Pole circumference compared to Code requirements

# POLE #7 WESTERN RED CEDAR CLASS 2/55 ft



# POLE #8 WESTERN RED CEDAR CLASS 2/50 ft

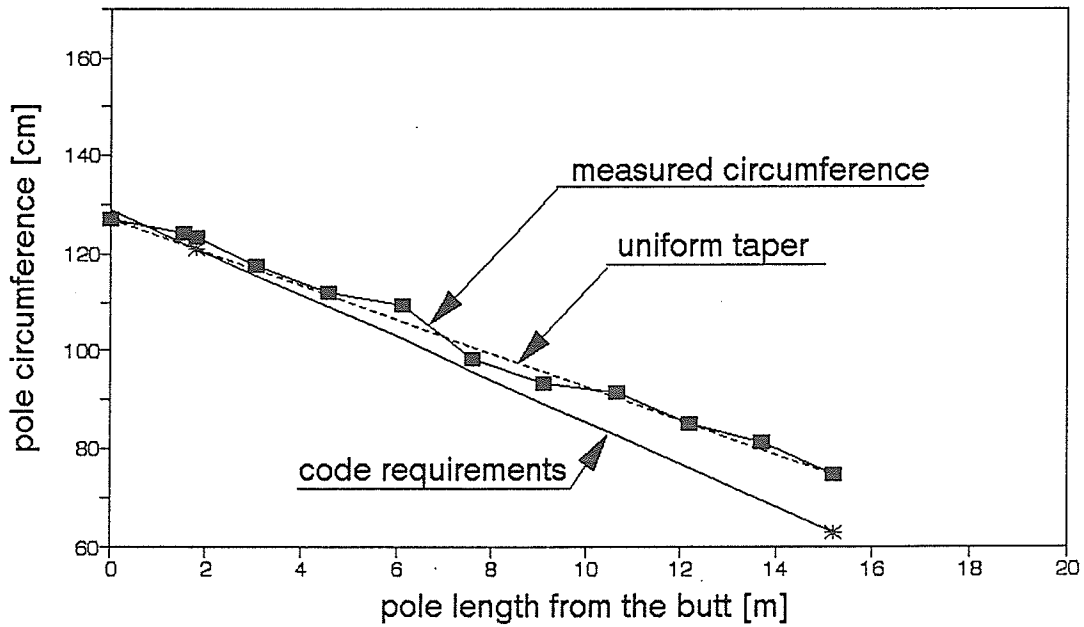
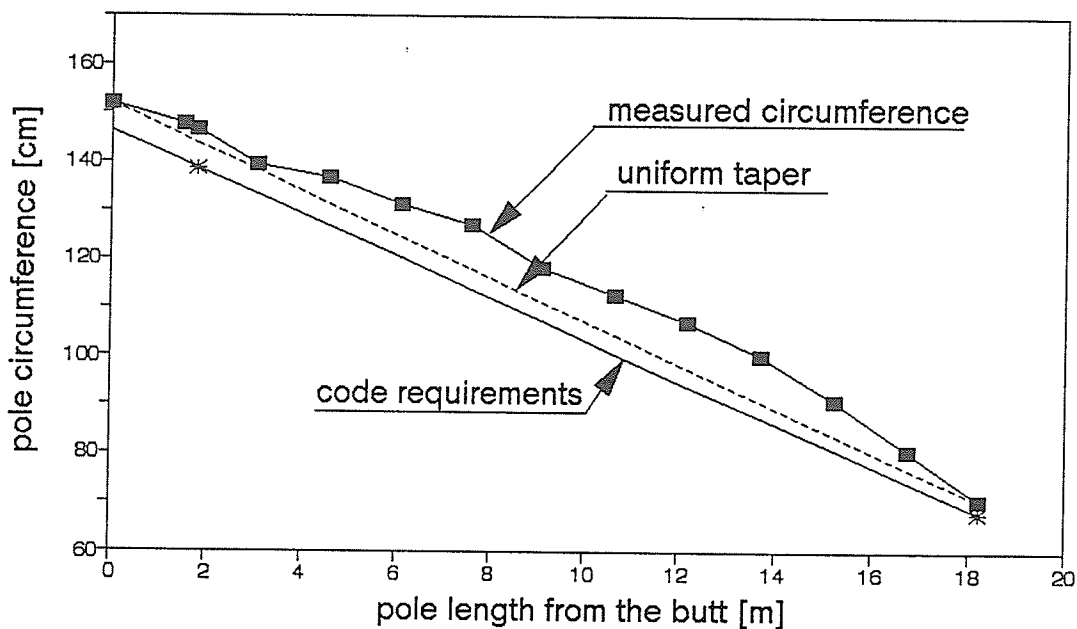


Figure 3.4. Pole circumference compared to Code requirements

## POLE #9 WESTERN RED CEDAR CLASS 1/60 ft



## POLE #10 WESTERN RED CEDAR CLASS 1/60 ft

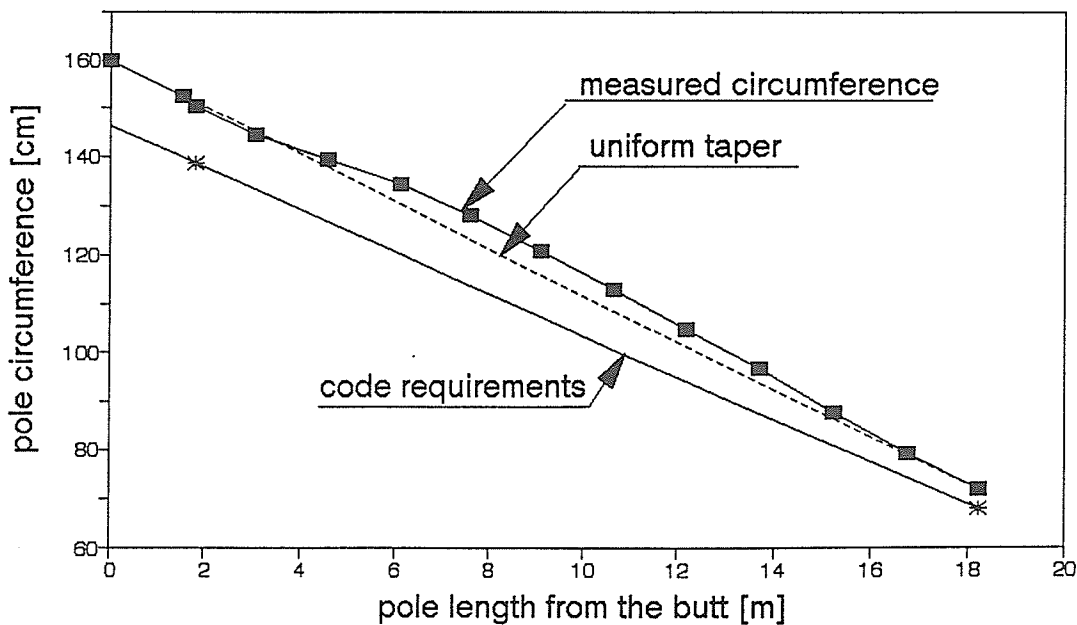


Figure 3.5. Pole circumference compared to Code requirements

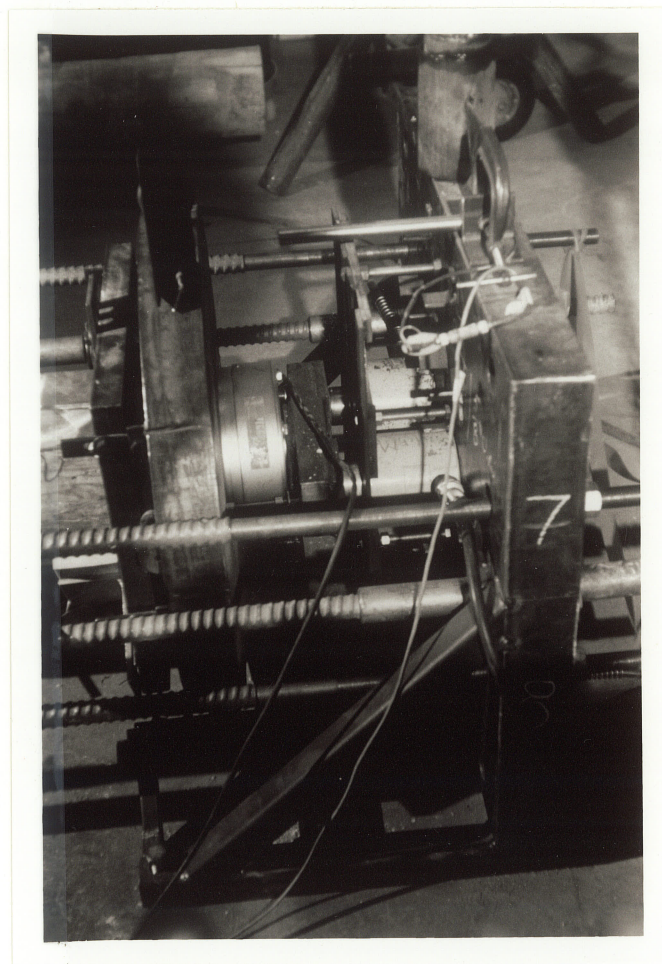


Figure 3.6. End support, equipped with hydraulic jacks to apply the load

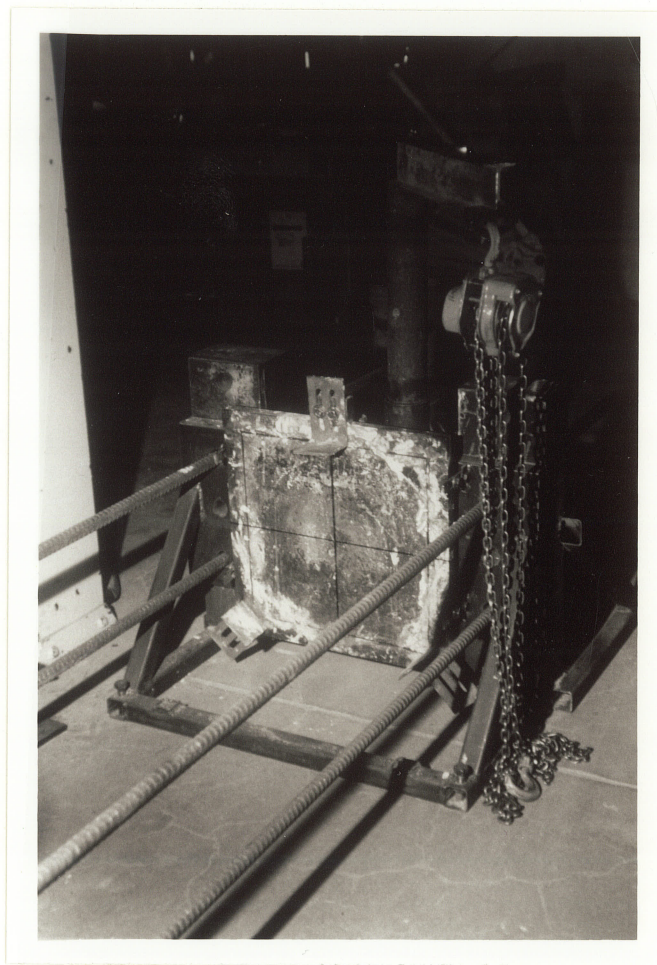


Figure 3.7. End support



Figure 3.8. Test set-up



Figure 3.9. Set of rulers for deflection measuring

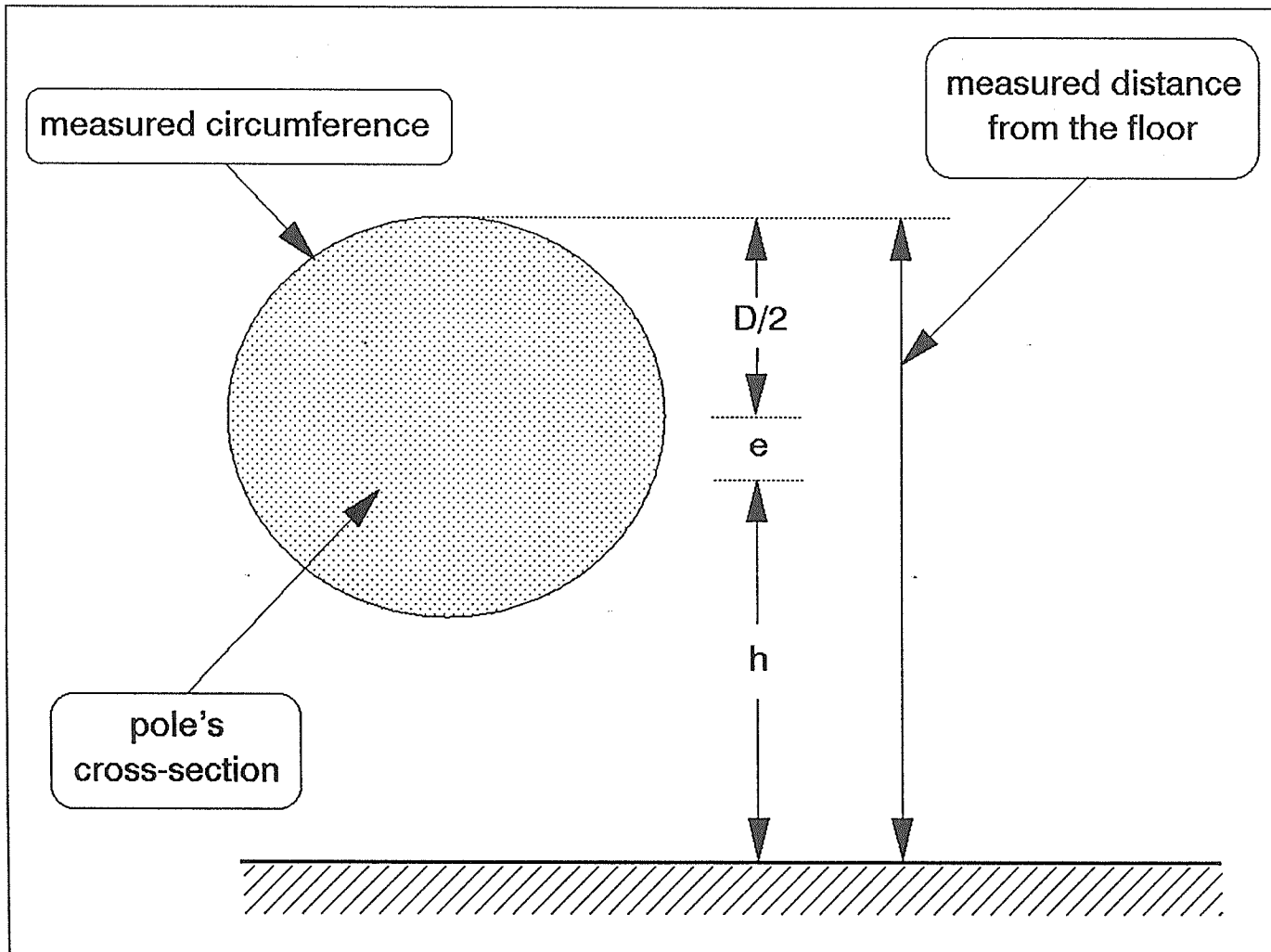


Figure 3.10. Initial out-of-straightness measuring

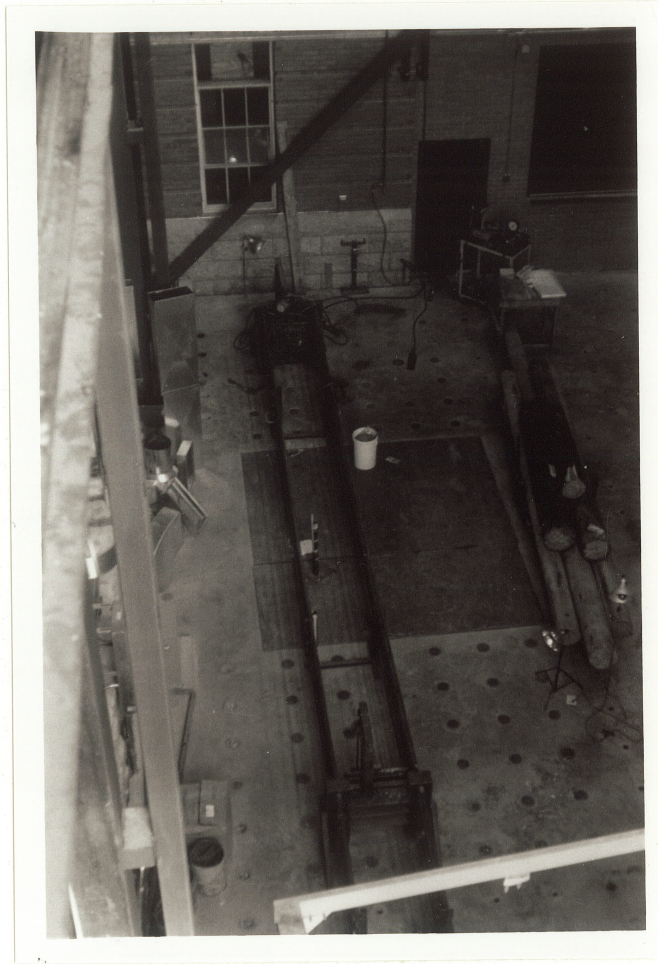


Figure 3.11. Modified testing frame

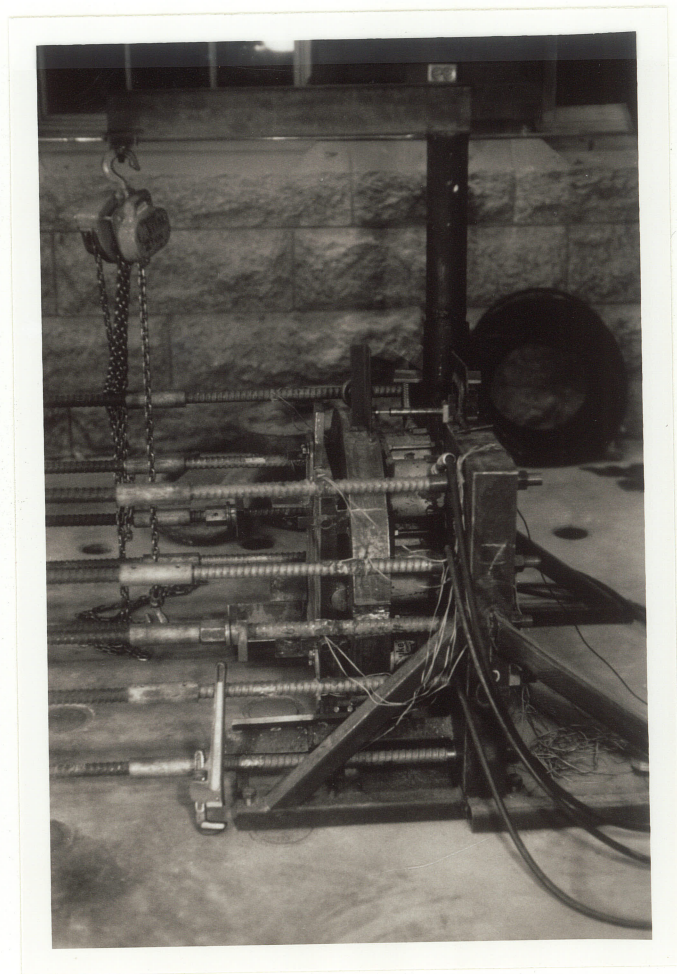
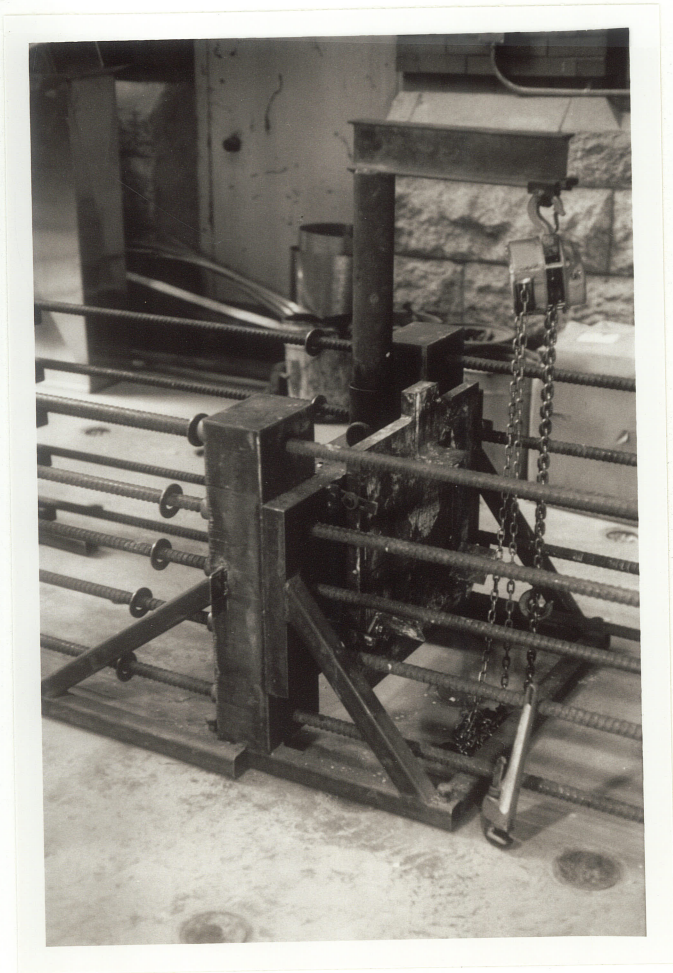


Figure 3.12. End fittings of the modified testing frame

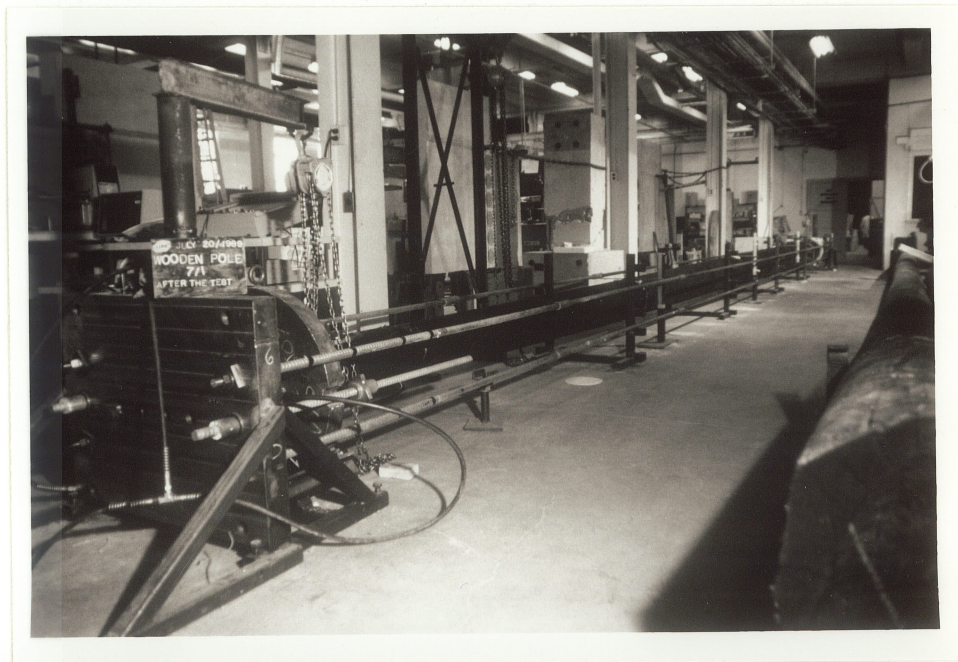
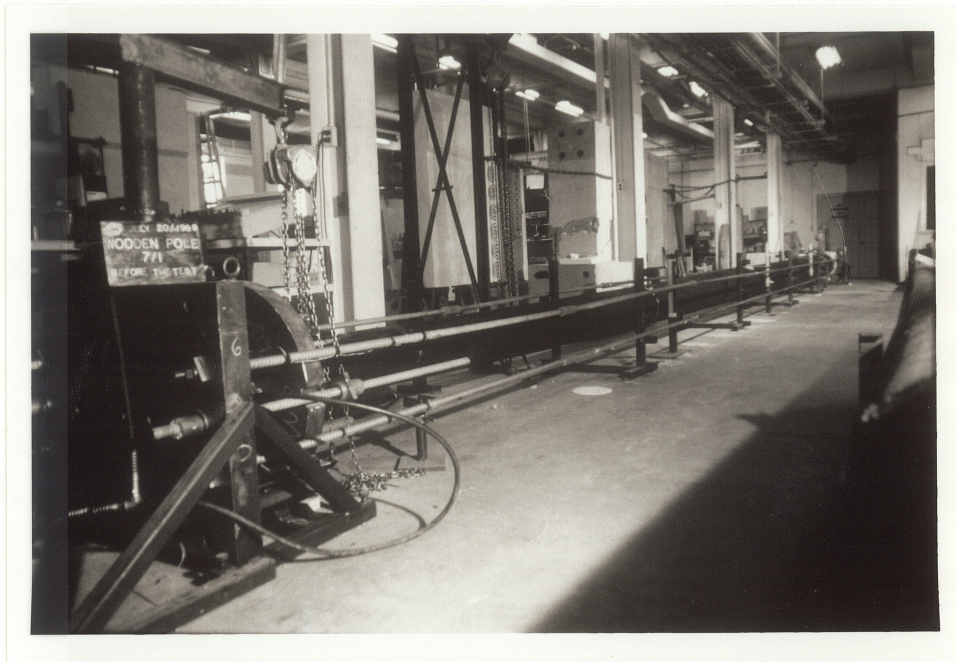


Figure 3.13. Test specimen before and after the test

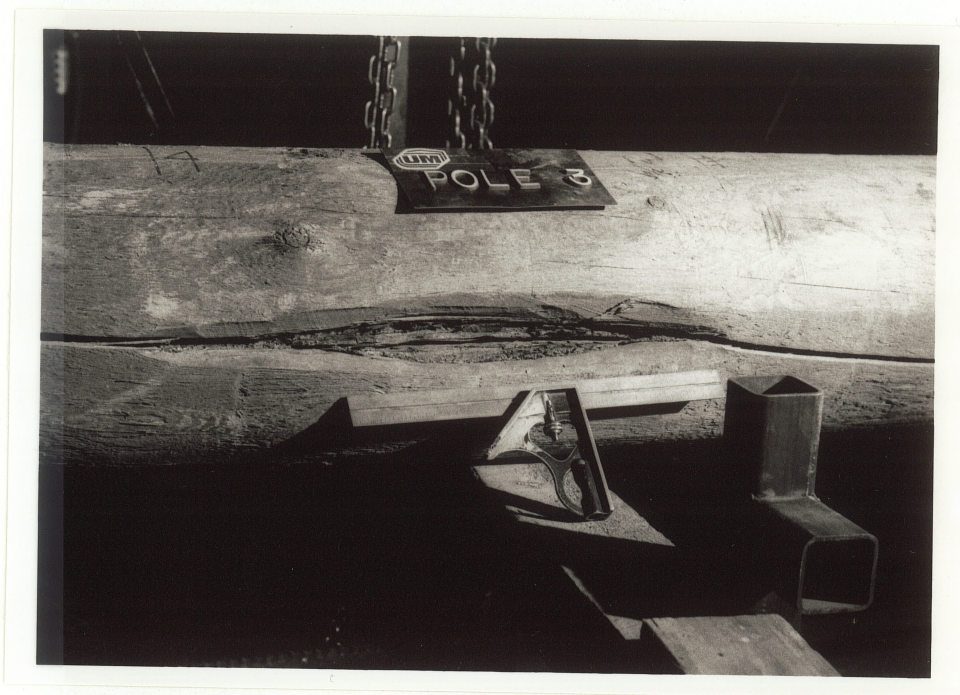


Figure 3.14. Two scars of the pole #3

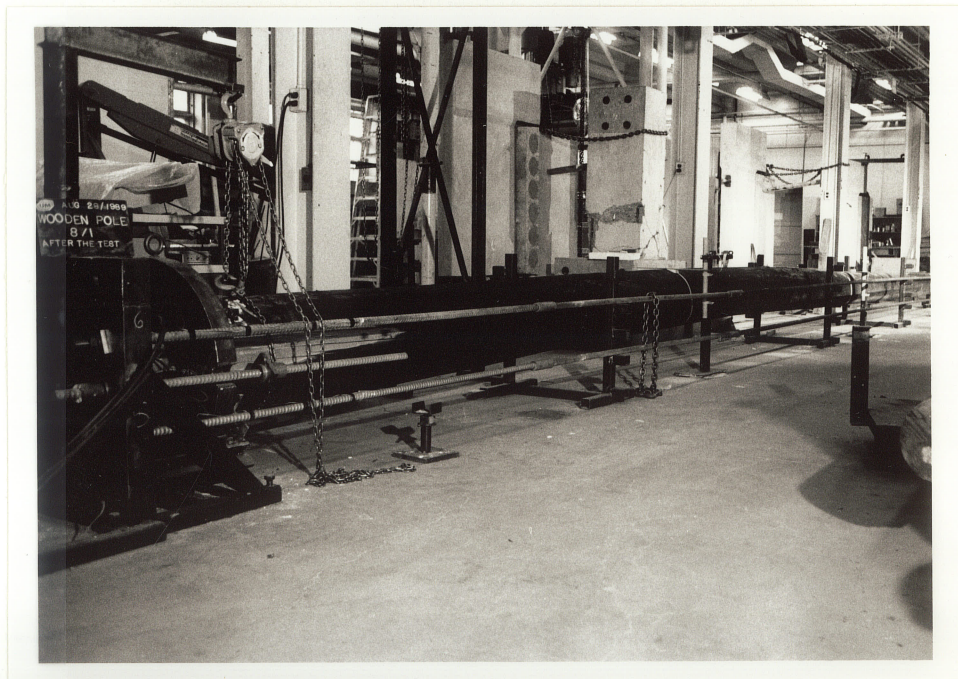


Figure 3.15. Pole #8

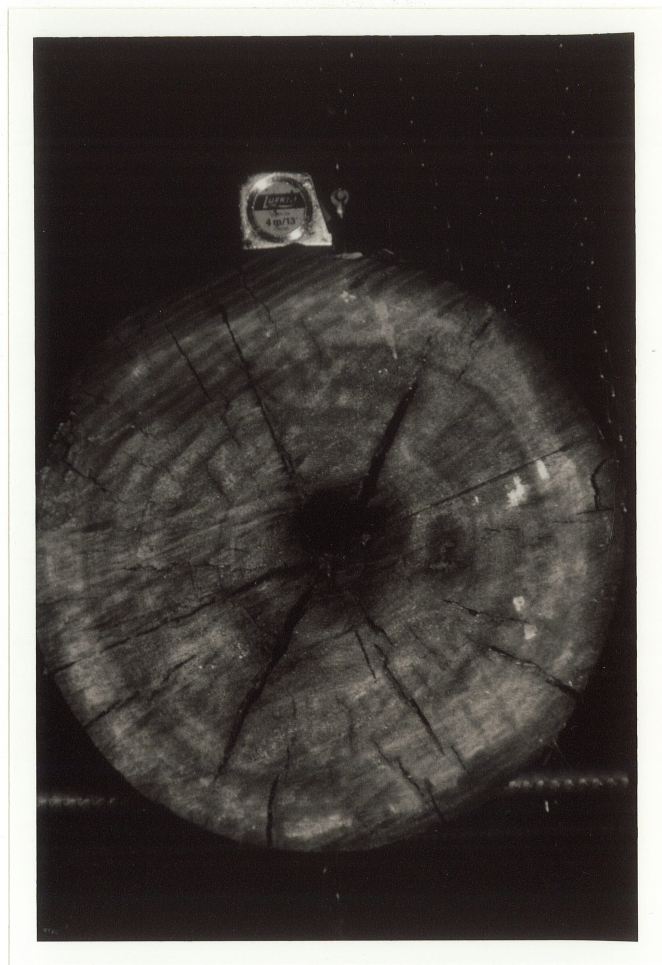


Figure 3.16. Hollow hart of the pole #9



Figure 3.17. Split near the butt of the pole #9

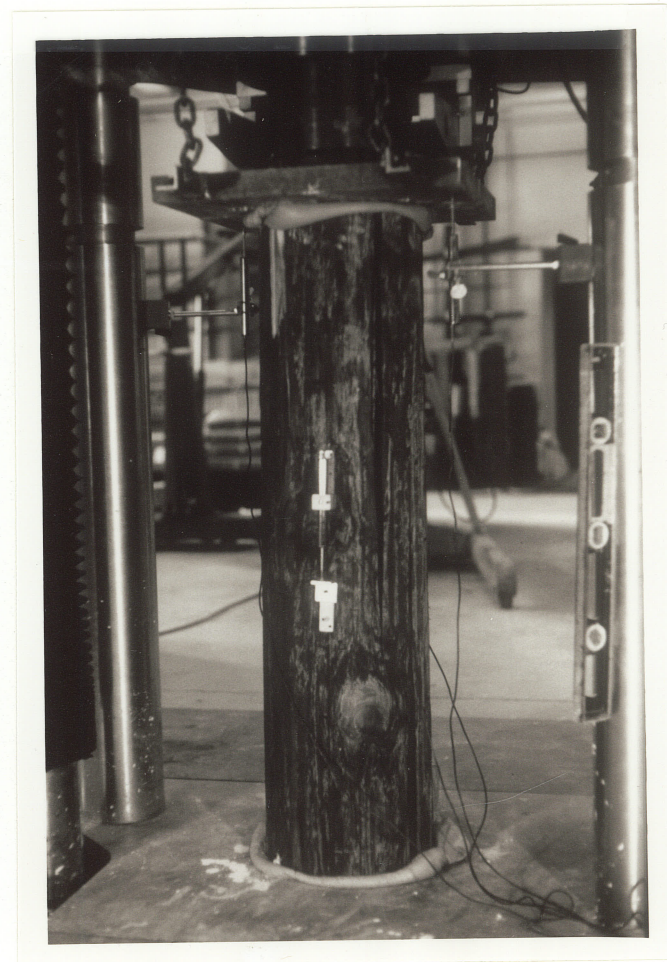
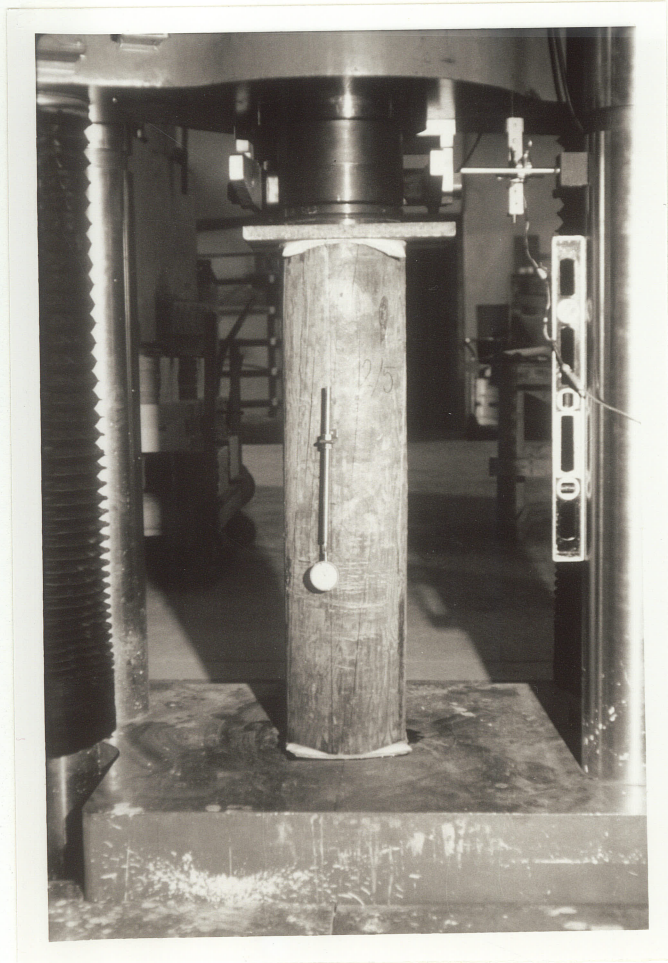


Figure 3.18. Compression parallel to the grain test setup



Figure 3.19. Bending test setup

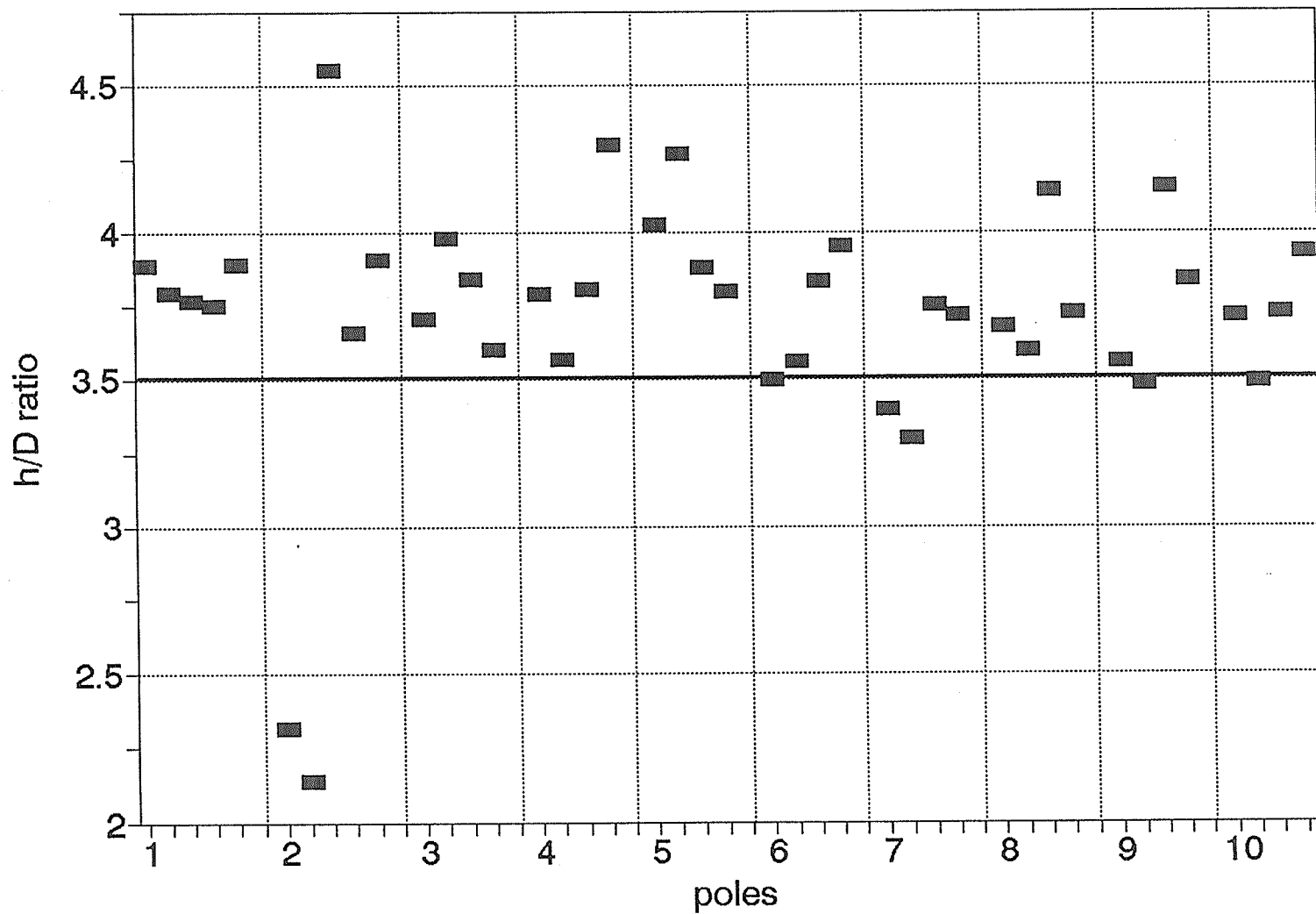


Figure 4.1. Height-diameter ratio for all compression test specimens

# LOGGEPOLE PINE

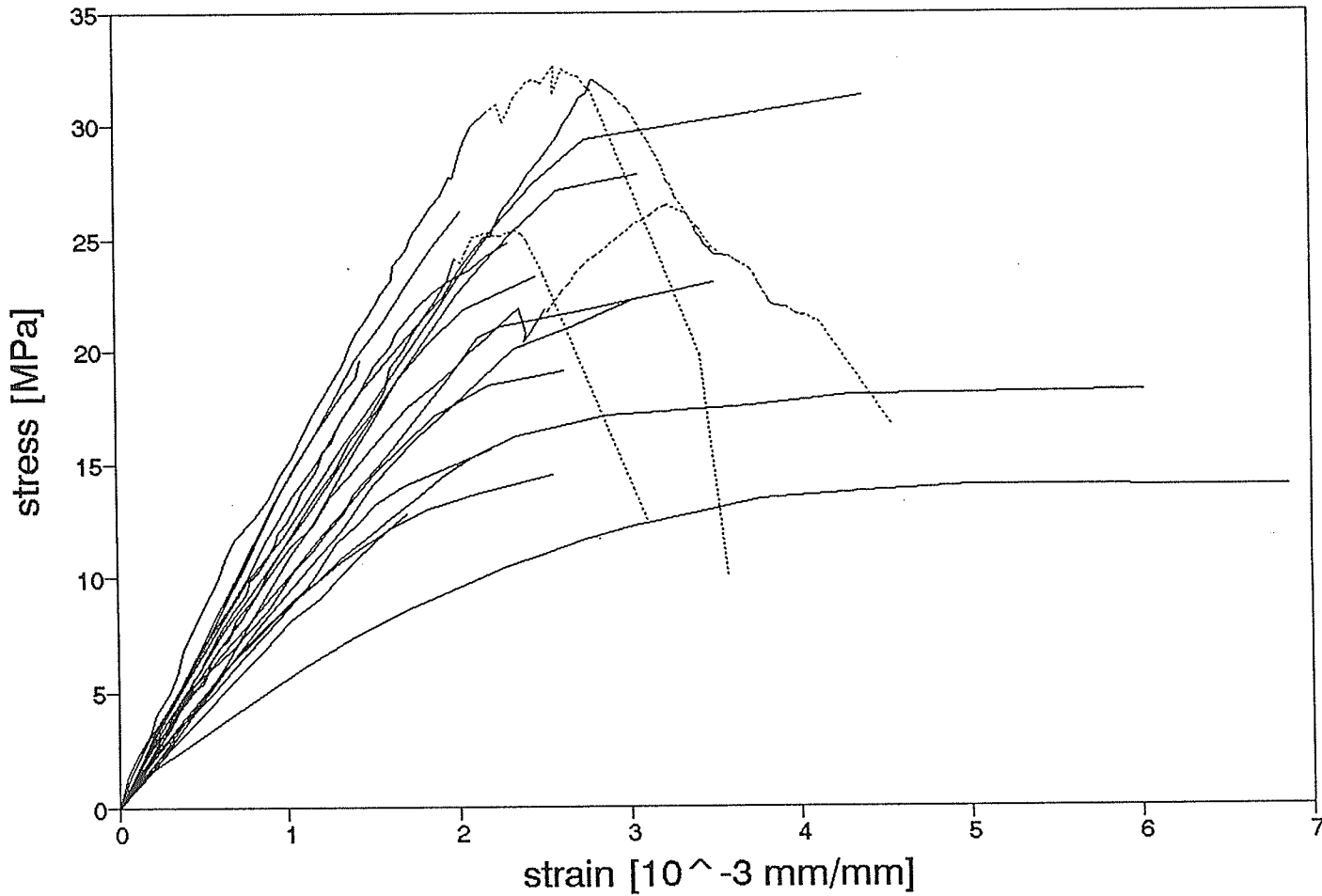


Figure 4.2. Stress-strain relationship for compression tests for Lodgepole Pine

# WESTERN RED CEDAR

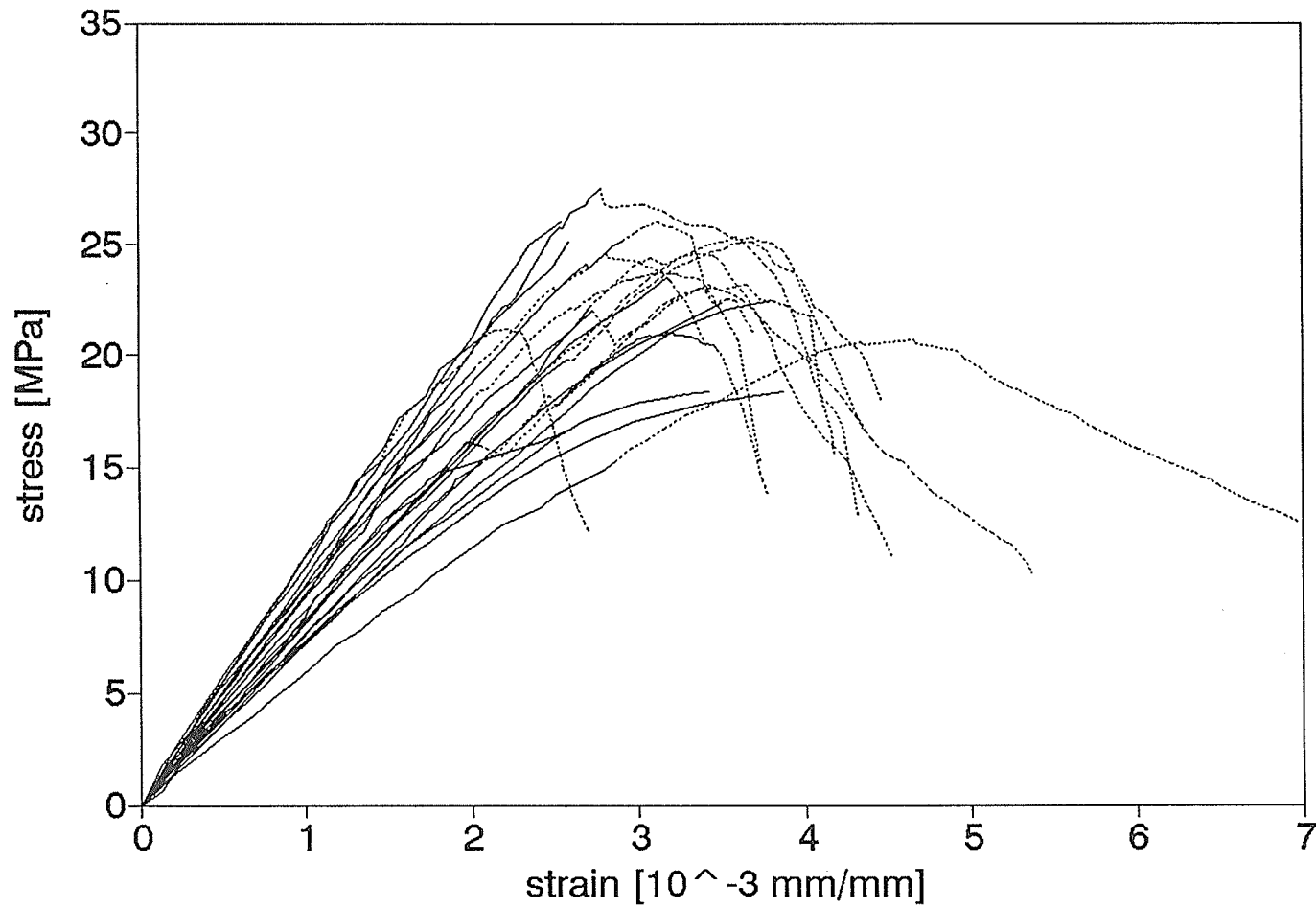
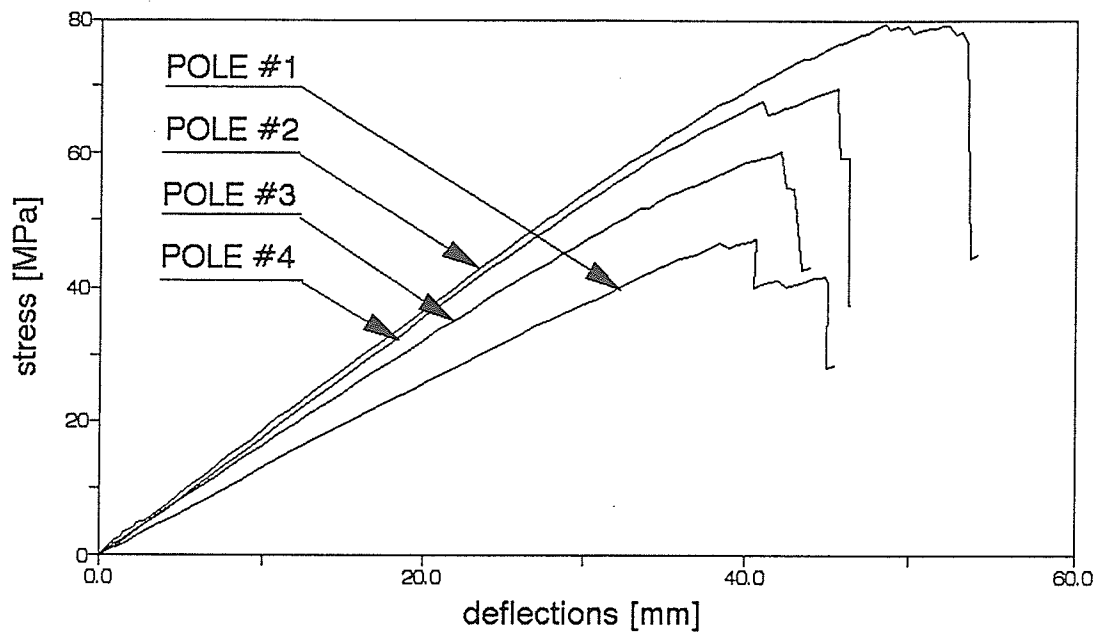


Figure 4.3. Stress-strain relationship for compression tests for Western Red Cedar

## LOGEPOLE PINE bending tests



## WESTERN RED CEDAR bending tests

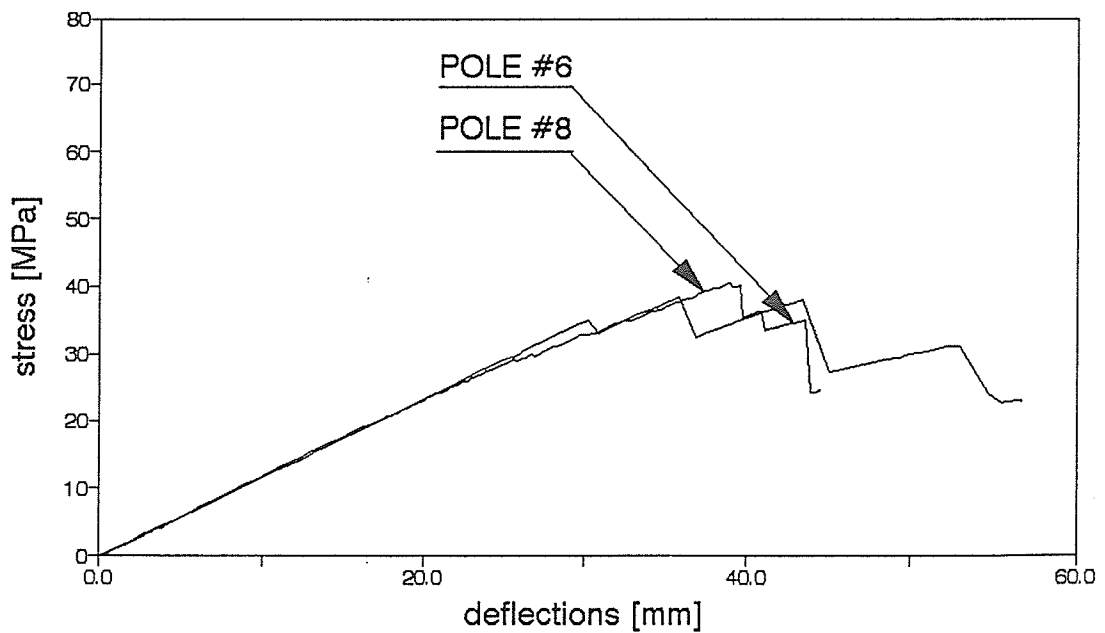


Figure 4.4. Stress-deflection relationship for bending tests

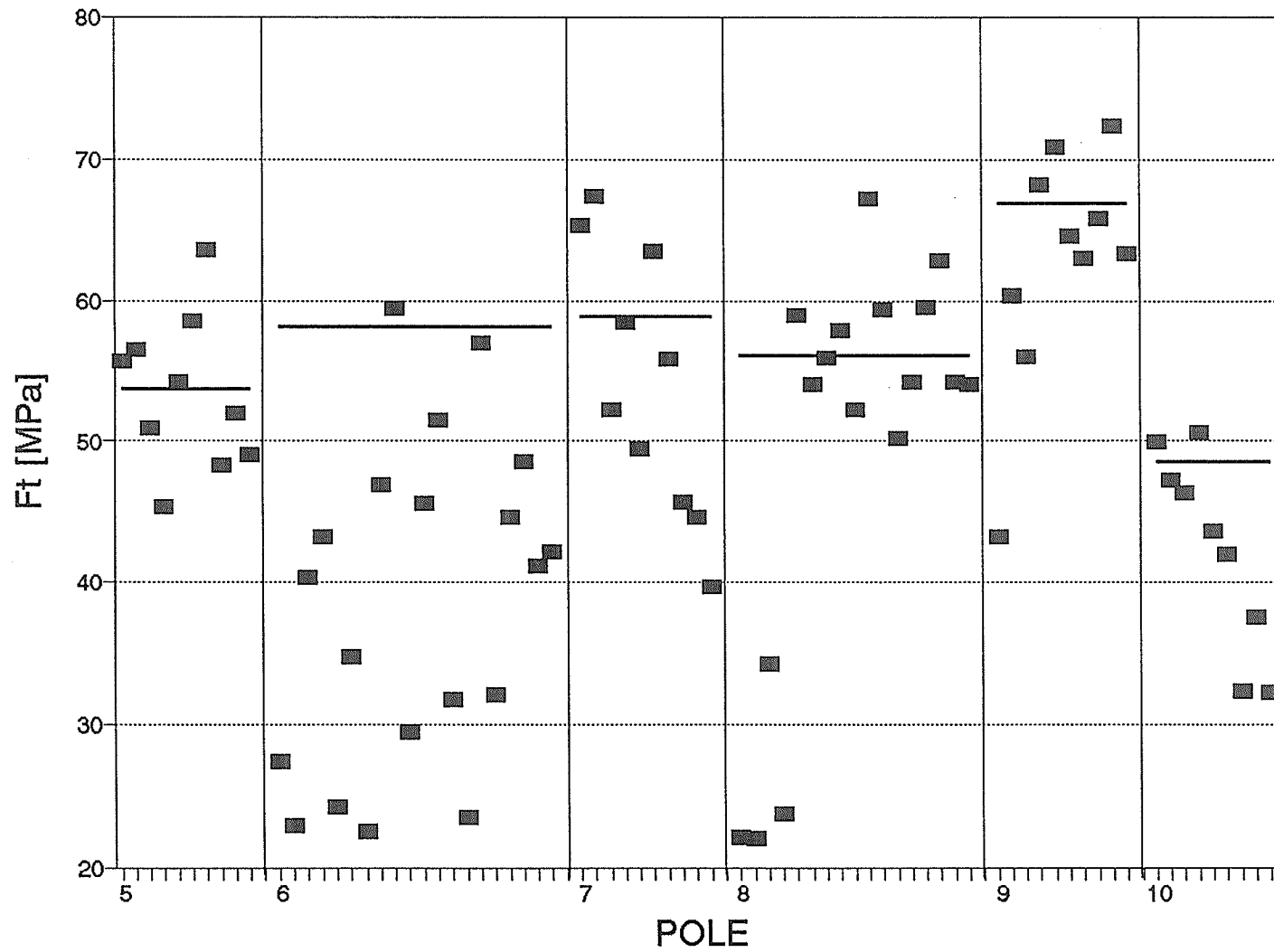
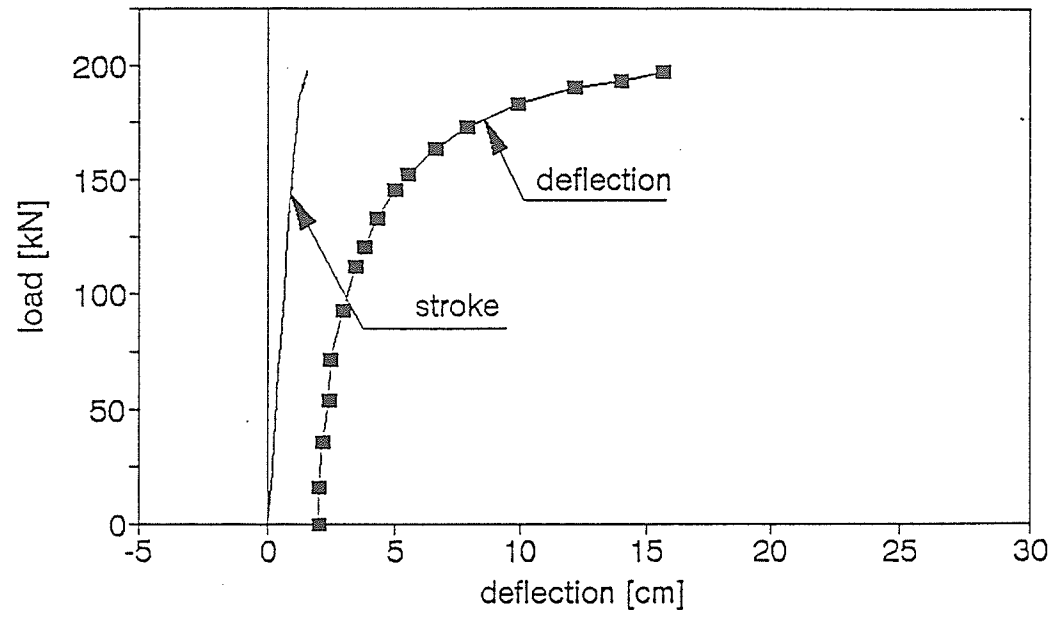


Figure 4.5. Tension test results

### POLE 7/1 DEFLECTION AT THE MIDSPAN



### DEFLECTED SHAPE OF THE POLE 7/1 UNDER DIFFERENT LOAD LEVELS

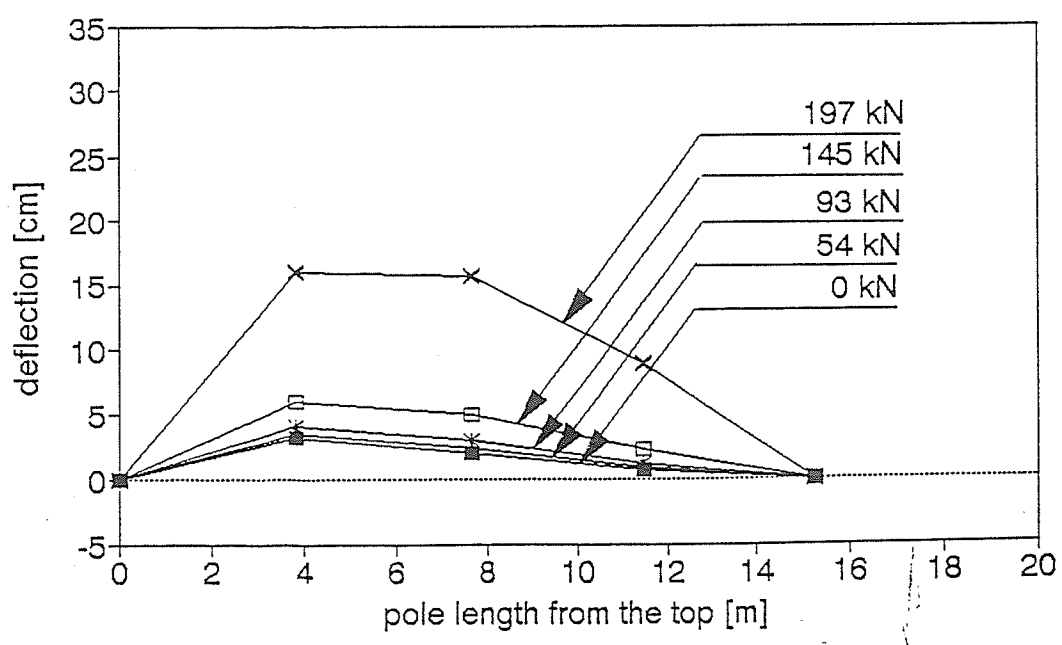
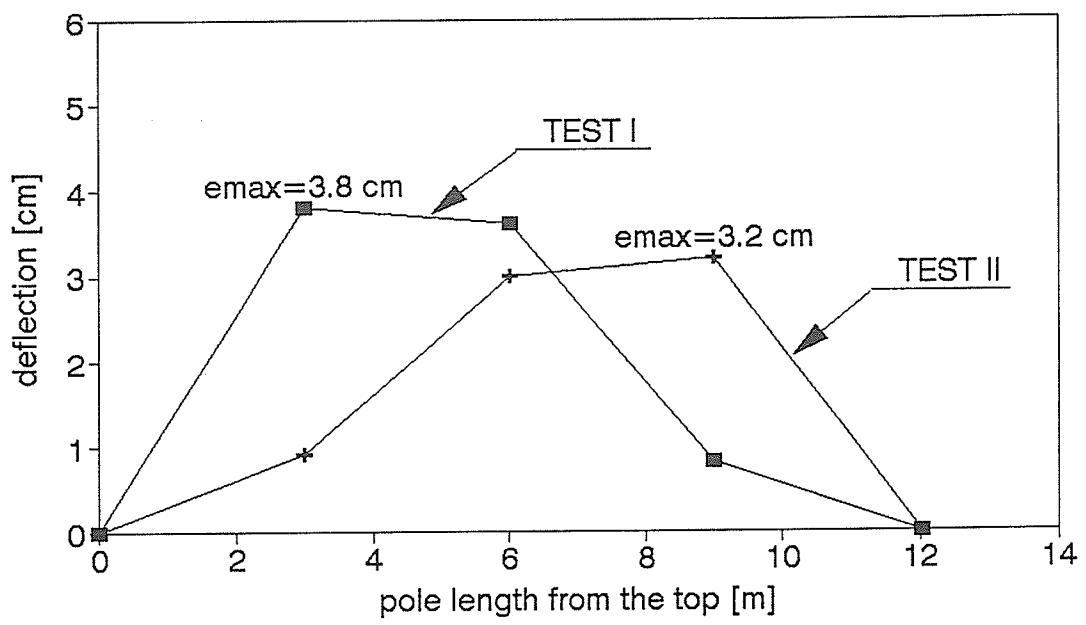


Figure 4.6. Typical load-deflection relationship and deflected shape of the pole 7/1

# DEFLECTED SHAPE OF THE POLE 2/1

LOAD P= 0.0kN



## POLE 2/1 DEFLECTION AT THE MIDSPAN COMPARED RESULTS OF TEST I AND TEST II

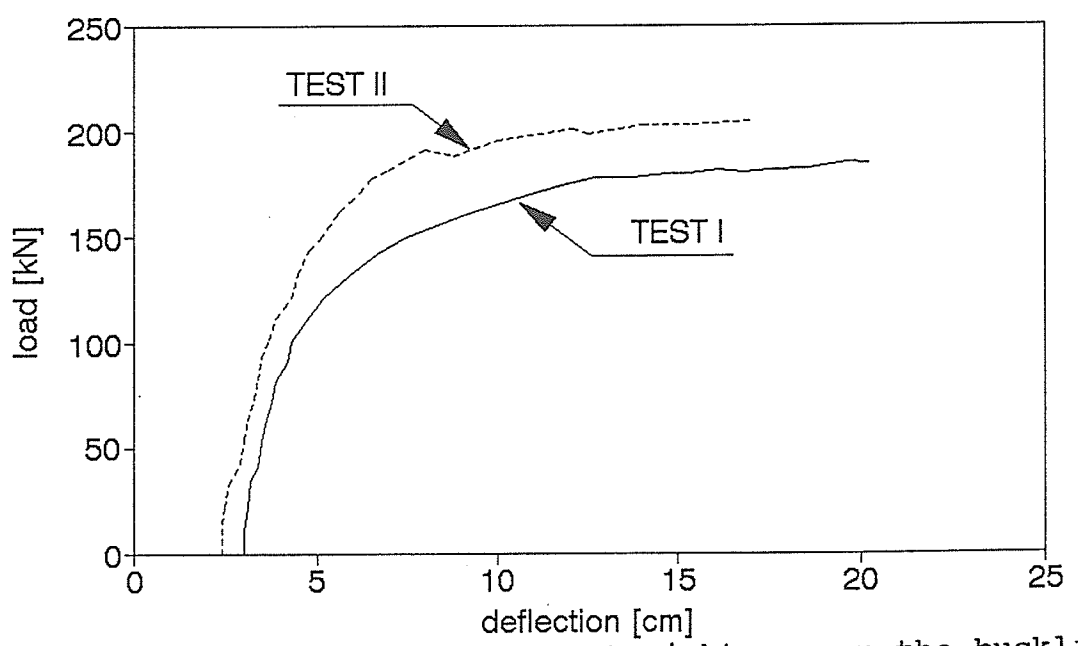


Figure 4.7. Effect of out-of-straightness on the buckling capacity of the pole

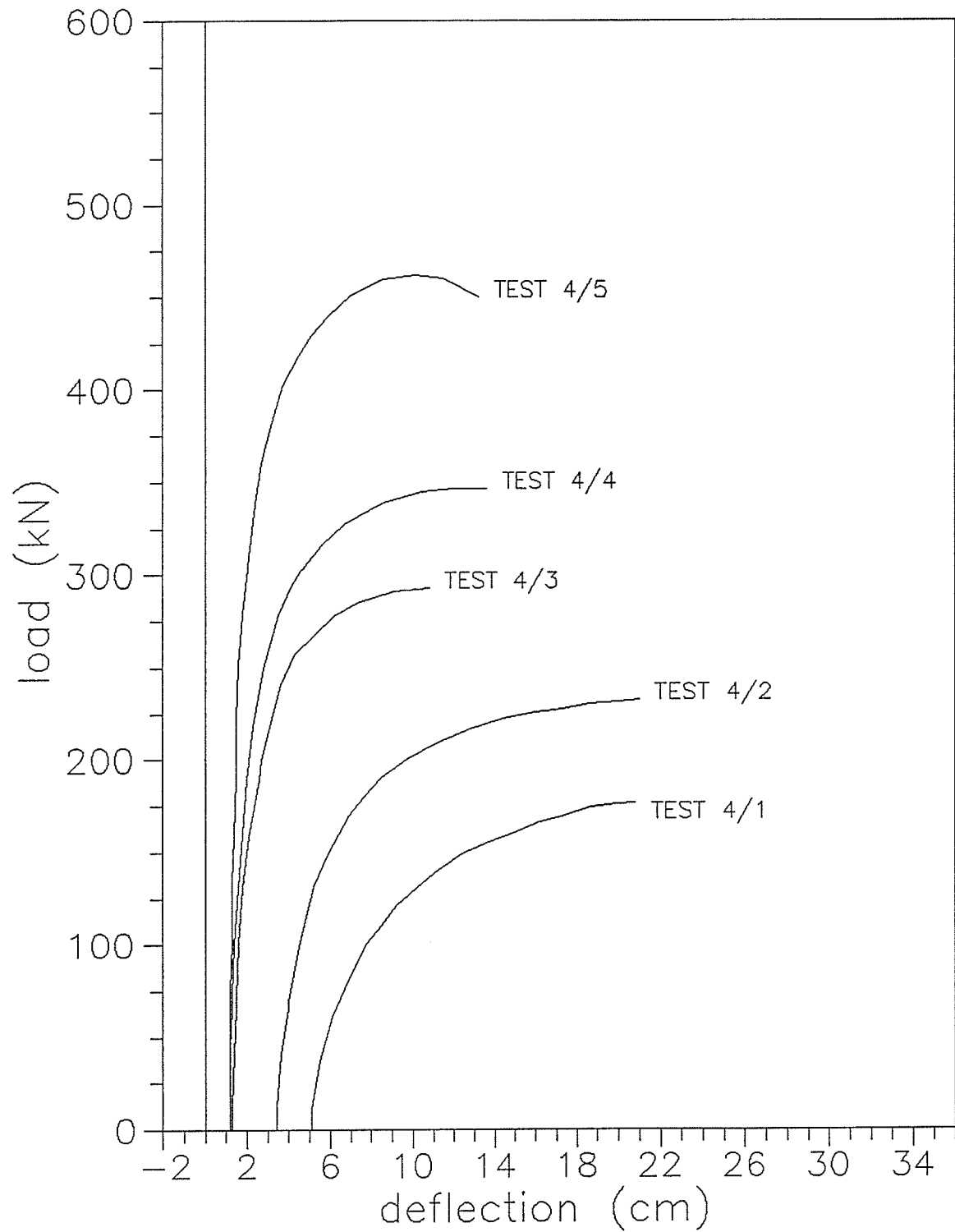


Figure 4.8. Typical load-deflection relationship of the test specimens originated from the same pole

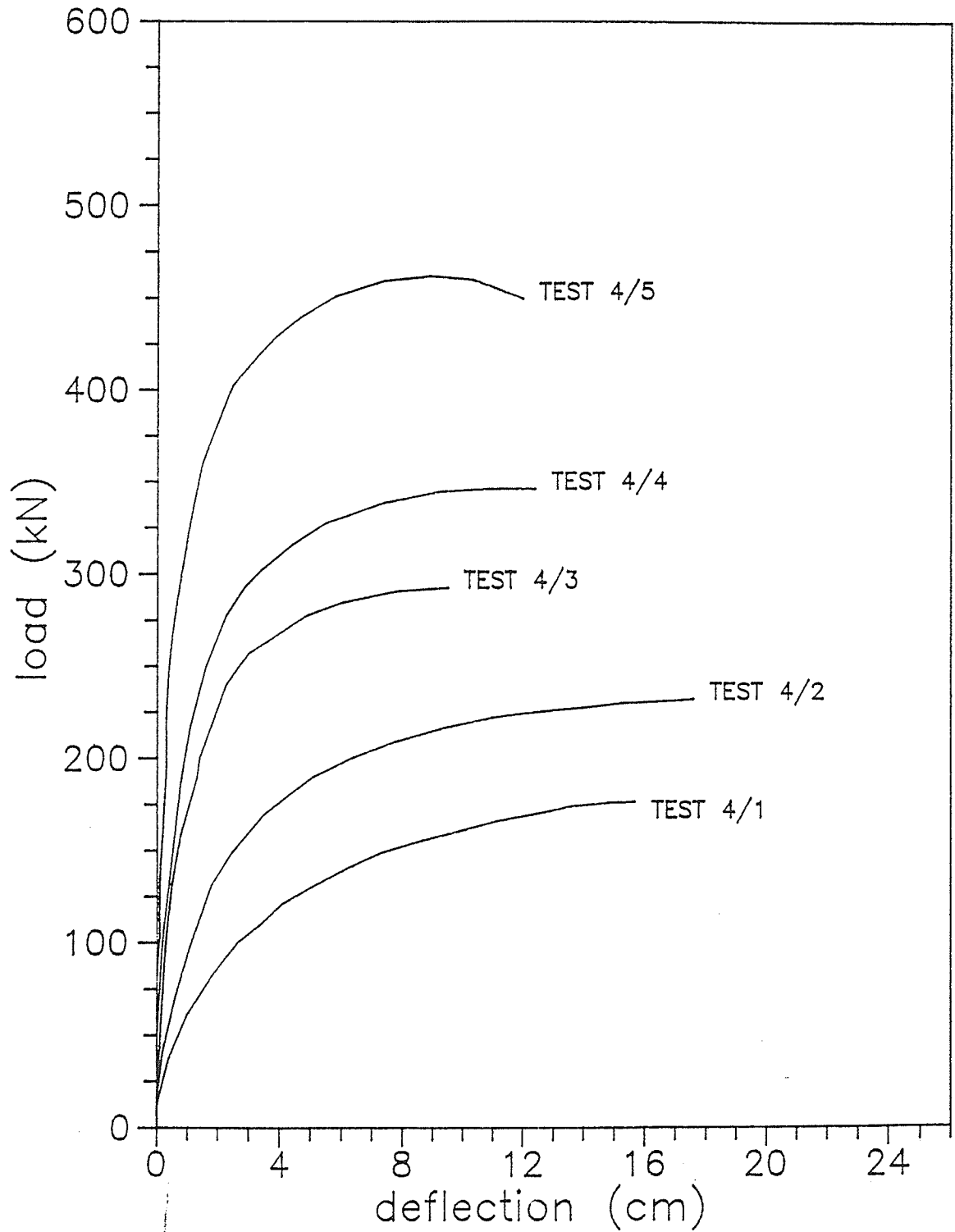


Figure 4.9. Typical load-relative deflections relationship for the specimens originated from the same pole

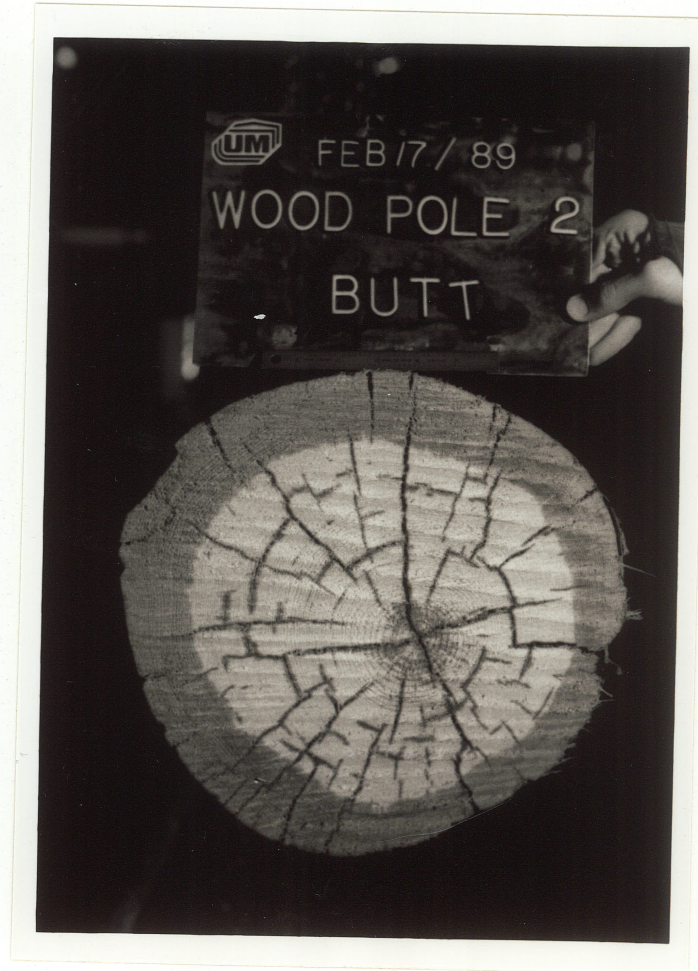
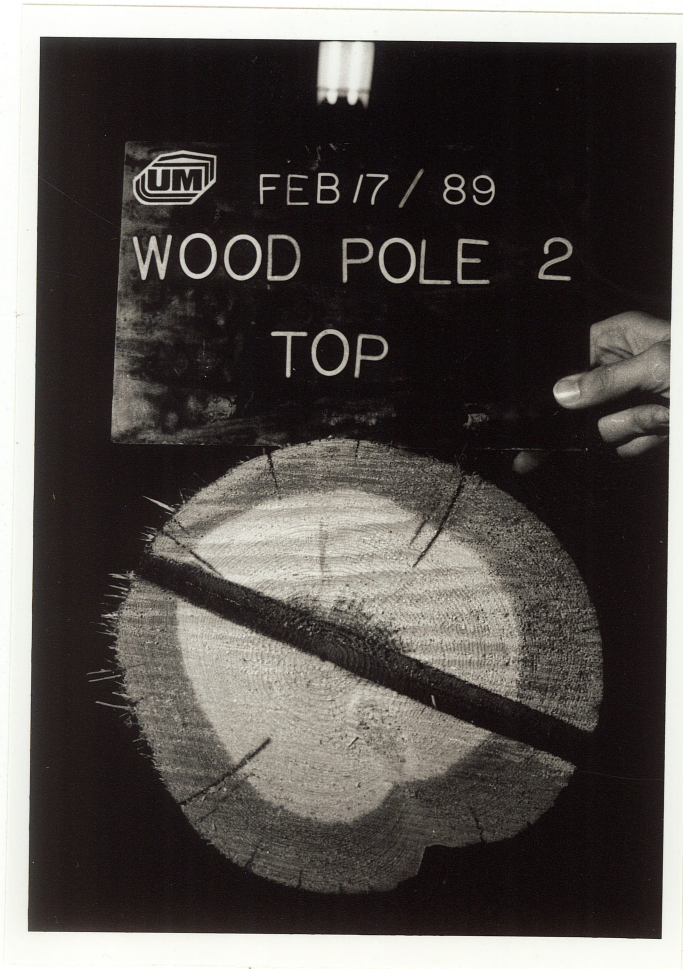


Figure 5.1. Imperfect circular cross-section of the pole #2

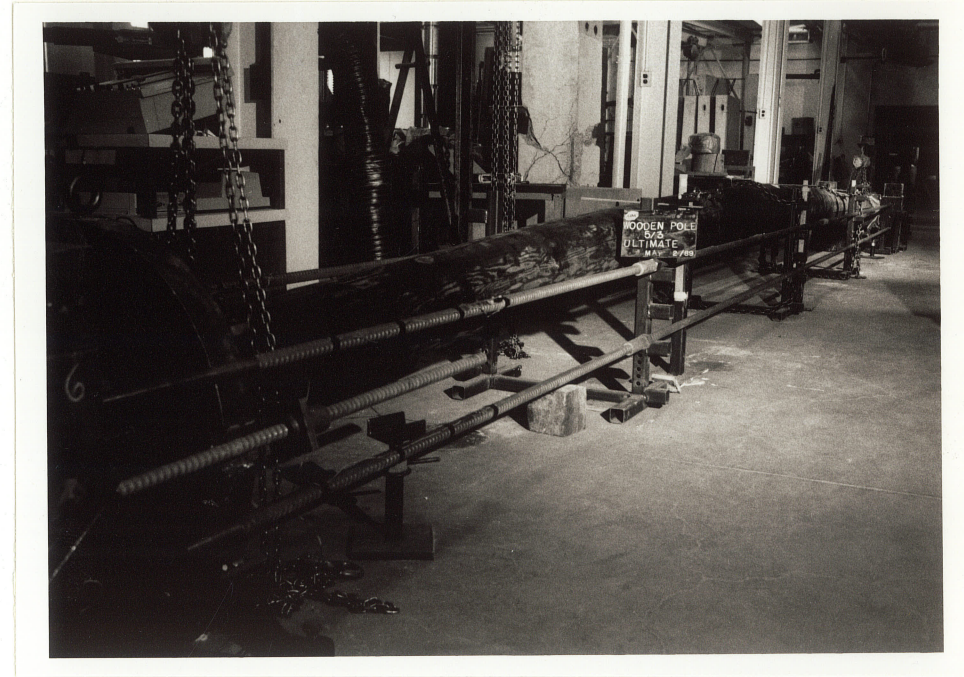
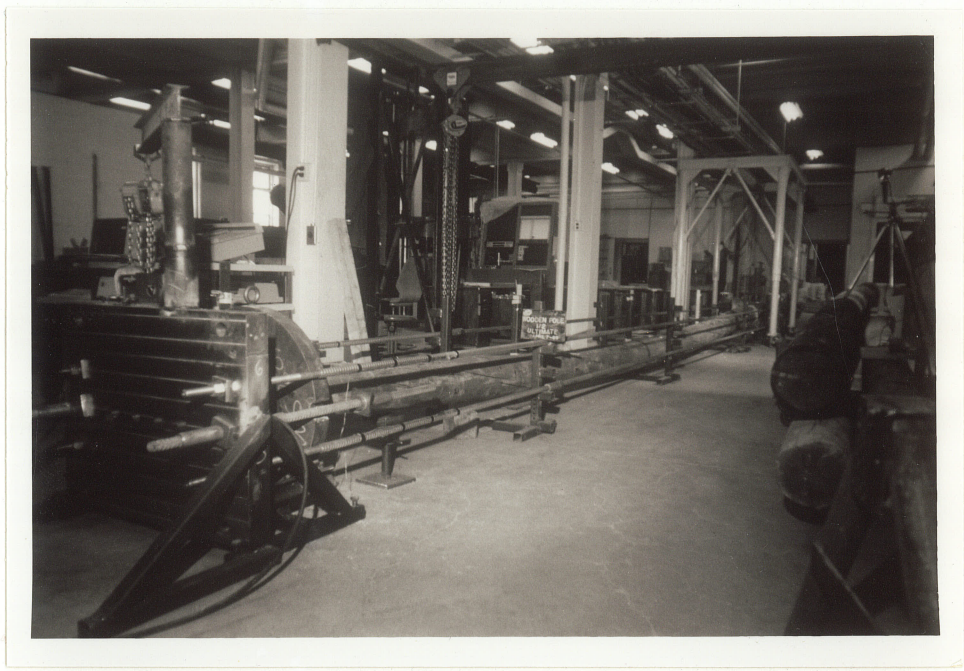


Figure 5.2. Two types of buckling behaviour

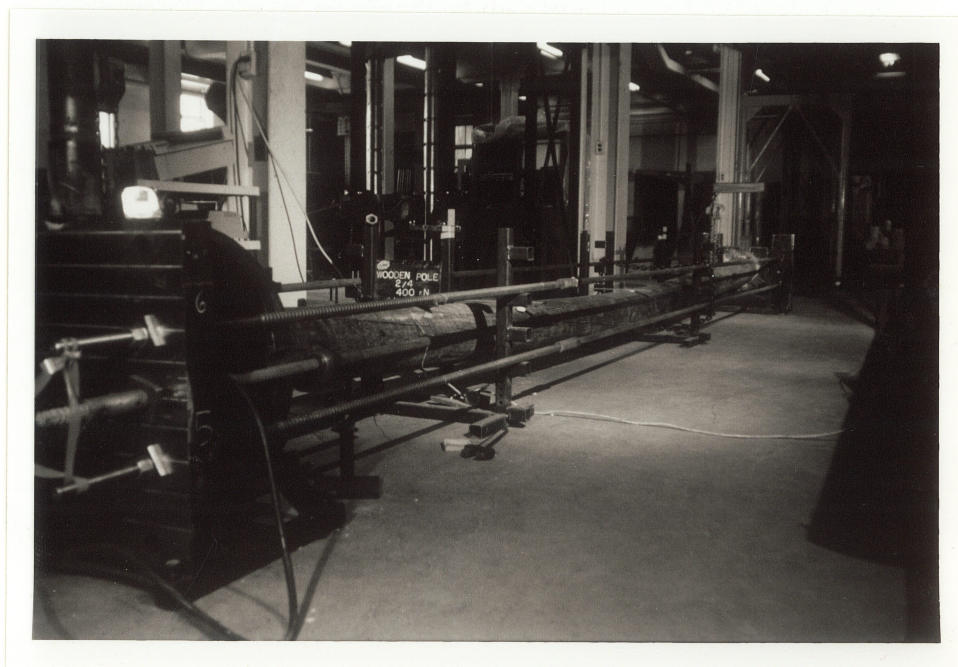
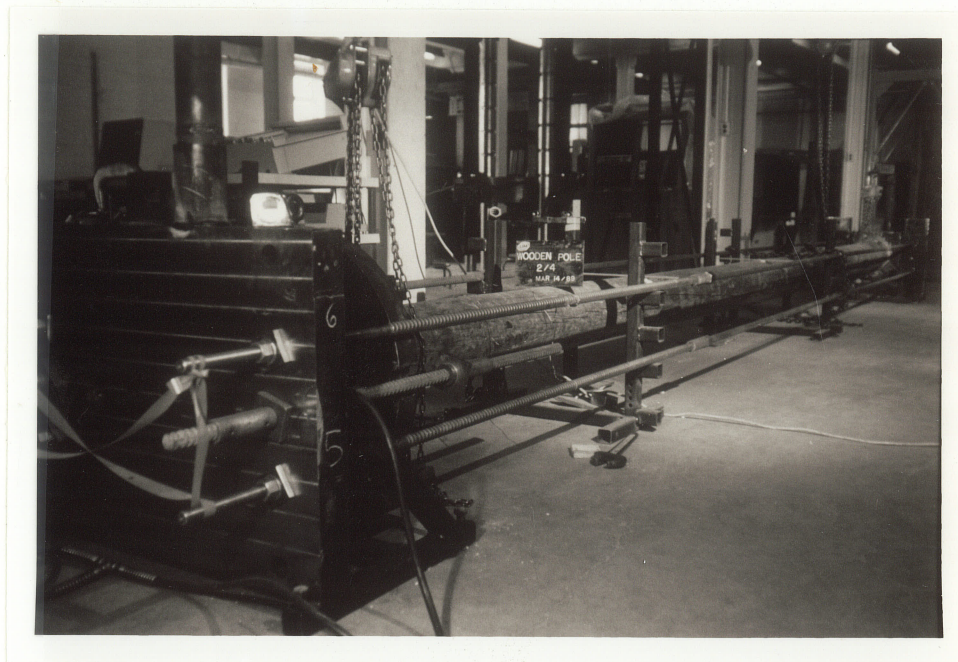


Figure 5.3. Pole before applying the load and at ultimate load

# Southwell plot

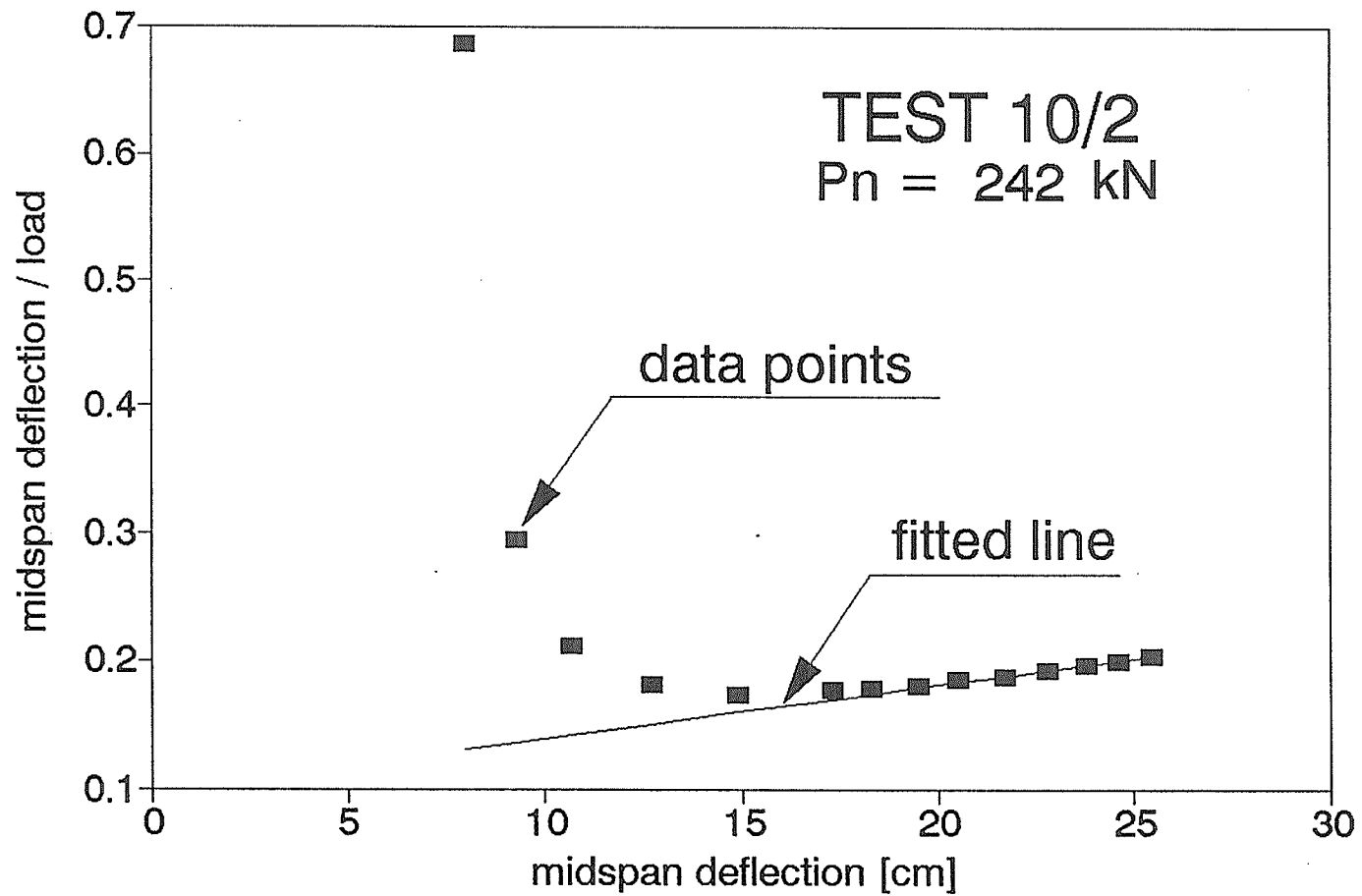


Figure 5.4. Typical Southwell plot

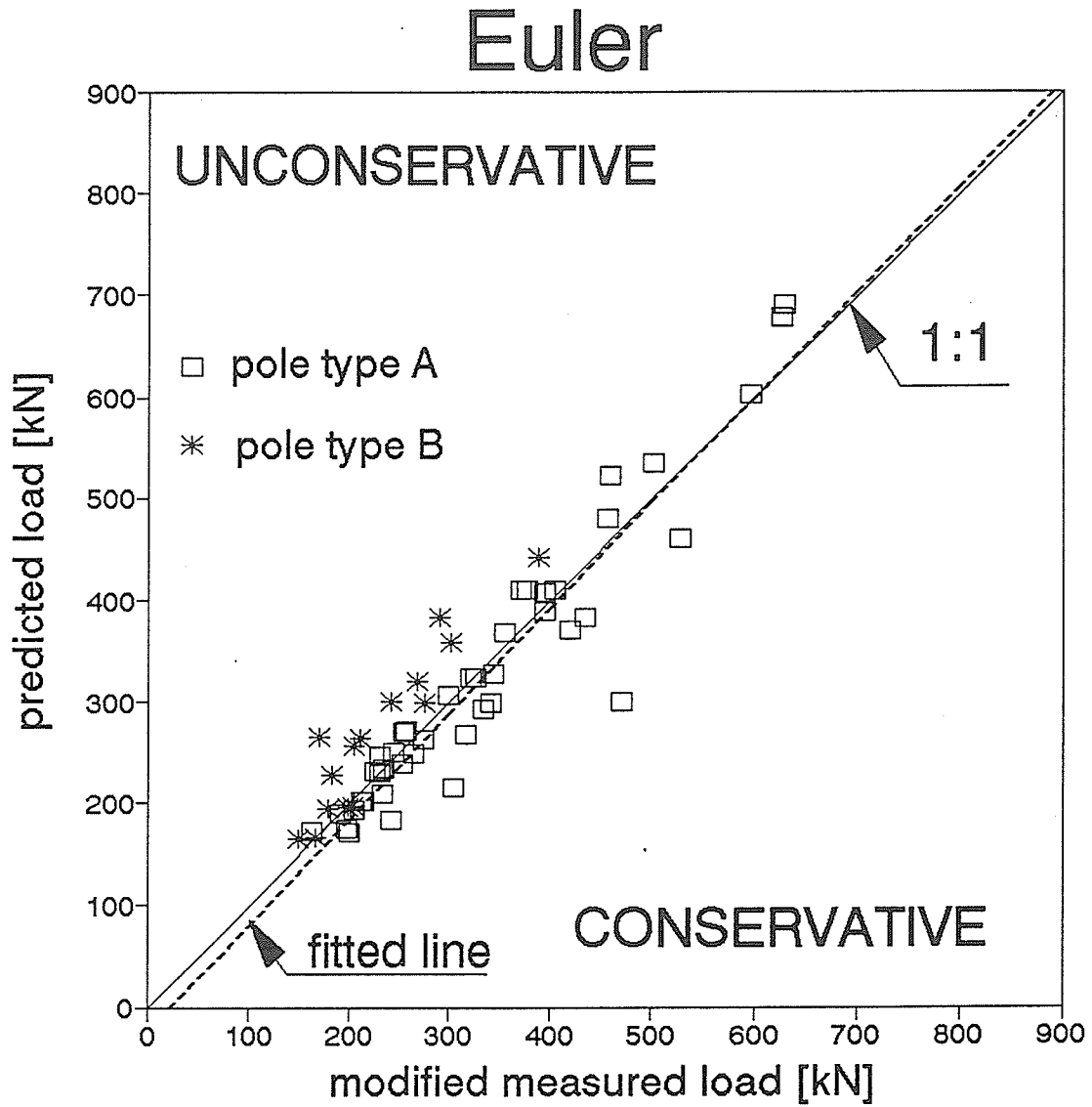


Figure 5.5. Critical load evaluated by Southwell plot compared to prediction of the Euler's formula

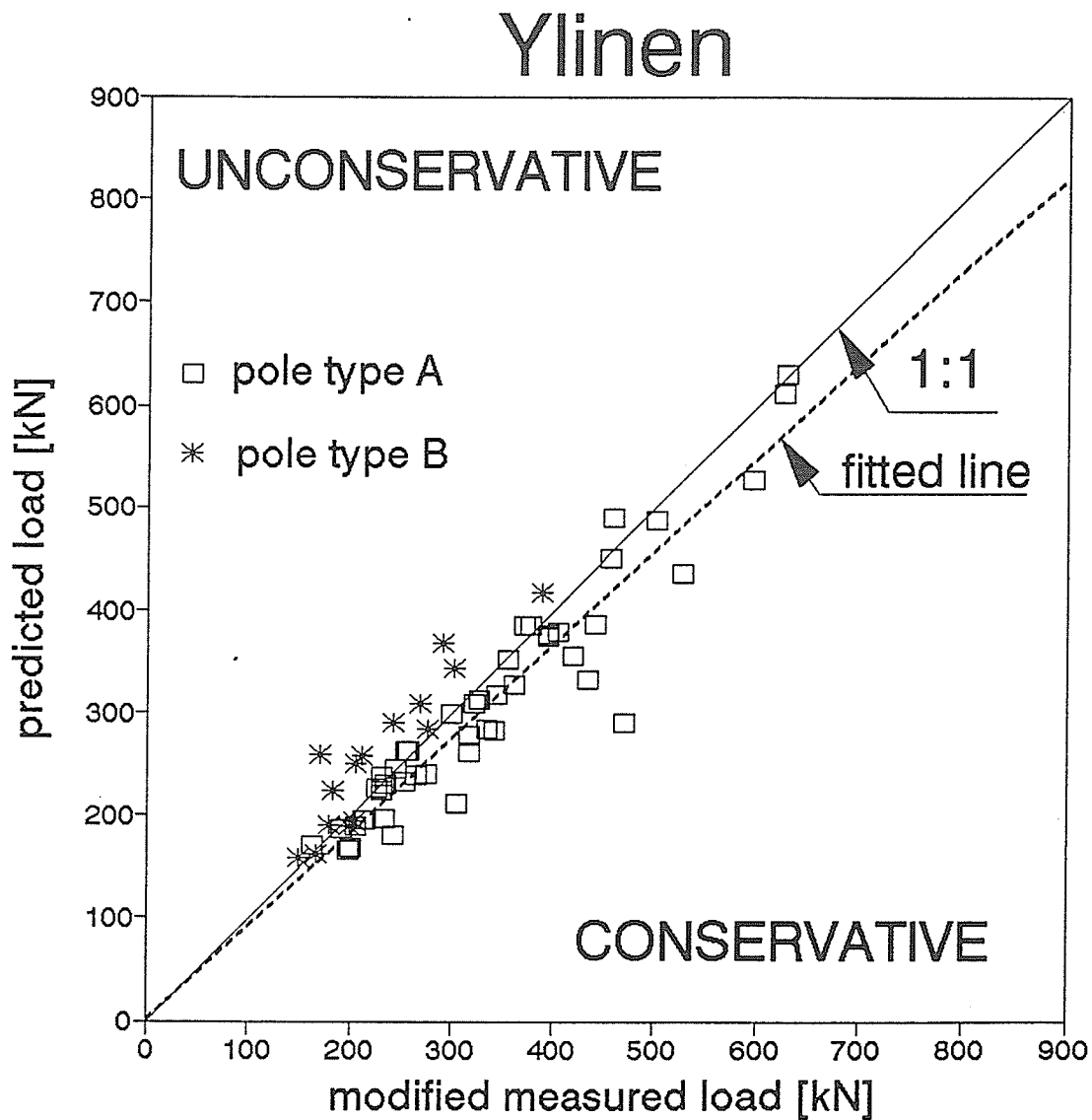


Figure 5.6. Critical load evaluated by Southwell plot compared to prediction of the Ylinen's column formula

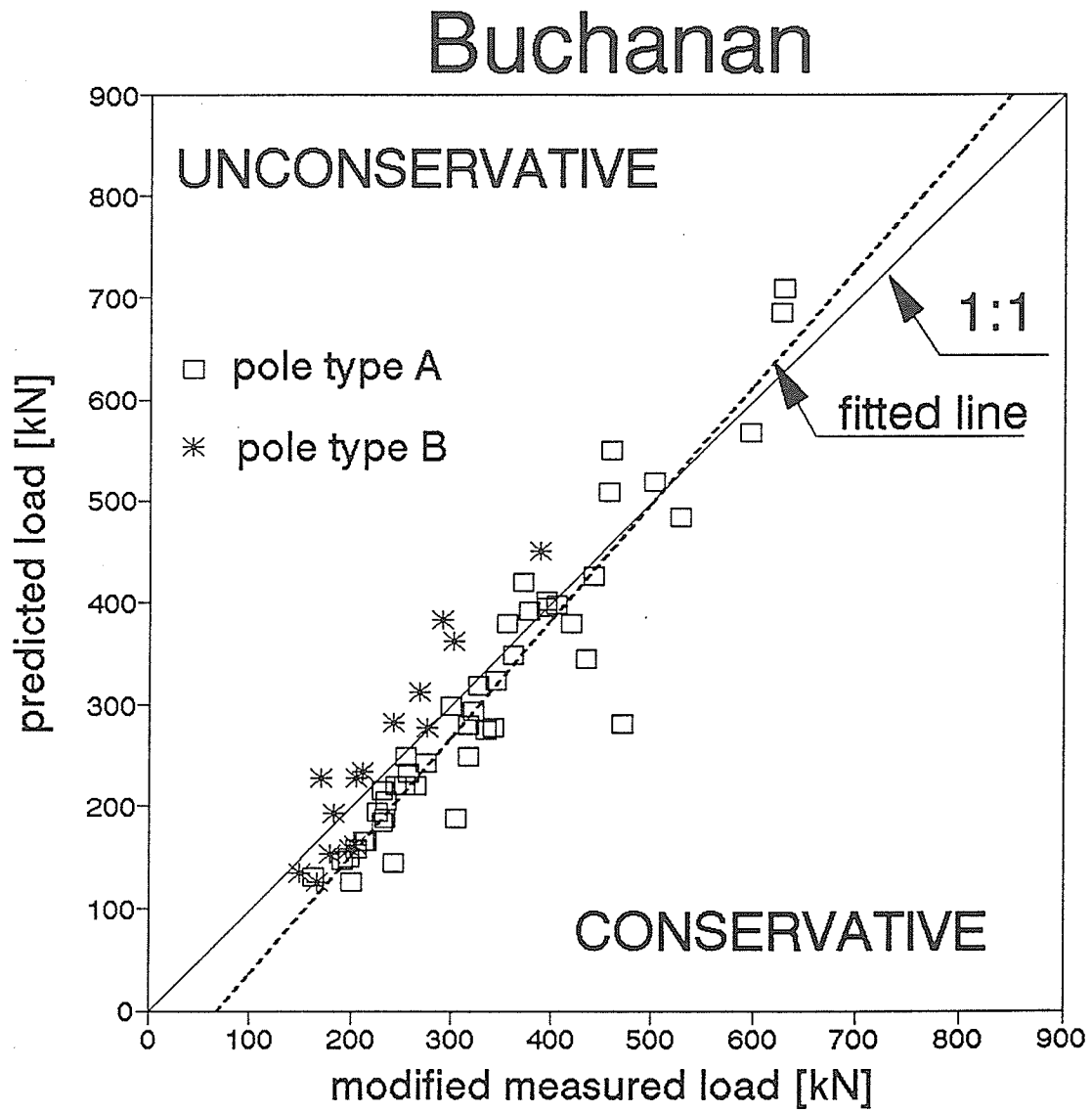


Figure 5.7. Critical load evaluated by Southwell plot compared to prediction of the Buchanan's formula

# Code equation

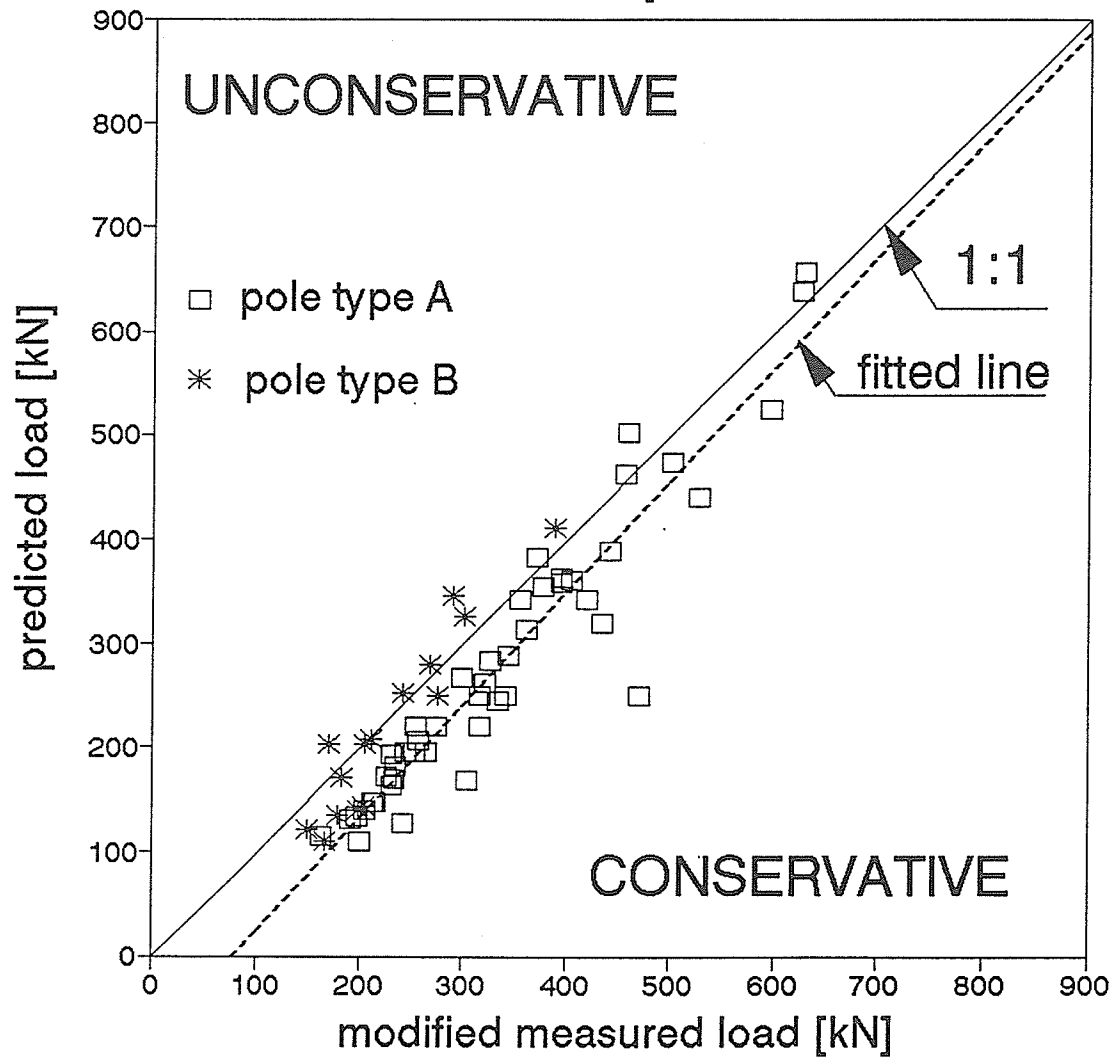
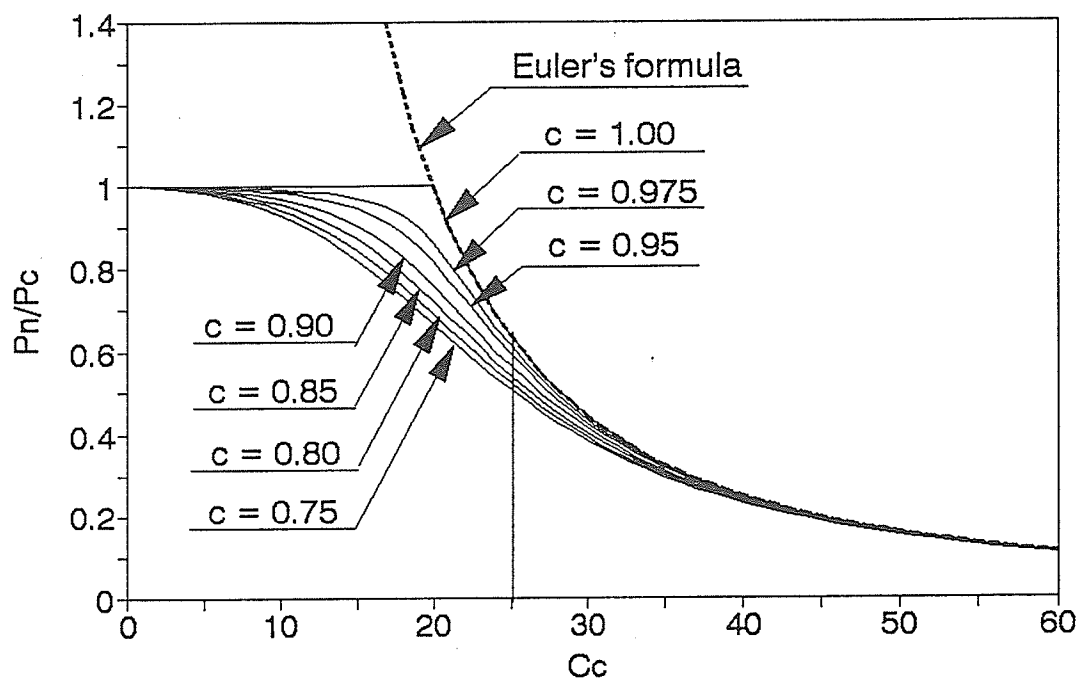


Figure 5.8. Critical load evaluated by Southwell plot compared to prediction of the Code equation

# LOGEPOLE PINE



# WESTERN RED CEDAR

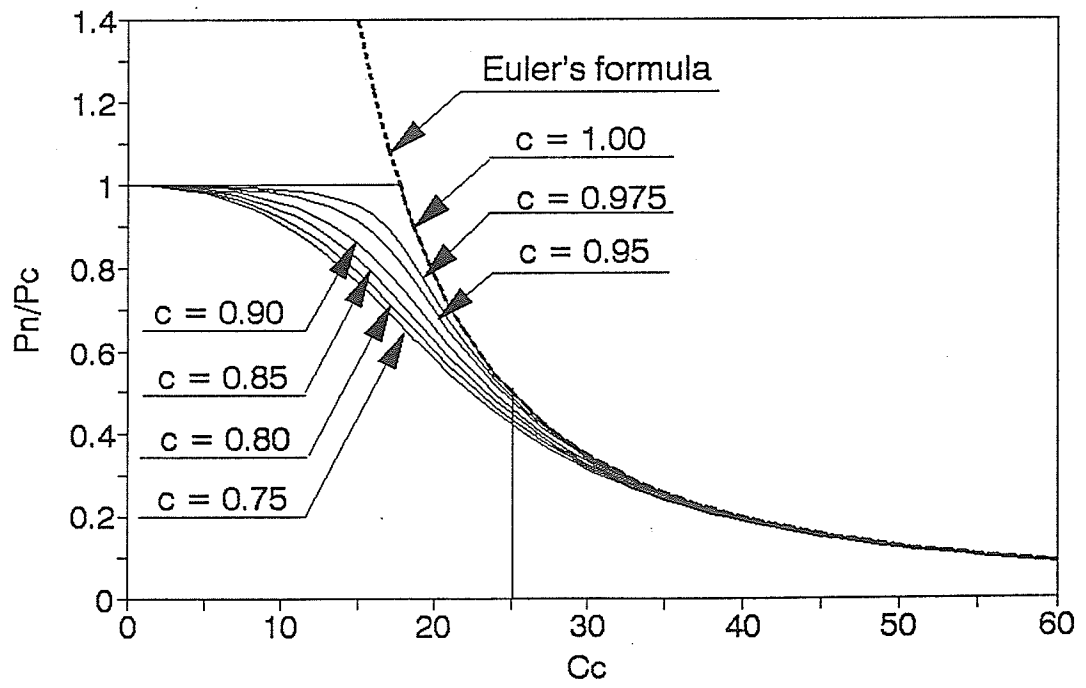


Figure 5.9. Influence of the coefficient  $c$  on predicted compression strength of the column by Ylinen's formula

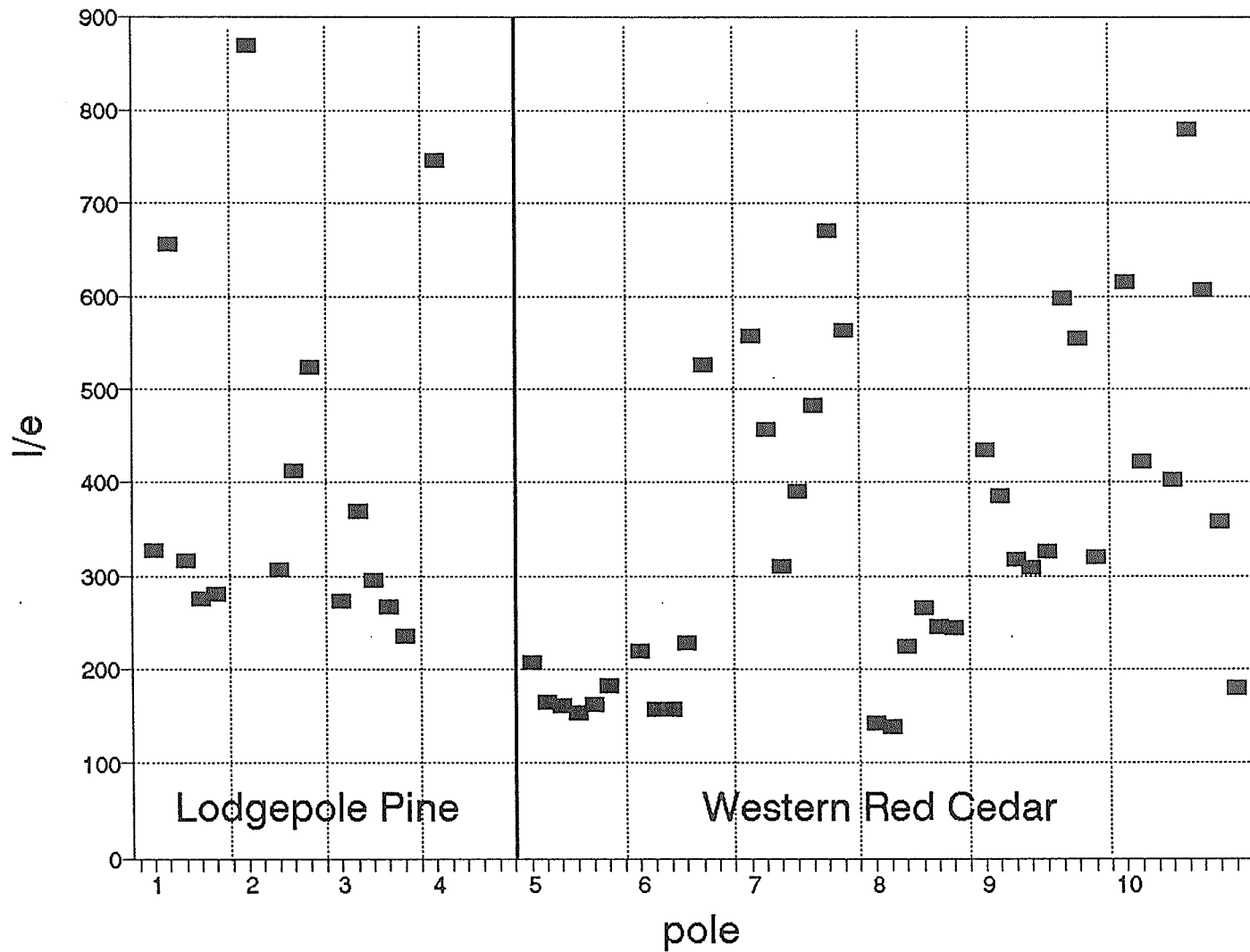


Figure 5.10. Ratio between pole's length and pole's out-of-straightness

# POLE 3/2

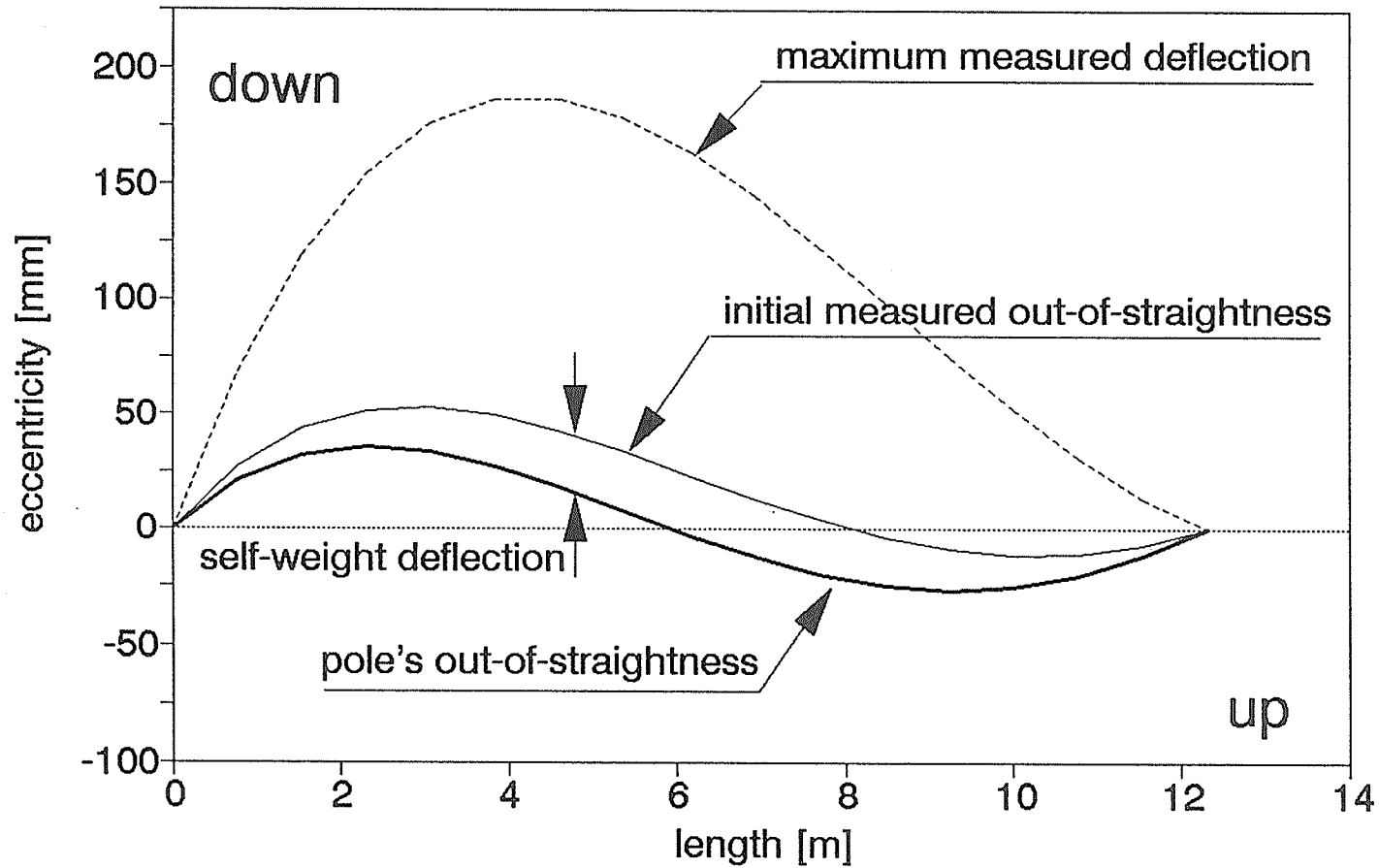


Figure 5.11. Typical pole shape at various loading stages

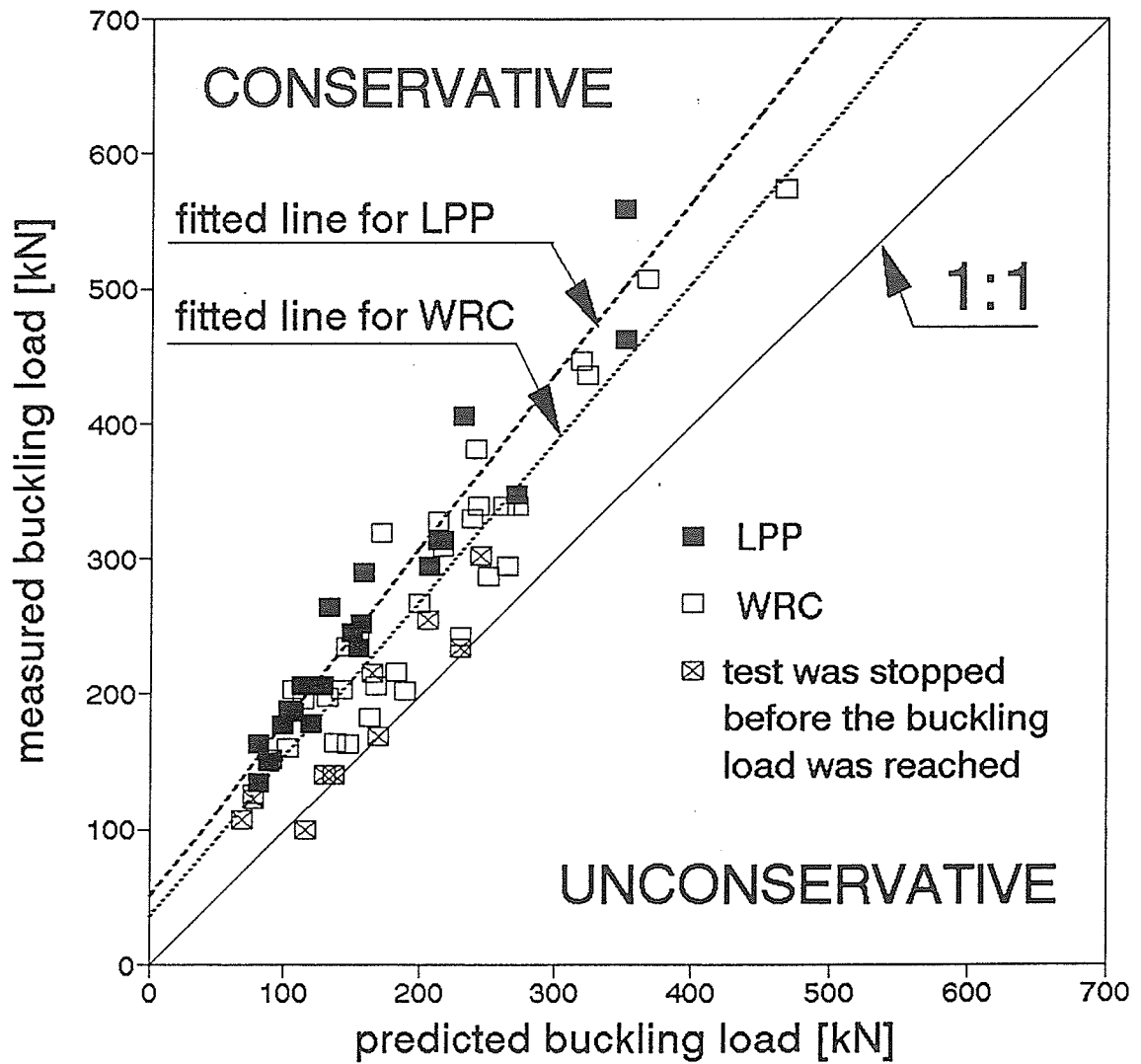


Figure 5.12. Predicted load by Buchanan's model compared to measured buckling load

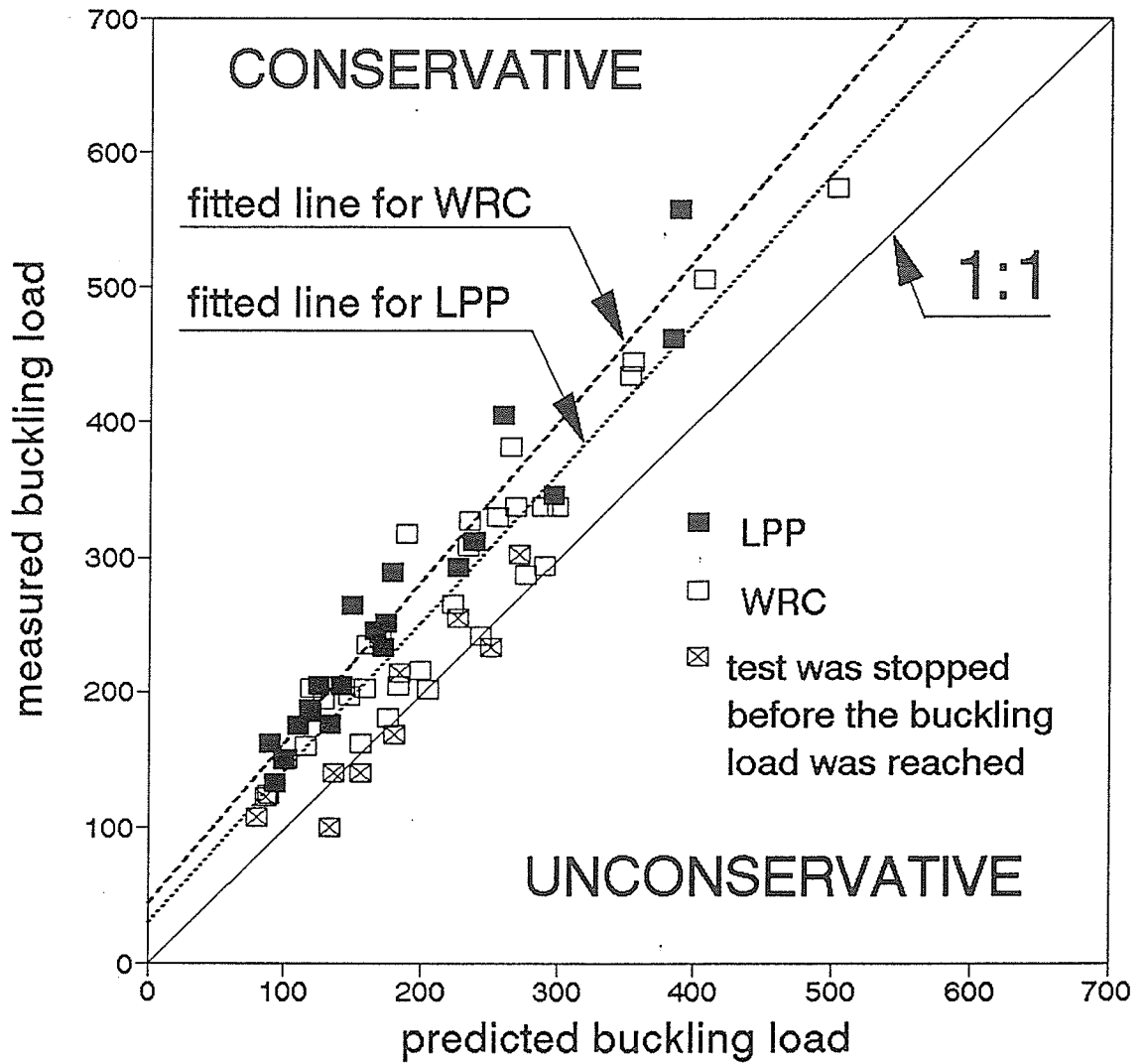


Figure 5.13. Predicted load by modified Buchanan's model compared to measured buckling load

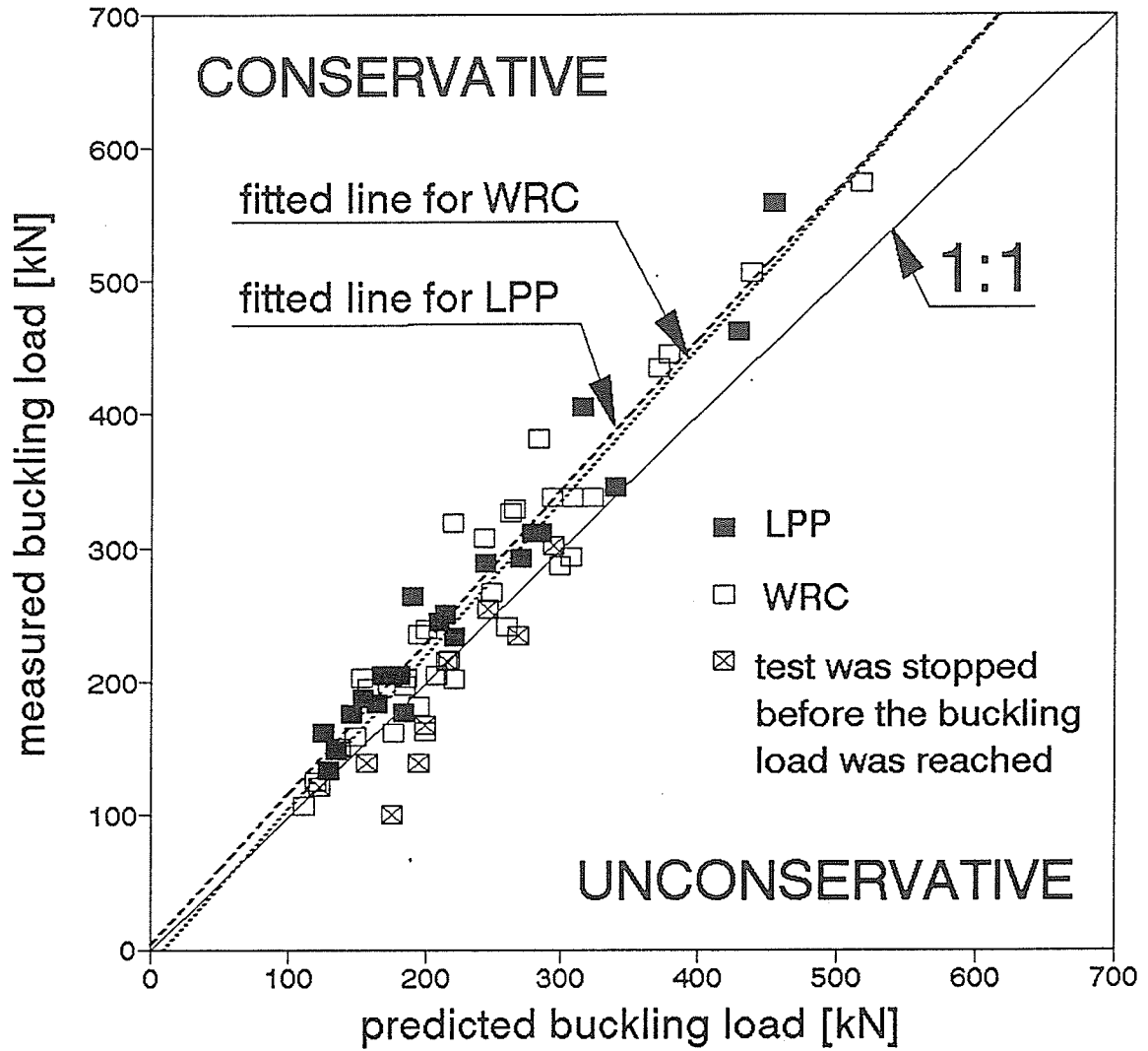


Figure 5.14. Predicted load by Zahn's model compared to measured buckling load

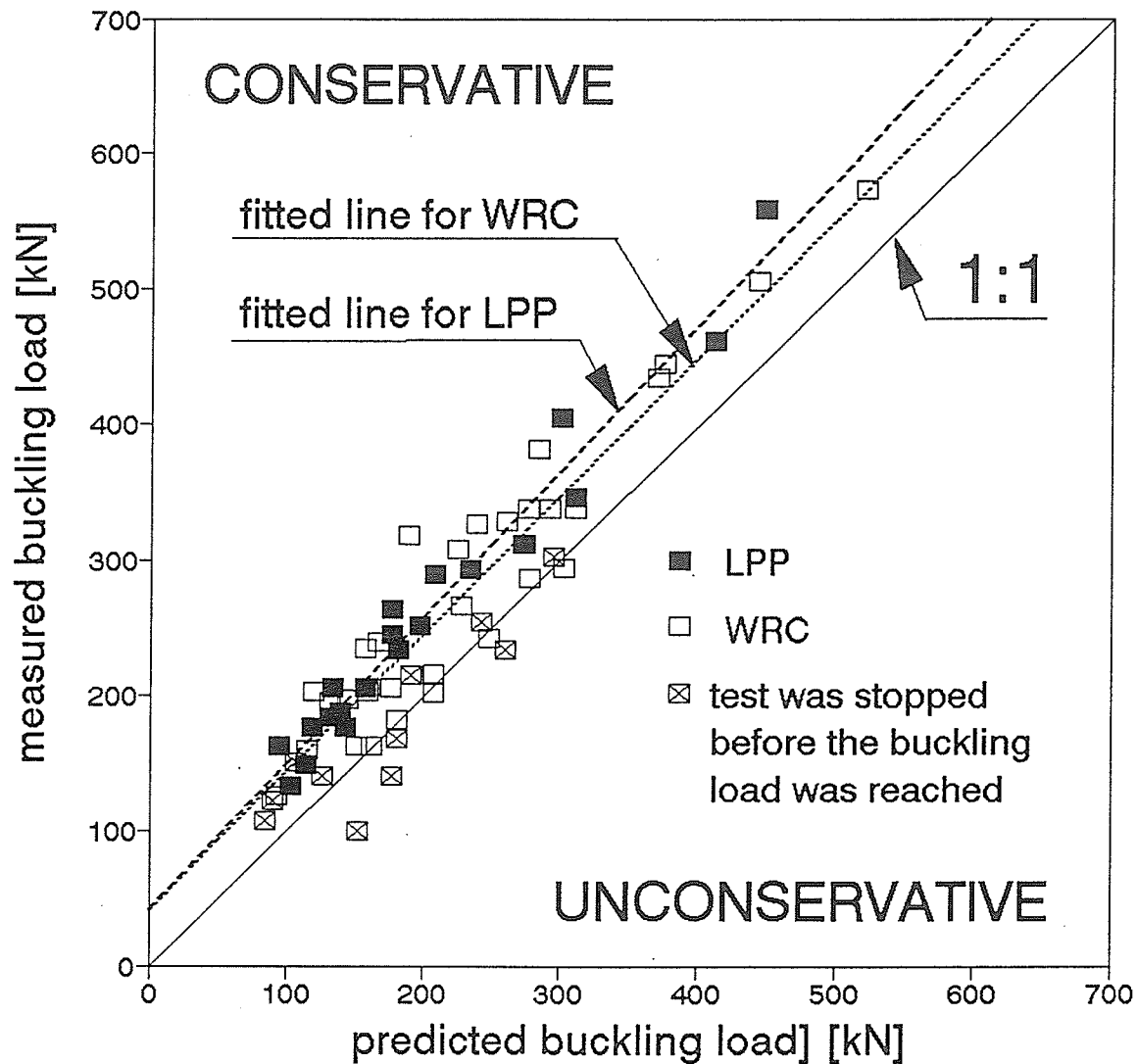
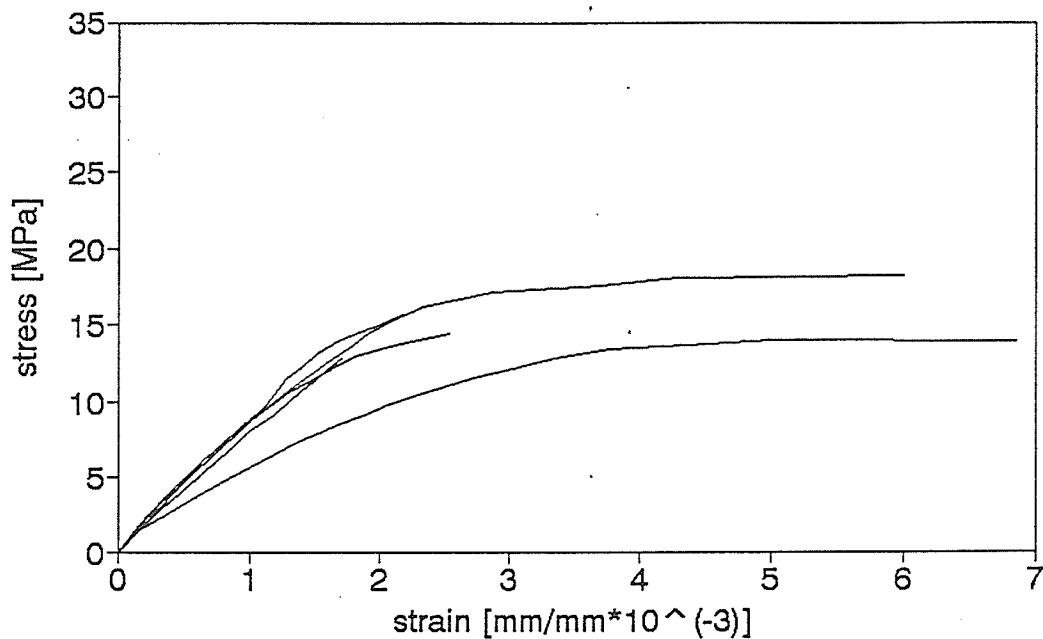


Figure 5.15. Predicted load by the Code model compared to measured buckling load

# APPENDIX A

# POLE #1 MATERIAL PROPERTIES

## TESTS 1 to 5



# POLE #2 MATERIAL PROPERTIES

## TESTS 1 to 5

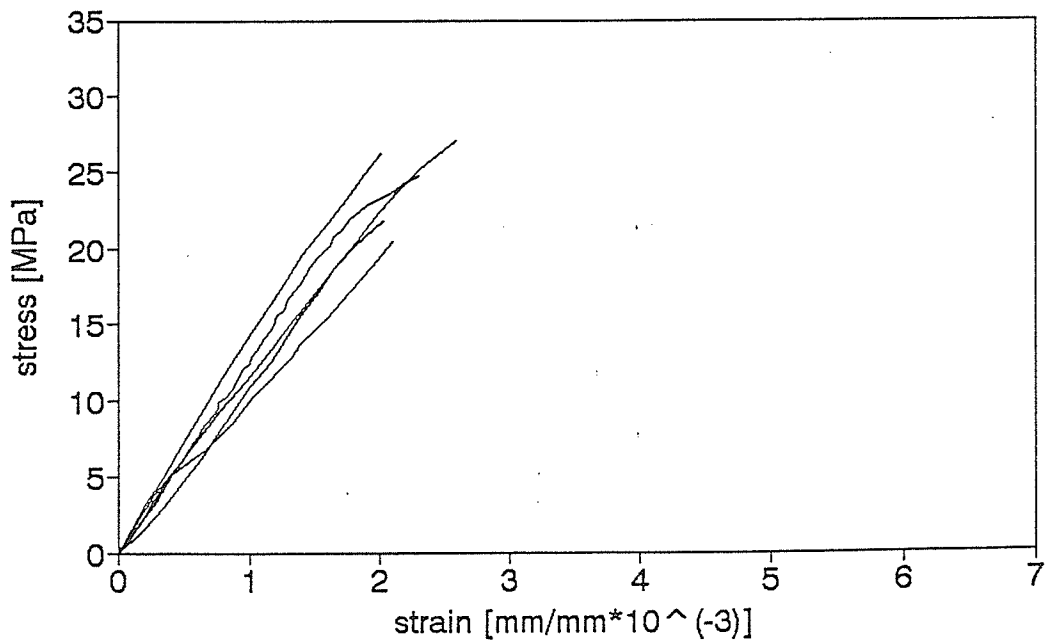
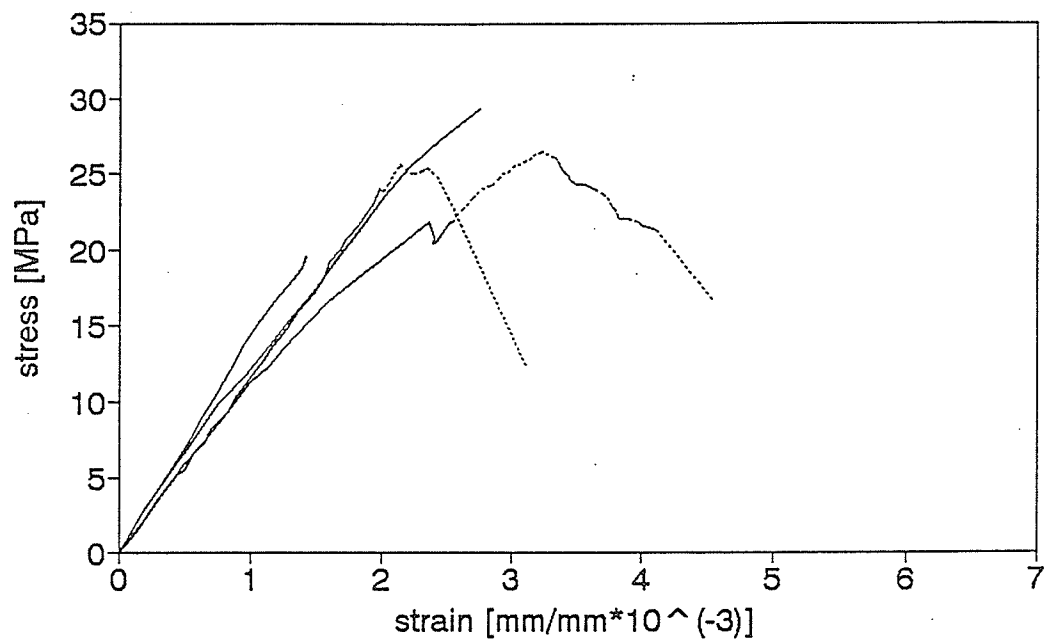


Figure A1.1. Stress-strain relationship for compression tests

## POLE #3 MATERIAL PROPERTIES TESTS 1 to 4



## POLE 4 MATERIAL PROPERTIES TESTS 1 to 4

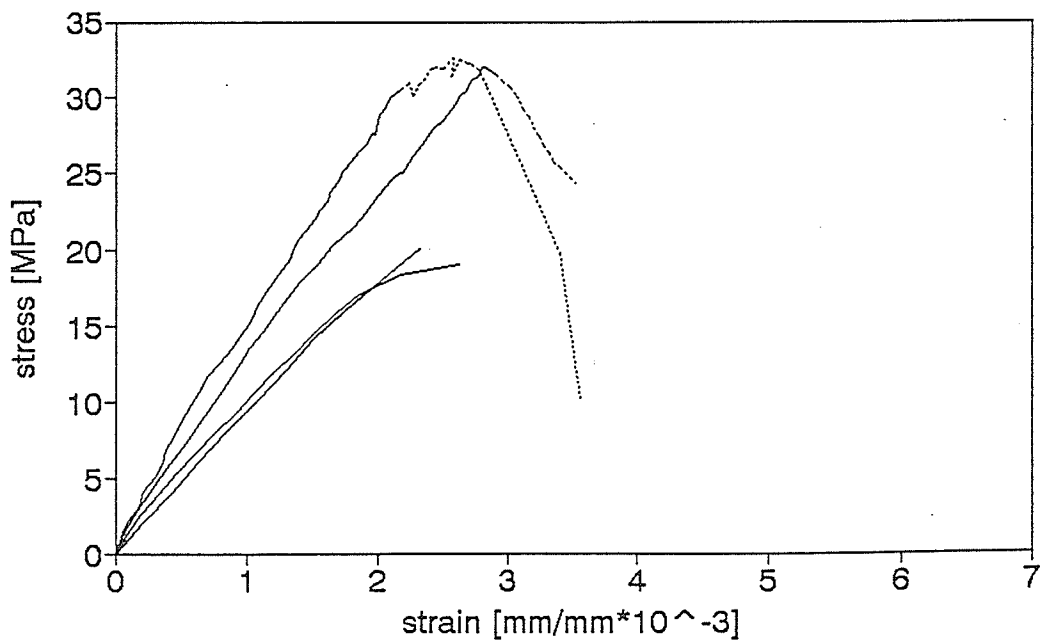
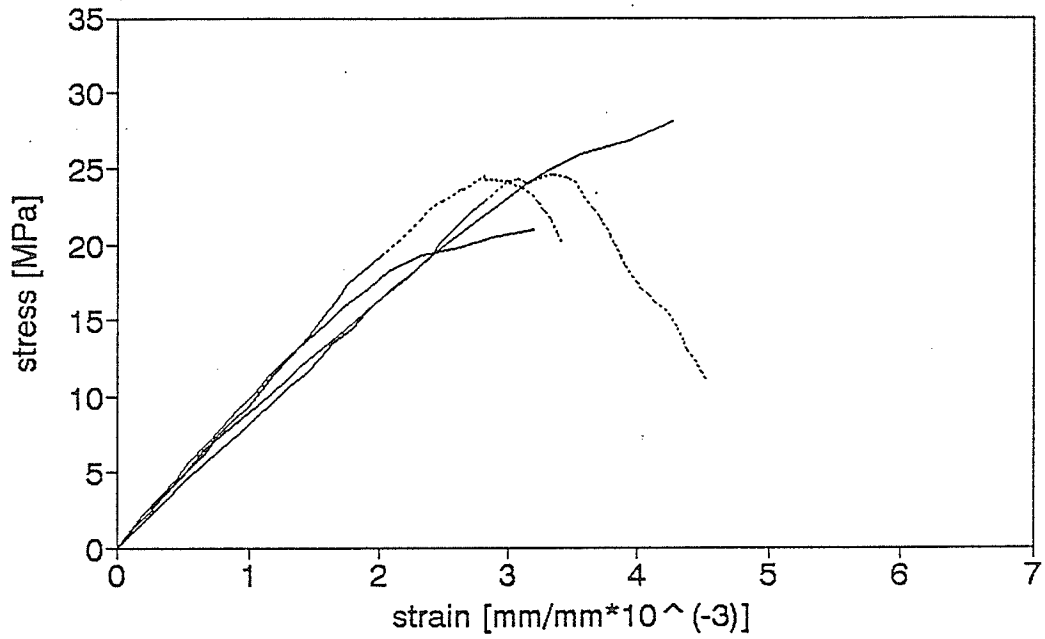


Figure A1.2. Stress-strain relationship for compression tests

# POLE #5 MATERIAL PROPERTIES

TESTS 1 to 4



# POLE #6 MATERIAL PROPERTIES

TESTS 1 to 4

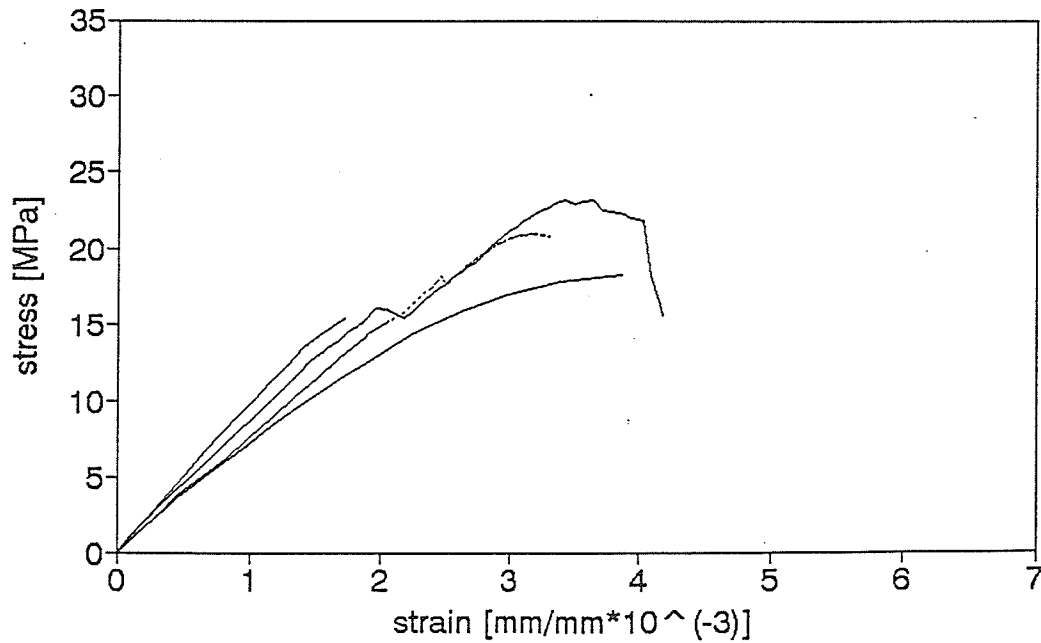
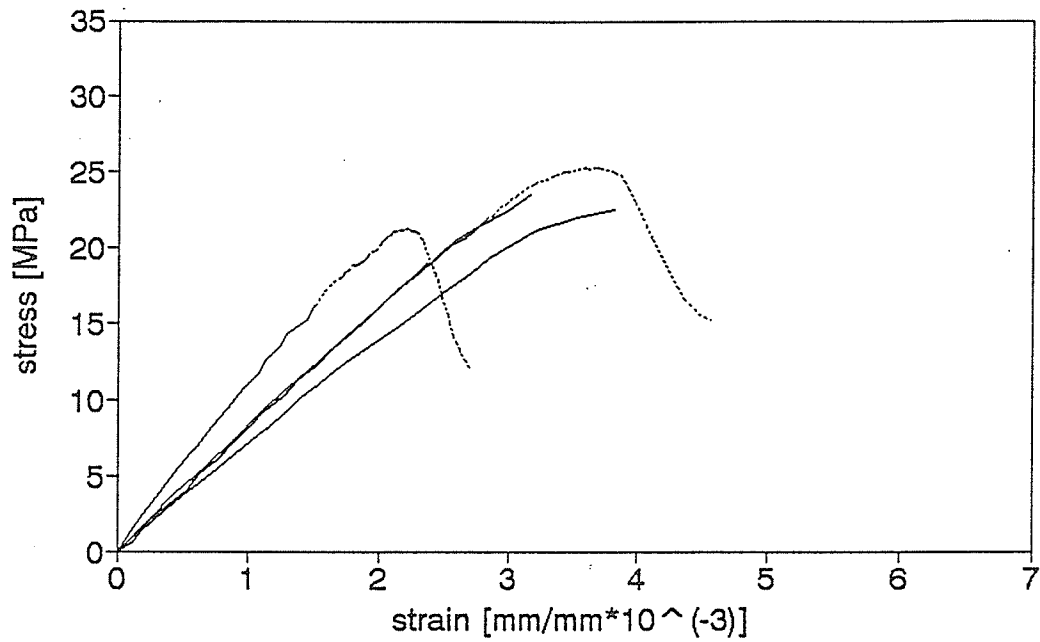


Figure A1.3. Stress-strain relationship for compression tests

# POLE #7 MATERIAL PROPERTIES

## TESTS 1 to 4



# POLE #8 MATERIAL PROPERTIES

## TESTS 1 to 4

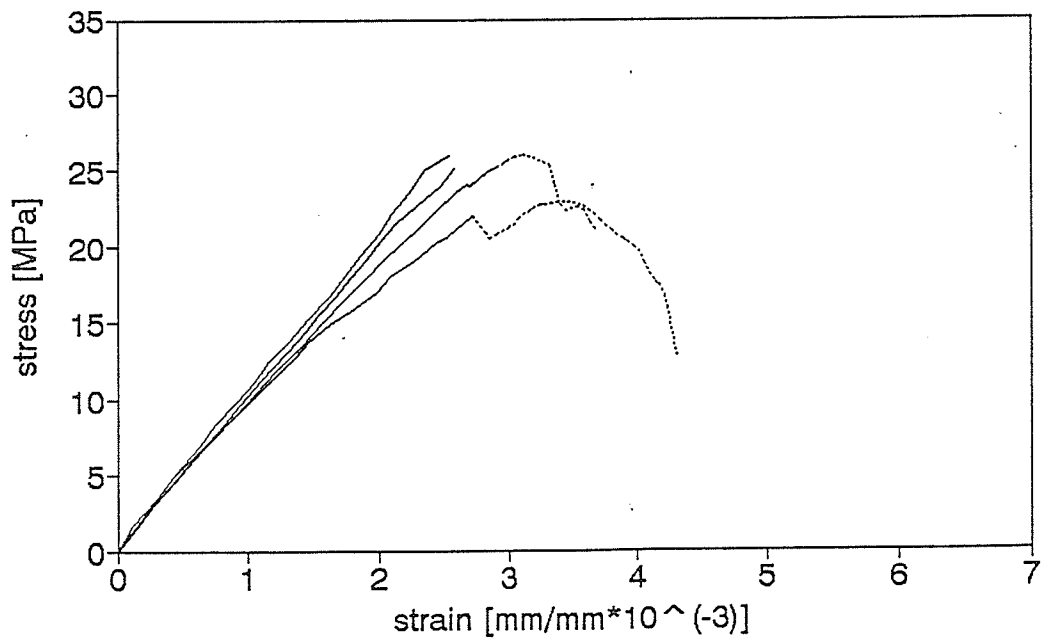
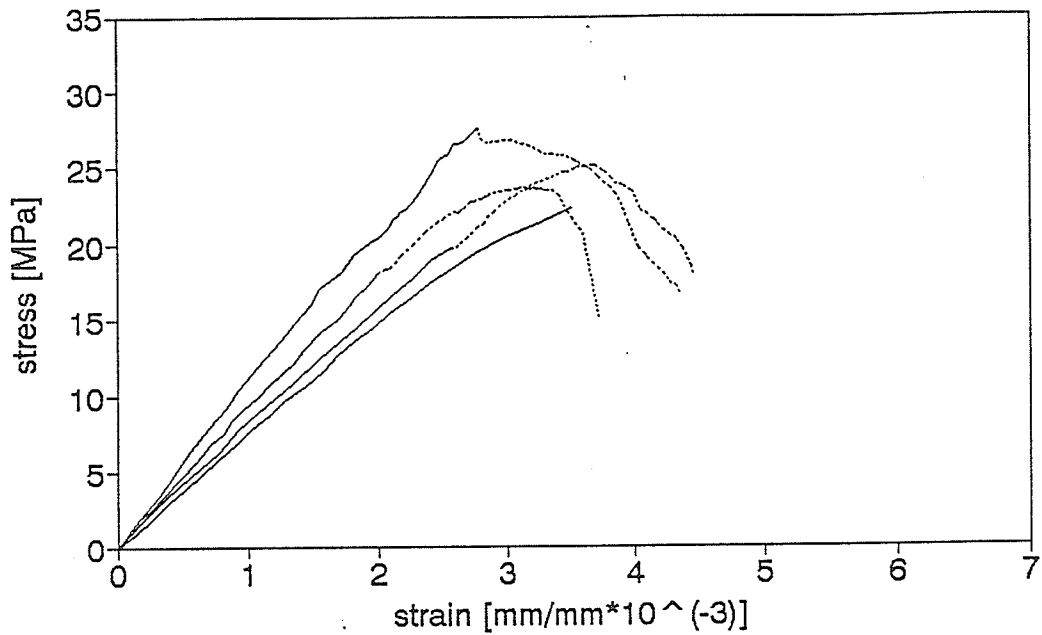


Figure A1.4. Stress-strain relationship for compression tests

## POLE #9 MATERIAL PROPERTIES

TESTS 1 to 4



## POLE #10 MATERIAL PROPERTIES

TESTS 1 to 4

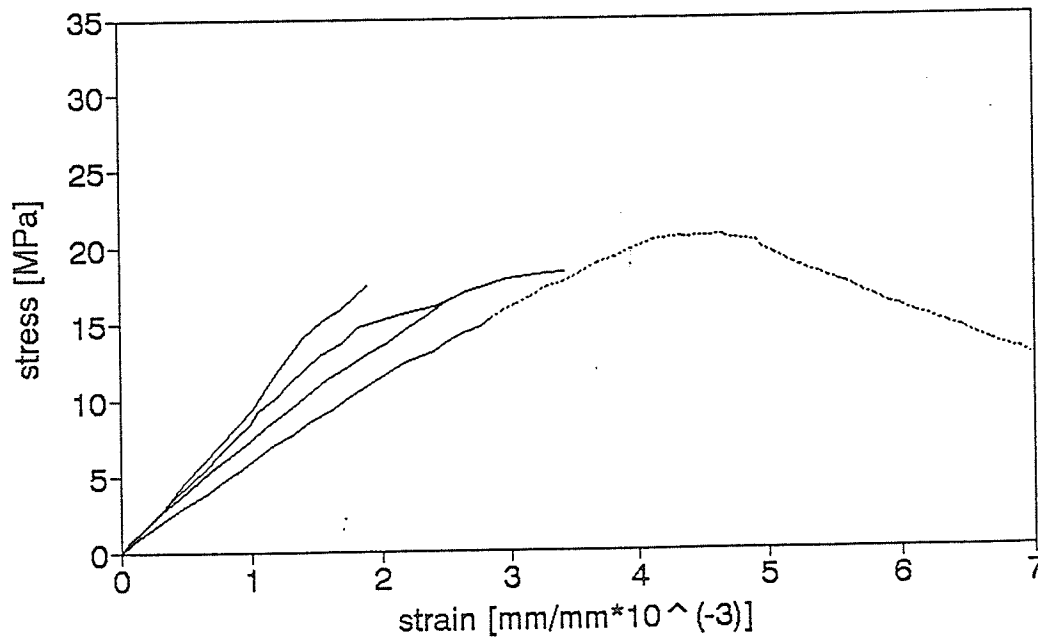
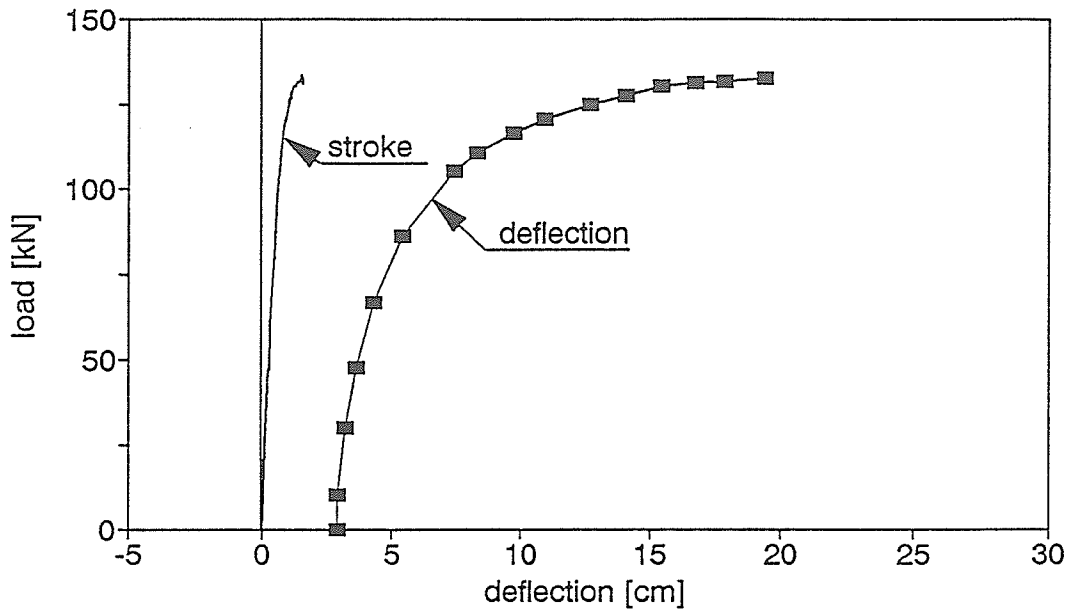


Figure A1.5. Stress-strain relationship for compression tests

## POLE 1/1 DEFLECTION AT THE MIDSPAN



## DEFLECTED SHAPE OF THE POLE 1/1 UNDER DIFFERENT LOAD LEVELS

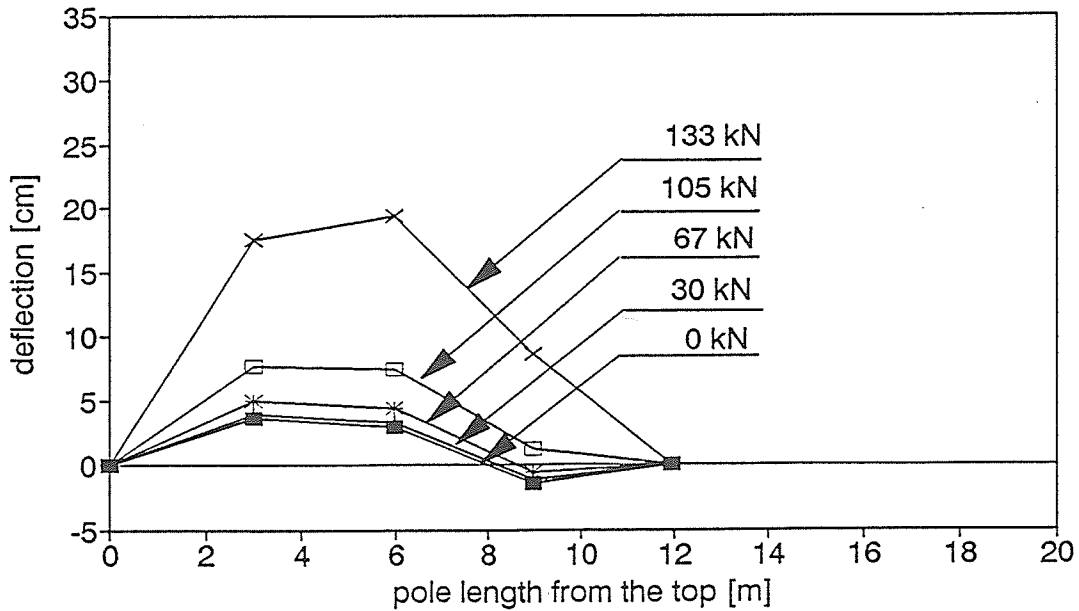
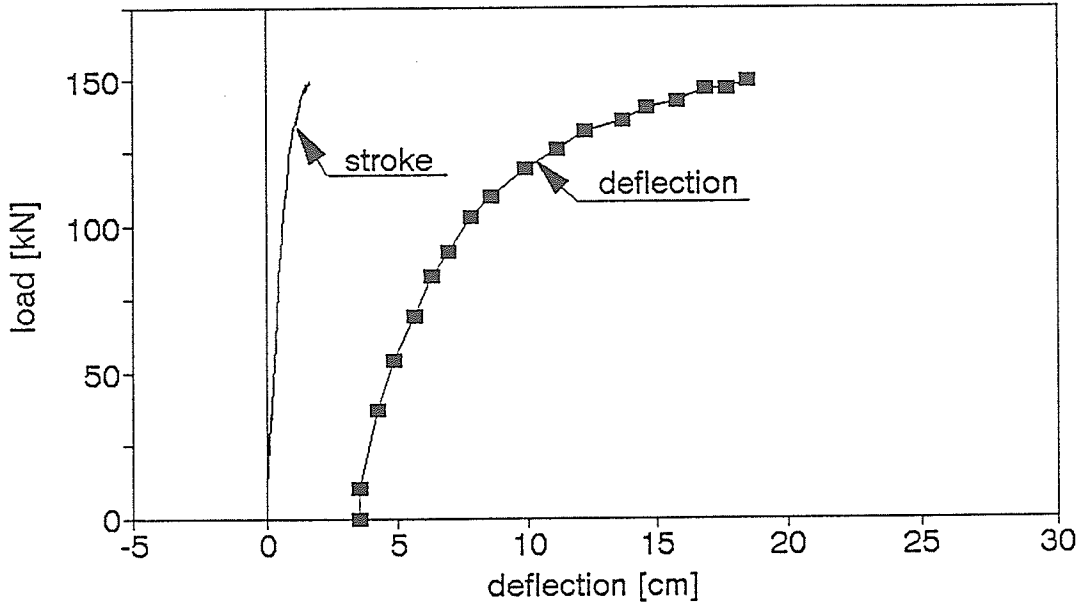


Figure A2.1. Load-deflection relationship and deflected shape of the pole

## POLE 1/2 DEFLECTION AT THE MIDSPAN



## DEFLECTED SHAPE OF THE POLE 1/2 UNDER DIFFERENT LOAD LEVELS

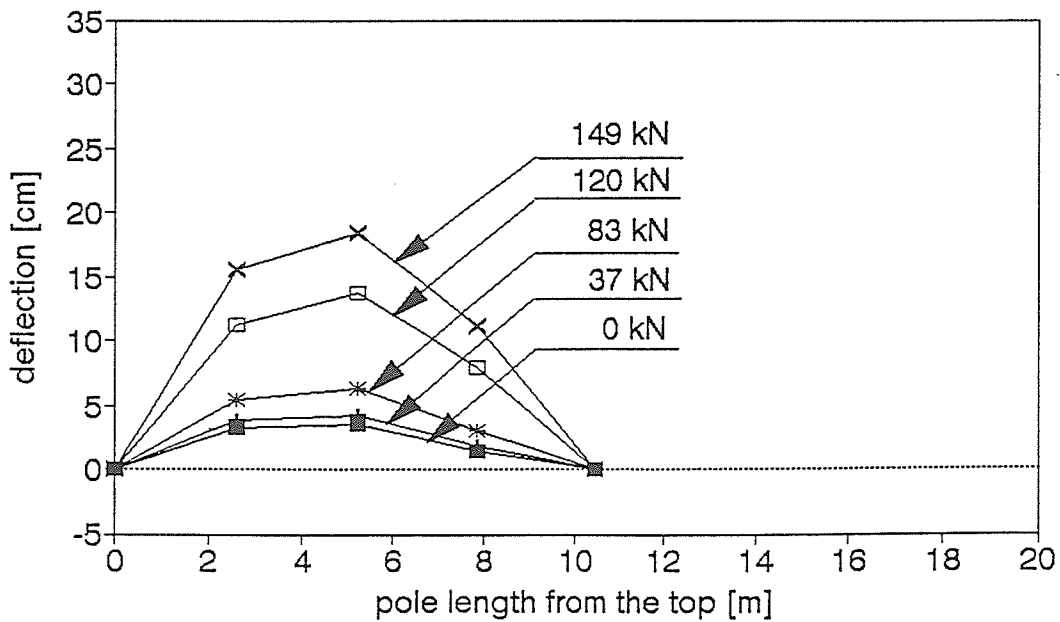
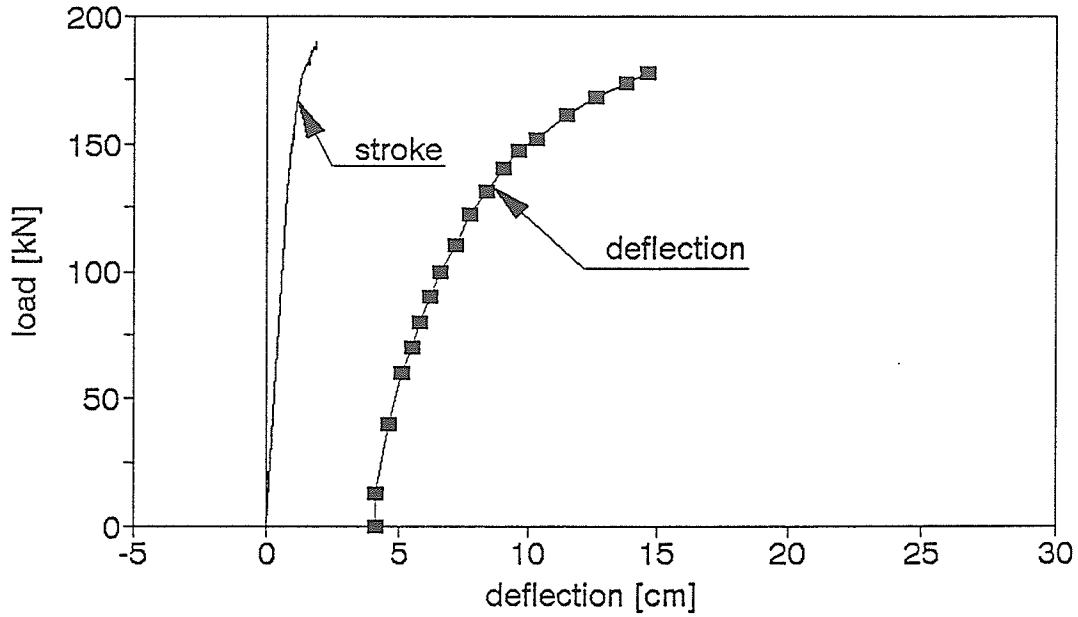


Figure A2.2. Load-deflection relationship and deflected shape of the pole

### POLE 1/3 DEFLECTION AT THE MIDSPAN



### DEFLECTED SHAPE OF THE POLE 1/3 UNDER DIFFERENT LOAD LEVELS

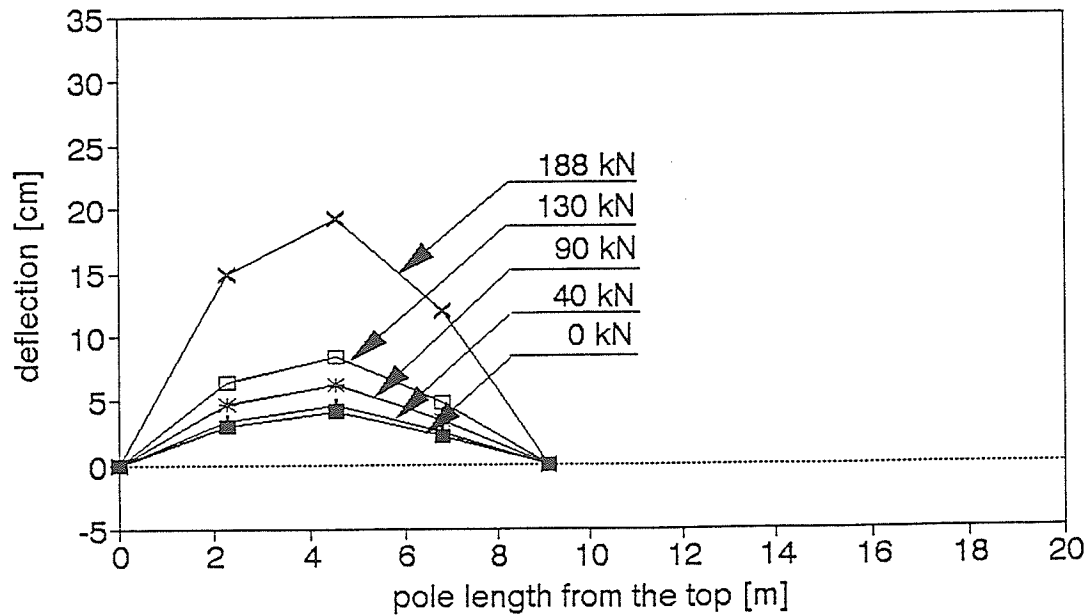
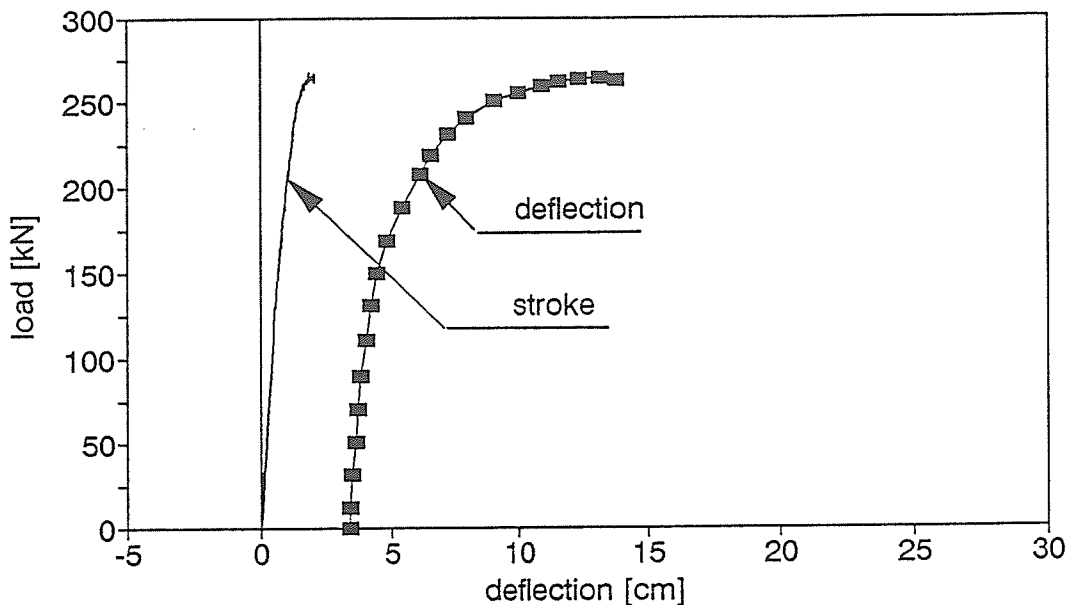


Figure A2.3. Load-deflection relationship and deflected shape of the pole

## POLE 1/4 DEFLECTION AT THE MIDSPAN



## DEFLECTED SHAPE OF THE POLE 1/4 UNDER DIFFERENT LOAD LEVELS

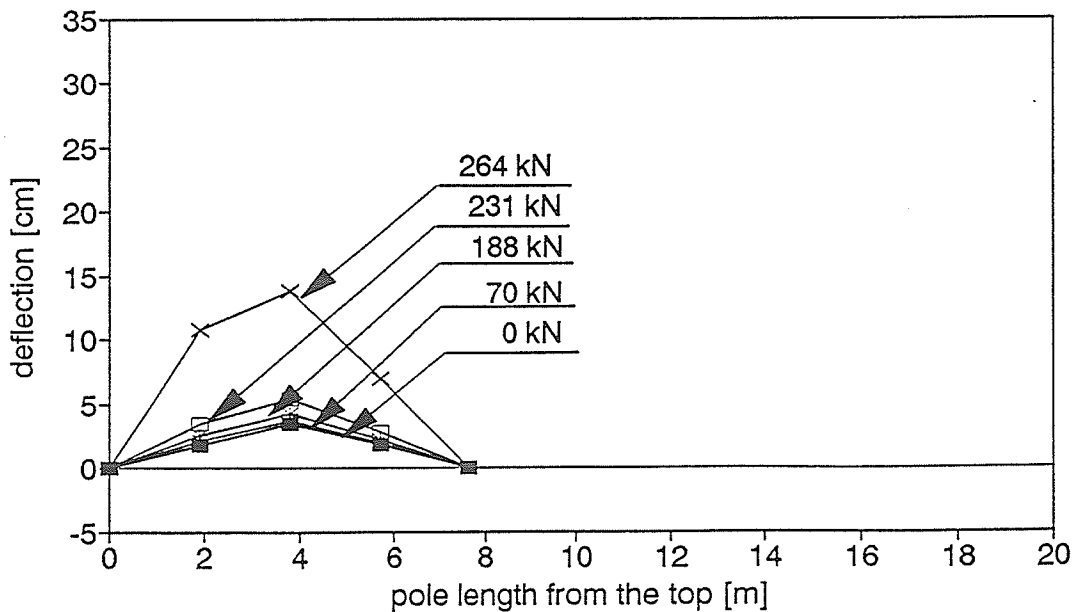
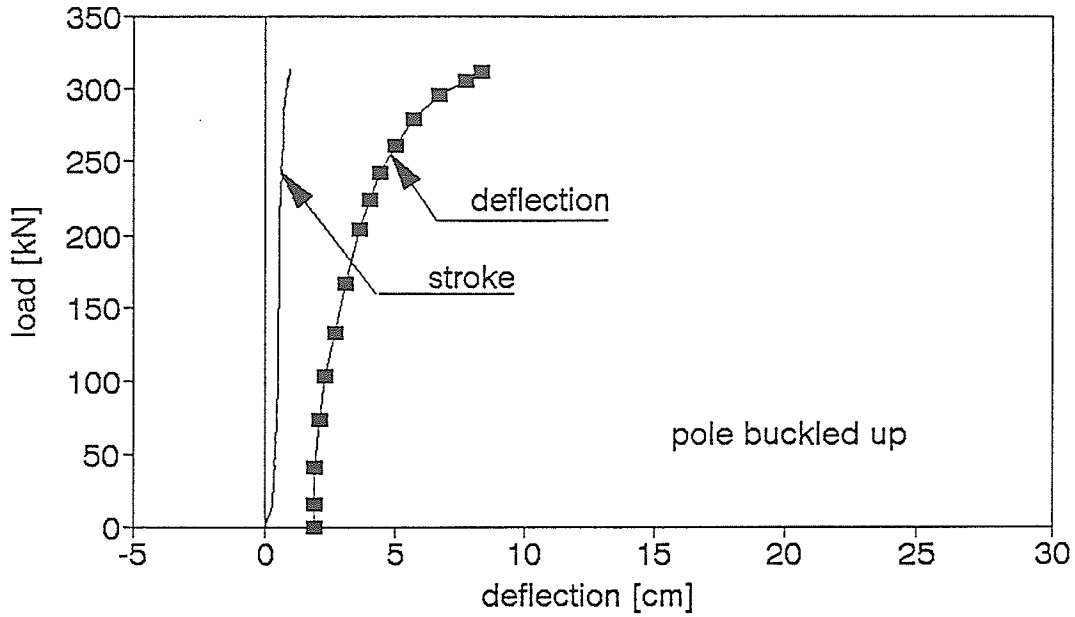


Figure A2.4. Load-deflection relationship and deflected shape of the pole

## POLE 1/5 DEFLECTION AT THE MIDSPAN



## DEFLECTED SHAPE OF THE POLE 1/5 UNDER DIFFERENT LOAD LEVELS

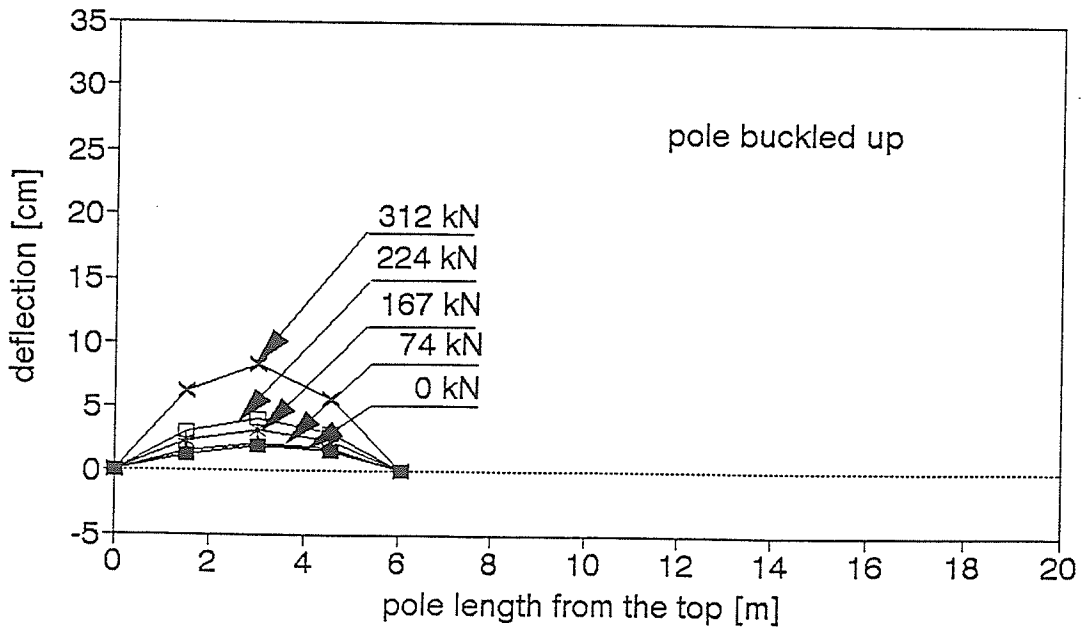
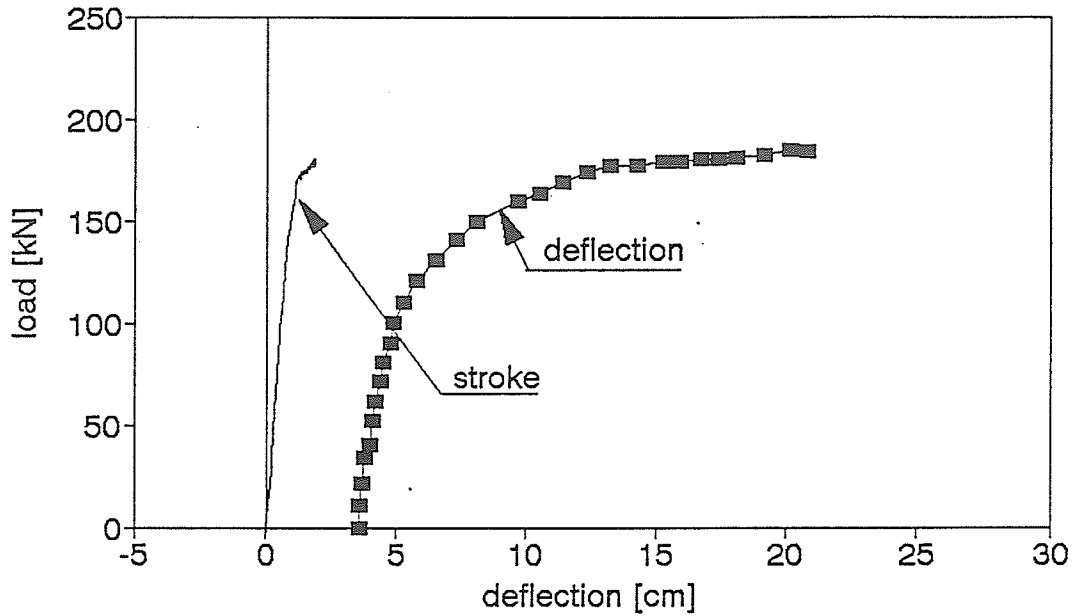


Figure A2.5. Load-deflection relationship and deflected shape of the pole

## POLE 2/1 test I DEFLECTION AT THE MIDSPAN



## DEFLECTED SHAPE OF THE POLE 2/1 UNDER DIFFERENT LOAD LEVELS (test I)

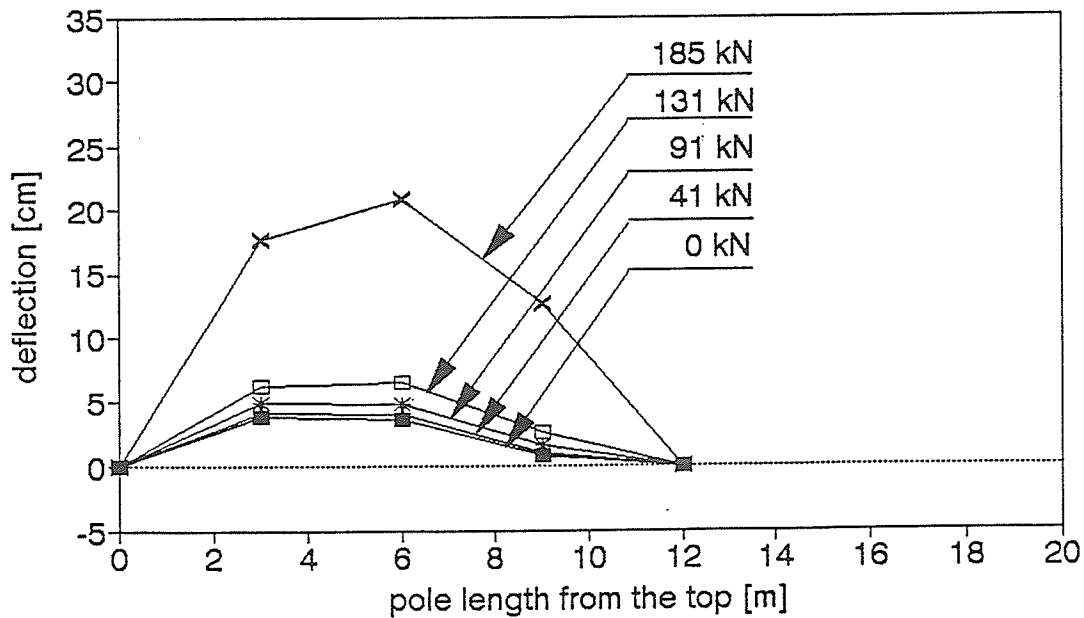
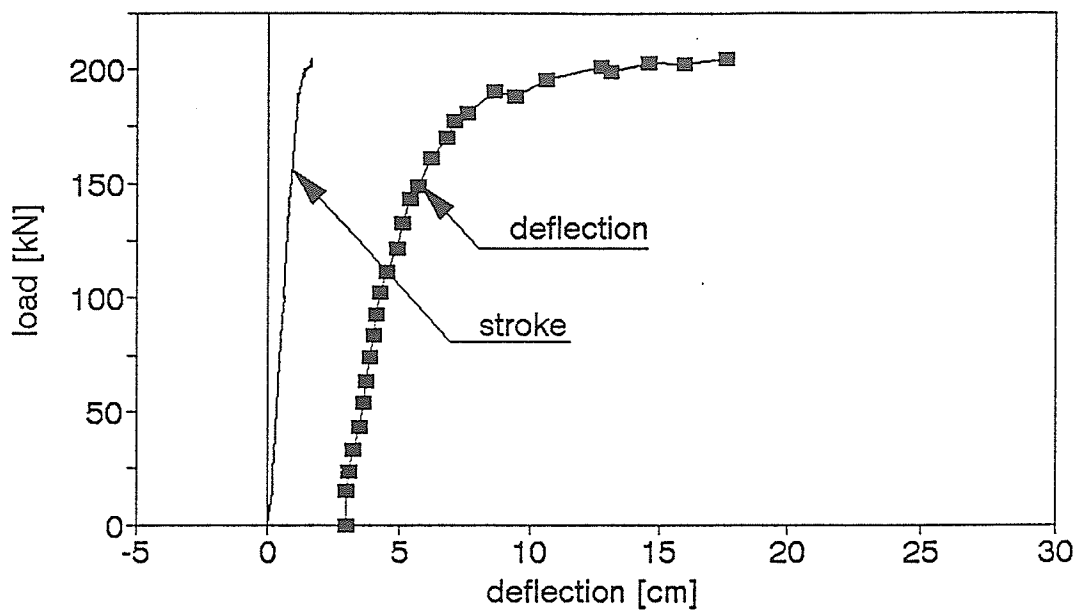


Figure A2.6. Load-deflection relationship and deflected shape of the pole

## POLE 2/1 test II DEFLECTION AT THE MIDSPAN



## DEFLECTED SHAPE OF THE POLE 2/1 UNDER DIFFERENT LOAD LEVELS (test II)

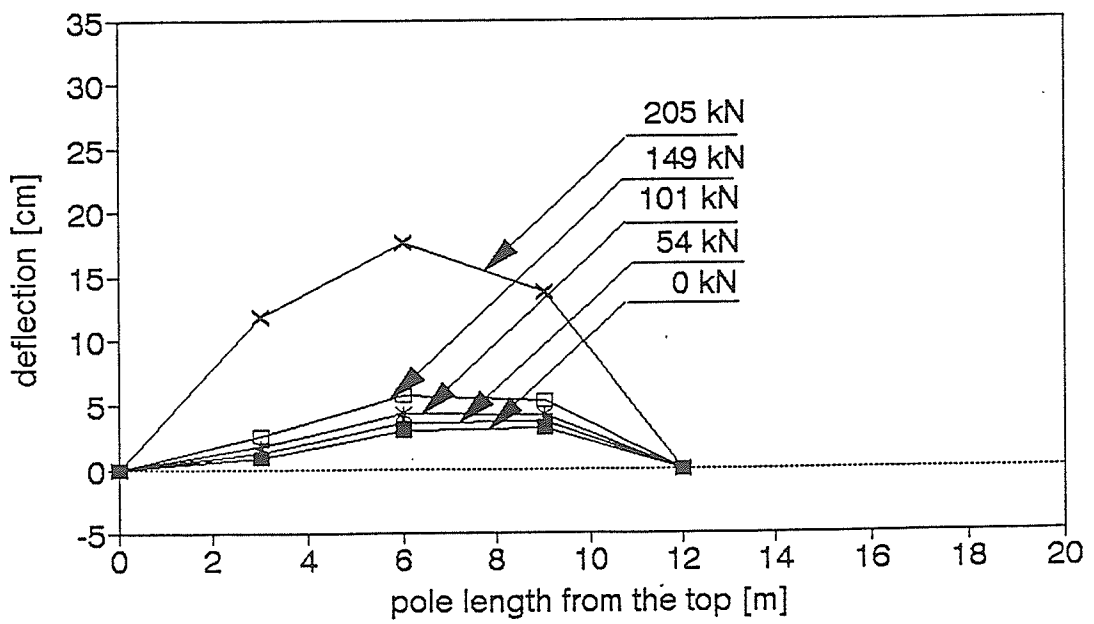
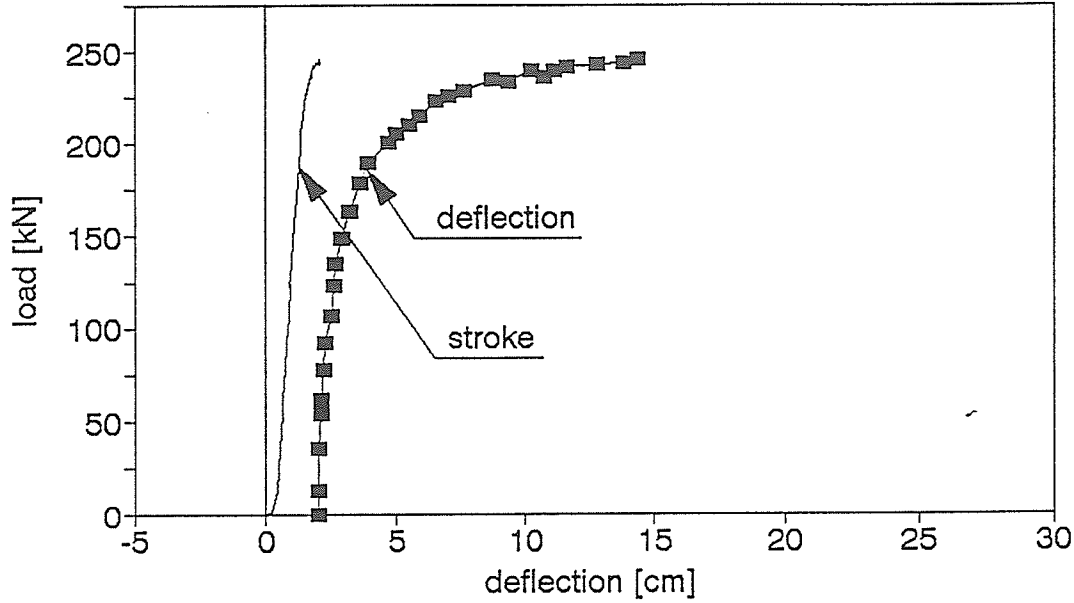


Figure A2.7. Load-deflection relationship and deflected shape of the pole

## POLE 2/2 DEFLECTION AT THE MIDSPAN



## DEFLECTED SHAPE OF THE POLE 2/2 UNDER DIFFERENT LOAD LEVELS

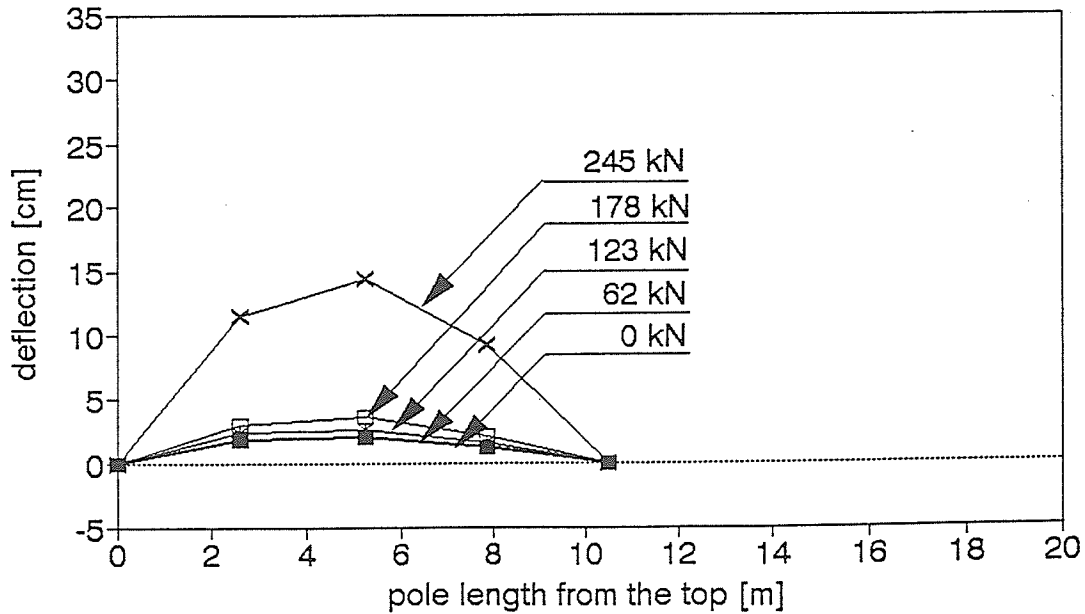
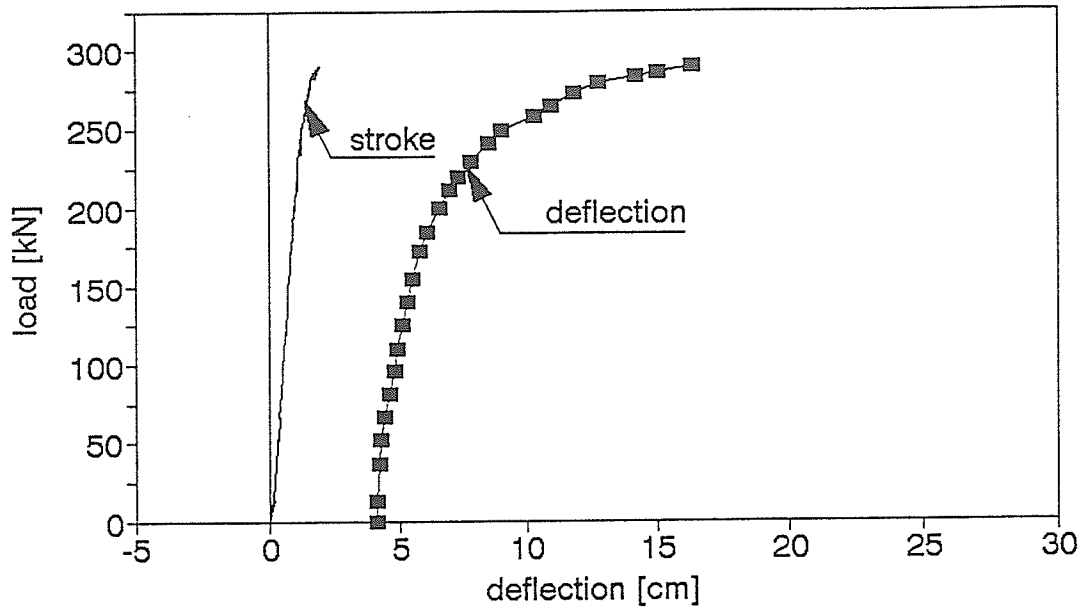


Figure A2.8. Load-deflection relationship and deflected shape of the pole

## POLE 2/3 DEFLECTION AT THE MIDSPAN



## DEFLECTED SHAPE OF THE POLE 2/3 UNDER DIFFERENT LOAD LEVELS

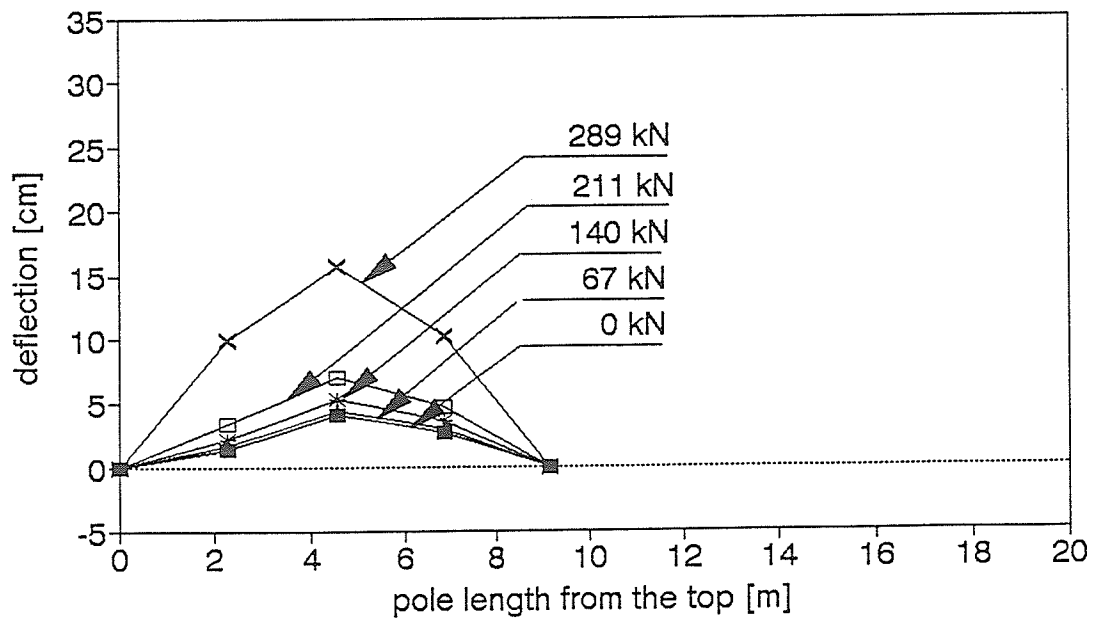
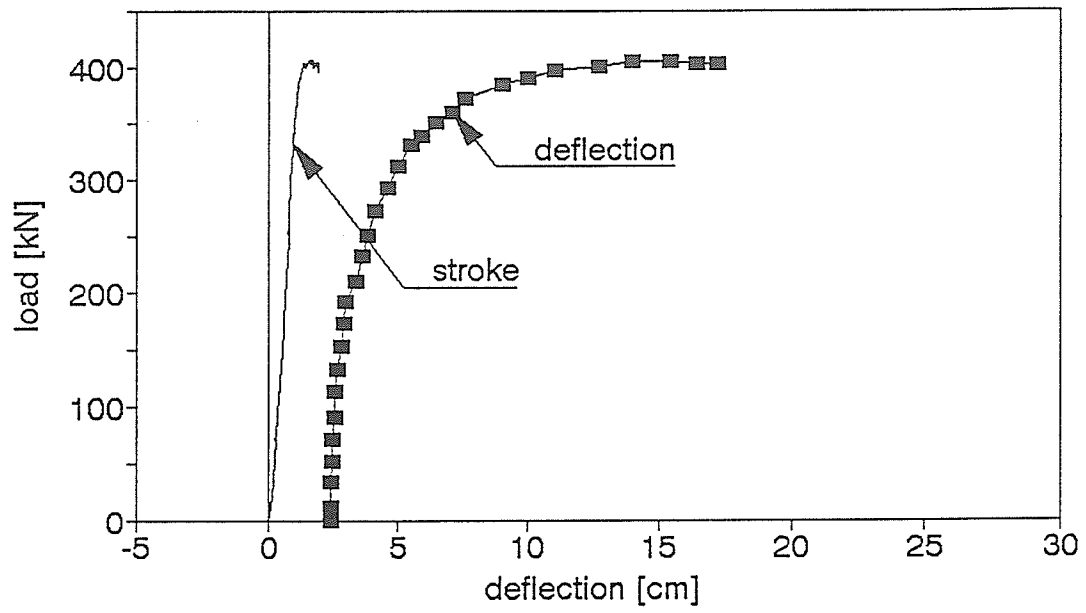


Figure A2.9. Load-deflection relationship and deflected shape of the pole

### POLE 2/4 DEFLECTION AT THE MIDSPAN



### DEFLECTED SHAPE OF THE POLE 2/4 UNDER DIFFERENT LOAD LEVELS

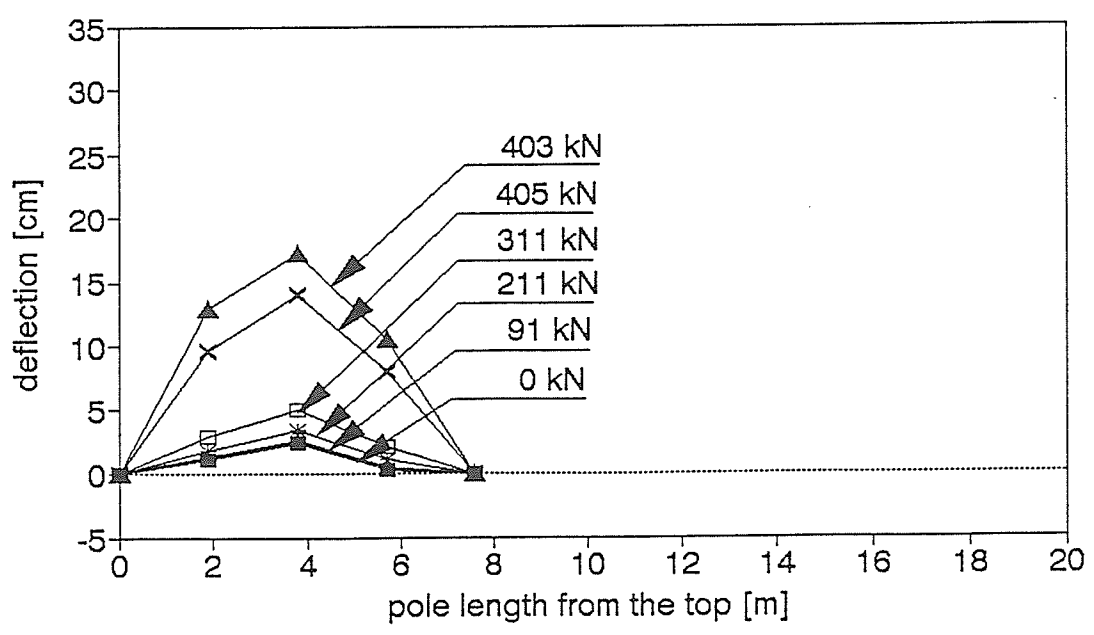
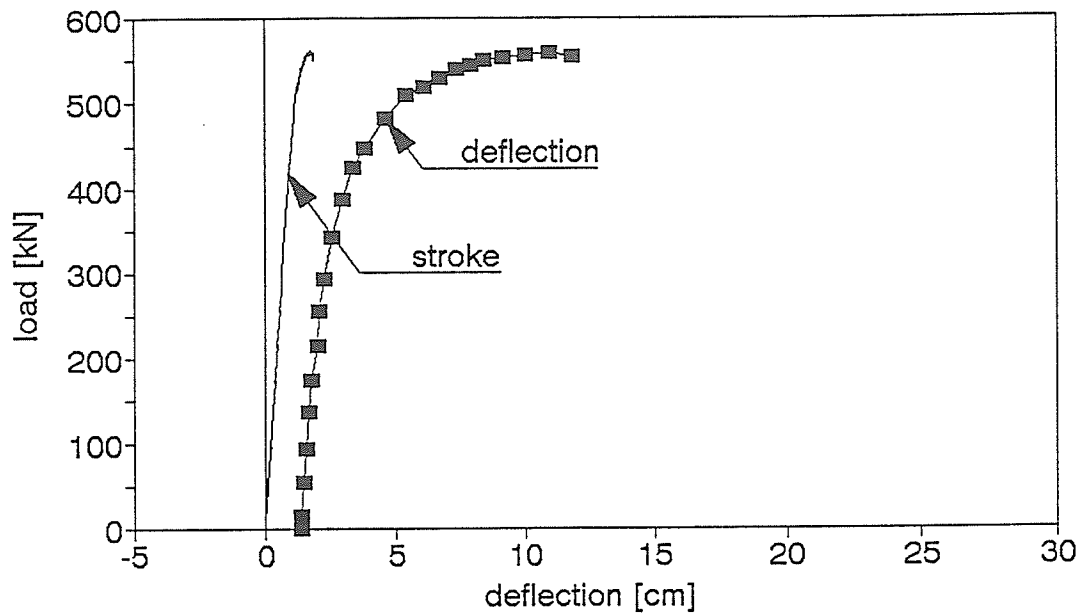


Figure A2.10. Load-deflection relationship and deflected shape of the pole

## POLE 2/5 DEFLECTION AT THE MIDSPAN



## DEFLECTED SHAPE OF THE POLE 2/5 UNDER DIFFERENT LOAD LEVELS

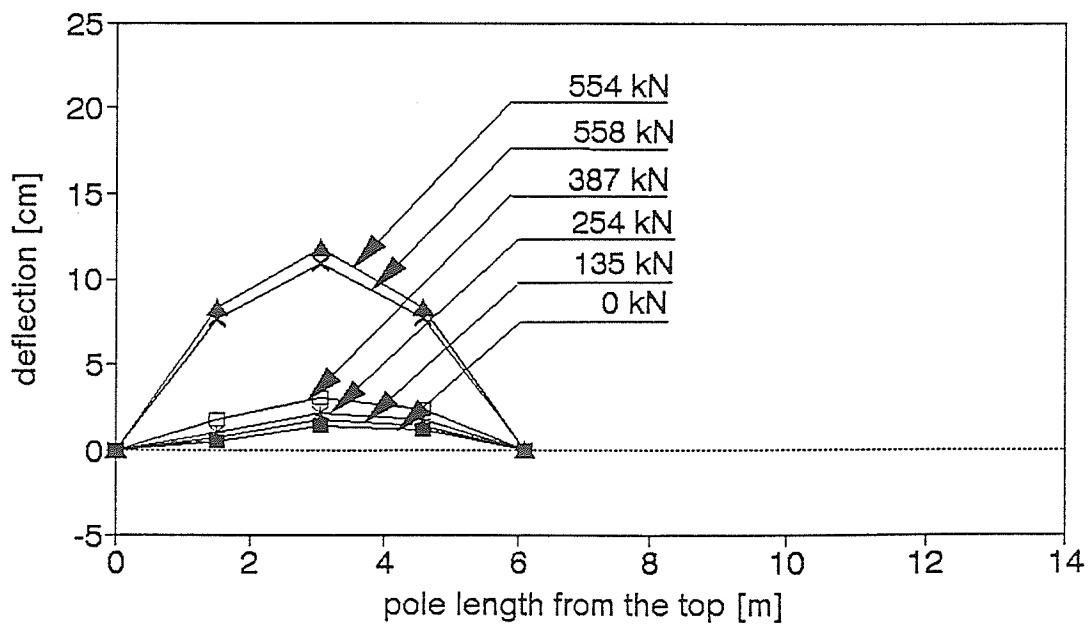
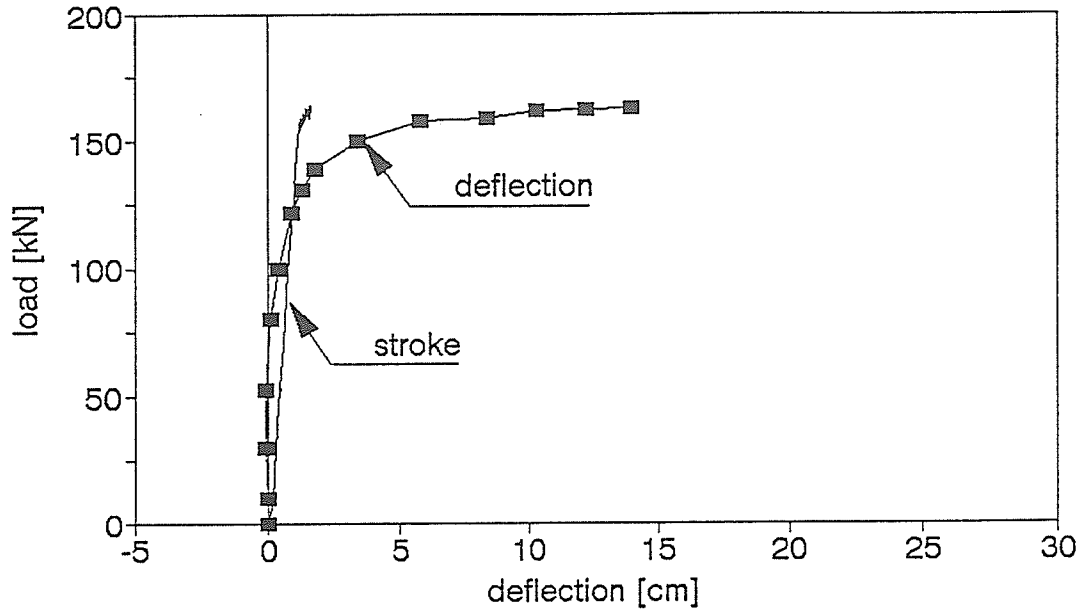


Figure A2.11. Load-deflection relationship and deflected shape of the pole

## POLE 3/1 DEFLECTION AT THE MIDSPAN



## DEFLECTED SHAPE OF THE POLE 3/1 UNDER DIFFERENT LOAD LEVELS

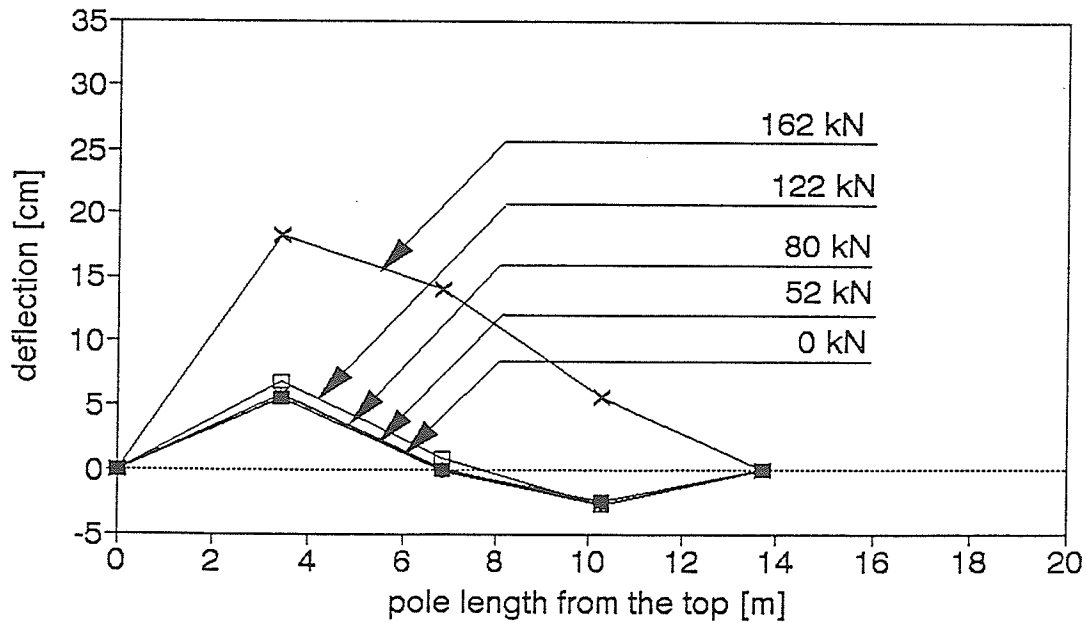
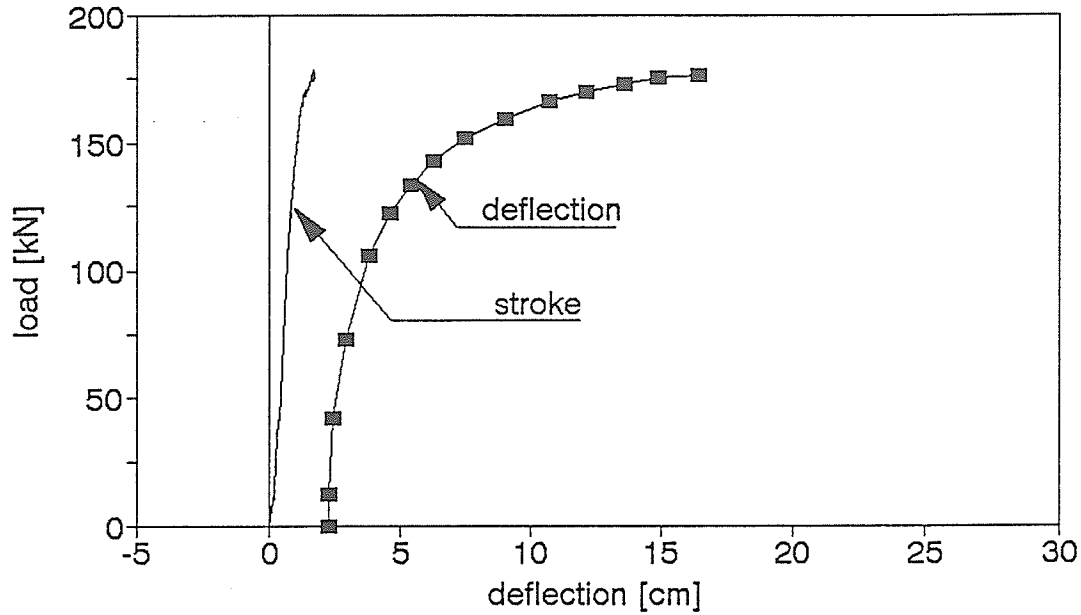


Figure A2.12. Load-deflection relationship and deflected shape of the pole

## POLE 3/2 DEFLECTION AT THE MIDSPAN



## DEFLECTED SHAPE OF THE POLE 3/2 UNDER DIFFERENT LOAD LEVELS

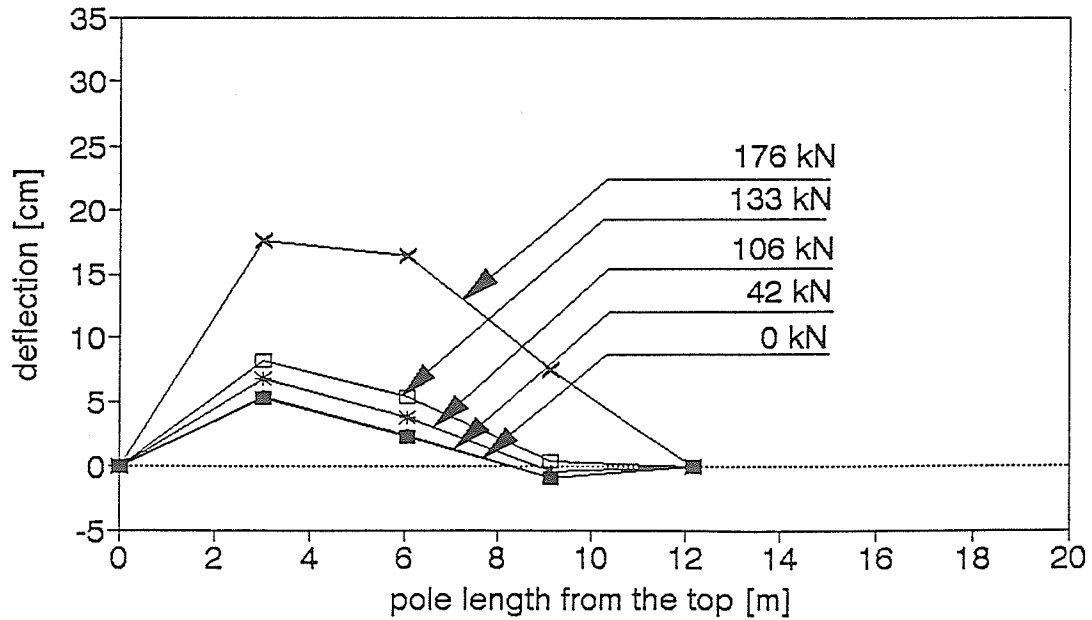
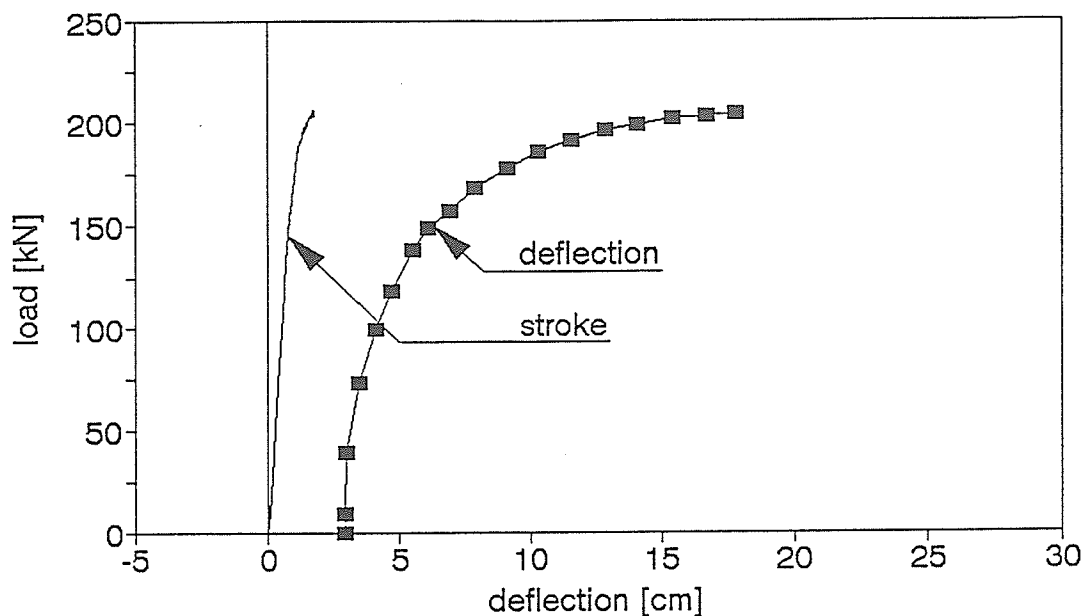


Figure A2.13. Load-deflection relationship and deflected shape of the pole

### POLE 3/3 DEFLECTION AT THE MIDSPAN



### DEFLECTED SHAPE OF THE POLE 3/3 UNDER DIFFERENT LOAD LEVELS

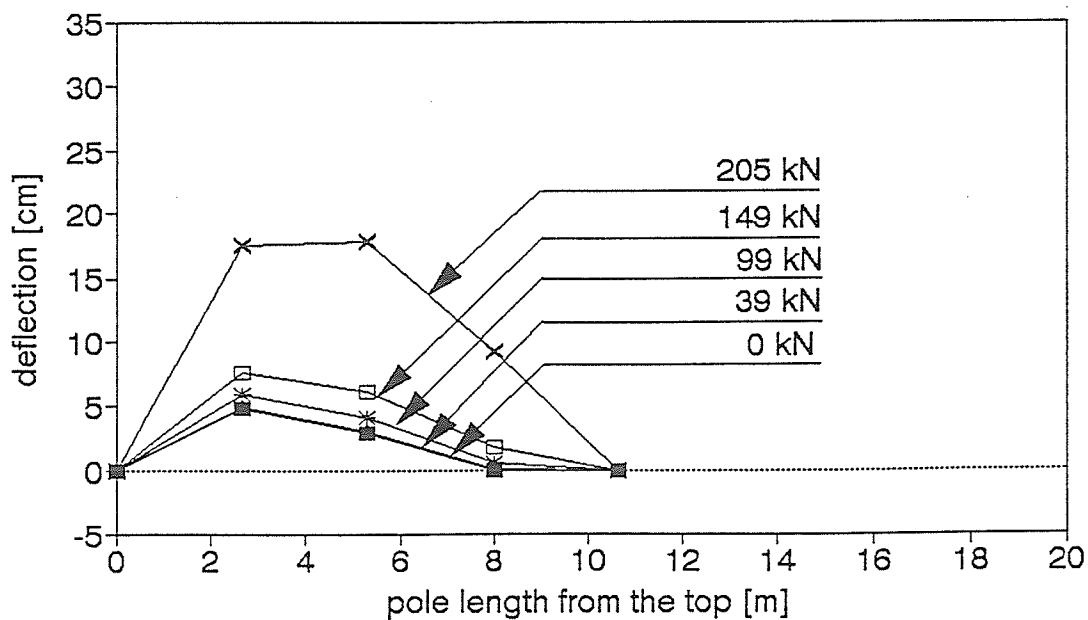
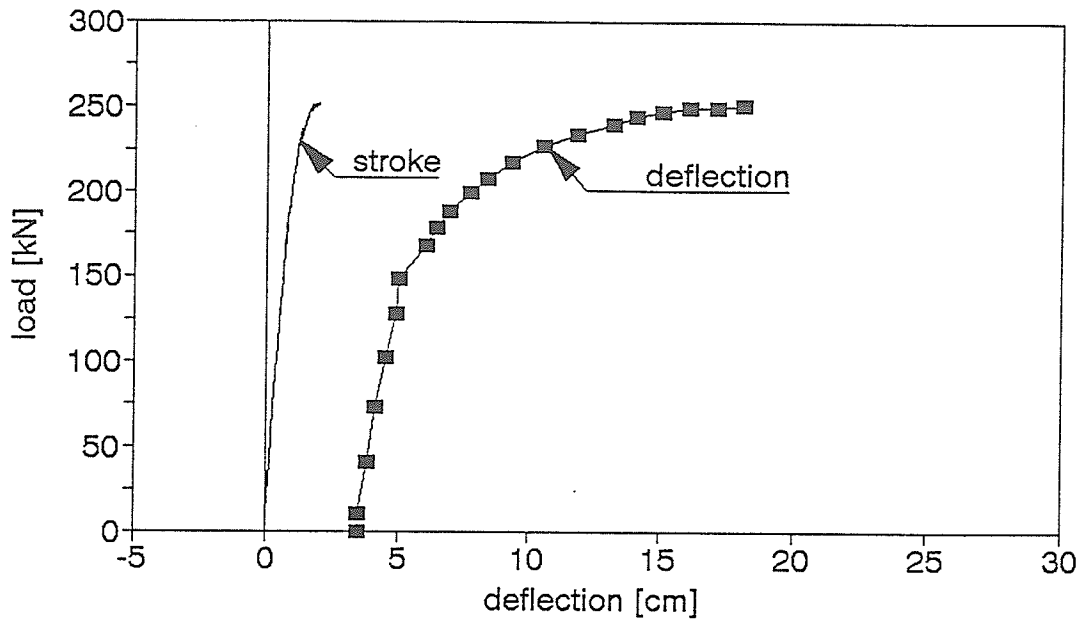


Figure A2.14. Load-deflection relationship and deflected shape of the pole

## POLE 3/4 DEFLECTION AT THE MIDSPAN



## DEFLECTED SHAPE OF THE POLE 3/4 UNDER DIFFERENT LOAD LEVELS

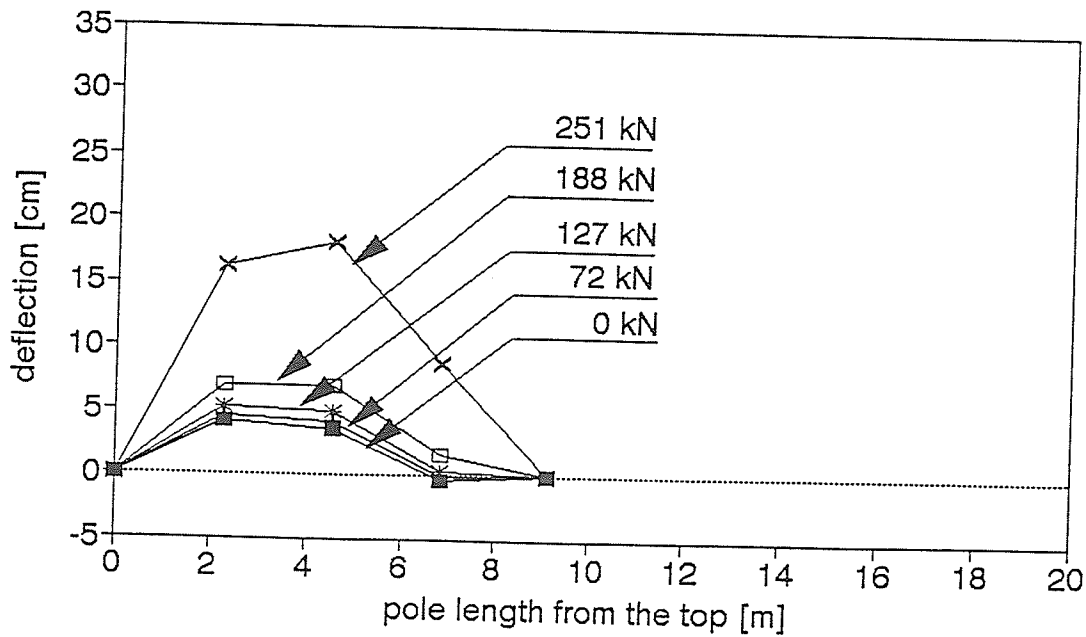
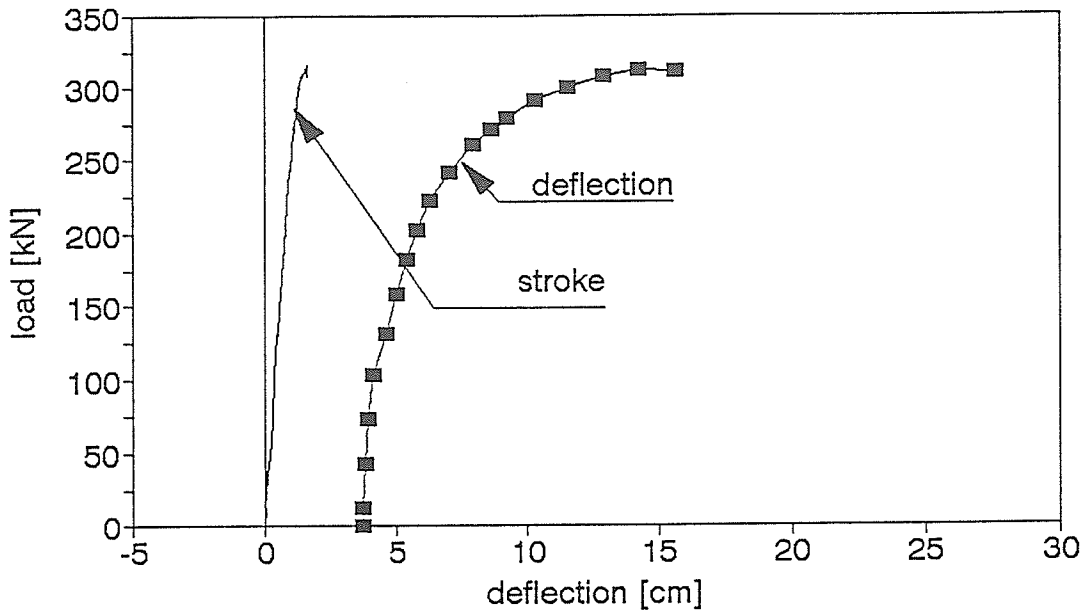


Figure A2.15. Load-deflection relationship and deflected shape of the pole

## POLE 3/5 DEFLECTION AT THE MIDSPAN



## DEFLECTED SHAPE OF THE POLE 3/5 UNDER DIFFERENT LOAD LEVELS

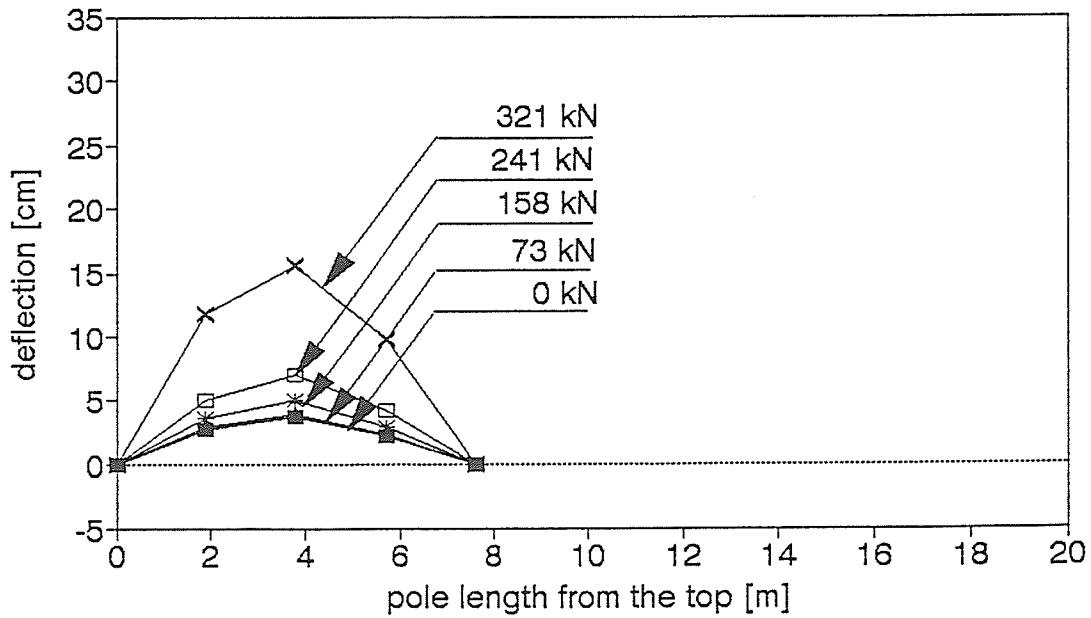
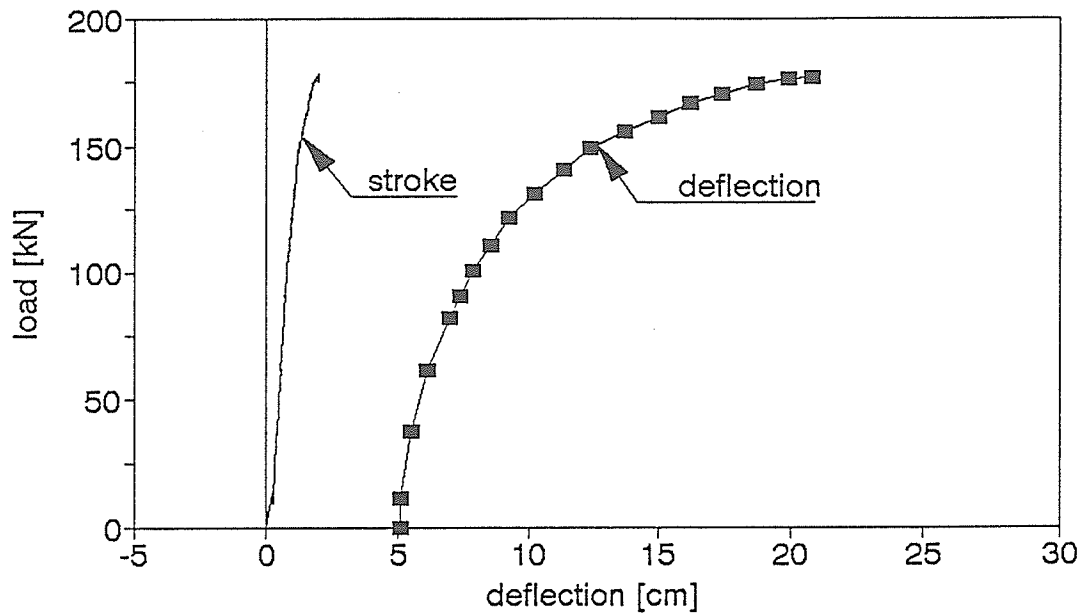


Figure A2.16. Load-deflection relationship and deflected shape of the pole

## POLE 4/1 DEFLECTION AT THE MIDSPAN



## DEFLECTED SHAPE OF THE POLE 4/1 UNDER DIFFERENT LOAD LEVELS

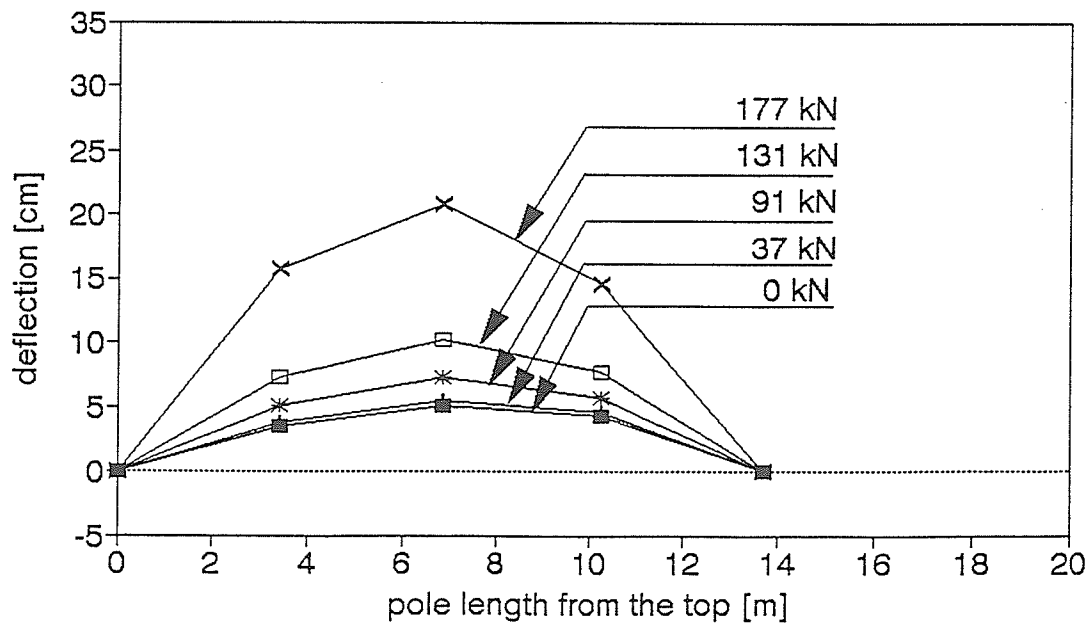
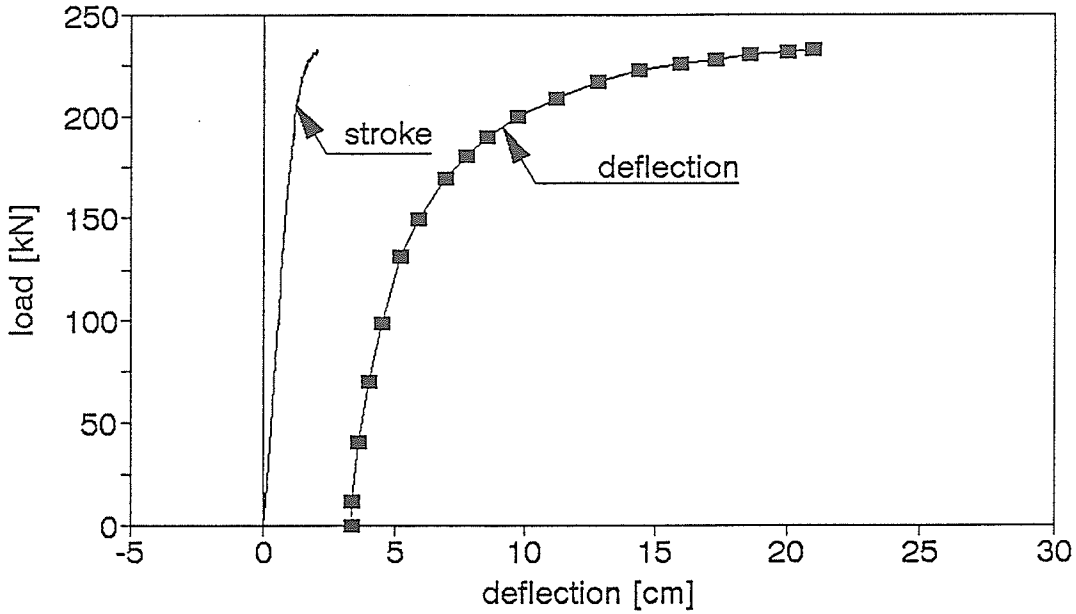


Figure A2.17. Load-deflection relationship and deflected shape of the pole

## POLE 4/2 DEFLECTION AT THE MIDSPAN



## DEFLECTED SHAPE OF THE POLE 4/2 UNDER DIFFERENT LOAD LEVELS

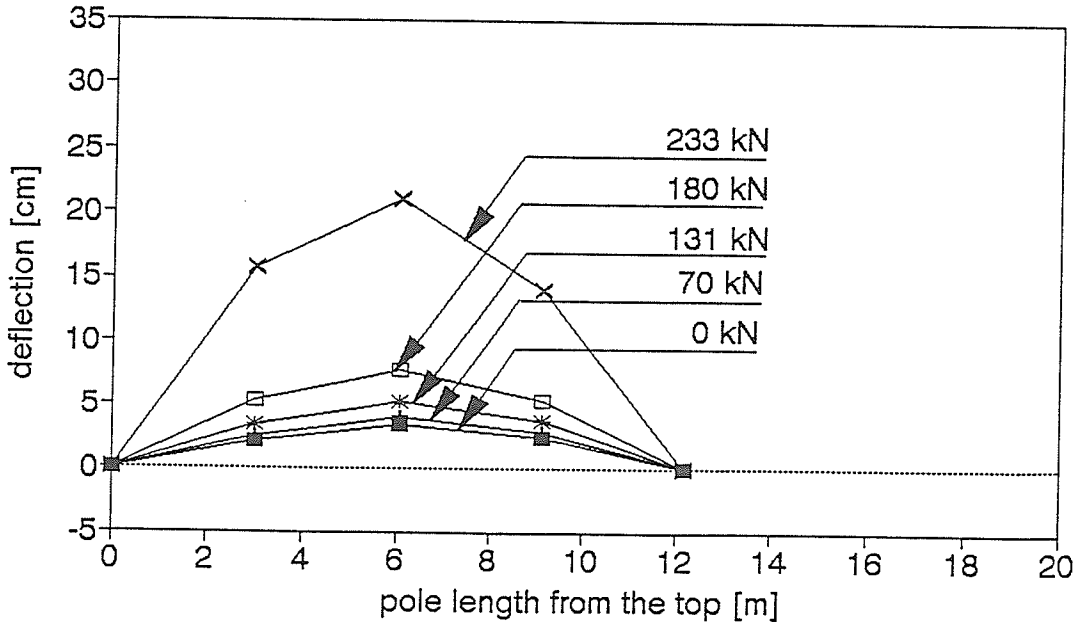
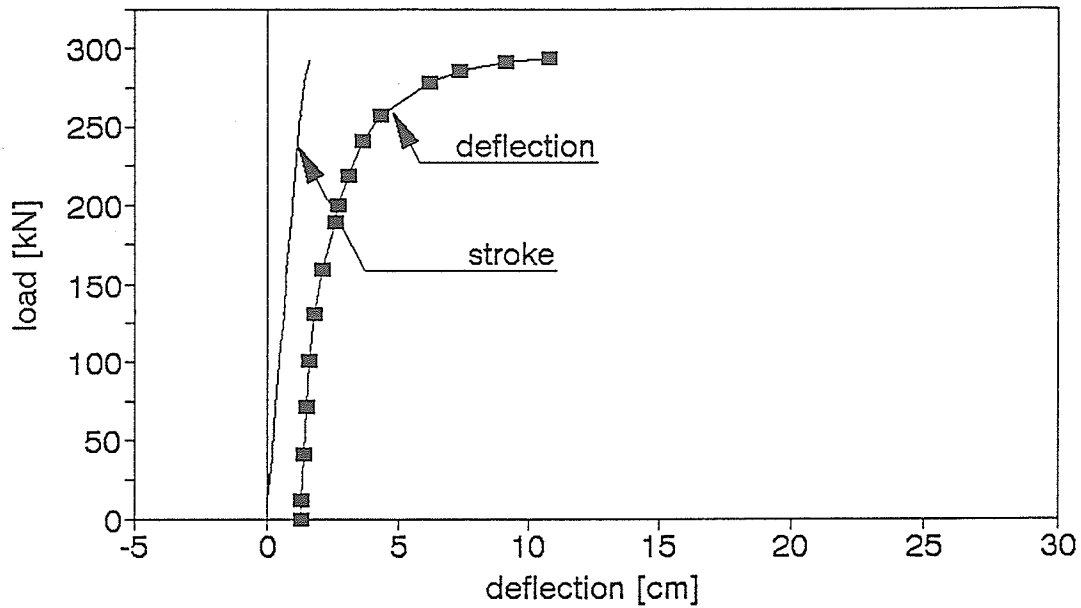


Figure A2.18. Load-deflection relationship and deflected shape of the pole

## POLE 4/3 DEFLECTION AT THE MIDSPAN



## DEFLECTED SHAPE OF THE POLE 4/3 UNDER DIFFERENT LOAD LEVELS

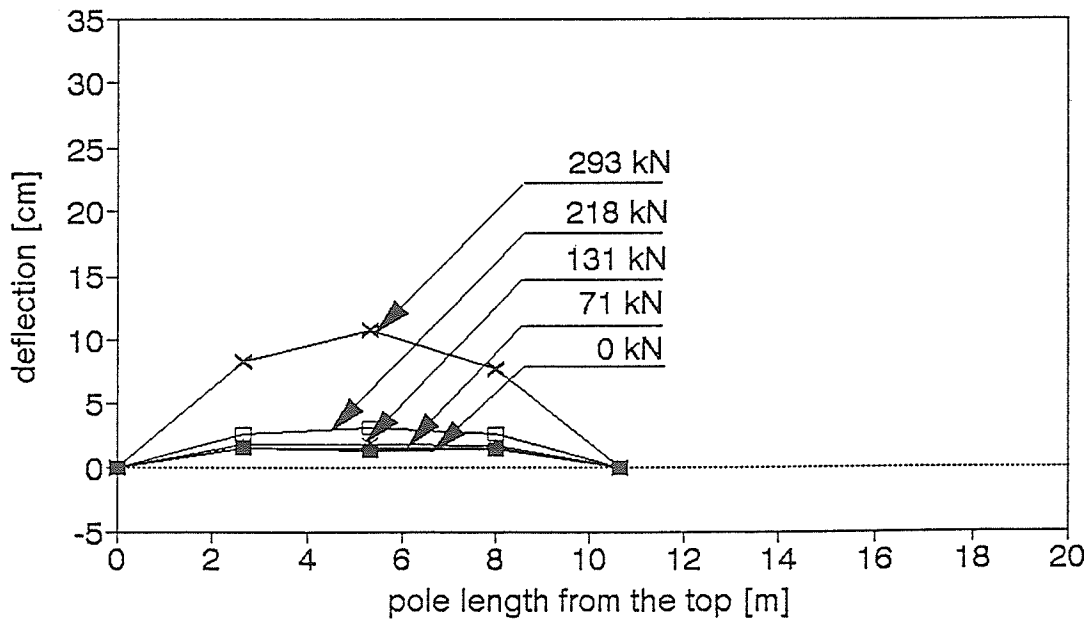
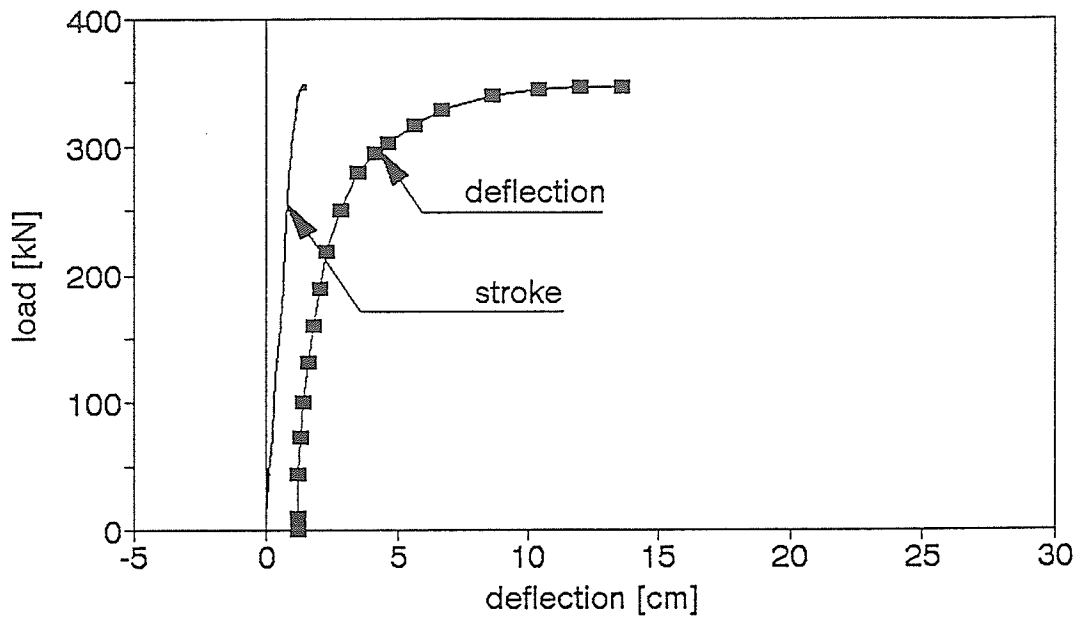


Figure A2.19. Load-deflection relationship and deflected shape of the pole

## POLE 4/4 DEFLECTION AT THE MIDSPAN



## DEFLECTED SHAPE OF THE POLE 4/4 UNDER DIFFERENT LOAD LEVELS

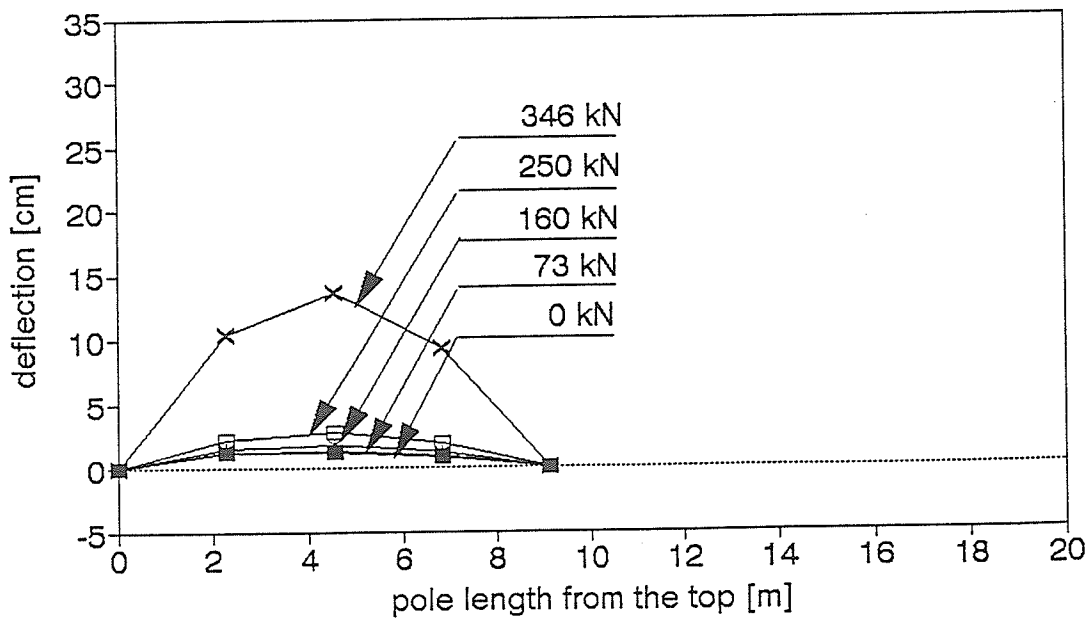
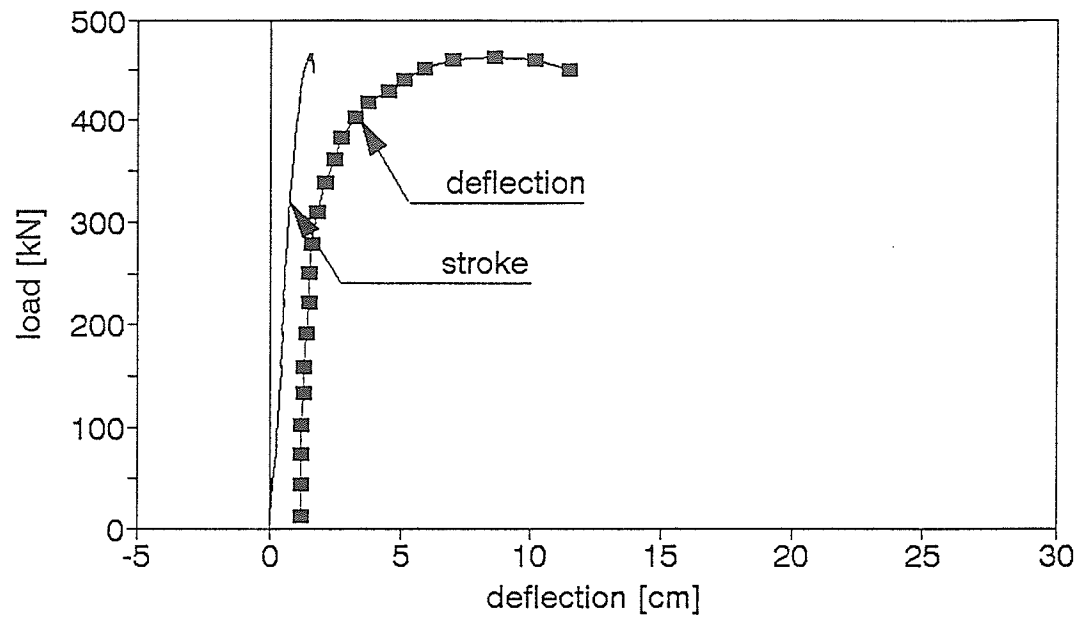


Figure A2.20. Load-deflection relationship and deflected shape of the pole

### POLE 4/5 DEFLECTION AT THE MIDSPAN



### DEFLECTED SHAPE OF THE POLE 4/5 UNDER DIFFERENT LOAD LEVELS

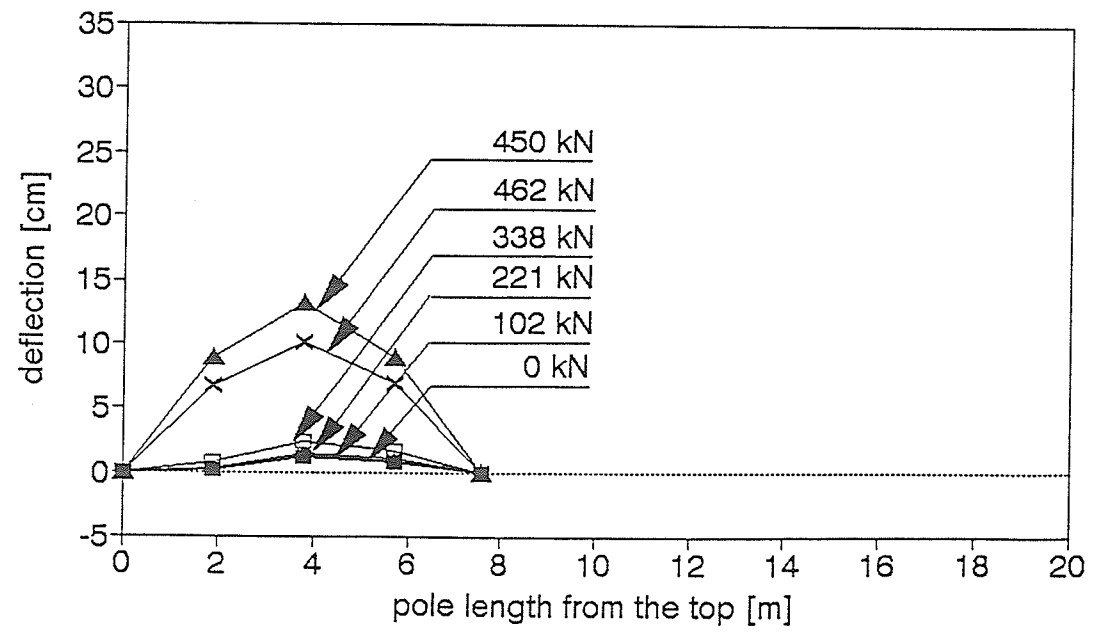
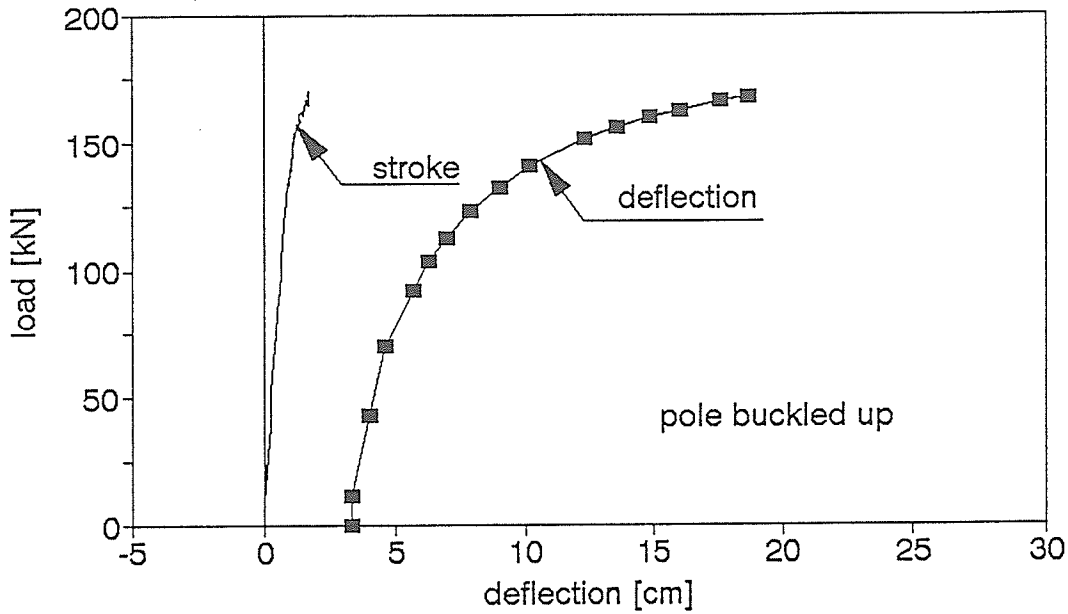


Figure A2.21. Load-deflection relationship and deflected shape of the pole

## POLE 5/1 DEFLECTION AT THE MIDSPAN



## DEFLECTED SHAPE OF THE POLE 5/1 UNDER DIFFERENT LOAD LEVELS

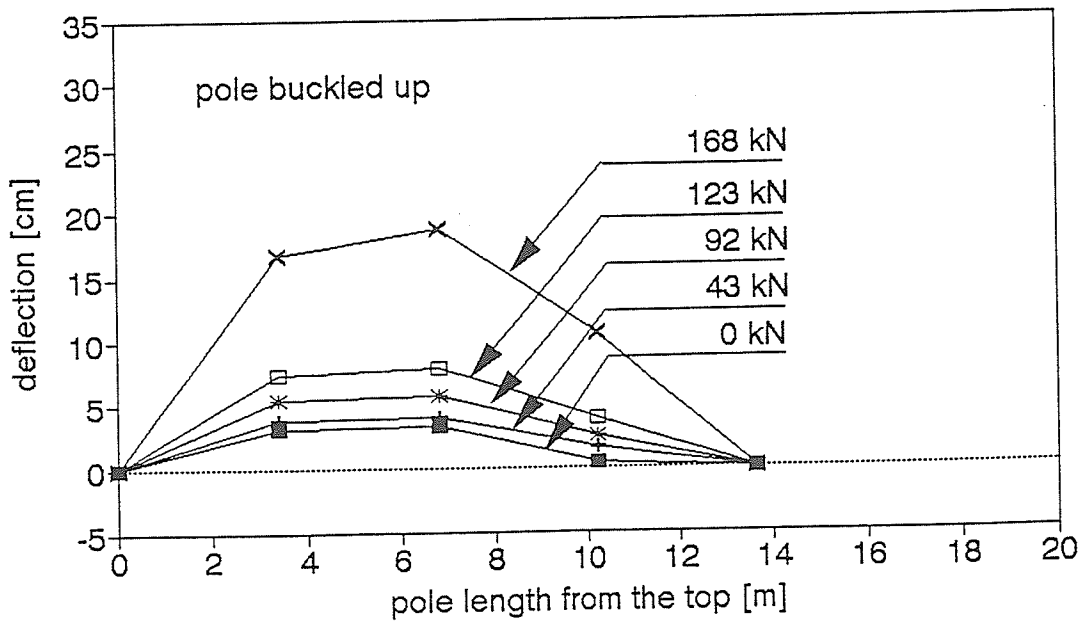
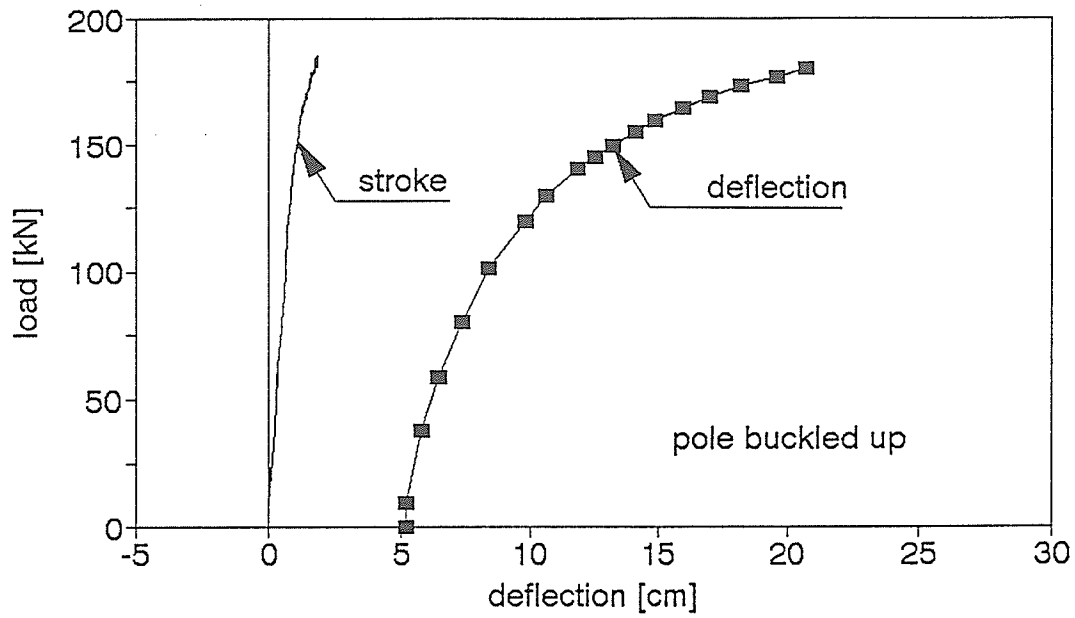


Figure A2.22. Load-deflection relationship and deflected shape of the pole

## POLE 5/2 DEFLECTION AT THE MIDSPAN



## DEFLECTED SHAPE OF THE POLE 5/2 UNDER DIFFERENT LOAD LEVELS

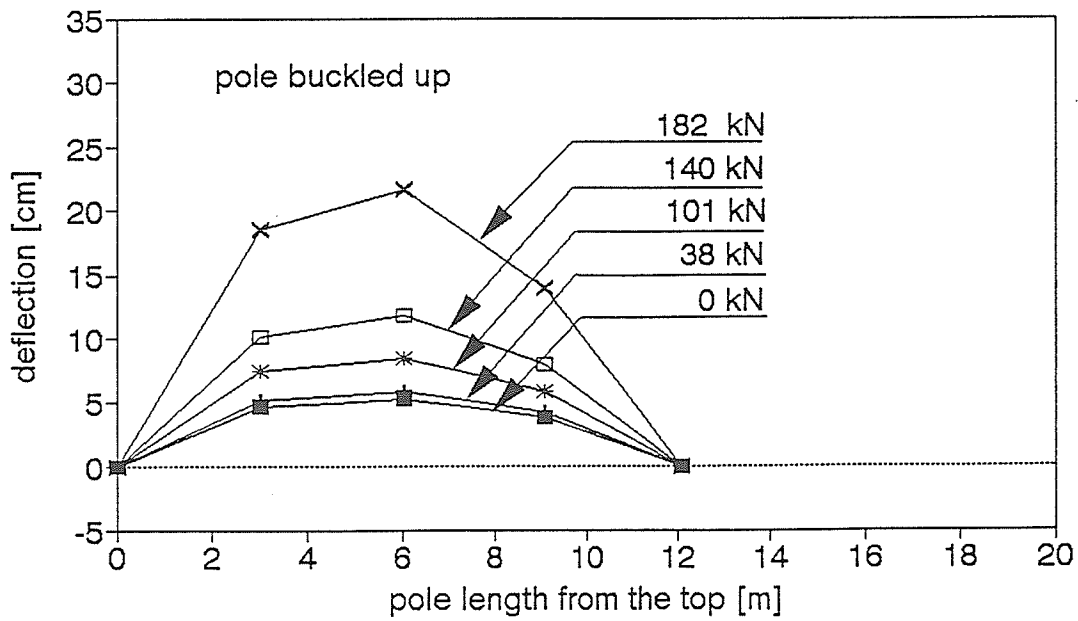
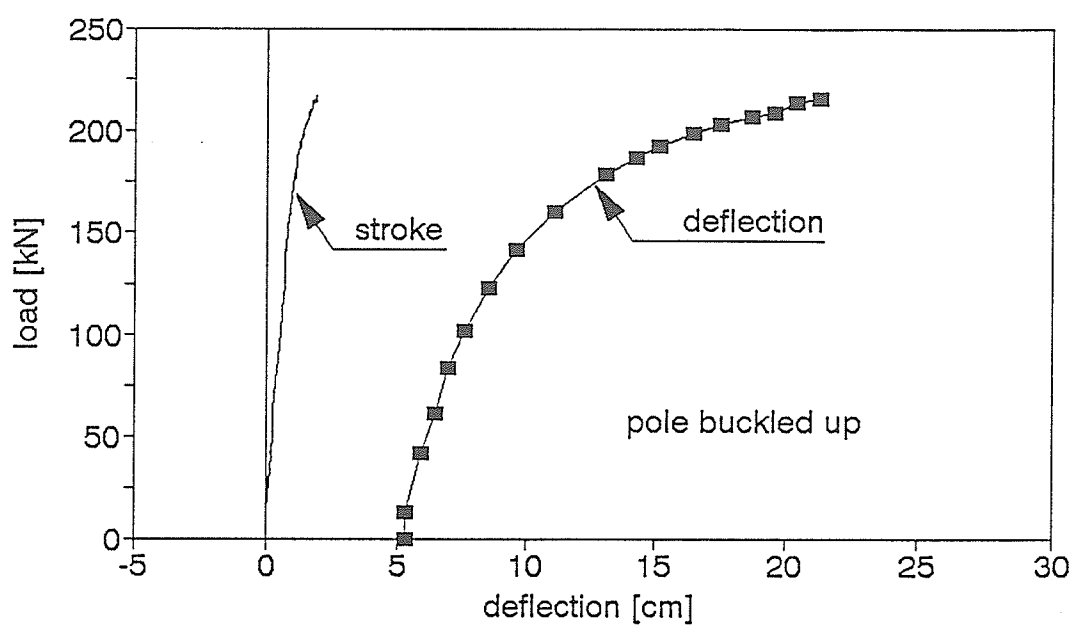


Figure A2.23. Load-deflection relationship and deflected shape of the pole

# POLE 5/3 DEFLECTION AT THE MIDSPAN



# DEFLECTED SHAPE OF THE POLE 5/3 UNDER DIFFERENT LOAD LEVELS

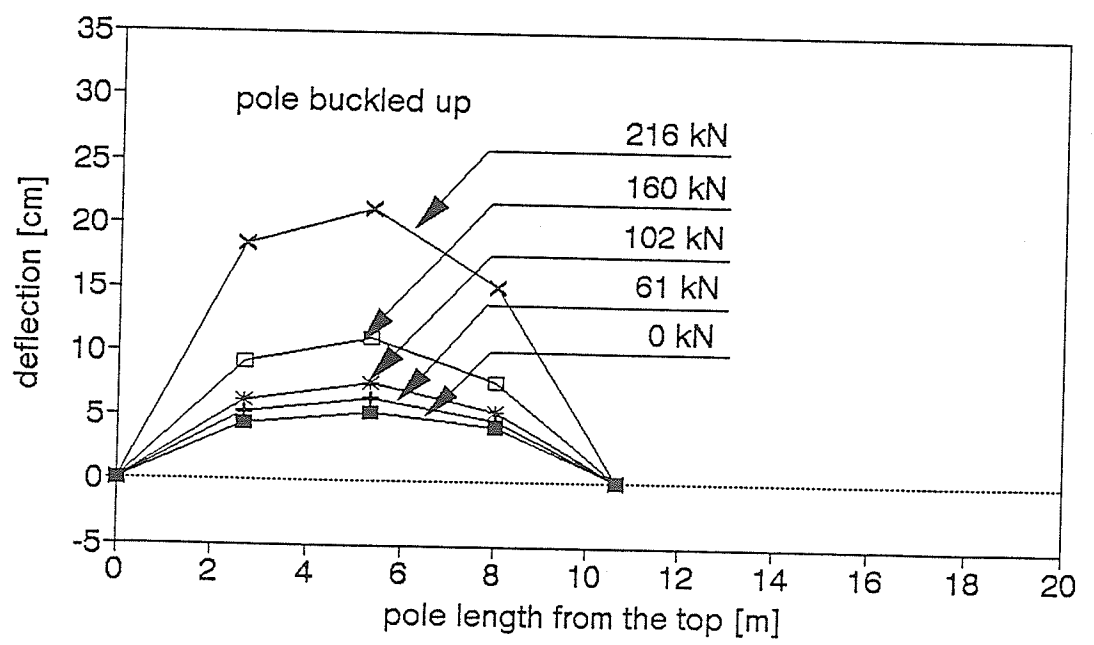
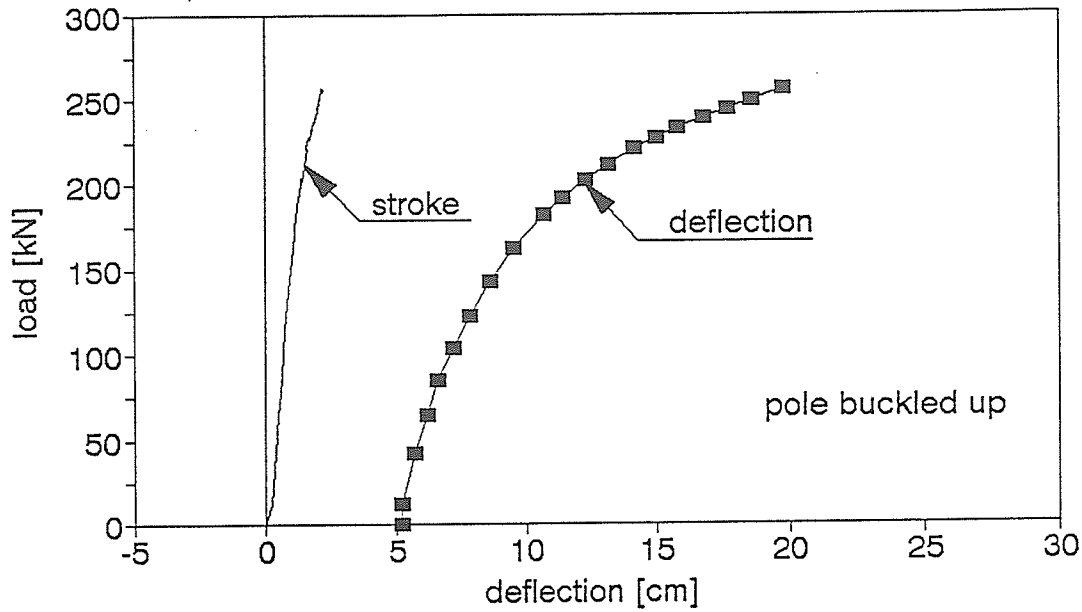


Figure A2.24. Load-deflection relationship and deflected shape of the pole

## POLE 5/4 DEFLECTION AT THE MIDSPAN



## DEFLECTED SHAPE OF THE POLE 5/4 UNDER DIFFERENT LOAD LEVELS

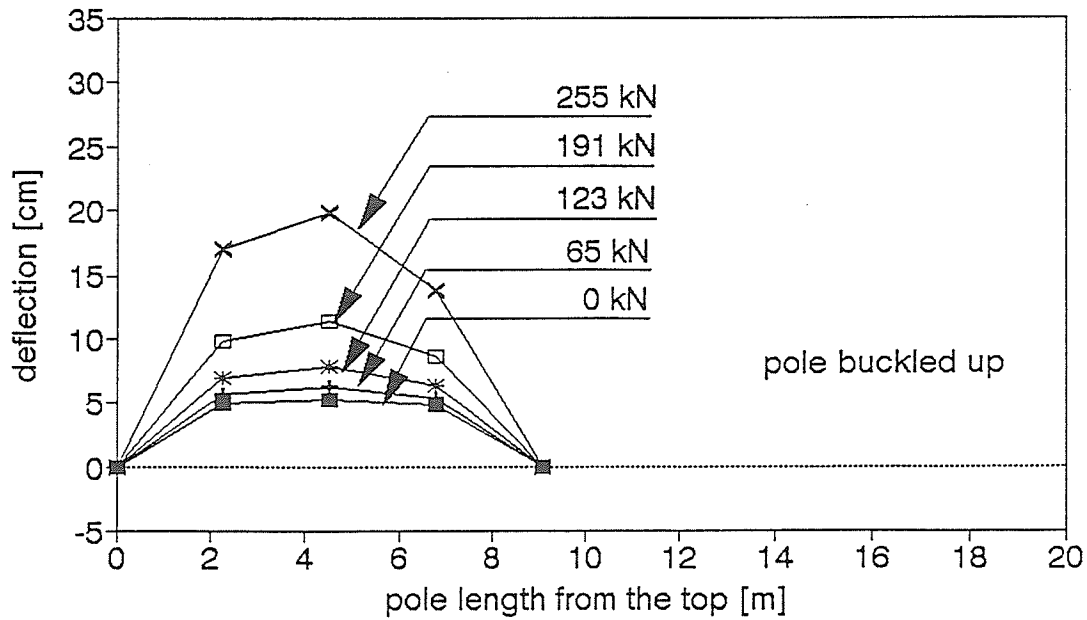
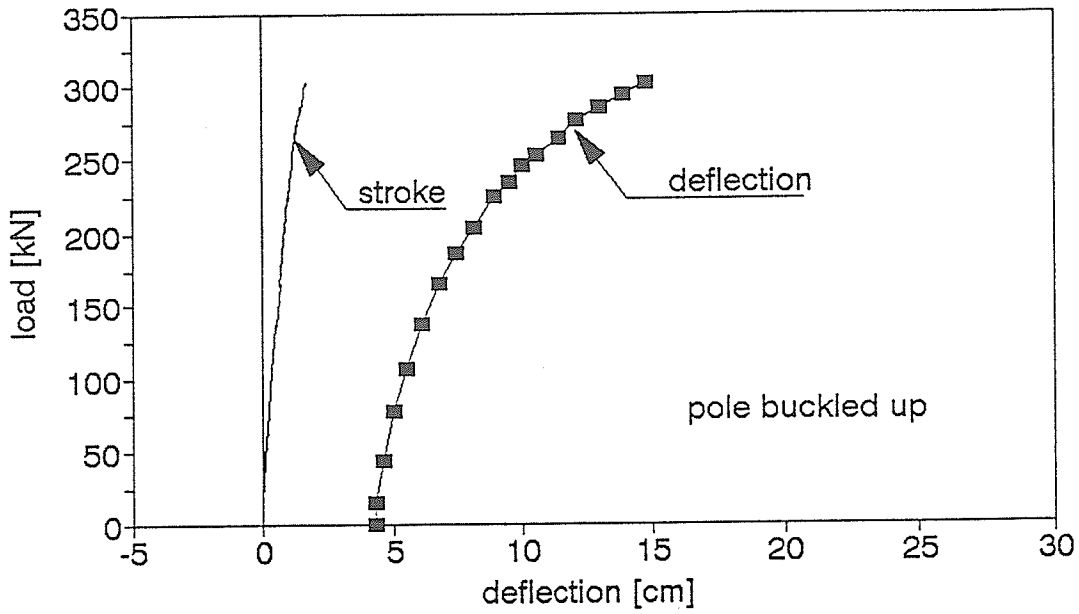


Figure A2.25. Load-deflection relationship and deflected shape of the pole

## POLE 5/5 DEFLECTION AT THE MIDSPAN



## DEFLECTED SHAPE OF THE POLE 5/5 UNDER DIFFERENT LOAD LEVELS

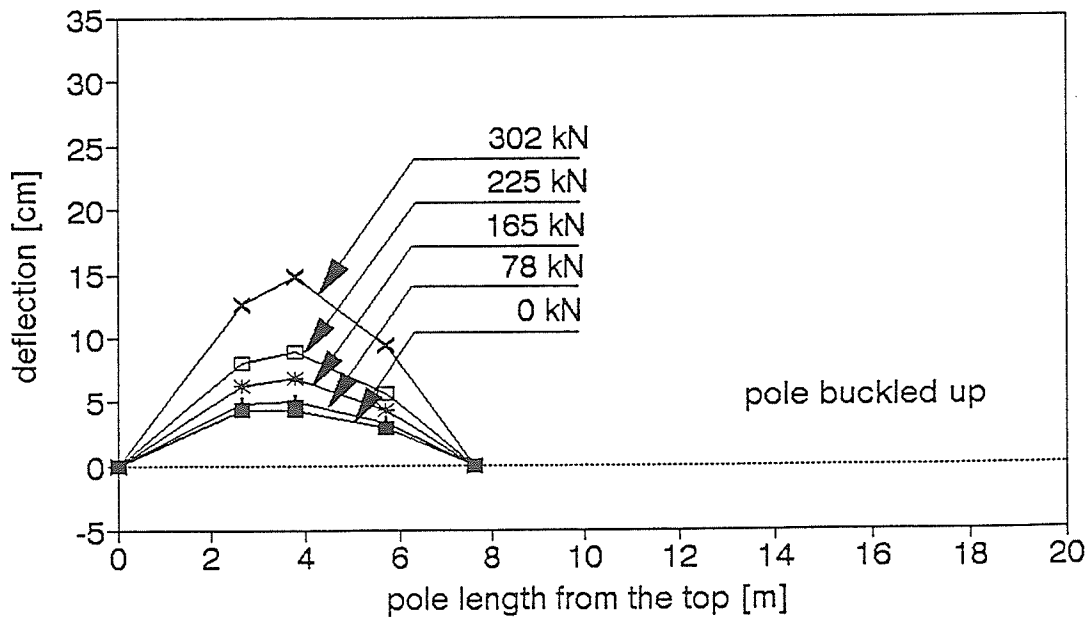
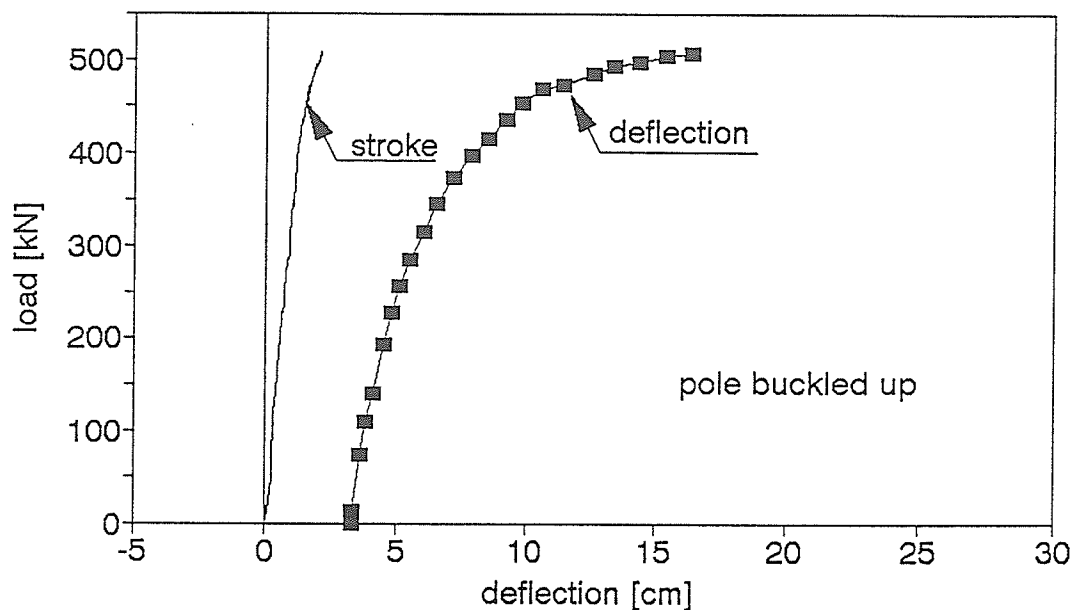


Figure A2.26. Load-deflection relationship and deflected shape of the pole

## POLE 5/6 DEFLECTION AT THE MIDSPAN



## DEFLECTED SHAPE OF THE POLE 5/6 UNDER DIFFERENT LOAD LEVELS

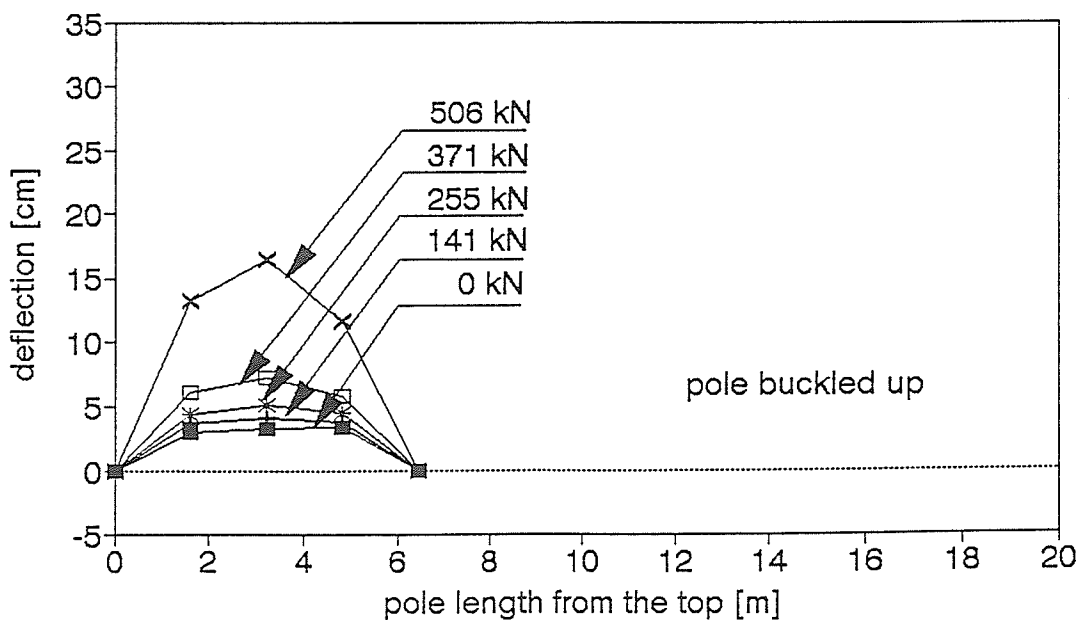
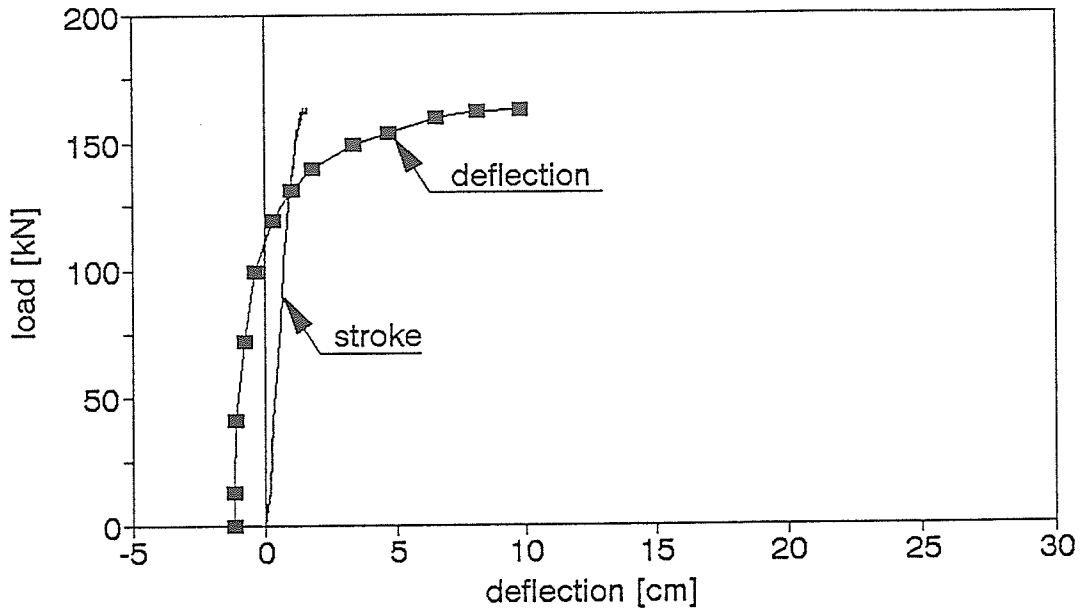


Figure A2.27. Load-deflection relationship and deflected shape of the pole

## POLE 6/1 DEFLECTION AT THE MIDSPAN



## DEFLECTED SHAPE OF THE POLE 6/1 UNDER DIFFERENT LOAD LEVELS

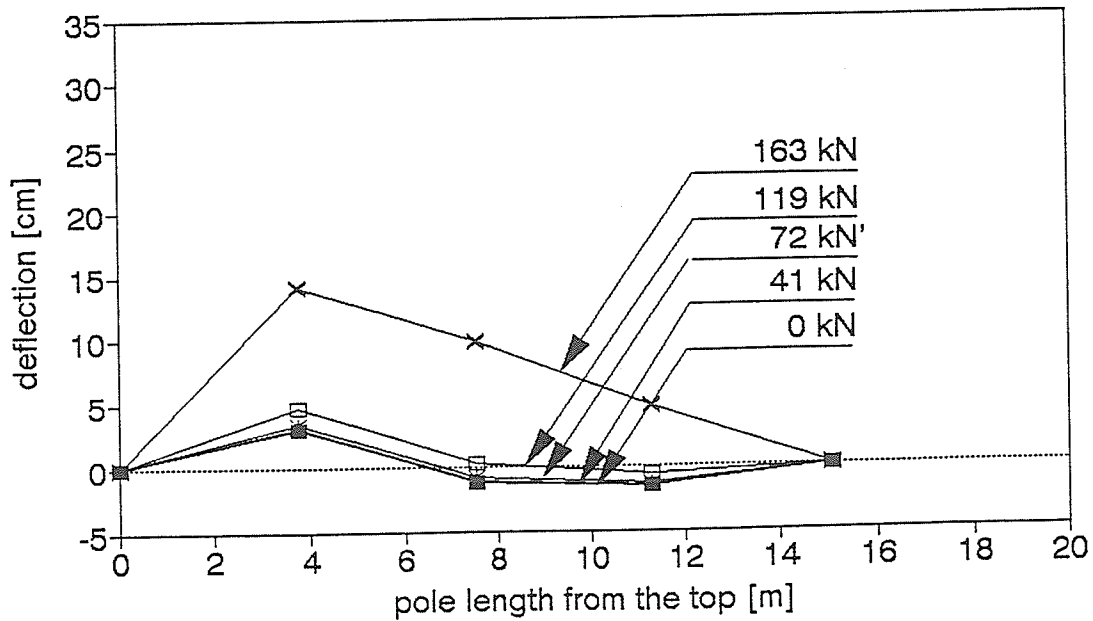
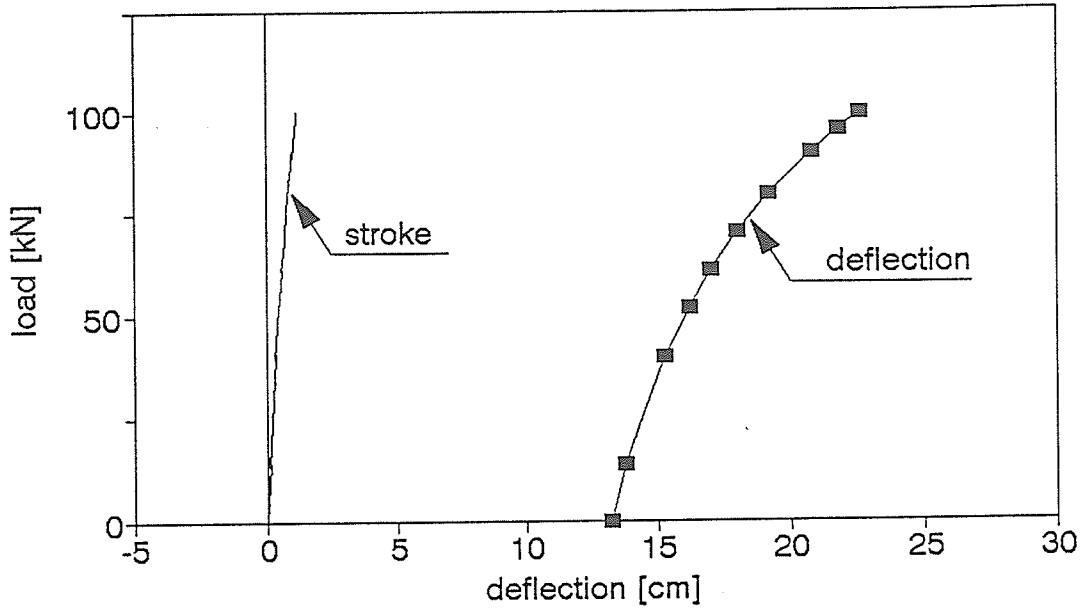


Figure A2.28. Load-deflection relationship and deflected shape of the pole

## POLE 6/2 DEFLECTION AT THE MIDSPAN



## DEFLECTED SHAPE OF THE POLE 6/2 UNDER DIFFERENT LOAD LEVELS

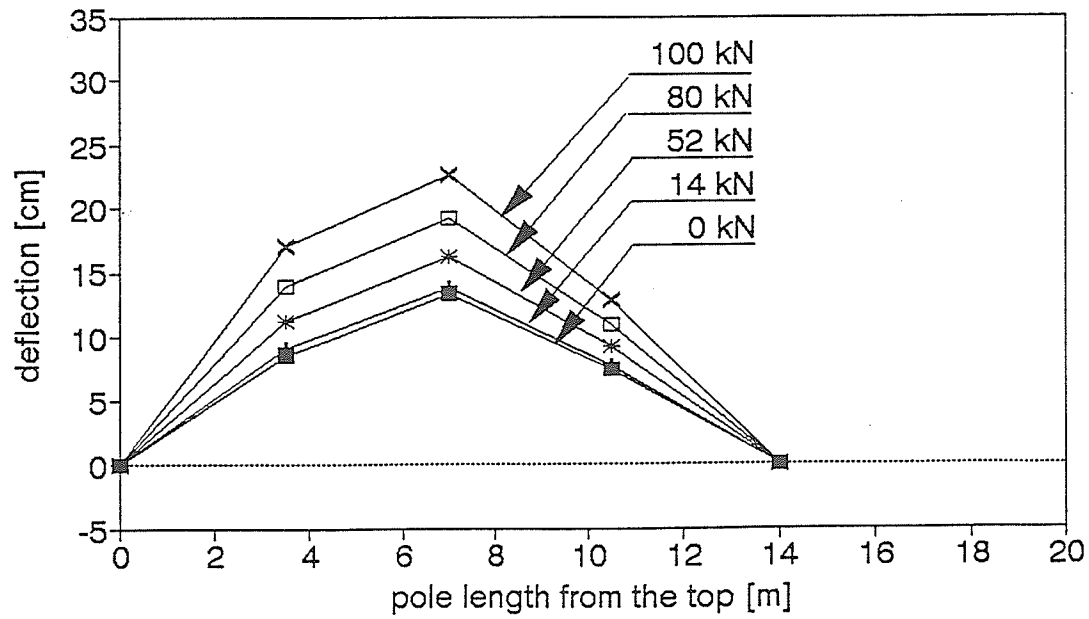
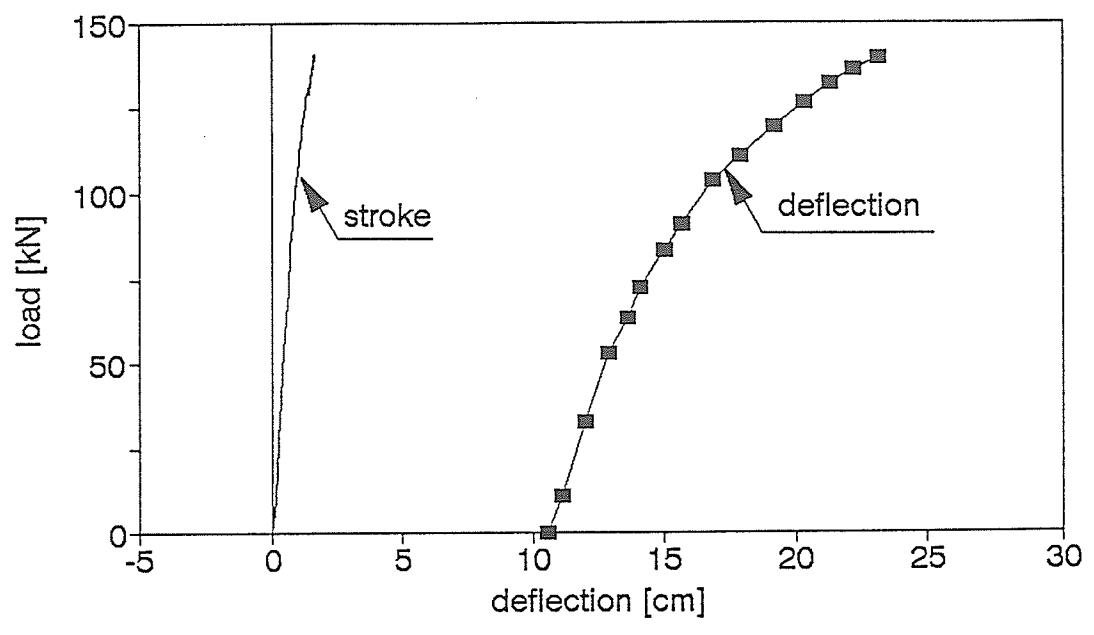


Figure A2.29. Load-deflection relationship and deflected shape of the pole

### POLE 6/3 DEFLECTION AT THE MIDSPAN



### DEFLECTED SHAPE OF THE POLE 6/3 UNDER DIFFERENT LOAD LEVELS

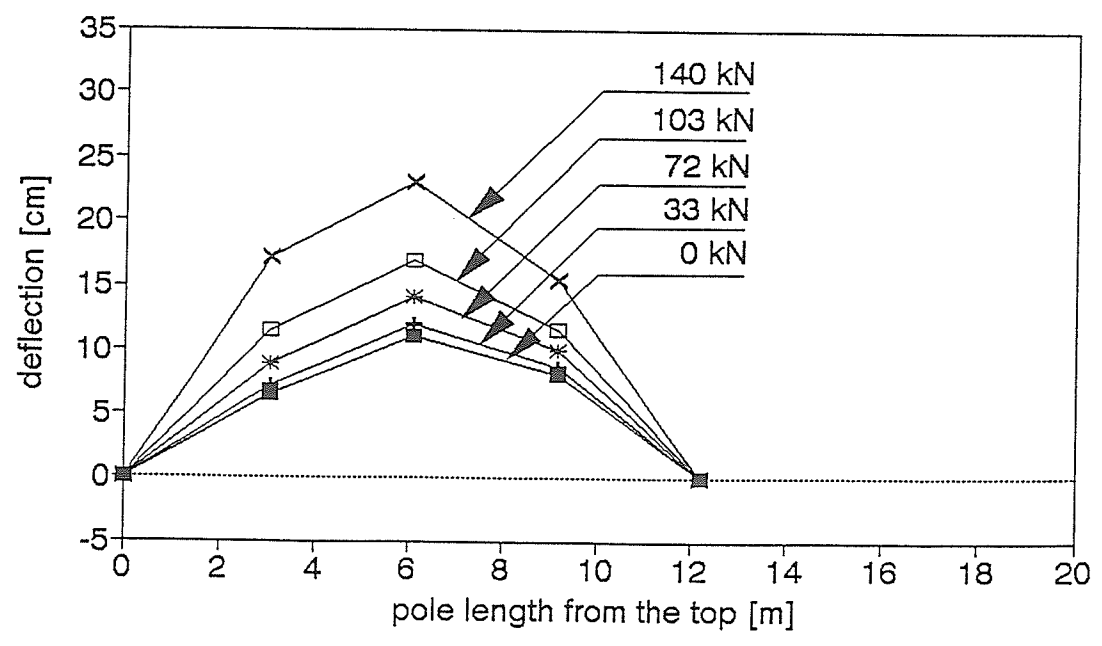
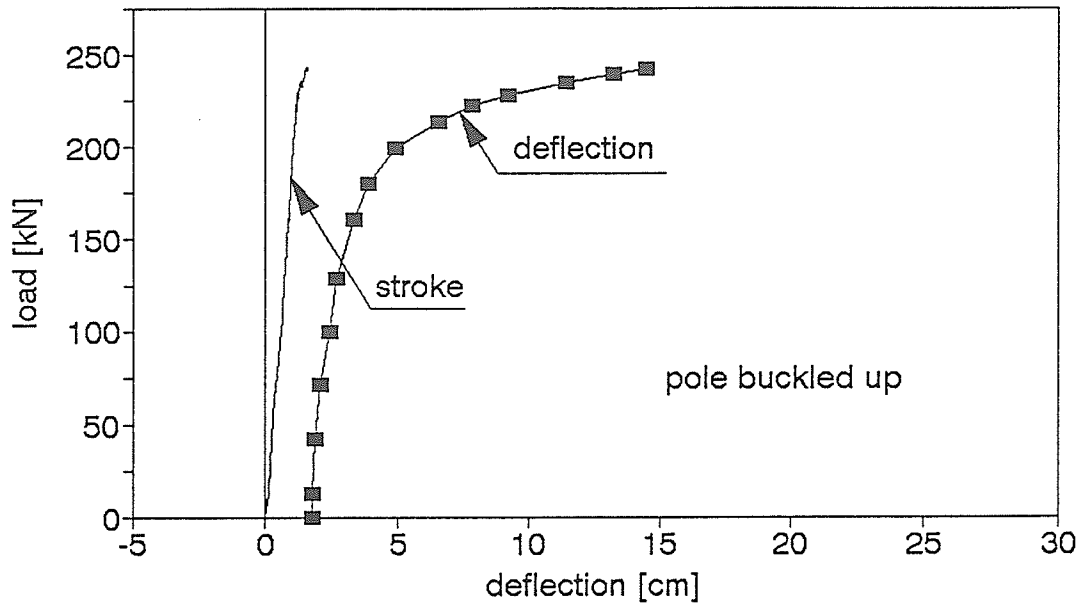


Figure A2.30. Load-deflection relationship and deflected shape of the pole

## POLE 6/4 DEFLECTION AT THE MIDSPAN



## DEFLECTED SHAPE OF THE POLE 6/4 UNDER DIFFERENT LOAD LEVELS

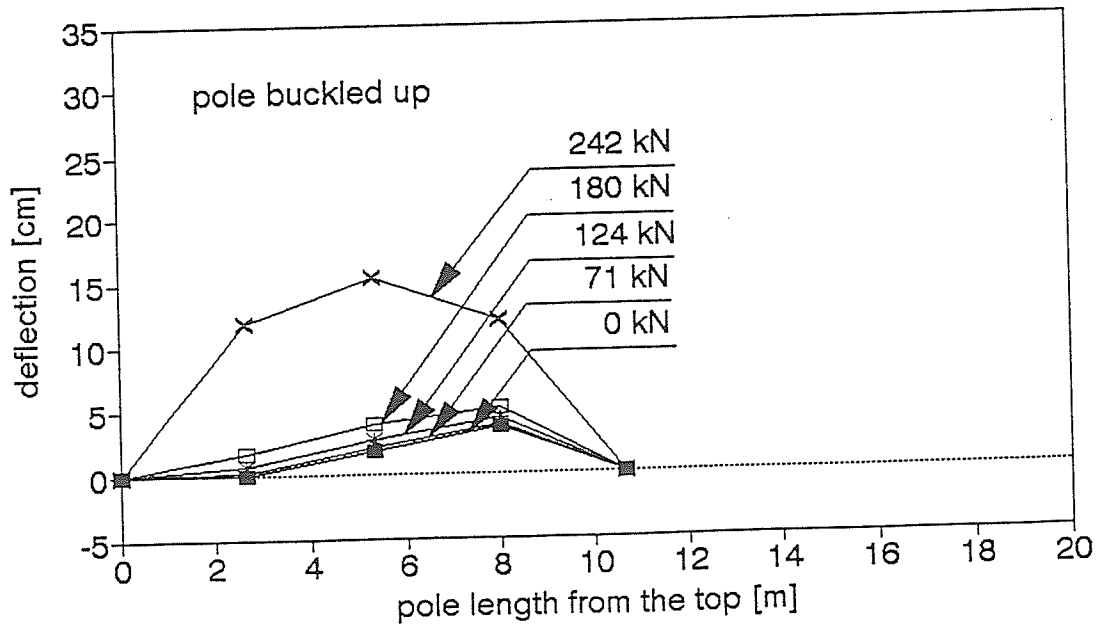
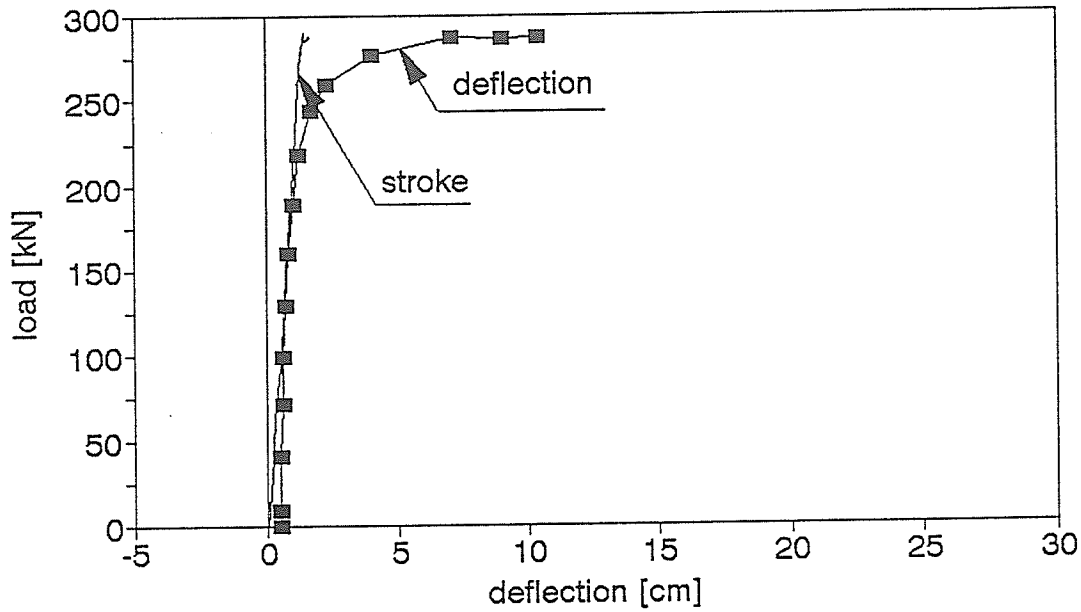


Figure A2.31. Load-deflection relationship and deflected shape of the pole

## POLE 6/5 DEFLECTION AT THE MIDSPAN



## DEFLECTED SHAPE OF THE POLE 6/5 UNDER DIFFERENT LOAD LEVELS

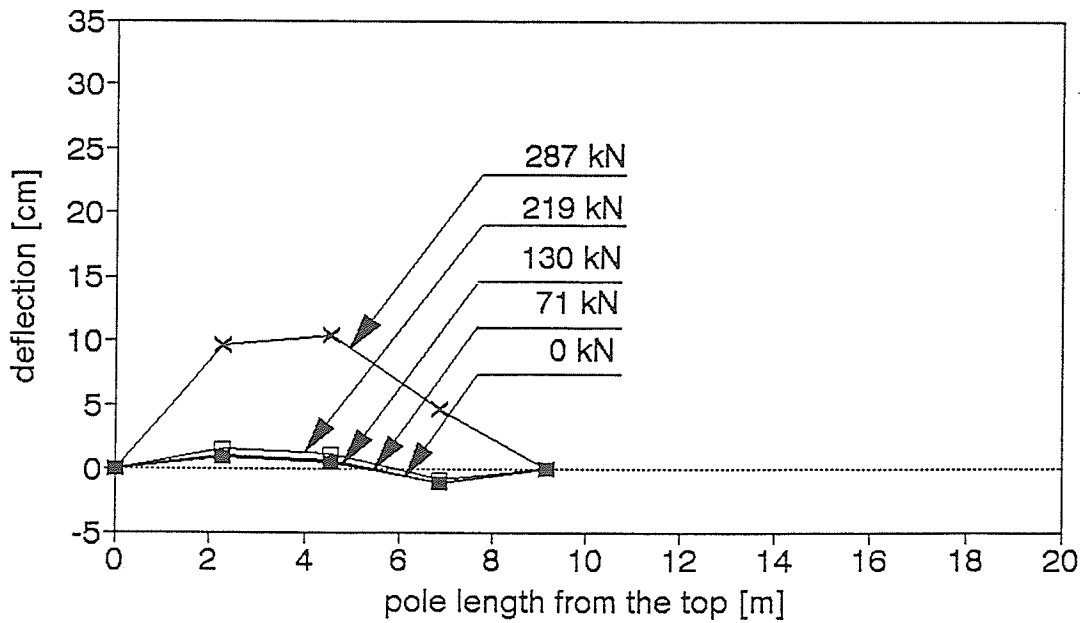
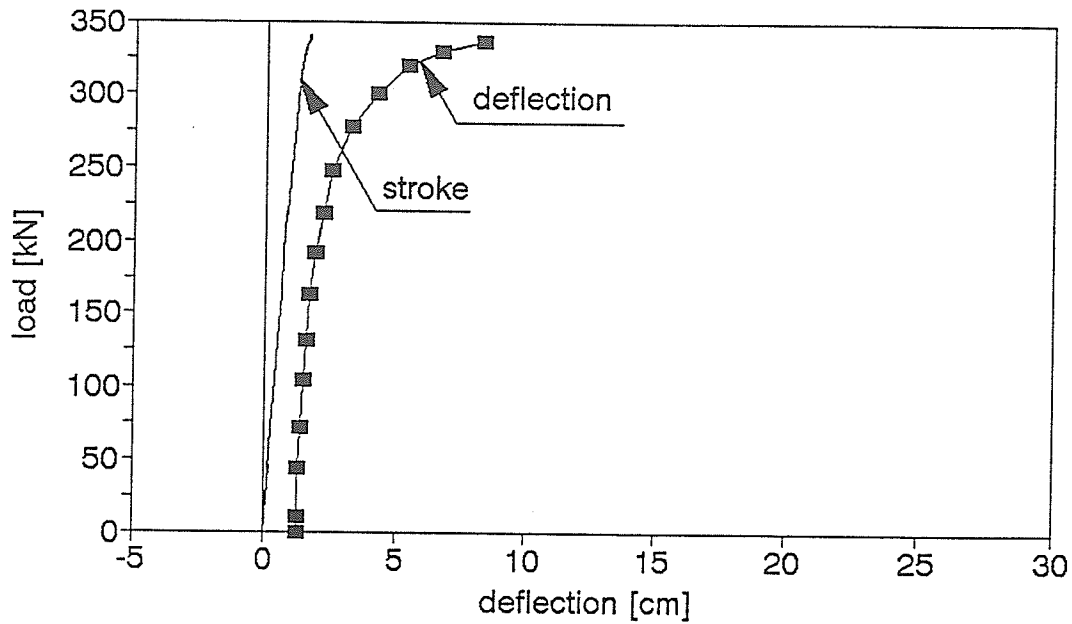


Figure A2.32. Load-deflection relationship and deflected shape of the pole

## POLE 6/6 DEFLECTION AT THE MIDSPAN



## DEFLECTED SHAPE OF THE POLE 6/6 UNDER DIFFERENT LOAD LEVELS

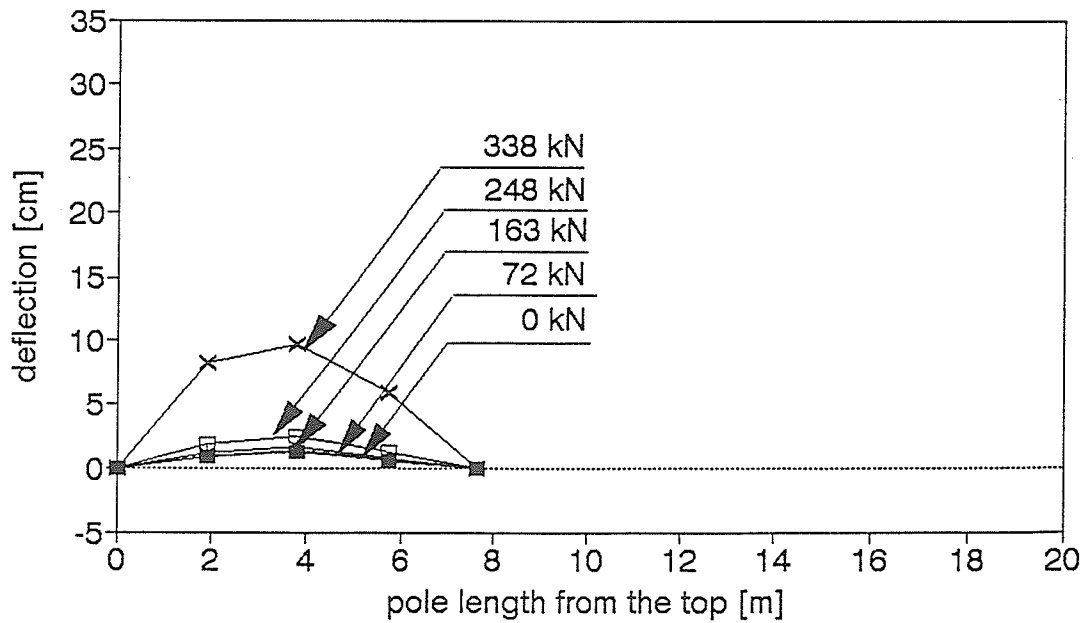
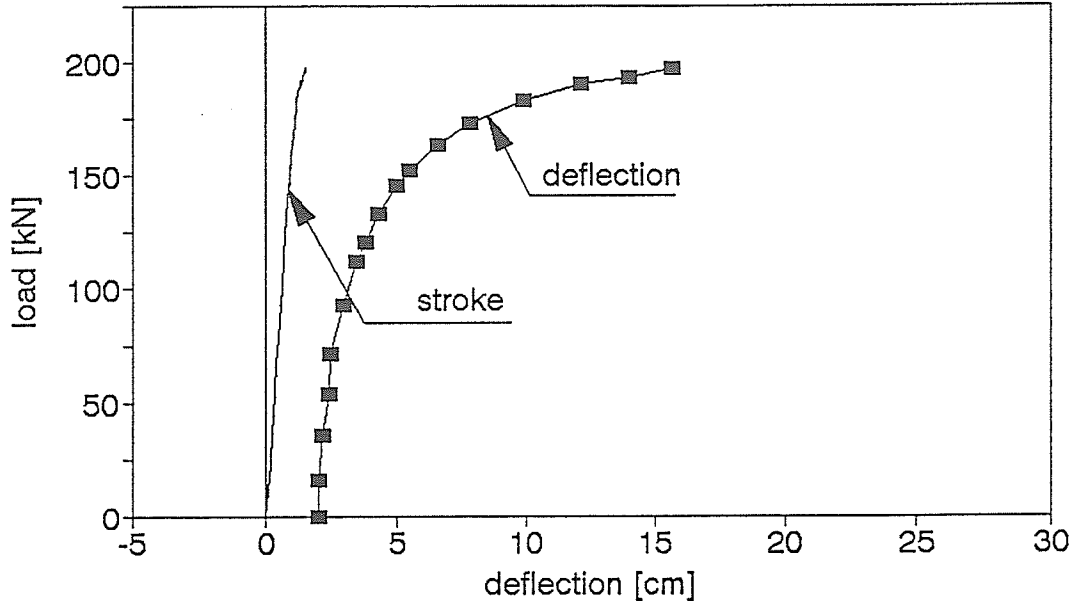


Figure A2.33. Load-deflection relationship and deflected shape of the pole

# POLE 7/1

## DEFLECTION AT THE MIDSPAN



## DEFLECTED SHAPE OF THE POLE 7/1 UNDER DIFFERENT LOAD LEVELS

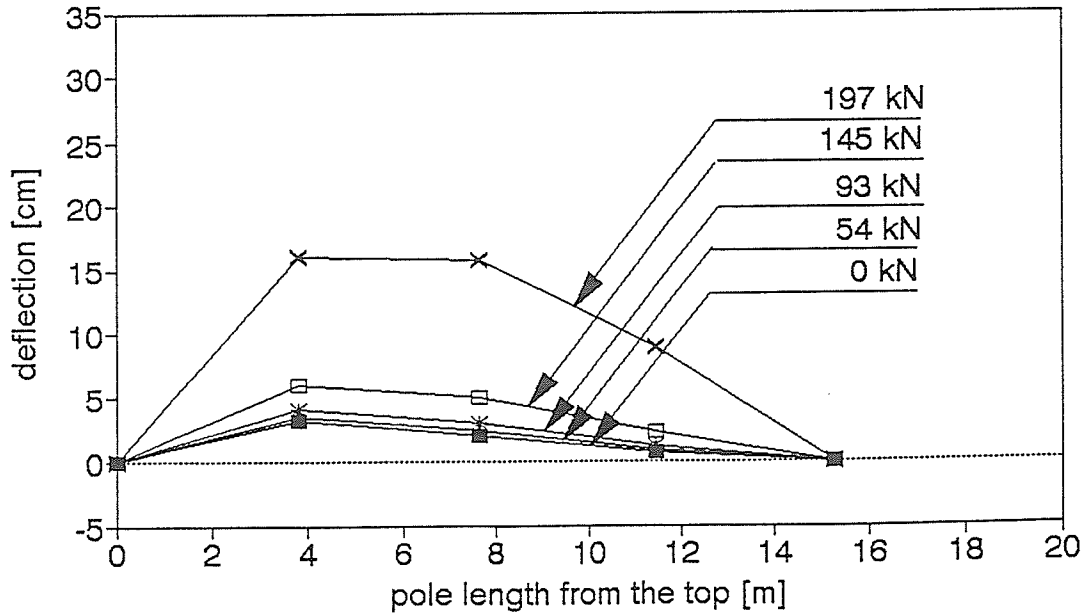
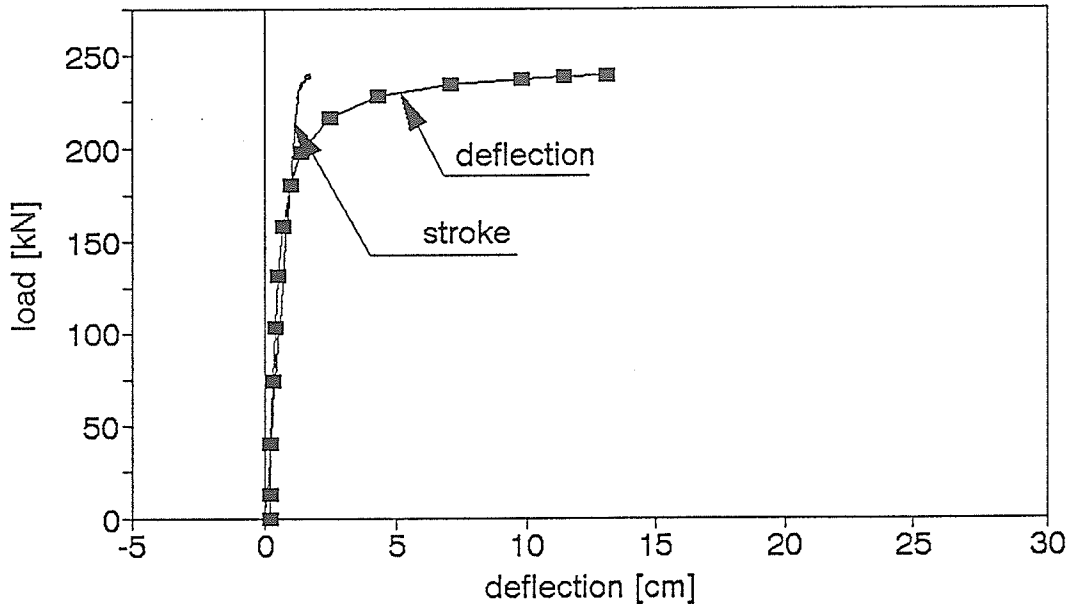


Figure A2.34. Load-deflection relationship and deflected shape of the pole

## POLE 7/2 DEFLECTION AT THE MIDSPAN



## DEFLECTED SHAPE OF THE POLE 7/2 UNDER DIFFERENT LOAD LEVELS

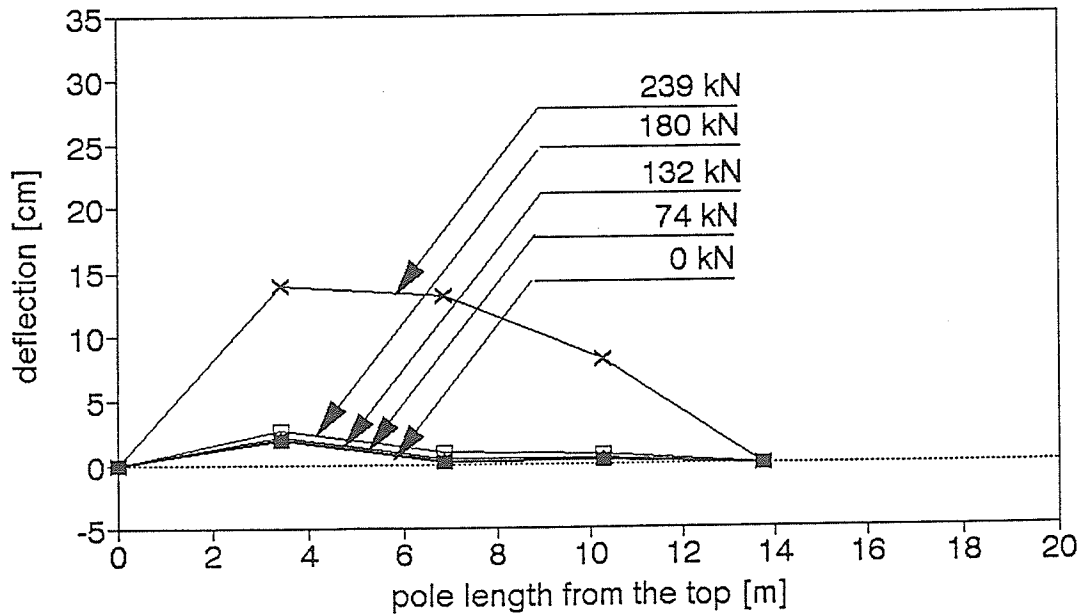
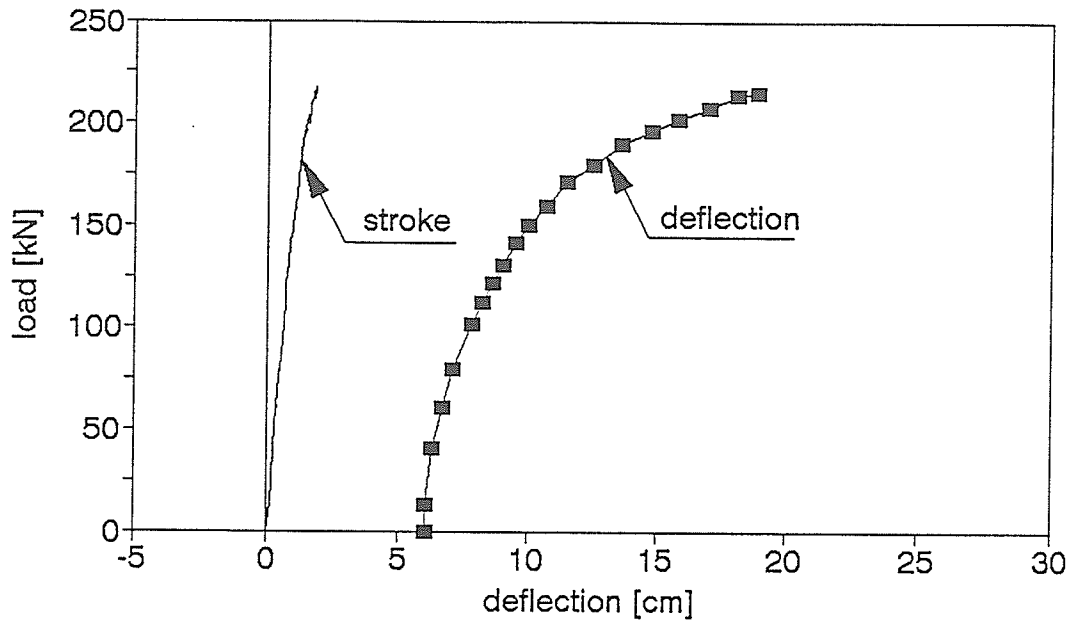


Figure A2.35. Load-deflection relationship and deflected shape of the pole

## POLE 7/3 DEFLECTION AT THE MIDSPAN



## DEFLECTED SHAPE OF THE POLE 7/3 UNDER DIFFERENT LOAD LEVELS

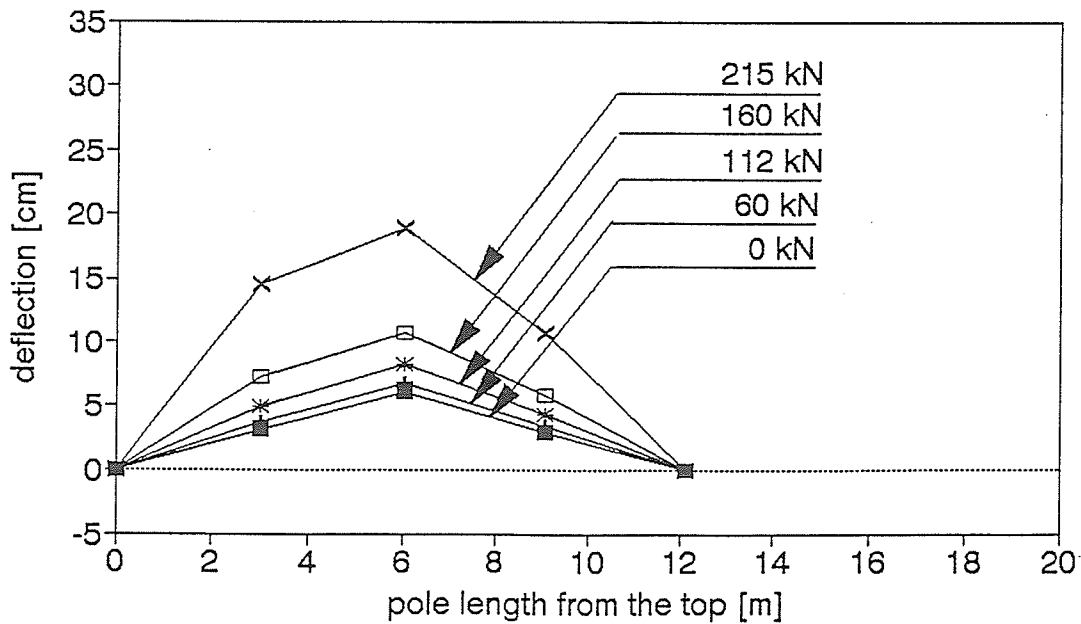
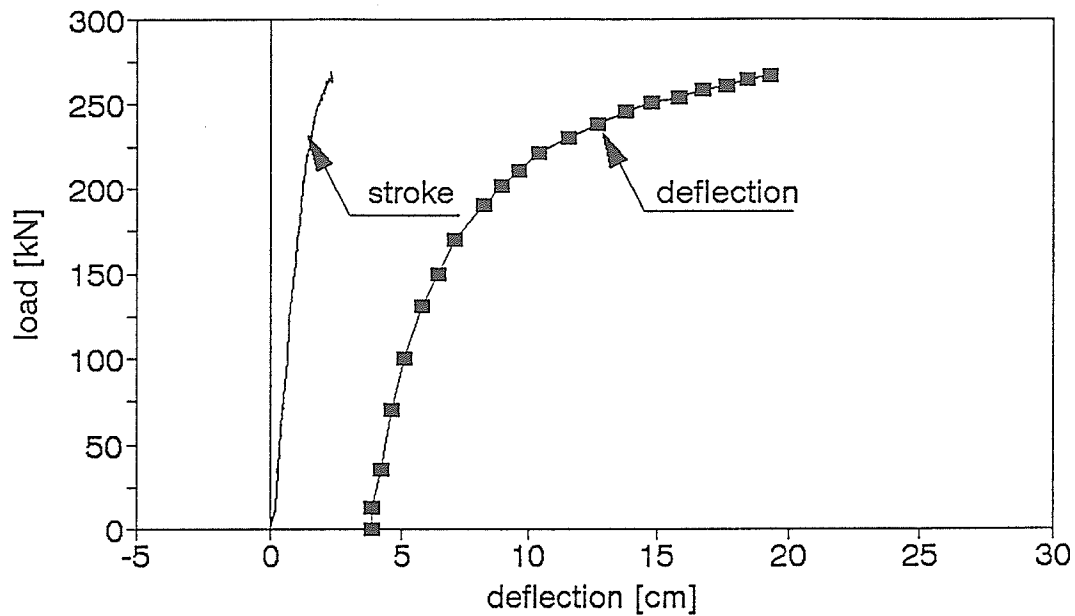


Figure A2.36. Load-deflection relationship and deflected shape of the pole

## POLE 7/4 DEFLECTION AT THE MIDSPAN



## DEFLECTED SHAPE OF THE POLE 7/4 UNDER DIFFERENT LOAD LEVELS

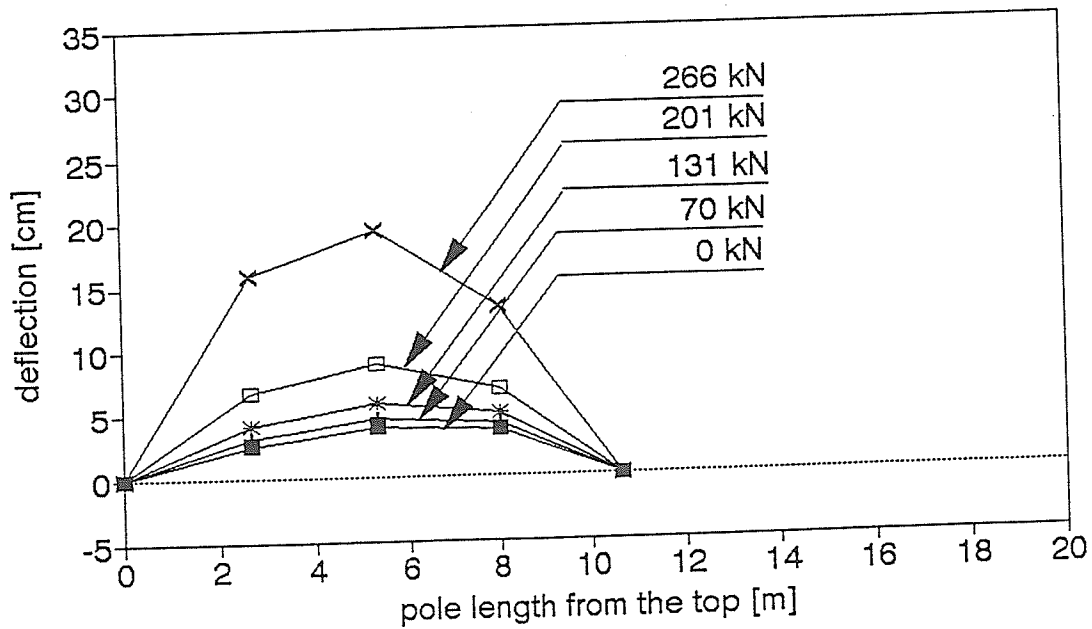
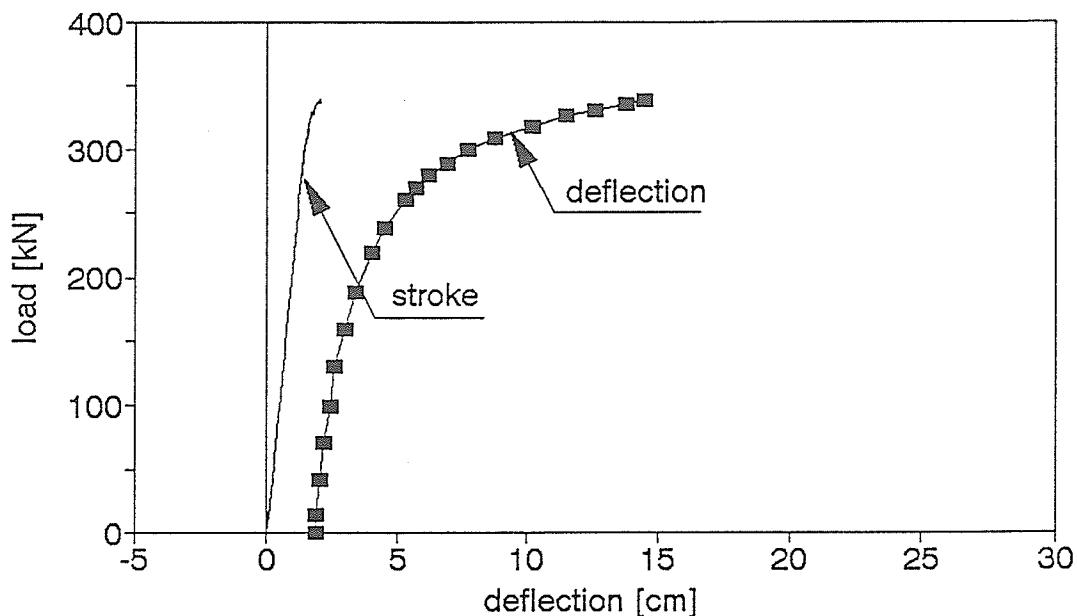


Figure A2.37. Load-deflection relationship and deflected shape of the pole

## POLE 7/5 DEFLECTION AT THE MIDSPAN



## DEFLECTED SHAPE OF THE POLE 7/5 UNDER DIFFERENT LOAD LEVELS

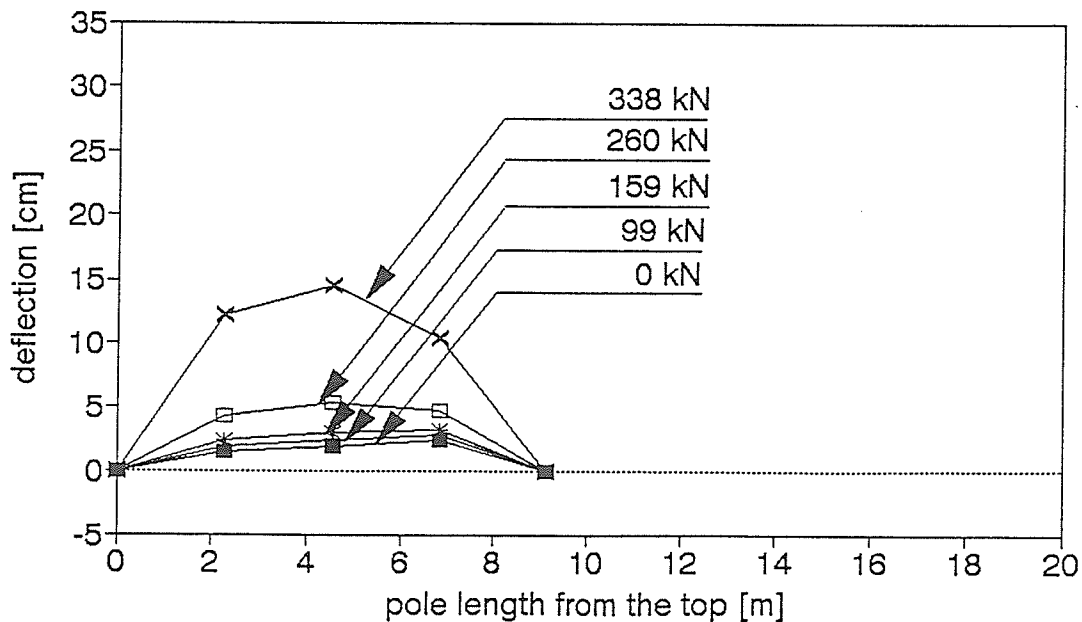
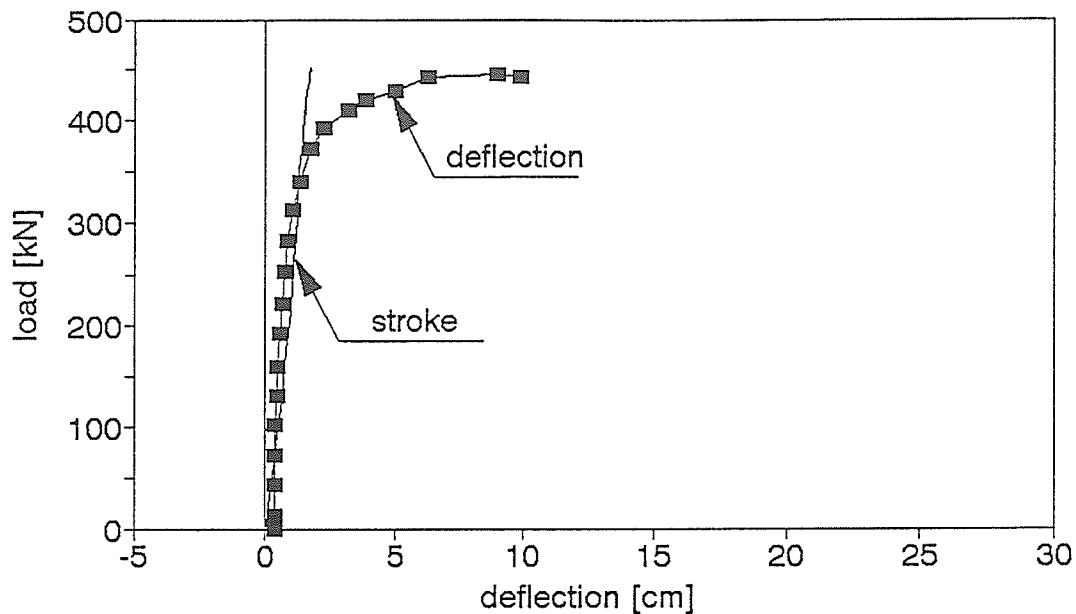


Figure A2.38. Load-deflection relationship and deflected shape of the pole

## POLE 7/6 DEFLECTION AT THE MIDSPAN



## DEFLECTED SHAPE OF THE POLE 7/6 UNDER DIFFERENT LOAD LEVELS

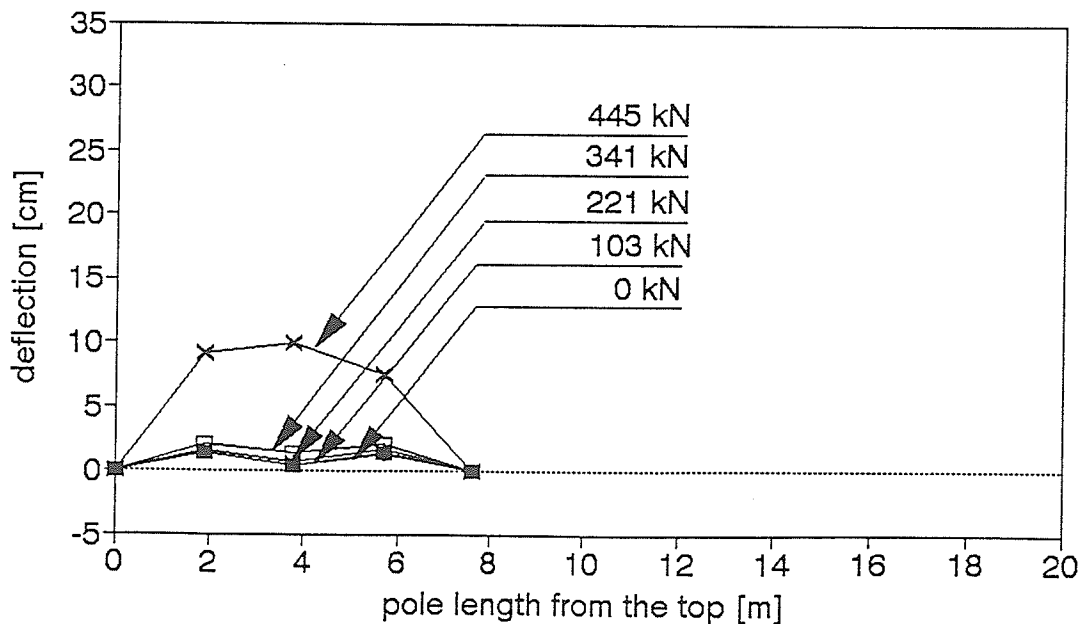
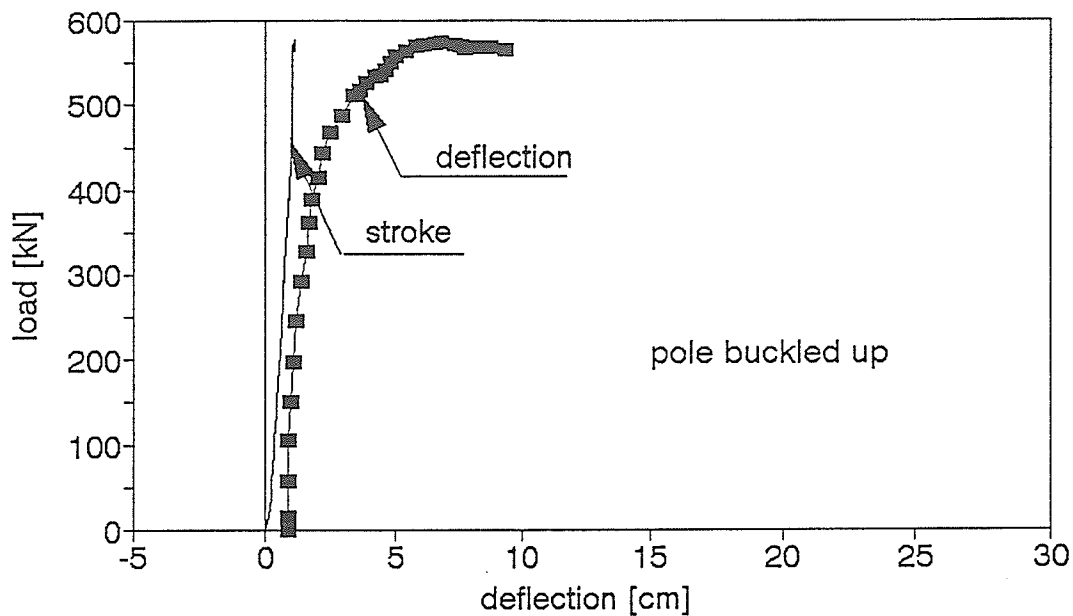


Figure A2.39. Load-deflection relationship and deflected shape of the pole

## POLE 7/7 DEFLECTION AT THE MIDSPAN



## DEFLECTED SHAPE OF THE POLE 7/7 UNDER DIFFERENT LOAD LEVELS

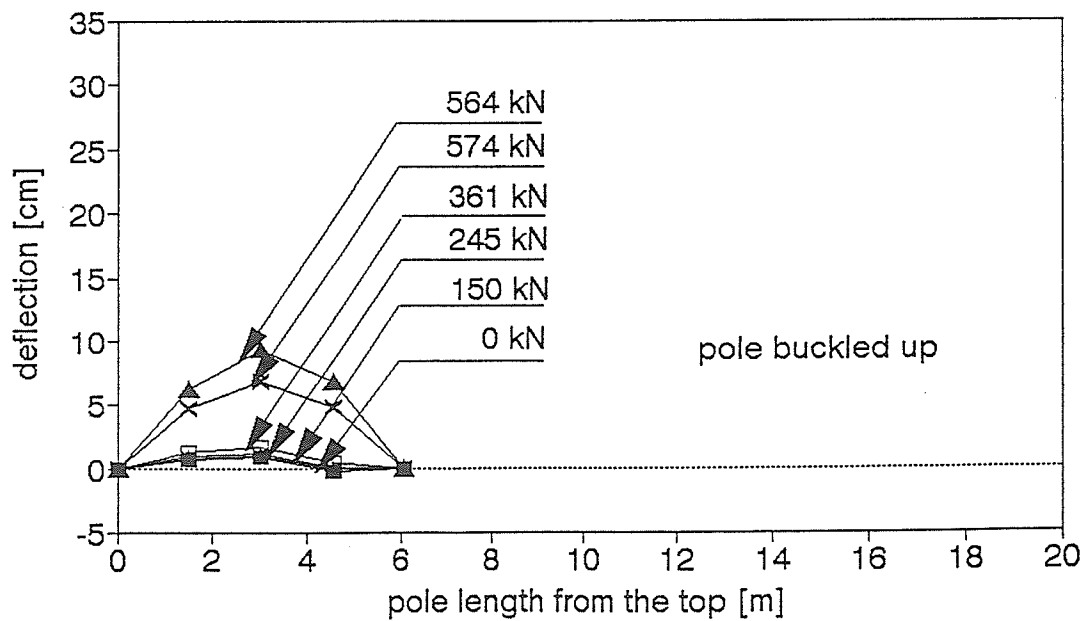
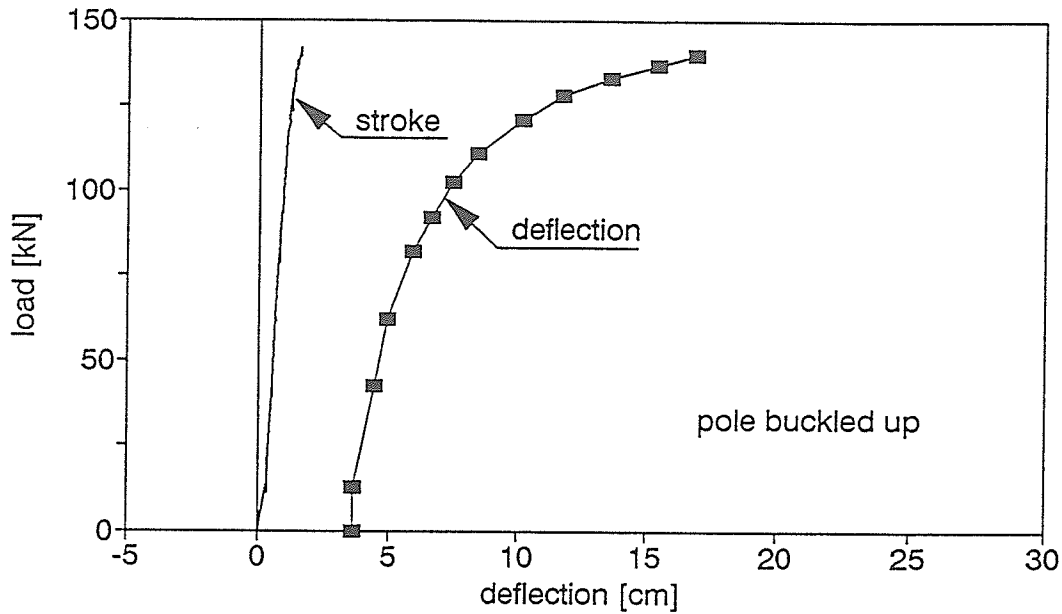


Figure A2.40. Load-deflection relationship and deflected shape of the pole

## POLE 8/1 DEFLECTION AT THE MIDSPAN



## DEFLECTED SHAPE OF THE POLE 8/1 UNDER DIFFERENT LOAD LEVELS

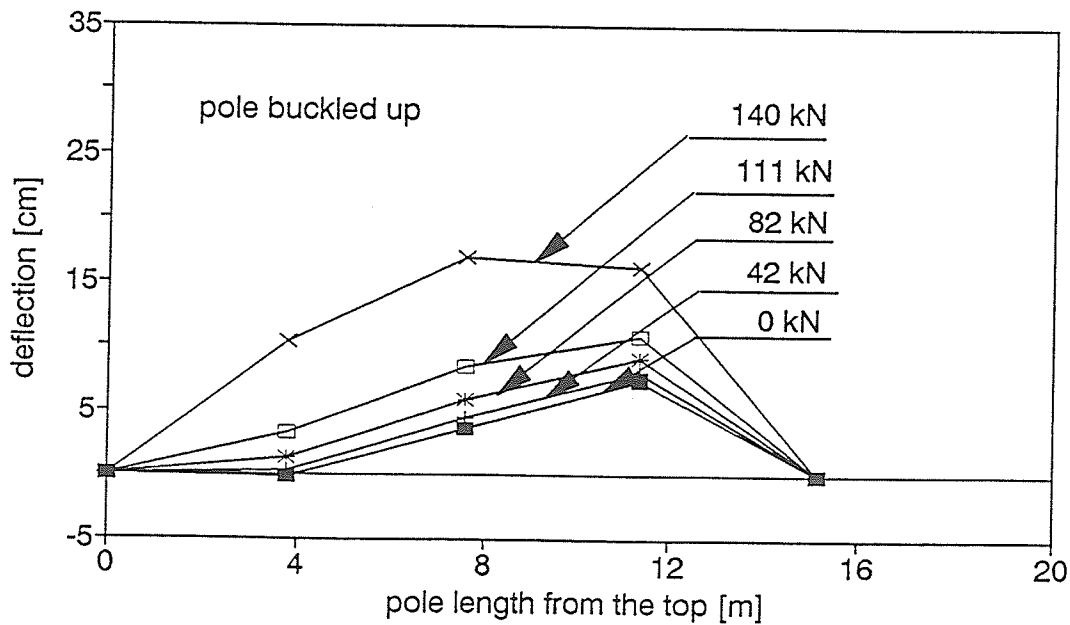
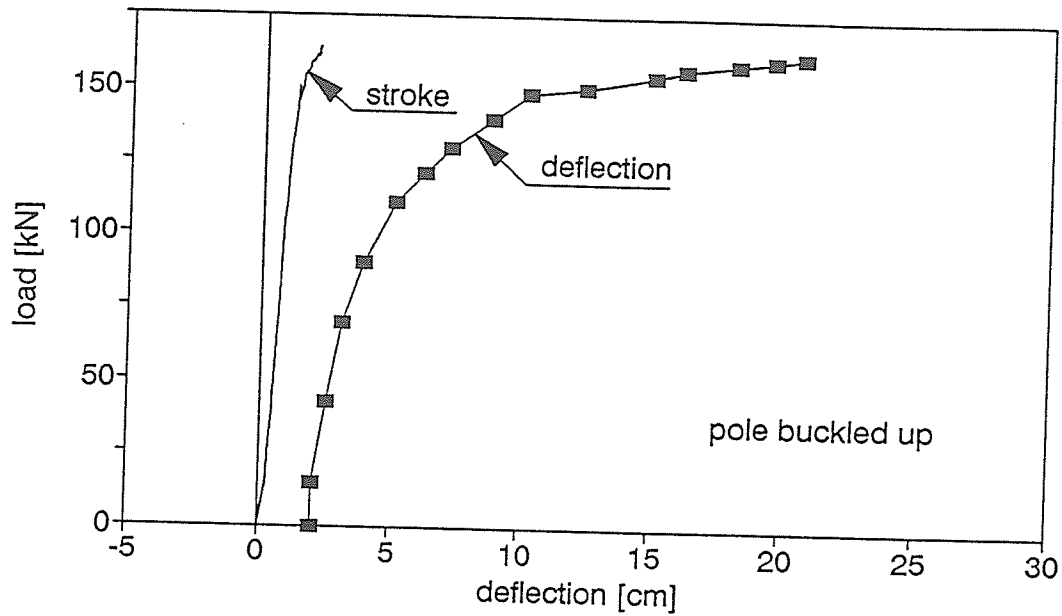


Figure A2.41. Load-deflection relationship and deflected shape of the pole

## POLE 8/2 DEFLECTION AT THE MIDSPAN



## DEFLECTED SHAPE OF THE POLE 8/2 UNDER DIFFERENT LOAD LEVELS

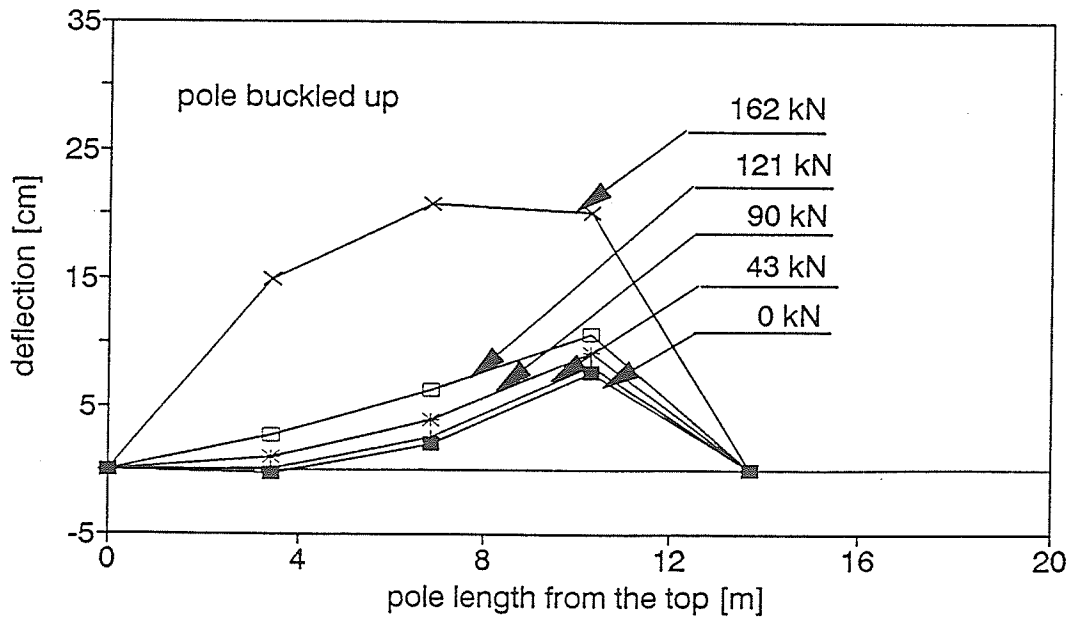
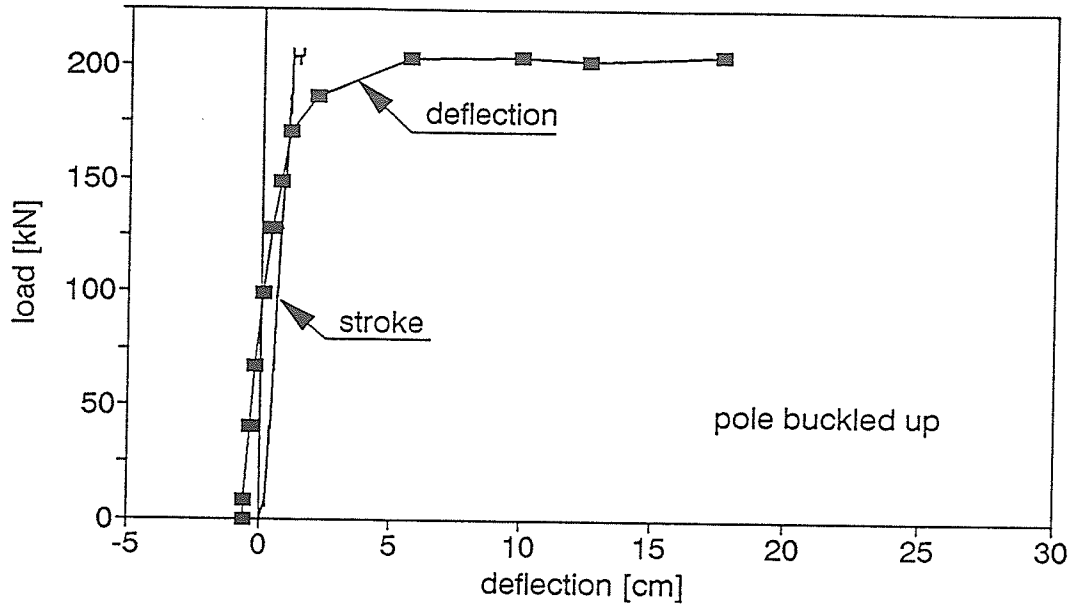


Figure A2.42. Load-deflection relationship and deflected shape of the pole

## POLE 8/3 DEFLECTION AT THE MIDSPAN



## DEFLECTED SHAPE OF THE POLE 8/3 UNDER DIFFERENT LOAD LEVELS

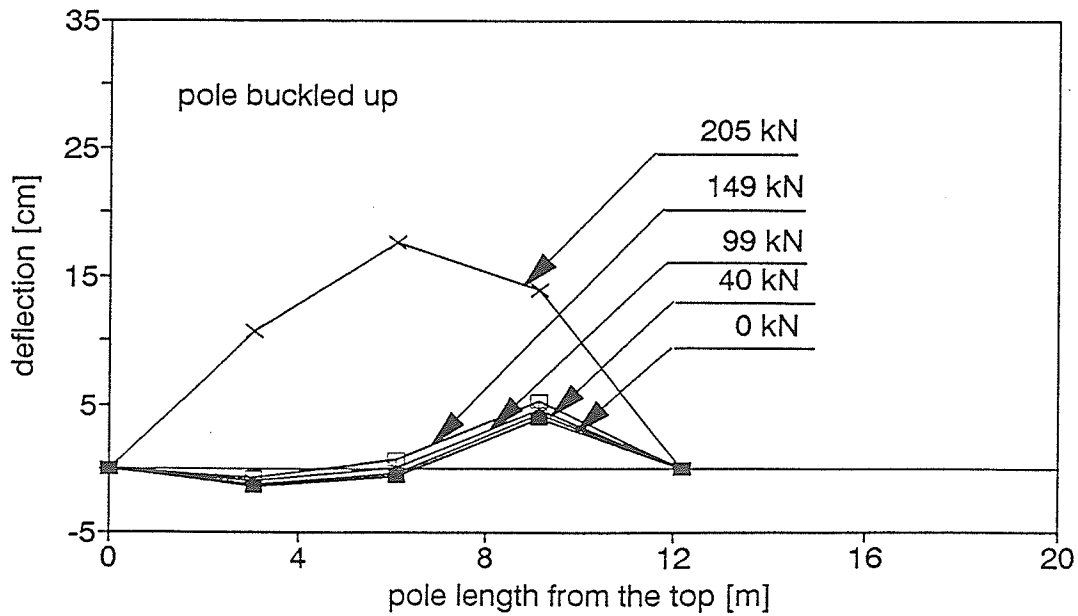
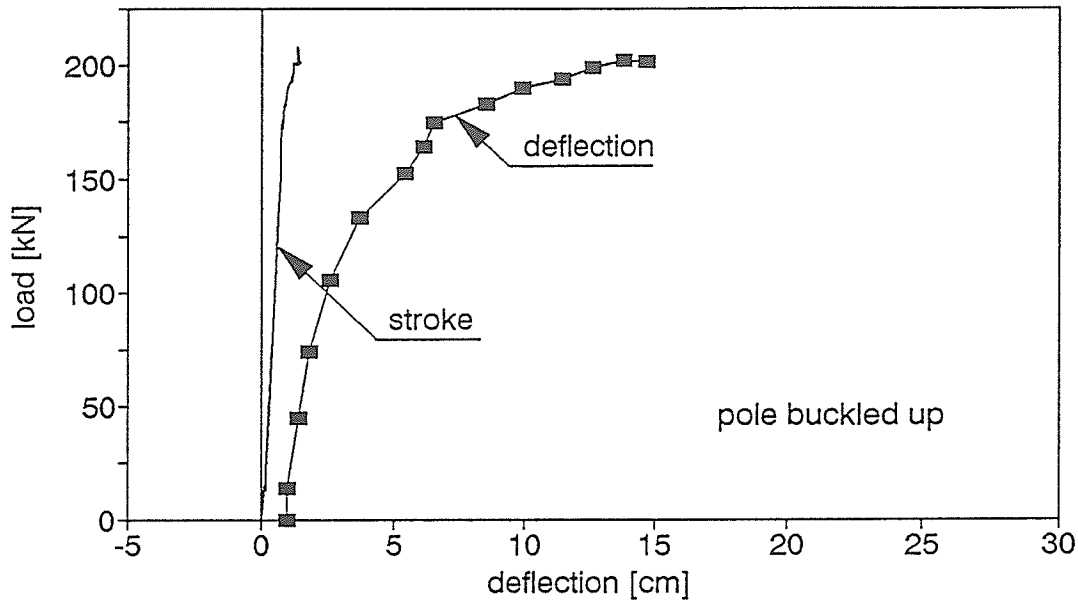


Figure A2.43. Load-deflection relationship and deflected shape of the pole

## POLE 8/4 DEFLECTION AT THE MIDSPAN



## DEFLECTED SHAPE OF THE POLE 8/4 UNDER DIFFERENT LOAD LEVELS

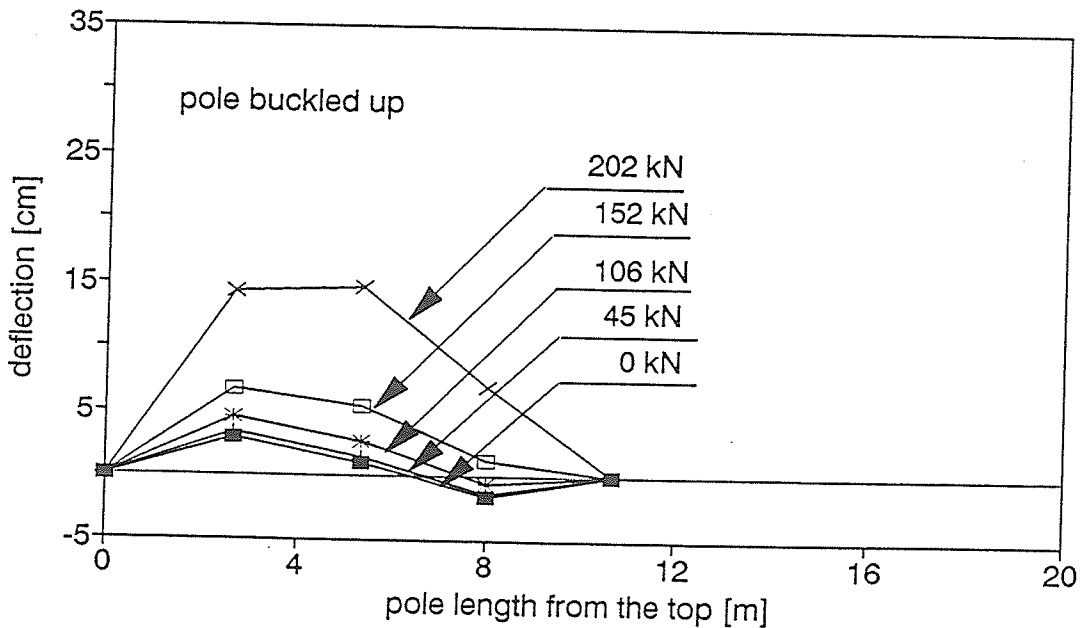
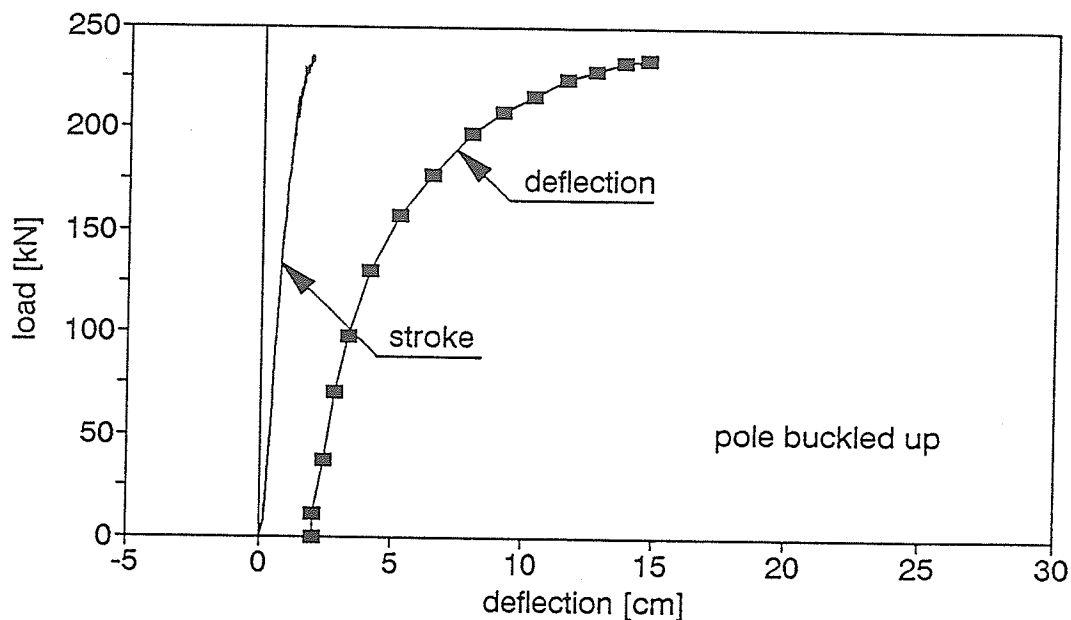


Figure A2.44. Load-deflection relationship and deflected shape of the pole

## POLE 8/5 DEFLECTION AT THE MIDSPAN



## DEFLECTED SHAPE OF THE POLE 8/5 UNDER DIFFERENT LOAD LEVELS

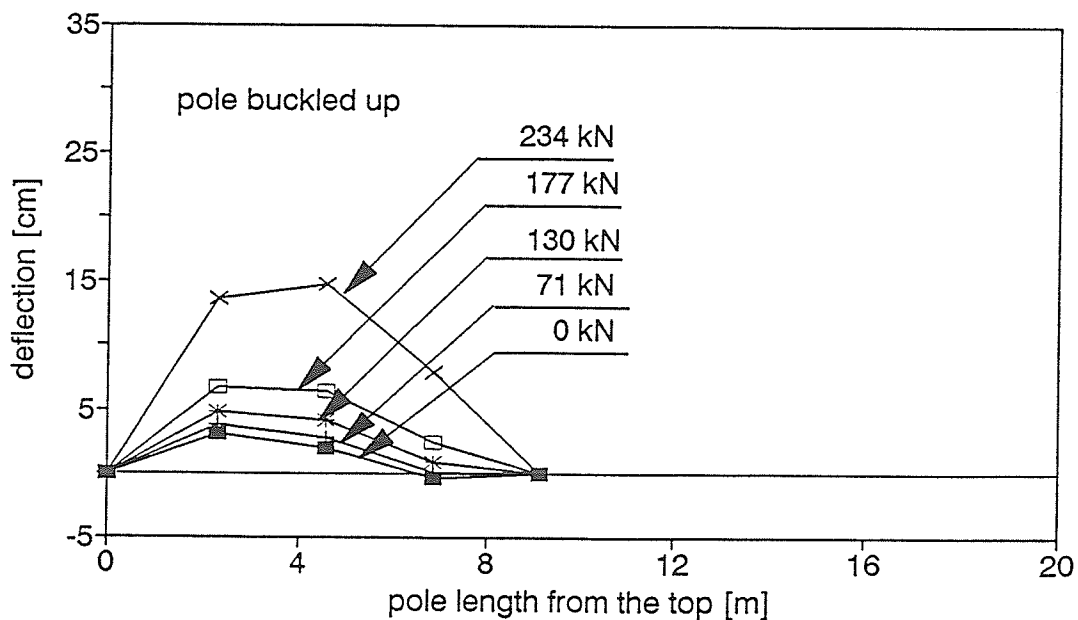
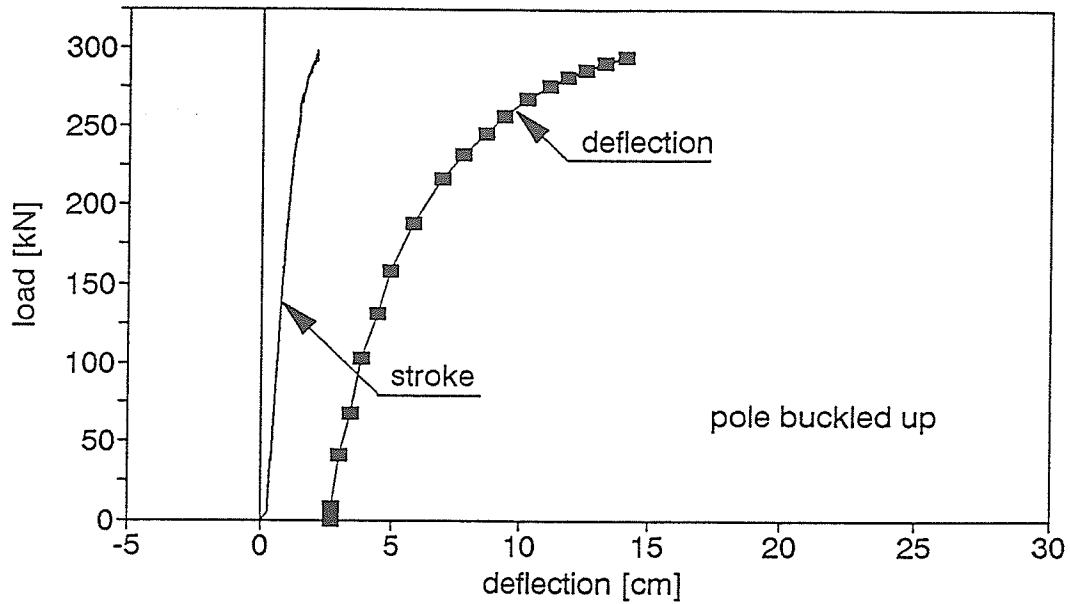


Figure A2.45. Load-deflection relationship and deflected shape of the pole

## POLE 8/6 DEFLECTION AT THE MIDSPAN



## DEFLECTED SHAPE OF THE POLE 8/6 UNDER DIFFERENT LOAD LEVELS

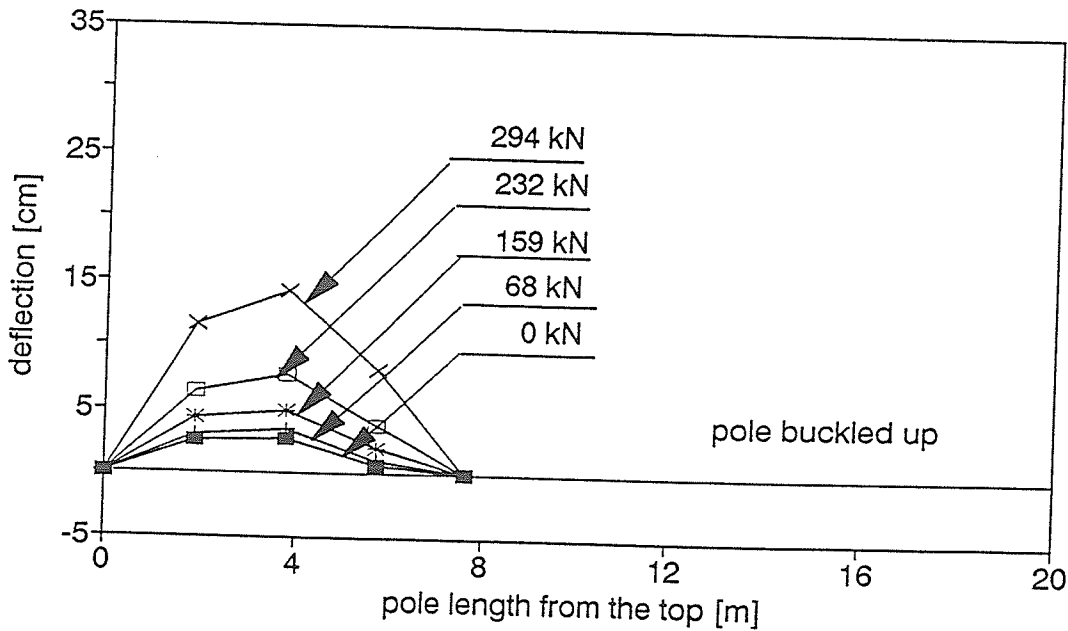
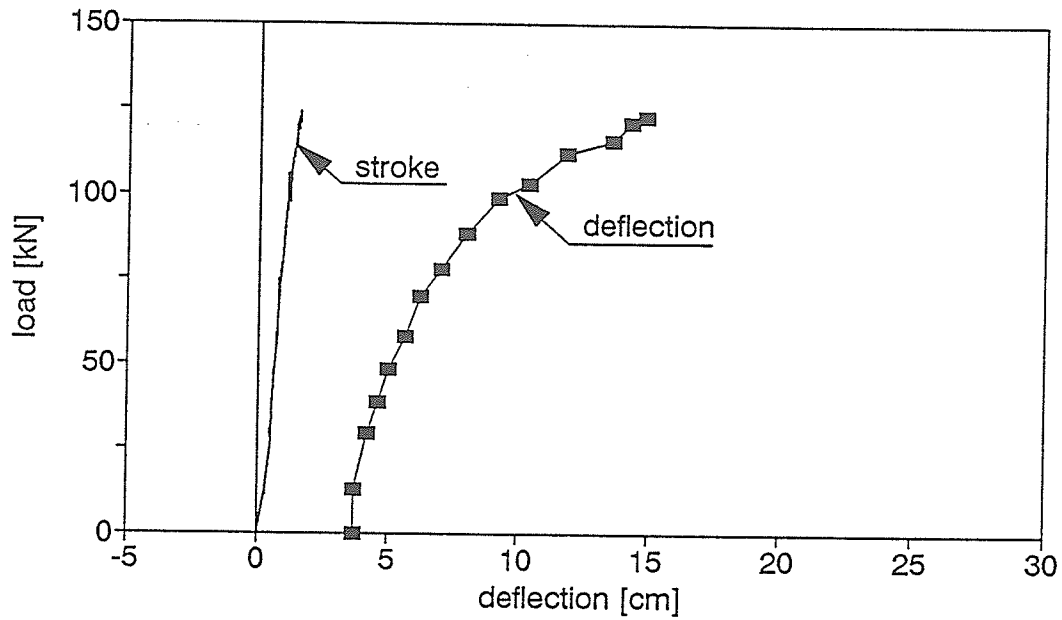


Figure A2.46. Load-deflection relationship and deflected shape of the pole

## POLE 9/1 DEFLECTION AT THE MIDSPAN



## DEFLECTED SHAPE OF THE POLE 9/1 UNDER DIFFERENT LOAD LEVELS

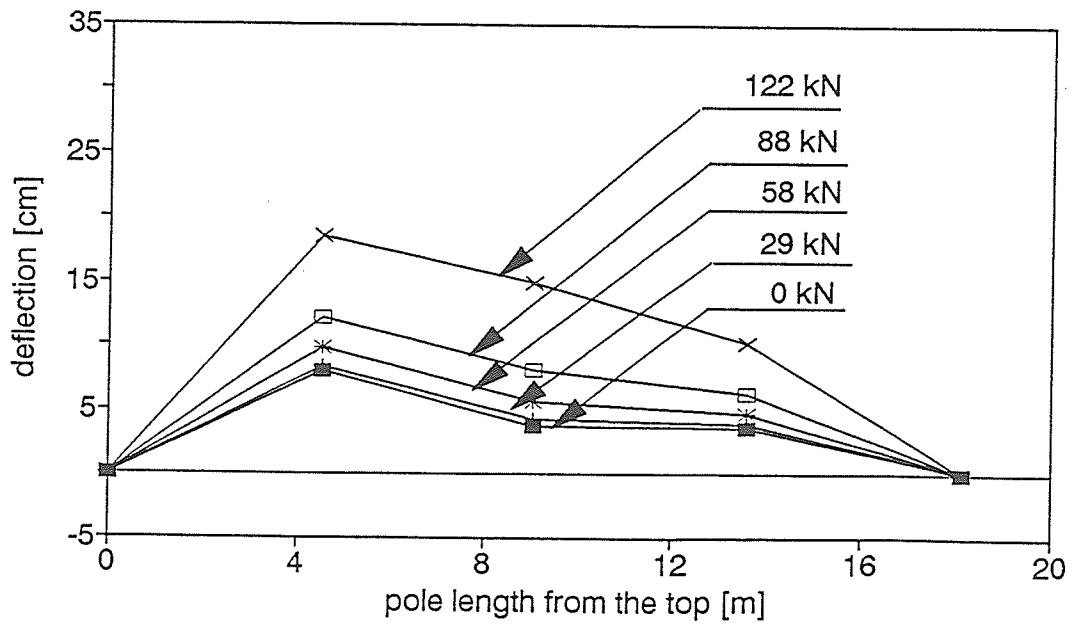
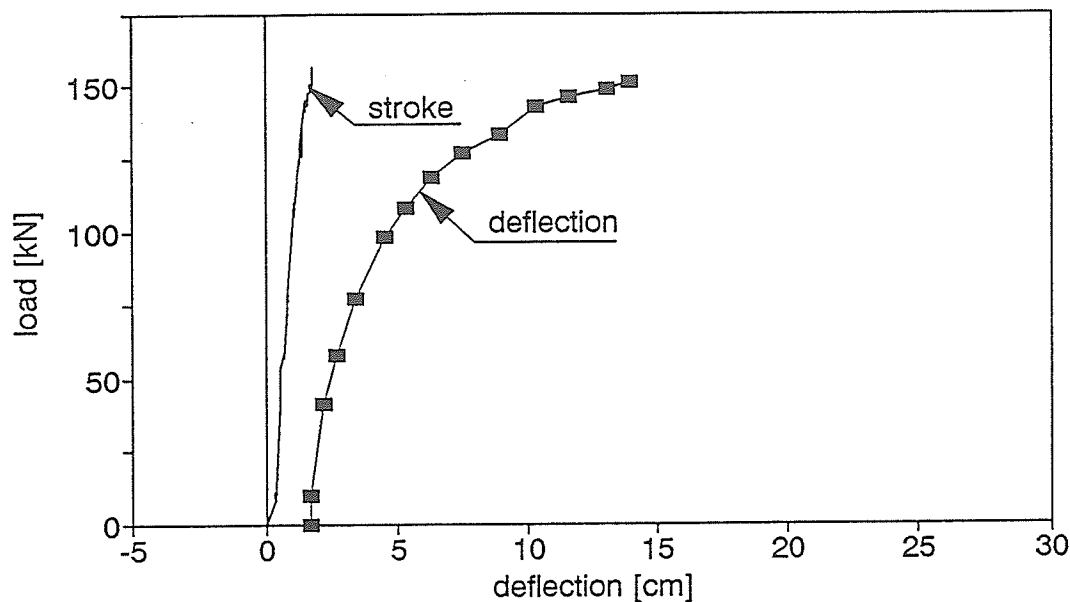


Figure A2.47. Load-deflection relationship and deflected shape of the pole

## POLE 9/2 DEFLECTION AT THE MIDSPAN



## DEFLECTED SHAPE OF THE POLE 9/2 UNDER DIFFERENT LOAD LEVELS

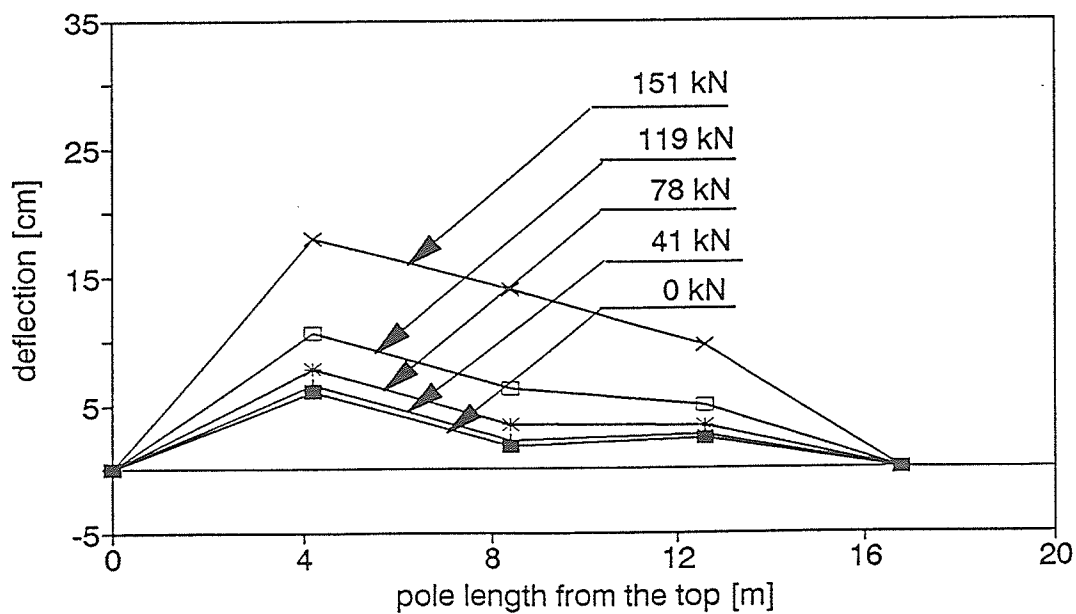
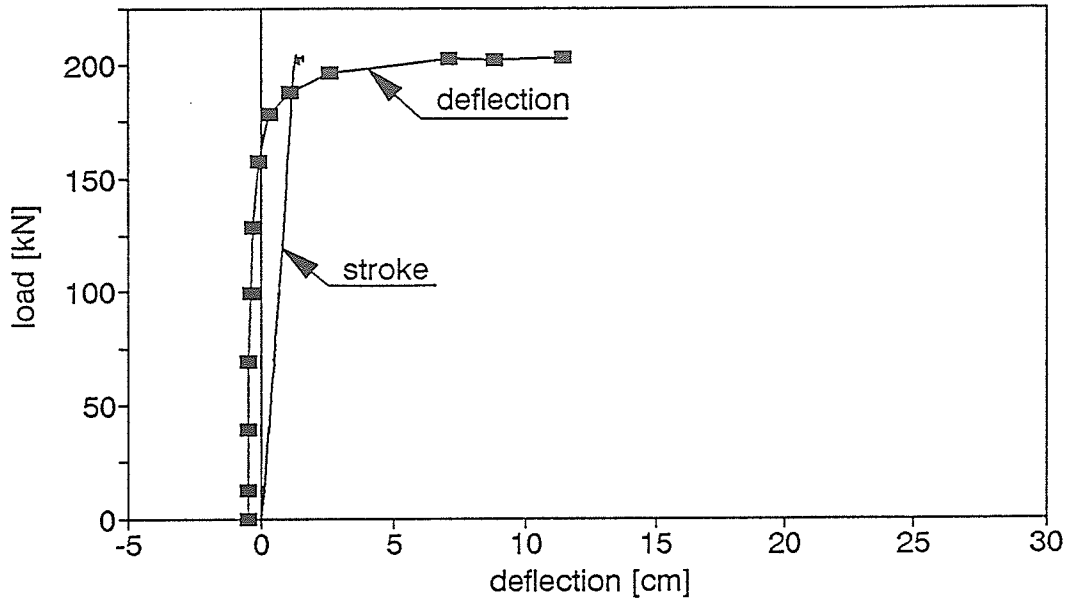


Figure A2.48. Load-deflection relationship and deflected shape of the pole

## POLE 9/3 DEFLECTION AT THE MIDSPAN



## DEFLECTED SHAPE OF THE POLE 9/3 UNDER DIFFERENT LOAD LEVELS

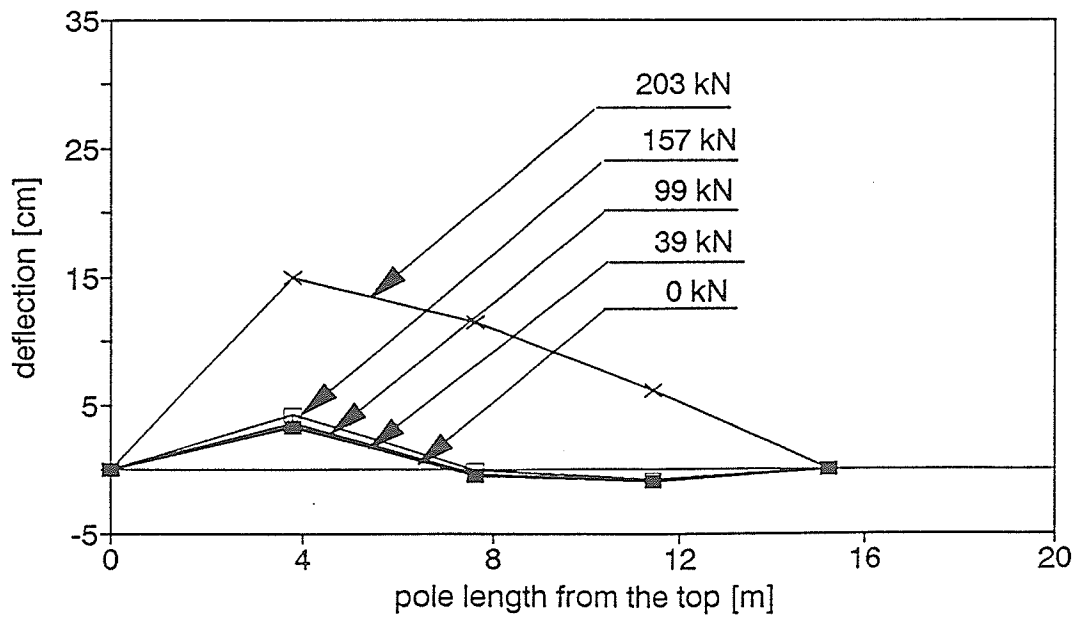
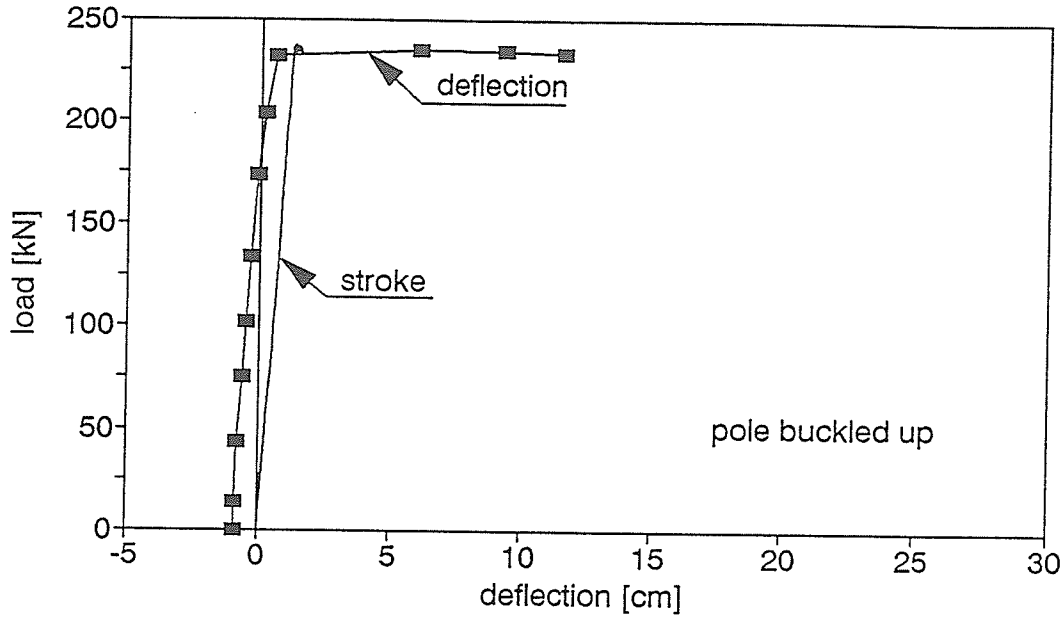


Figure A2.49. Load-deflection relationship and deflected shape of the pole

### POLE 9/4 DEFLECTION AT THE MIDSPAN



### DEFLECTED SHAPE OF THE POLE 9/4 UNDER DIFFERENT LOAD LEVELS

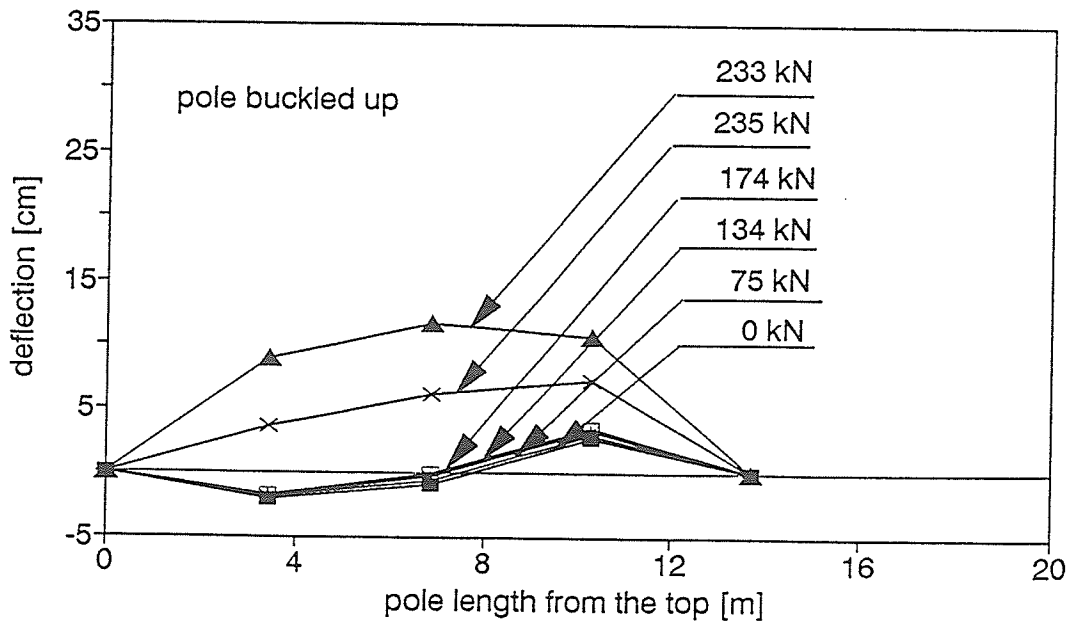
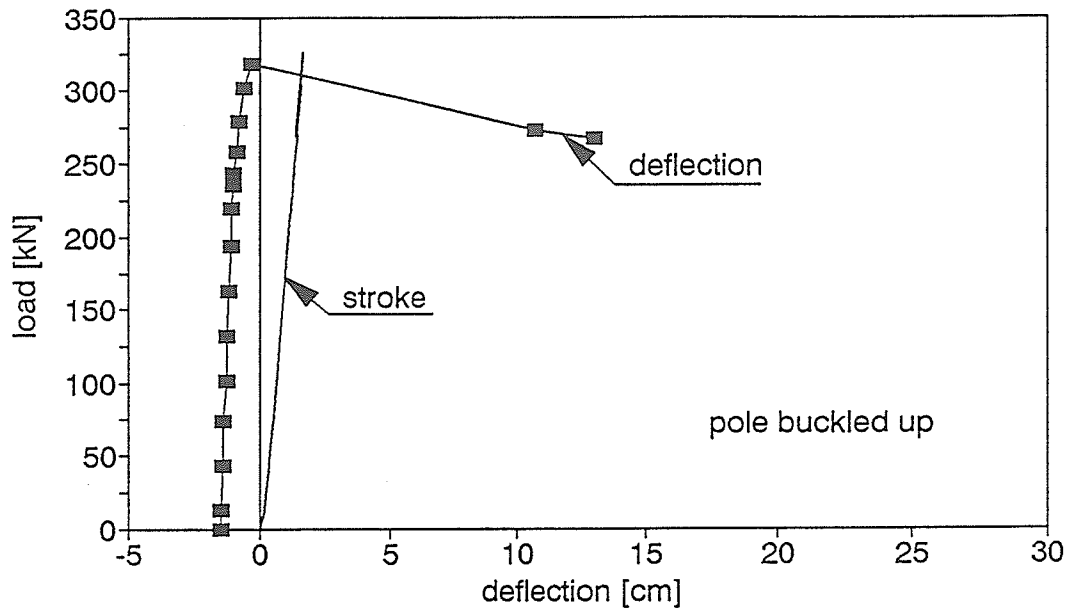


Figure A2.50. Load-deflection relationship and deflected shape of the pole

## POLE 9/5 DEFLECTION AT THE MIDSPAN



## DEFLECTED SHAPE OF THE POLE 9/5 UNDER DIFFERENT LOAD LEVELS

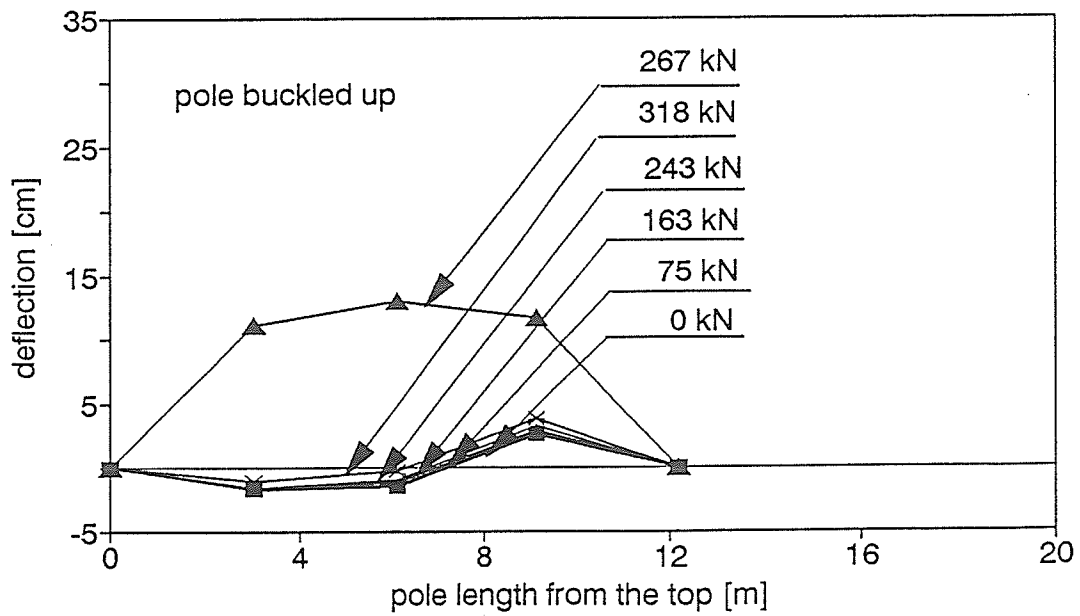
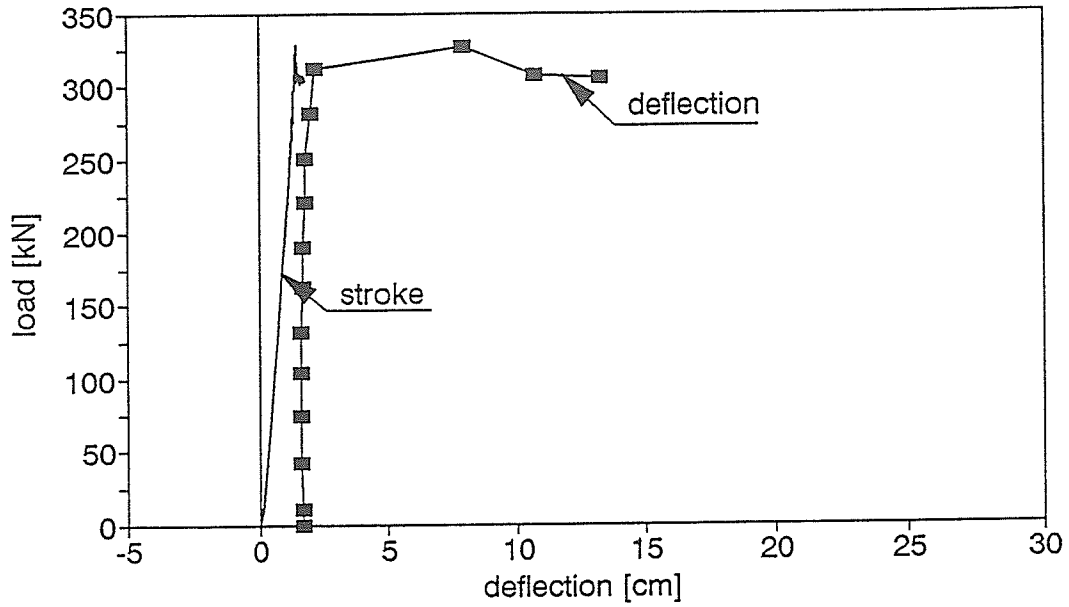


Figure A2.51. Load-deflection relationship and deflected shape of the pole

### POLE 9/6 DEFLECTION AT THE MIDSPAN



### DEFLECTED SHAPE OF THE POLE 9/6 UNDER DIFFERENT LOAD LEVELS

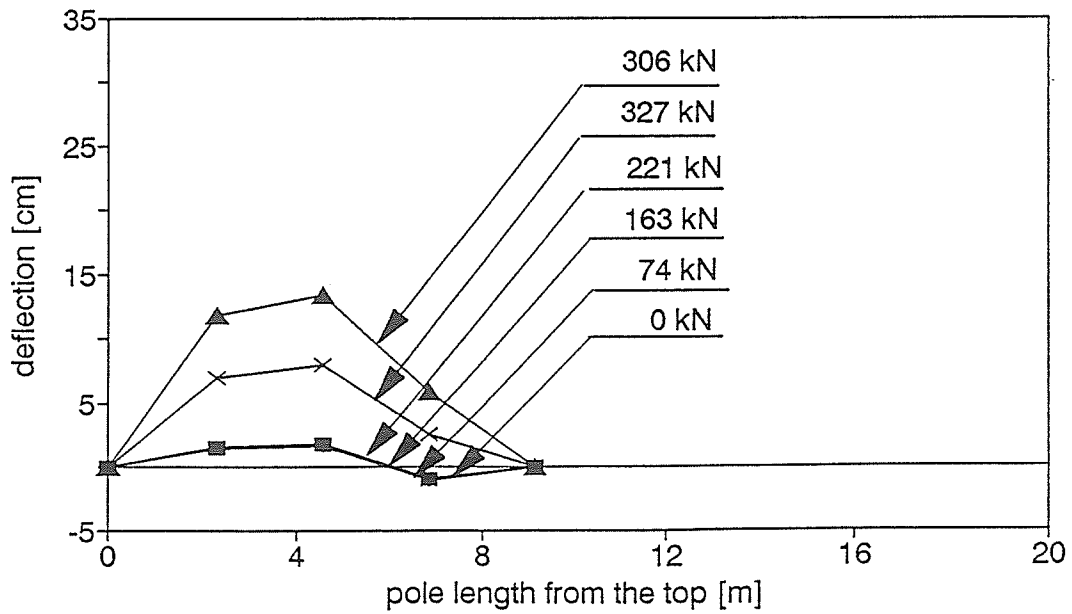
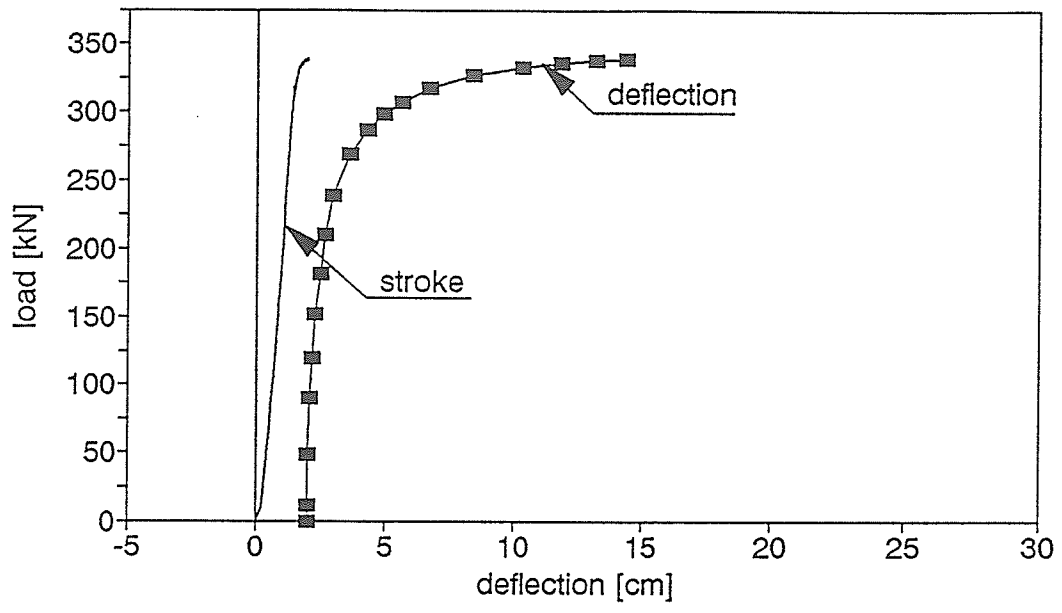


Figure A2.52. Load-deflection relationship and deflected shape of the pole

# POLE 9/7

## DEFLECTION AT THE MIDSPAN



## DEFLECTED SHAPE OF THE POLE 9/7

### UNDER DIFFERENT LOAD LEVELS

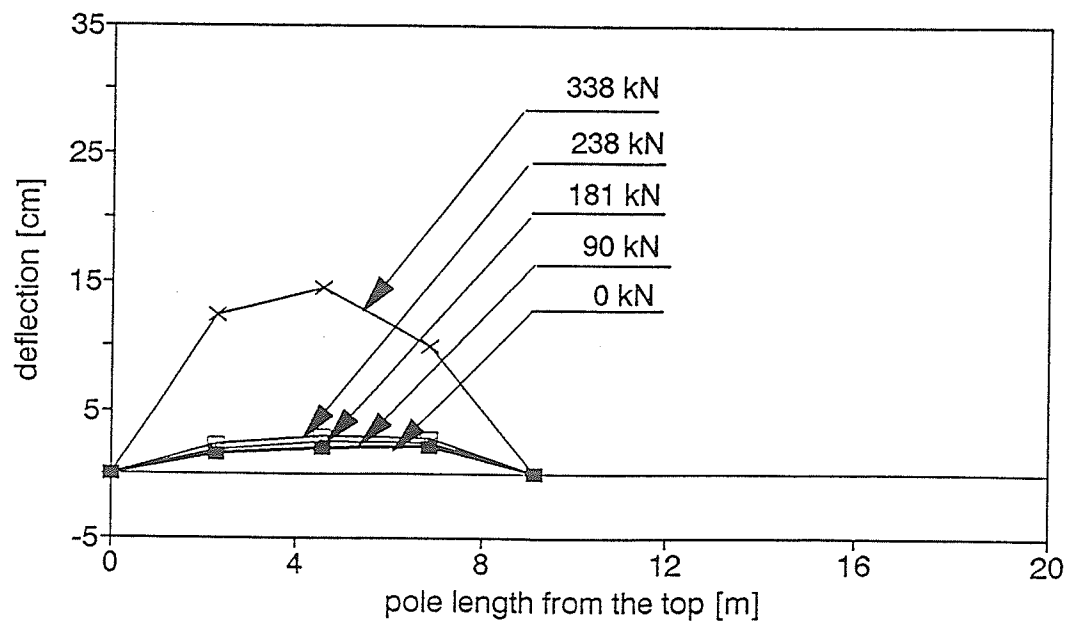
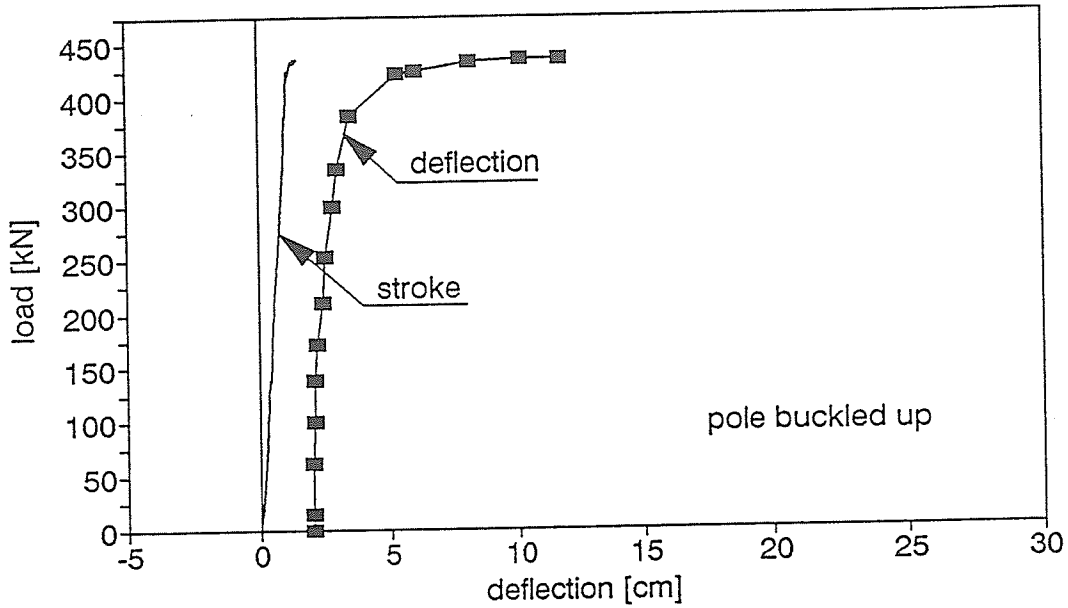


Figure A2.53. Load-deflection relationship and deflected shape of the pole

## POLE 9/8 DEFLECTION AT THE MIDSPAN



## DEFLECTED SHAPE OF THE POLE 9/8 UNDER DIFFERENT LOAD LEVELS

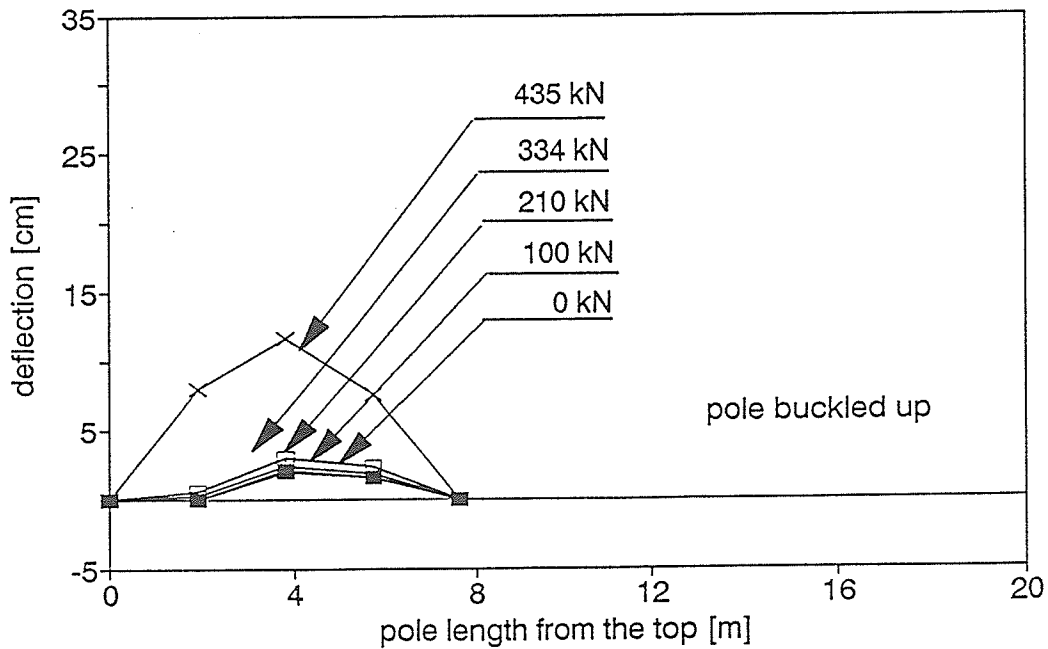
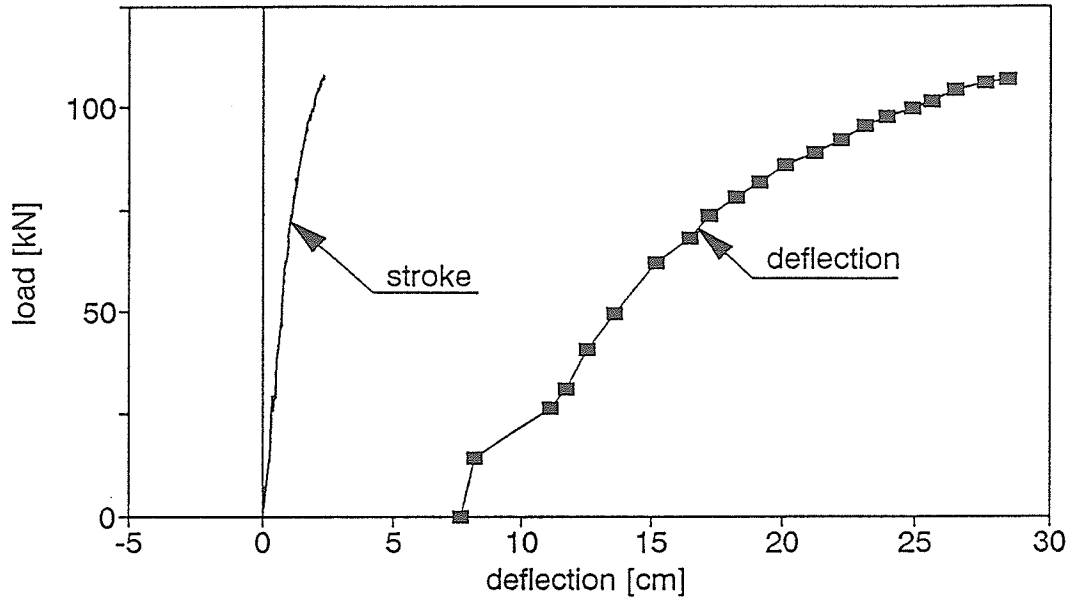


Figure A2.54. Load-deflection relationship and deflected shape of the pole

## POLE 10/1 DEFLECTION AT THE MIDSPAN



## DEFLECTED SHAPE OF THE POLE 10/1 UNDER DIFFERENT LOAD LEVELS

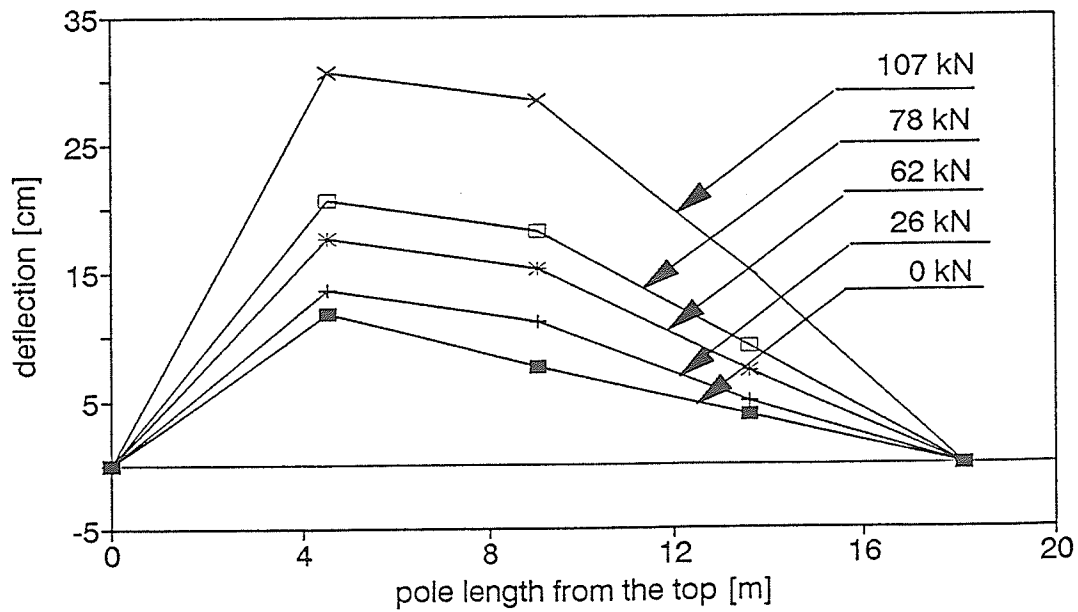
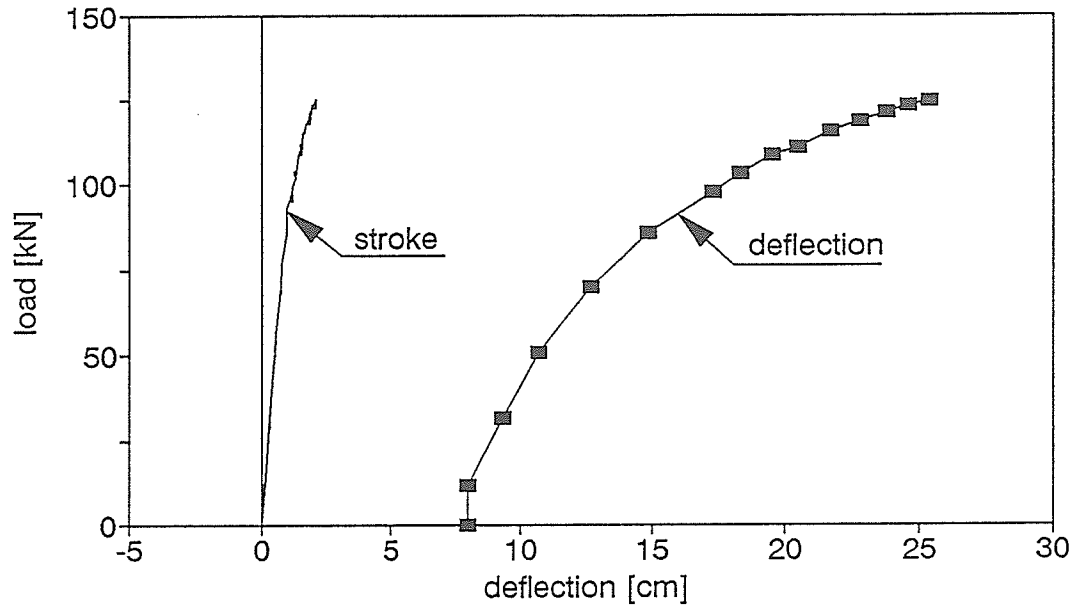


Figure A2.55. Load-deflection relationship and deflected shape of the pole

## POLE 10/2 DEFLECTION AT THE MIDSPAN



## DEFLECTED SHAPE OF THE POLE 10/2 UNDER DIFFERENT LOAD LEVELS

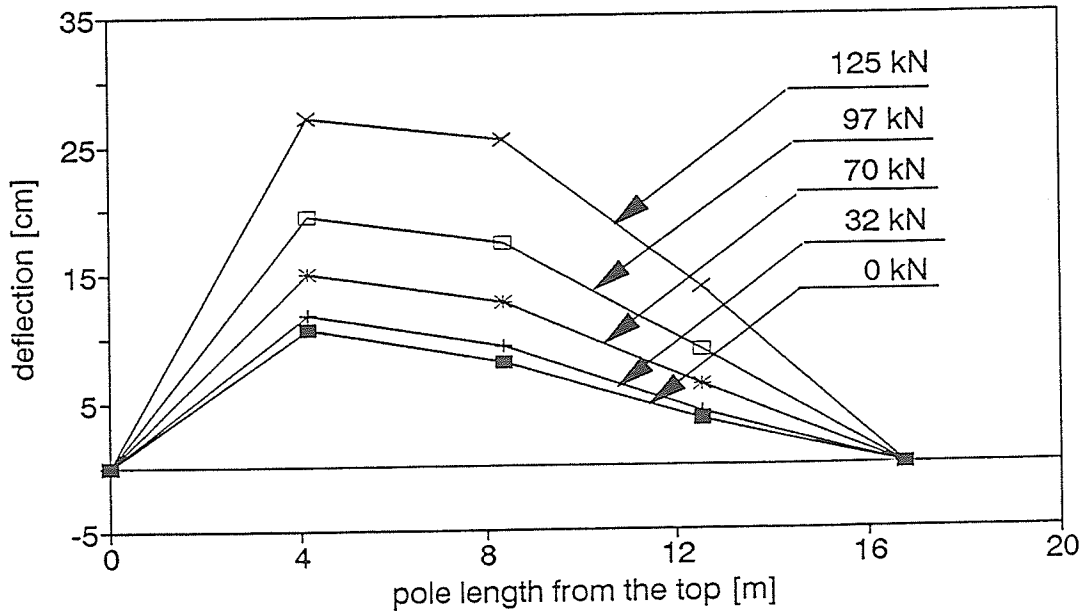
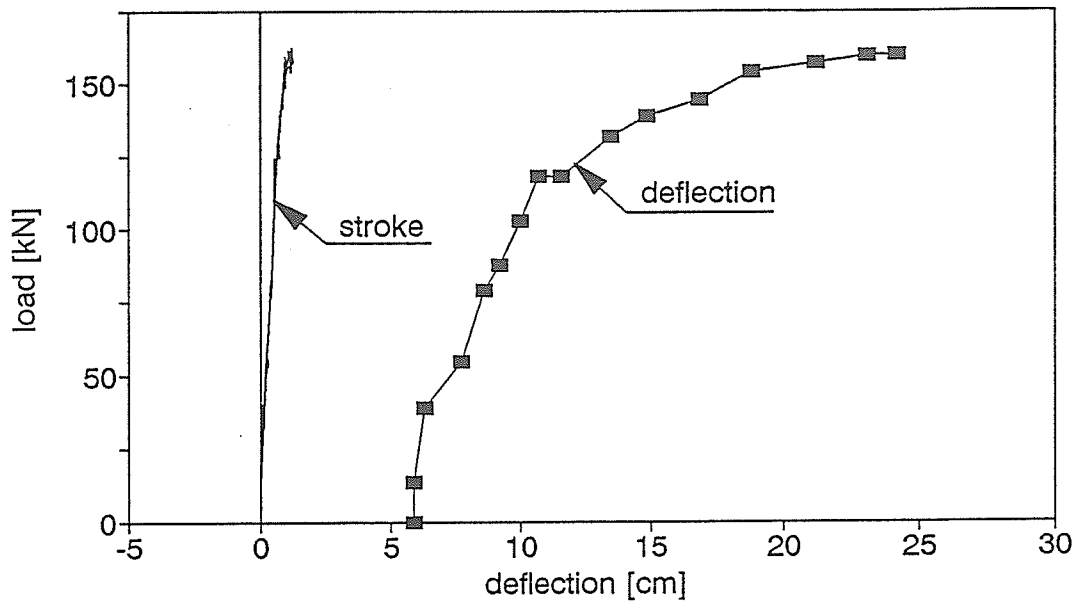


Figure A2.56. Load-deflection relationship and deflected shape of the pole

## POLE 10/3 DEFLECTION AT THE MIDSPAN



## DEFLECTED SHAPE OF THE POLE 10/3 UNDER DIFFERENT LOAD LEVELS

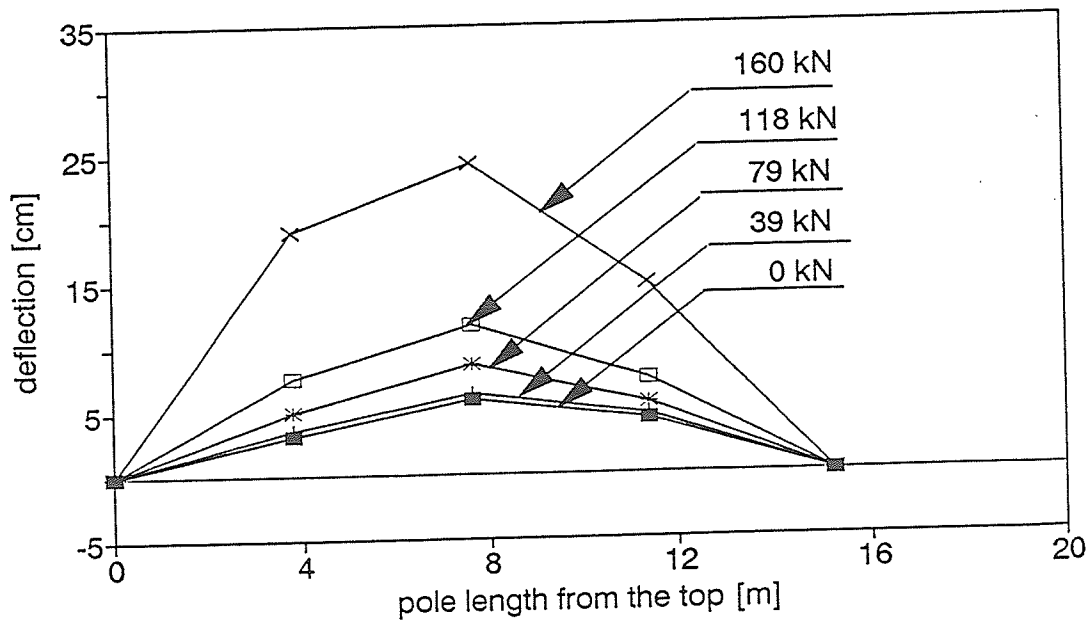
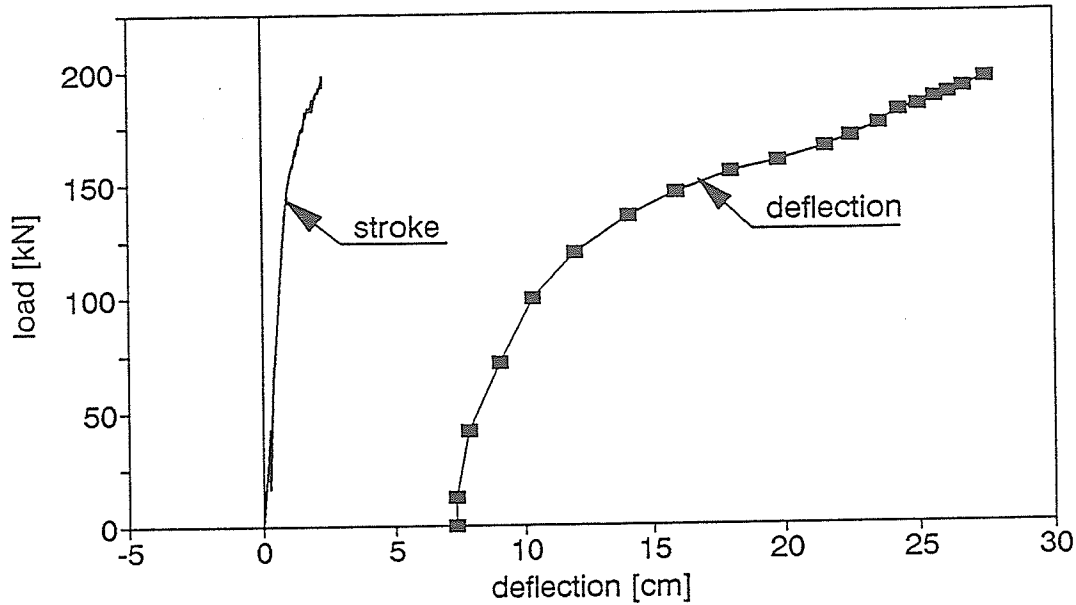


Figure A2.57. Load-deflection relationship and deflected shape of the pole

## POLE 10/4 DEFLECTION AT THE MIDSPAN



## DEFLECTED SHAPE OF THE POLE 10/4 UNDER DIFFERENT LOAD LEVELS

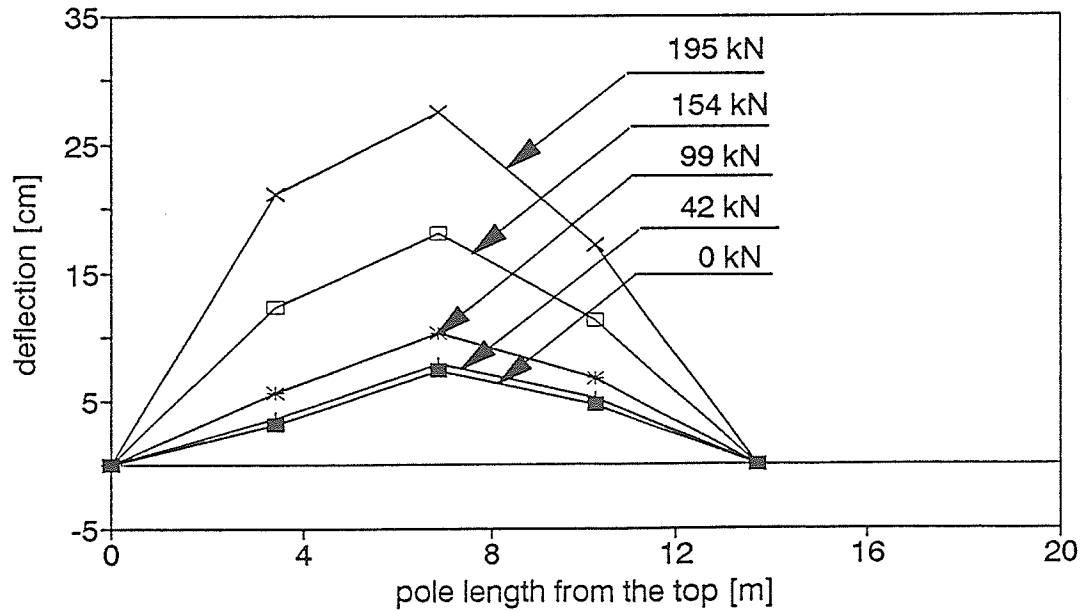
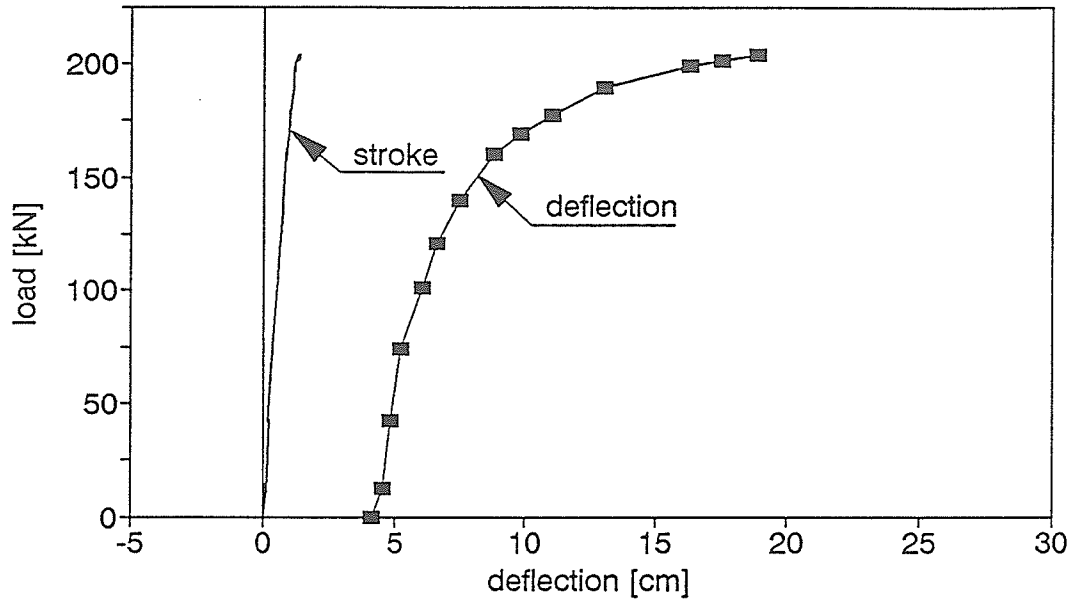


Figure A2.58. Load-deflection relationship and deflected shape of the pole

## POLE 10/5 DEFLECTION AT THE MIDSPAN



## DEFLECTED SHAPE OF THE POLE 10/5 UNDER DIFFERENT LOAD LEVELS

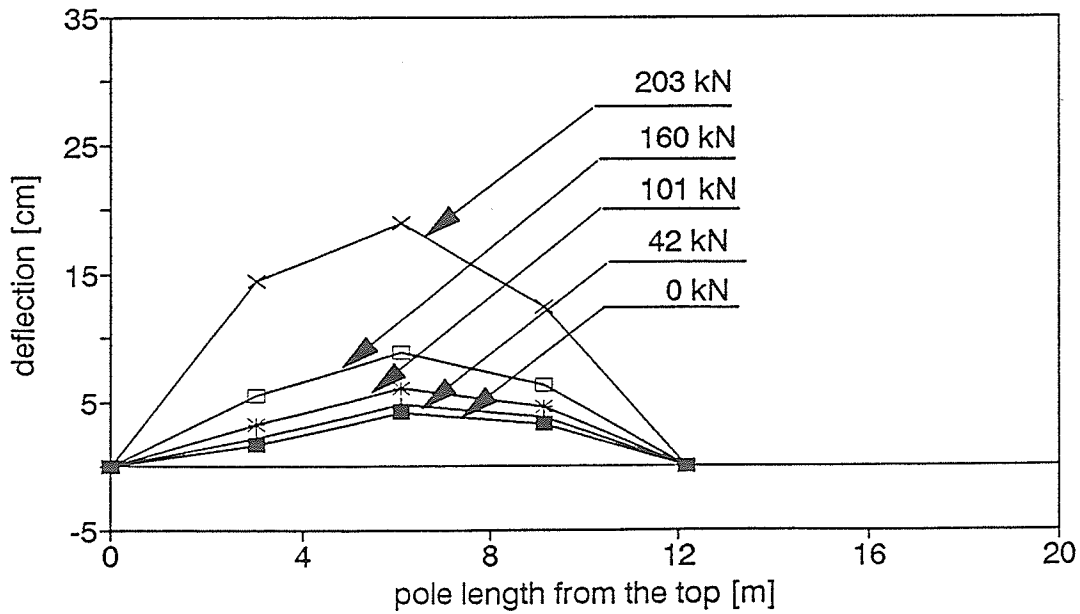
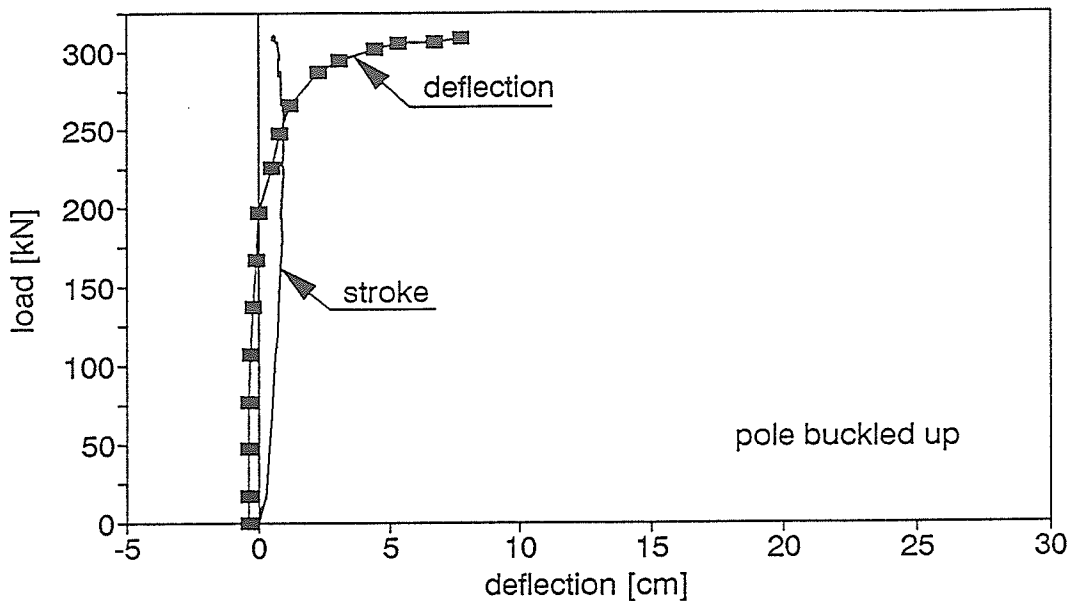


Figure A2.59. Load-deflection relationship and deflected shape of the pole

## POLE 10/6 DEFLECTION AT THE MIDSPAN



## DEFLECTED SHAPE OF THE POLE 10/6 UNDER DIFFERENT LOAD LEVELS

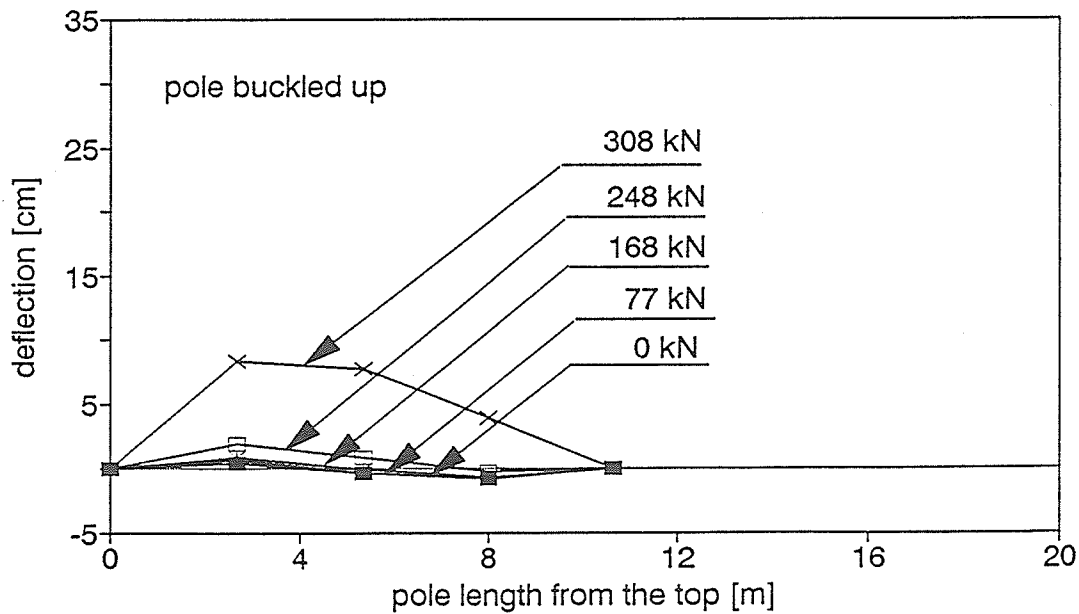
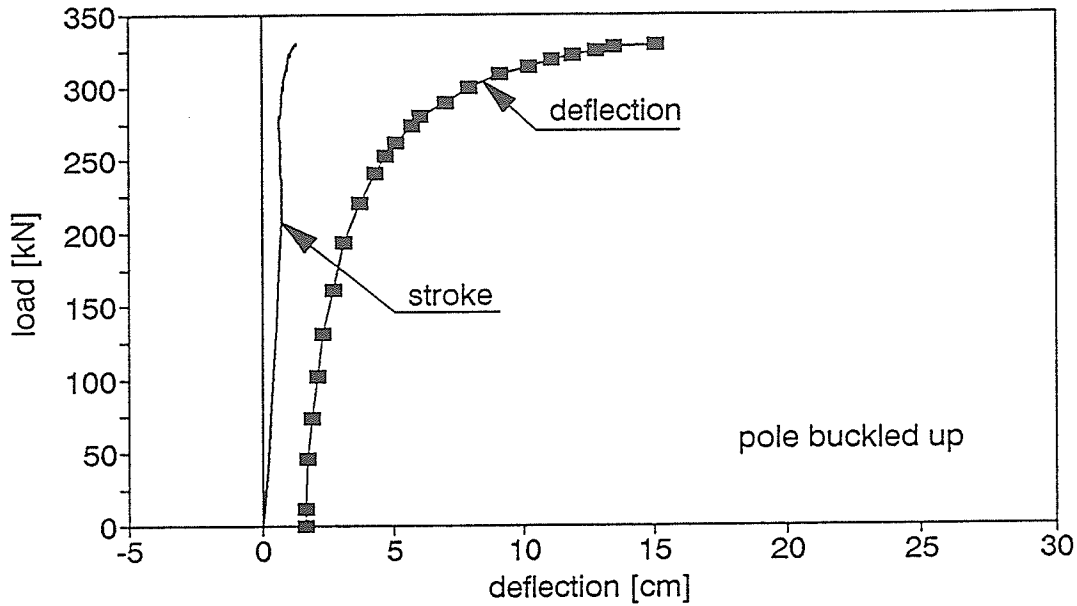


Figure A2.60. Load-deflection relationship and deflected shape of the pole

## POLE 10/7 DEFLECTION AT THE MIDSPAN



## DEFLECTED SHAPE OF THE POLE 10/7 UNDER DIFFERENT LOAD LEVELS

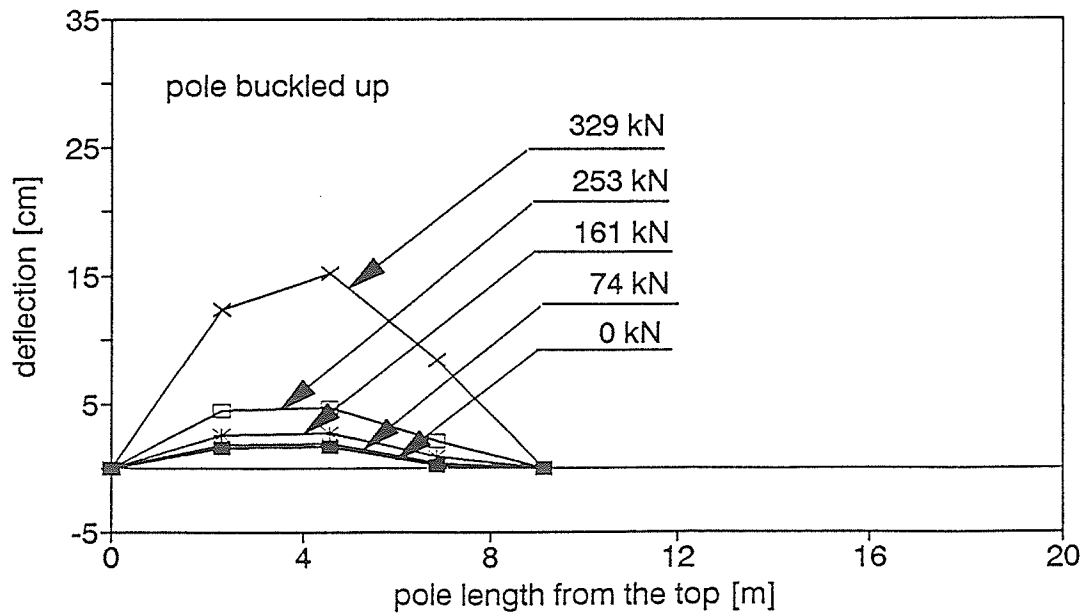
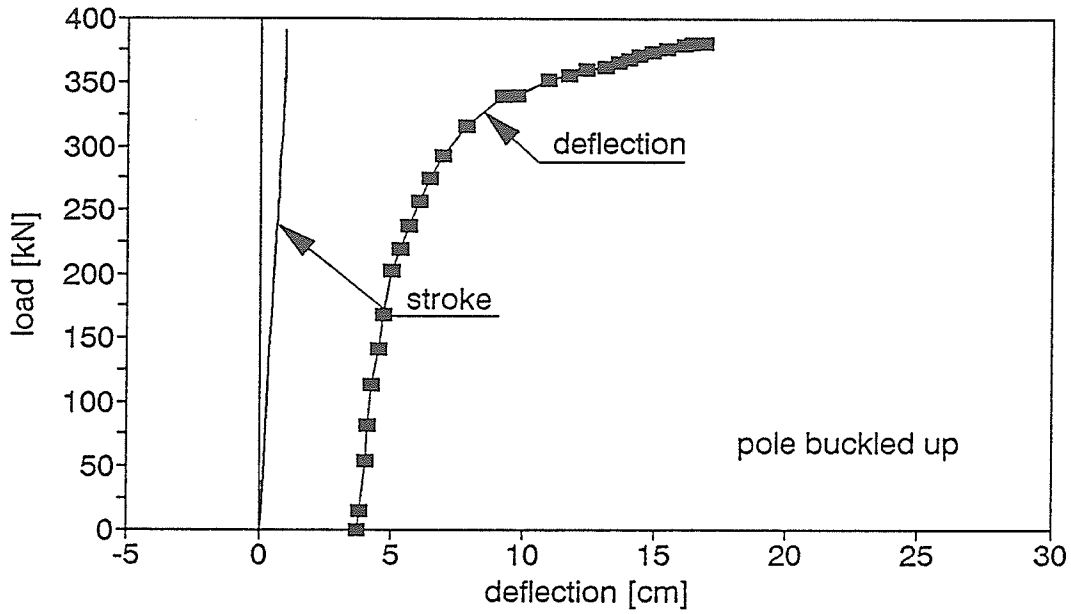


Figure A2.61. Load-deflection relationship and deflected shape of the pole

## POLE 10/8 DEFLECTION AT THE MIDSPAN



## DEFLECTED SHAPE OF THE POLE 10/8 UNDER DIFFERENT LOAD LEVELS

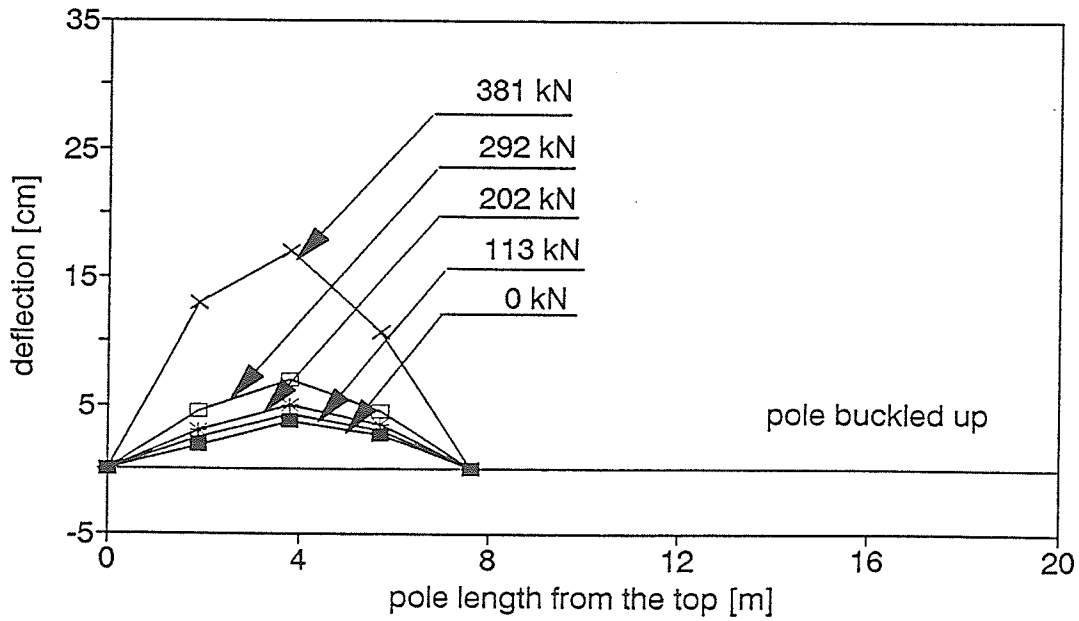


Figure A2.62. Load-deflection relationship and deflected shape of the pole

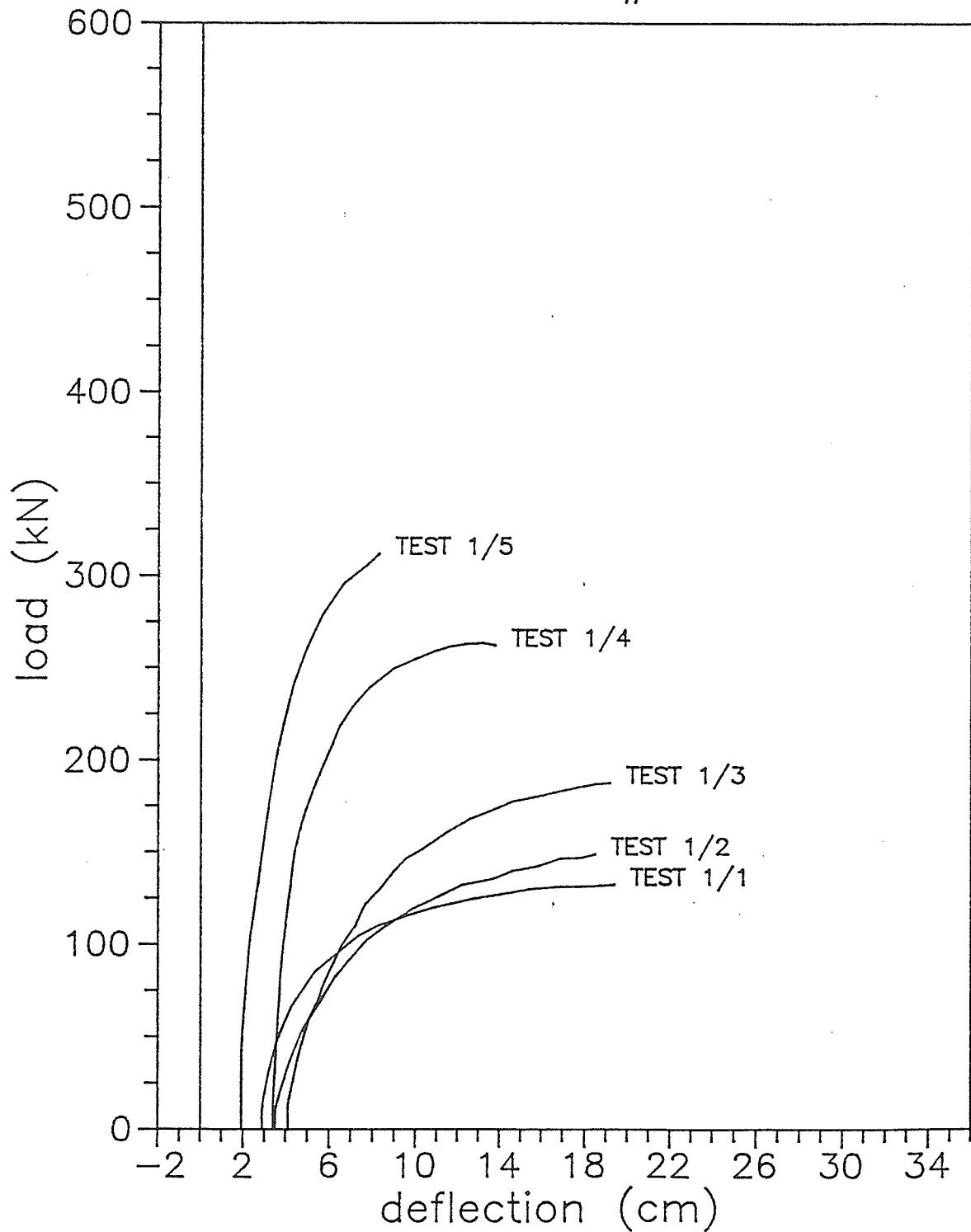


Figure A3.1. Load-deflection relationship of the test specimens originated from the same pole

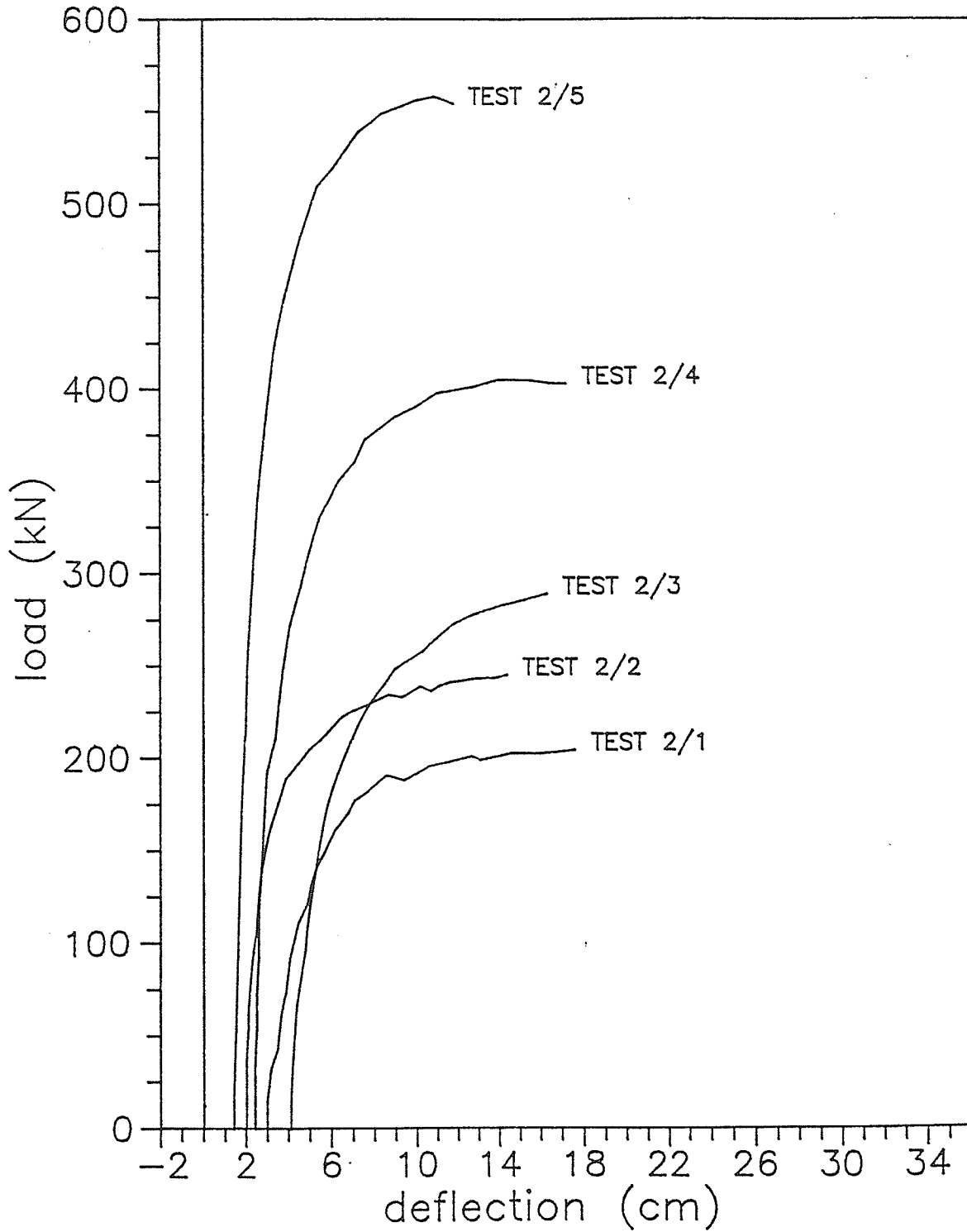


Figure A3.2. Load-deflection relationship of the test specimens originated from the same pole

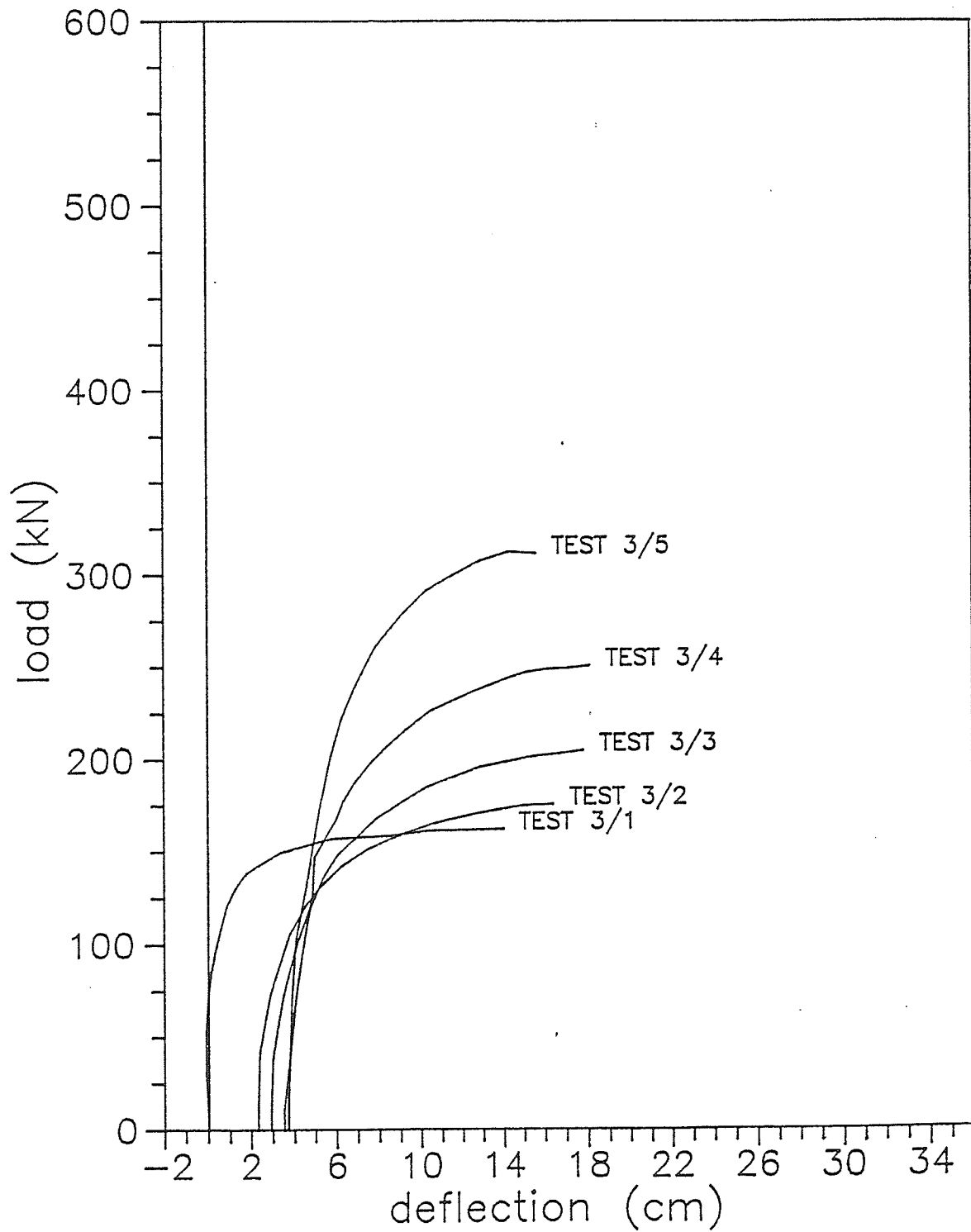


Figure A3.3. Load-deflection relationship of the test specimens originated from the same pole

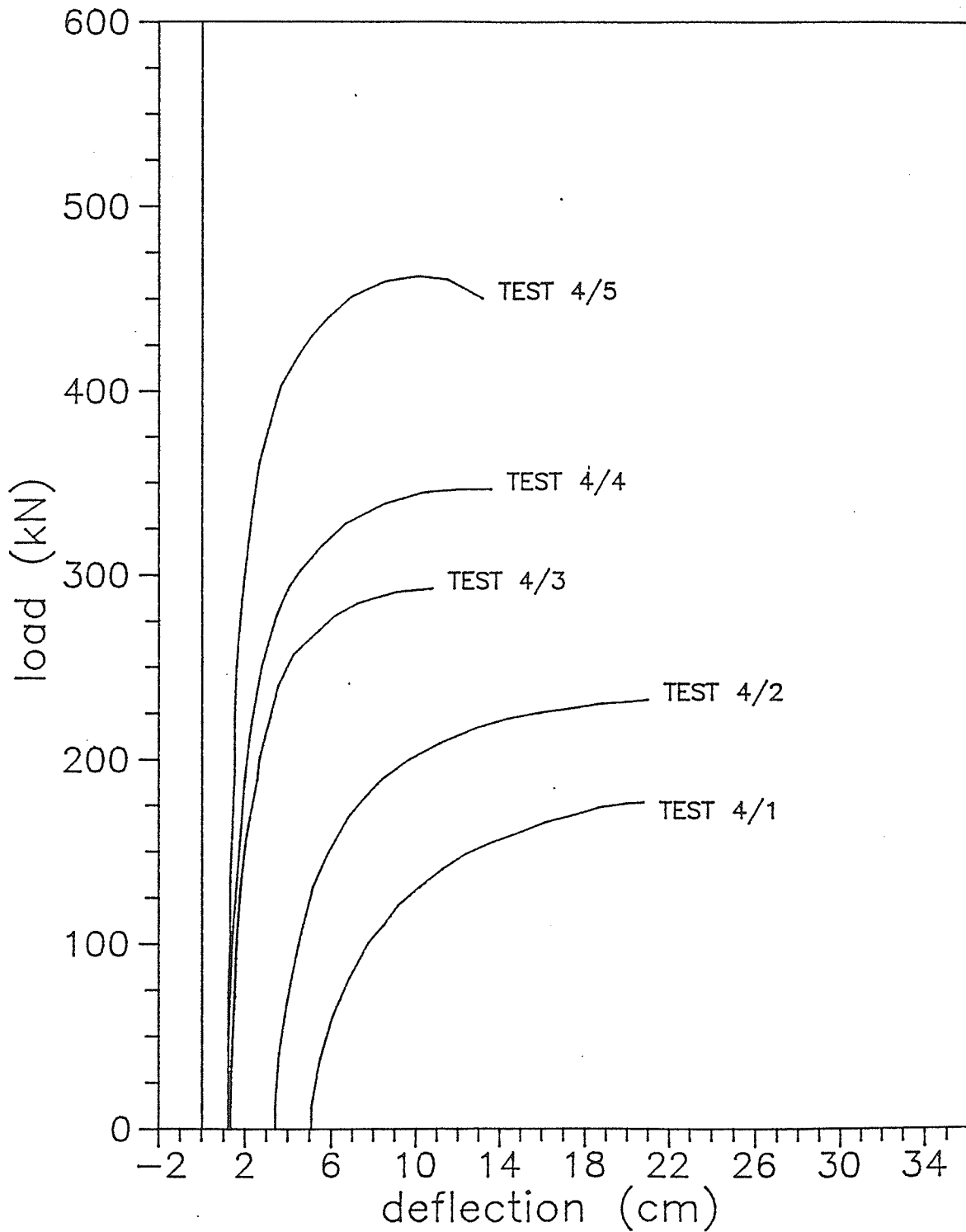


Figure A3.4. Load-deflection relationship of the test specimens originated from the same pole

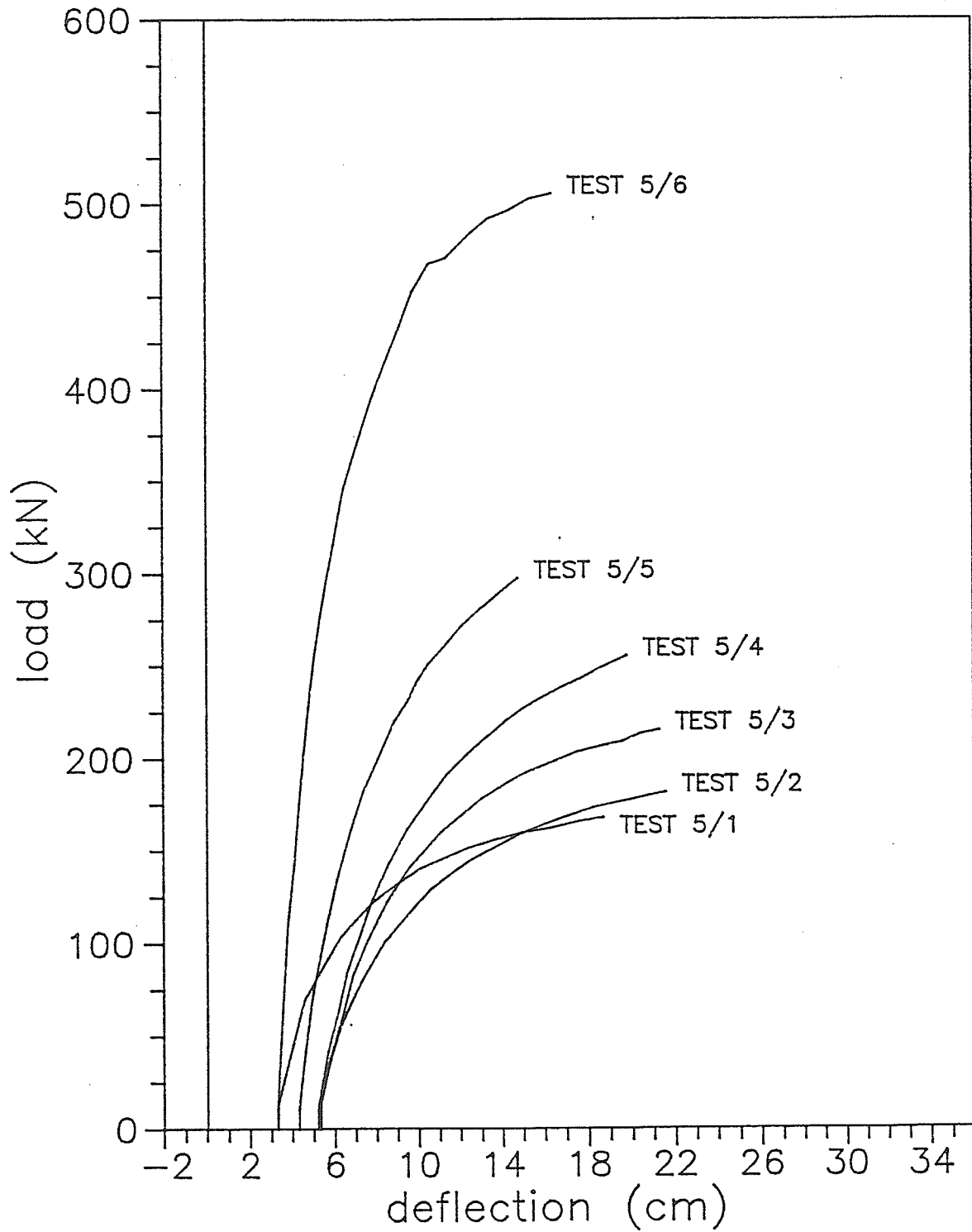


Figure A3.5. Load-deflection relationship of the test specimens originated from the same pole

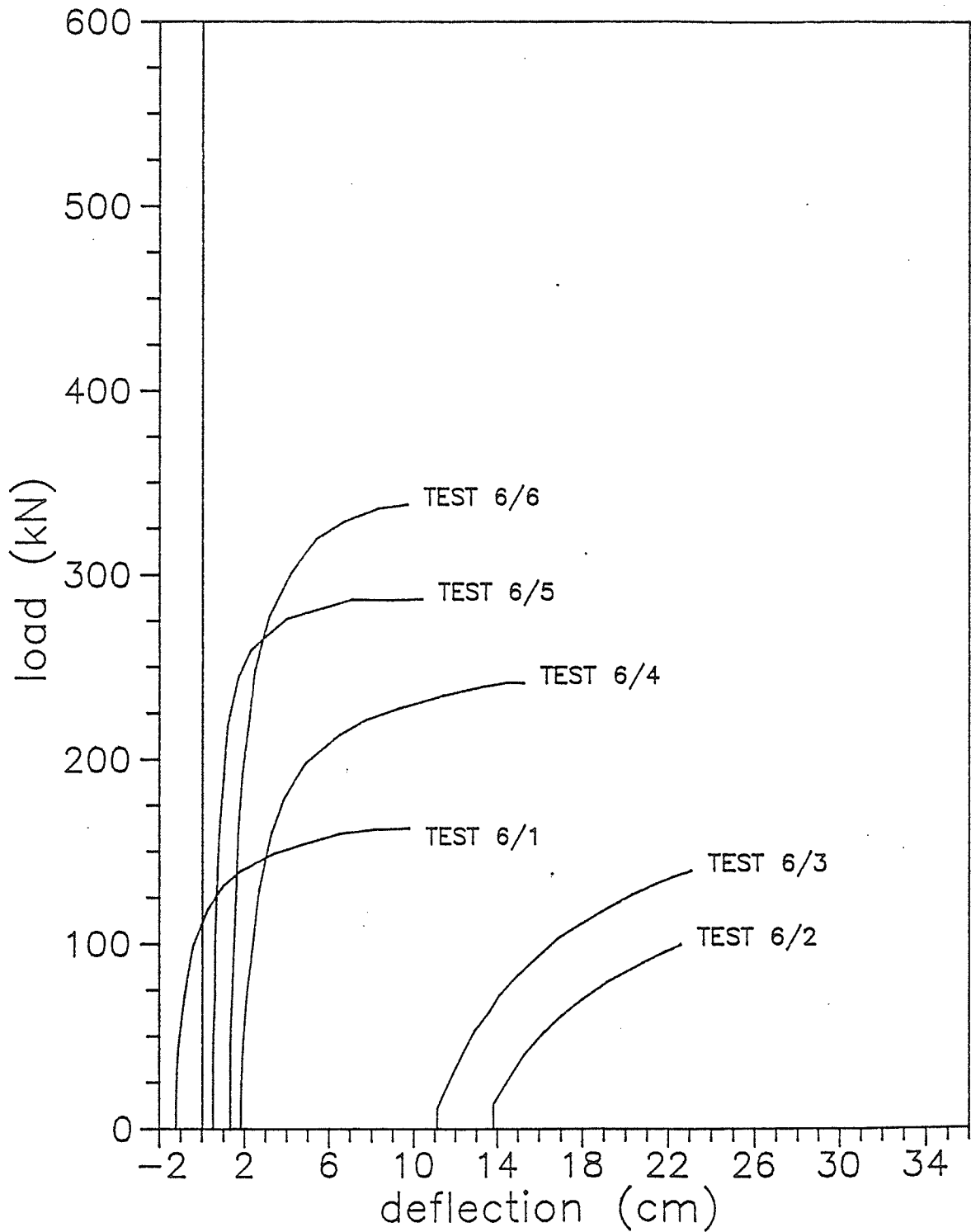


Figure A3.6. Load-deflection relationship of the test specimens originated from the same pole

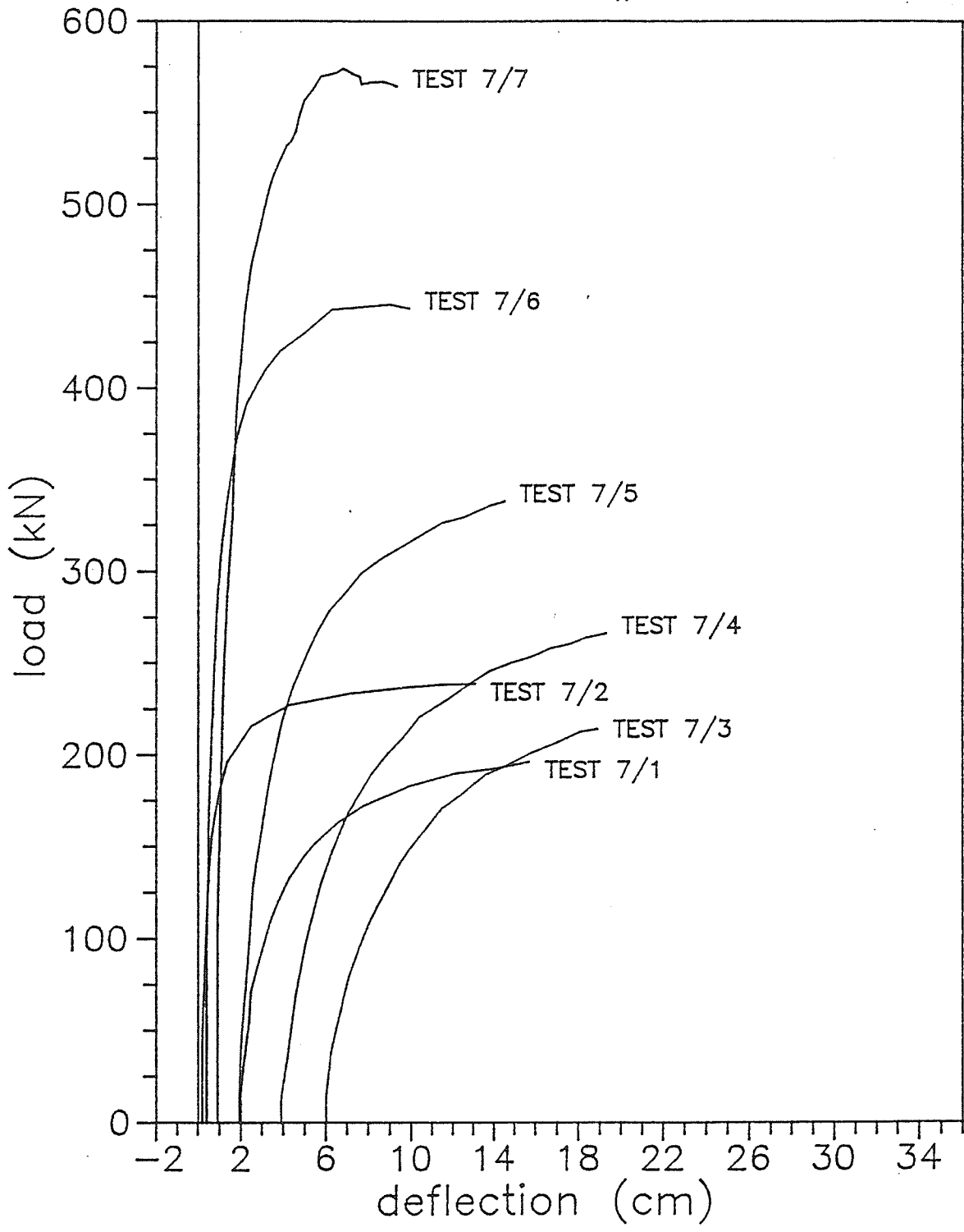


Figure A3.7. Load-deflection relationship of the test specimens originated from the same pole

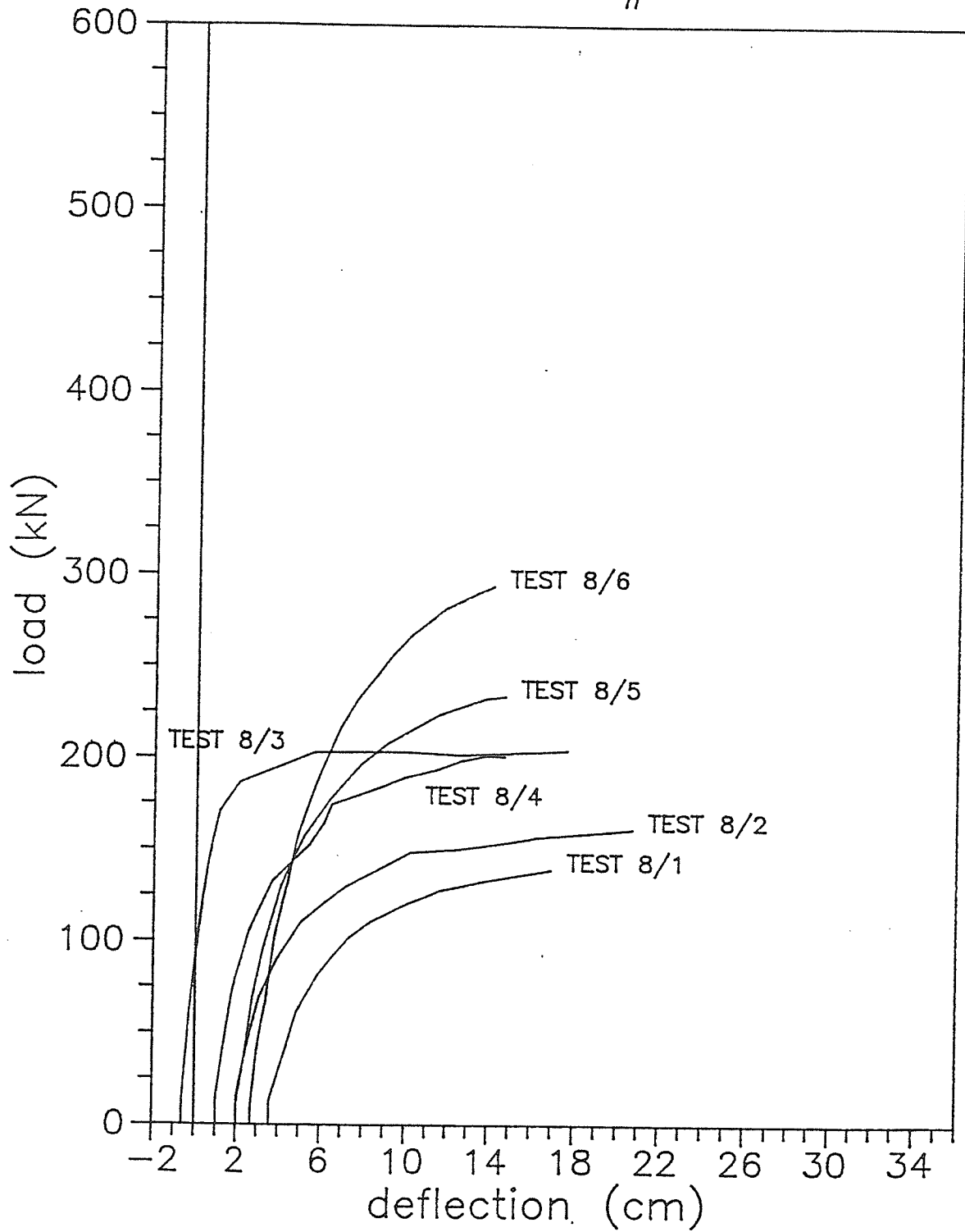


Figure A3.8. Load-deflection relationship of the test specimens originated from the same pole

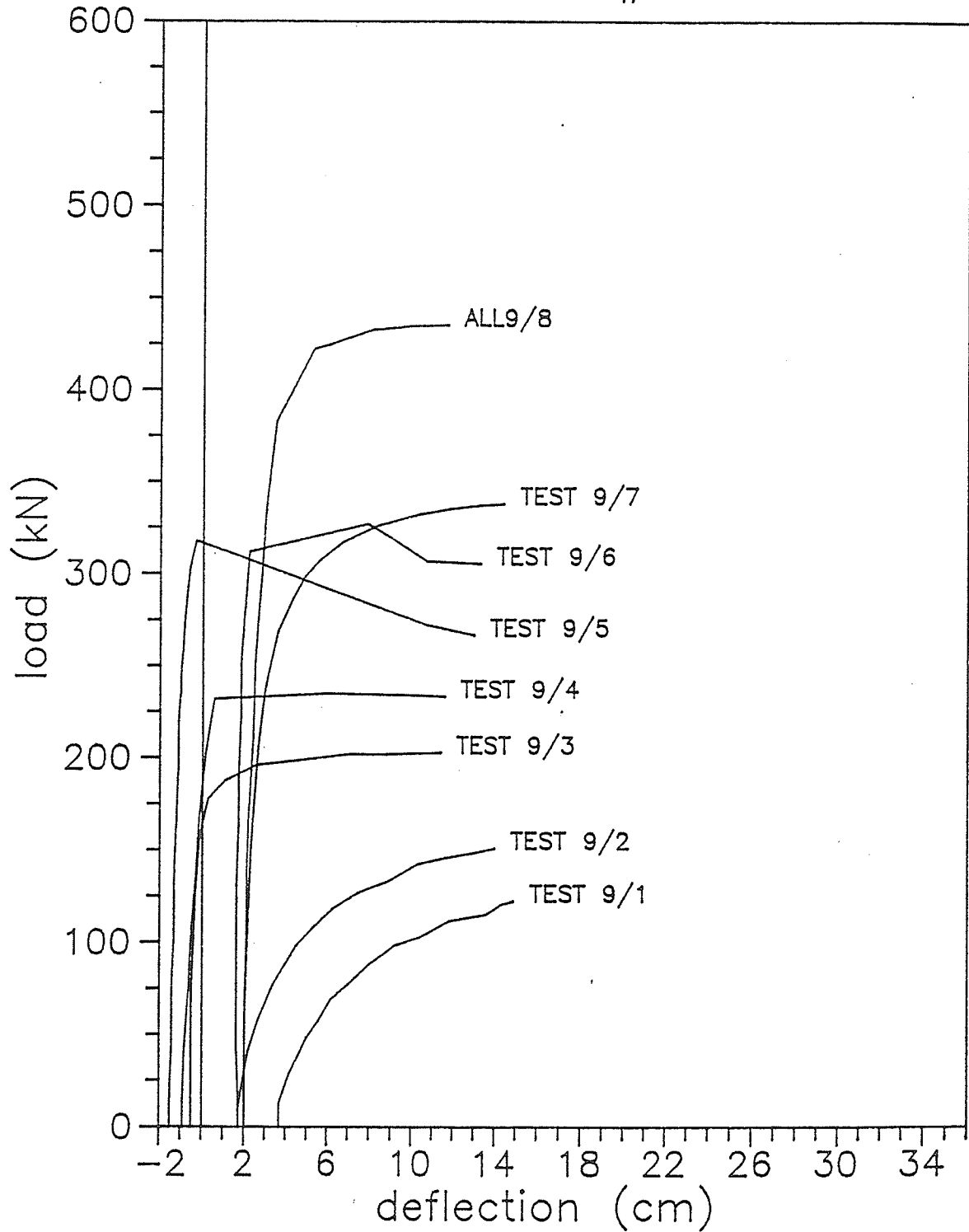


Figure A3.9. Load-deflection relationship of the test specimens originated from the same pole

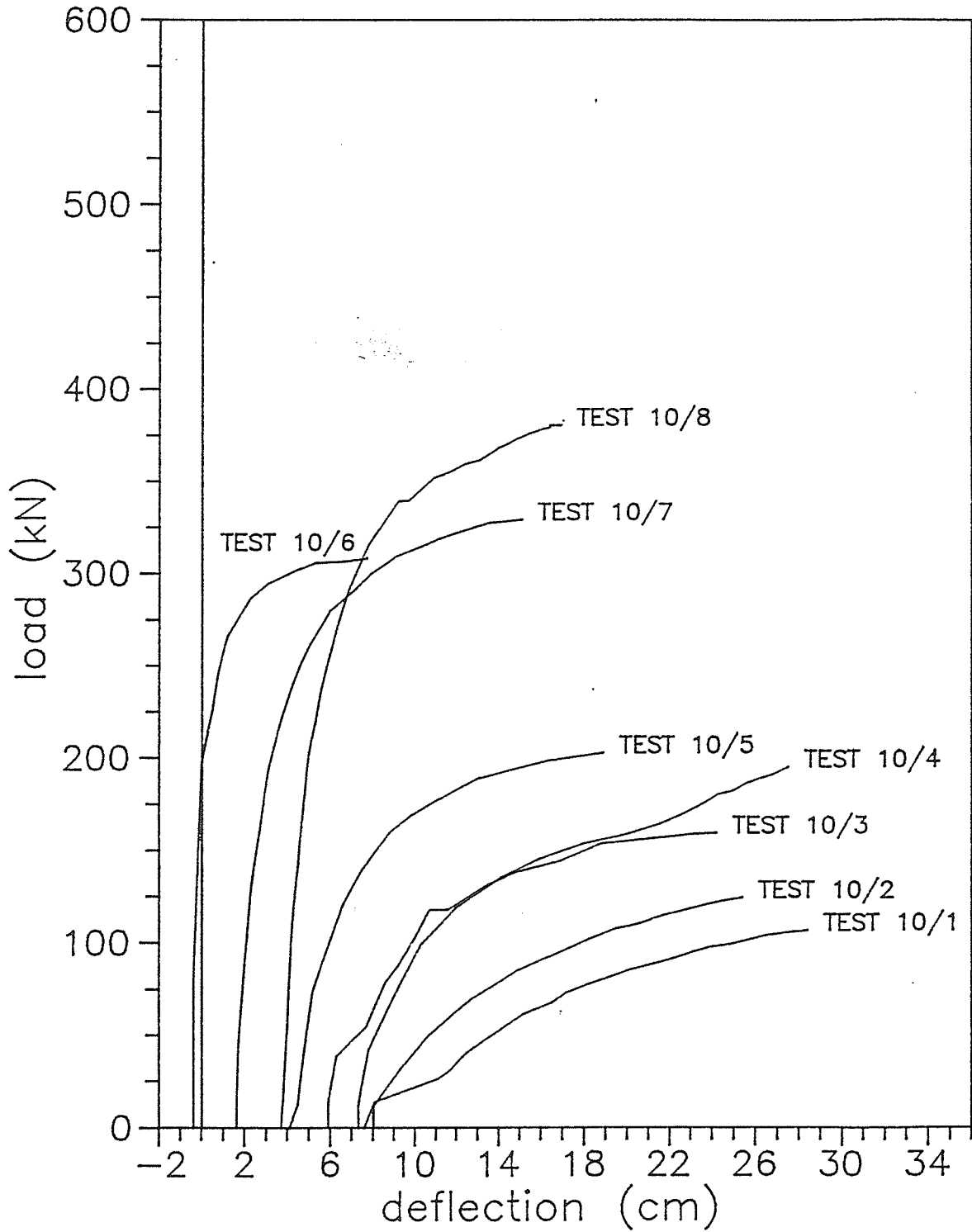


Figure A3.10. Load-deflection relationship of the test specimens originated from the same pole

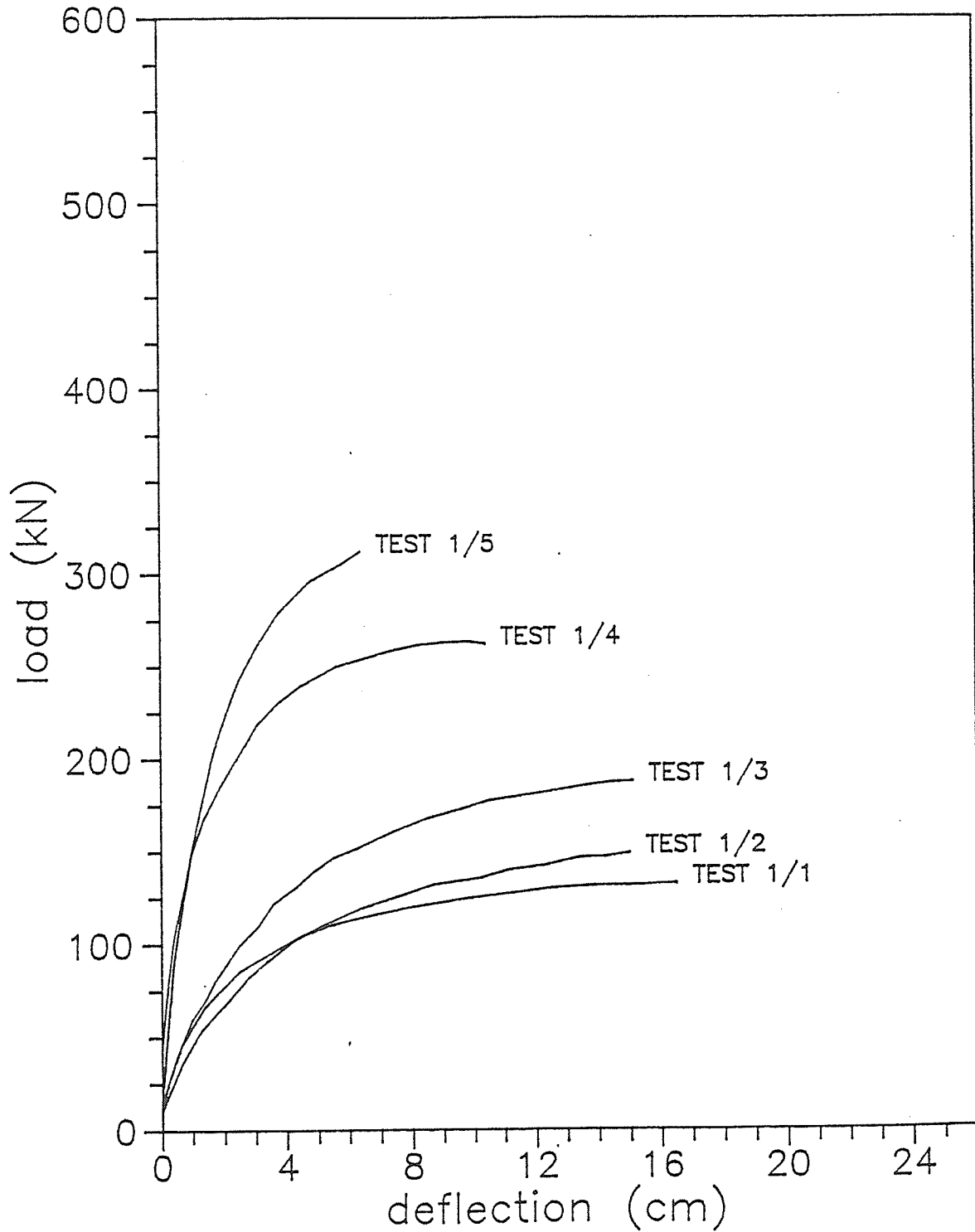


Figure A4.1. Load-relative deflection relationship of the test specimens originated from the same pole

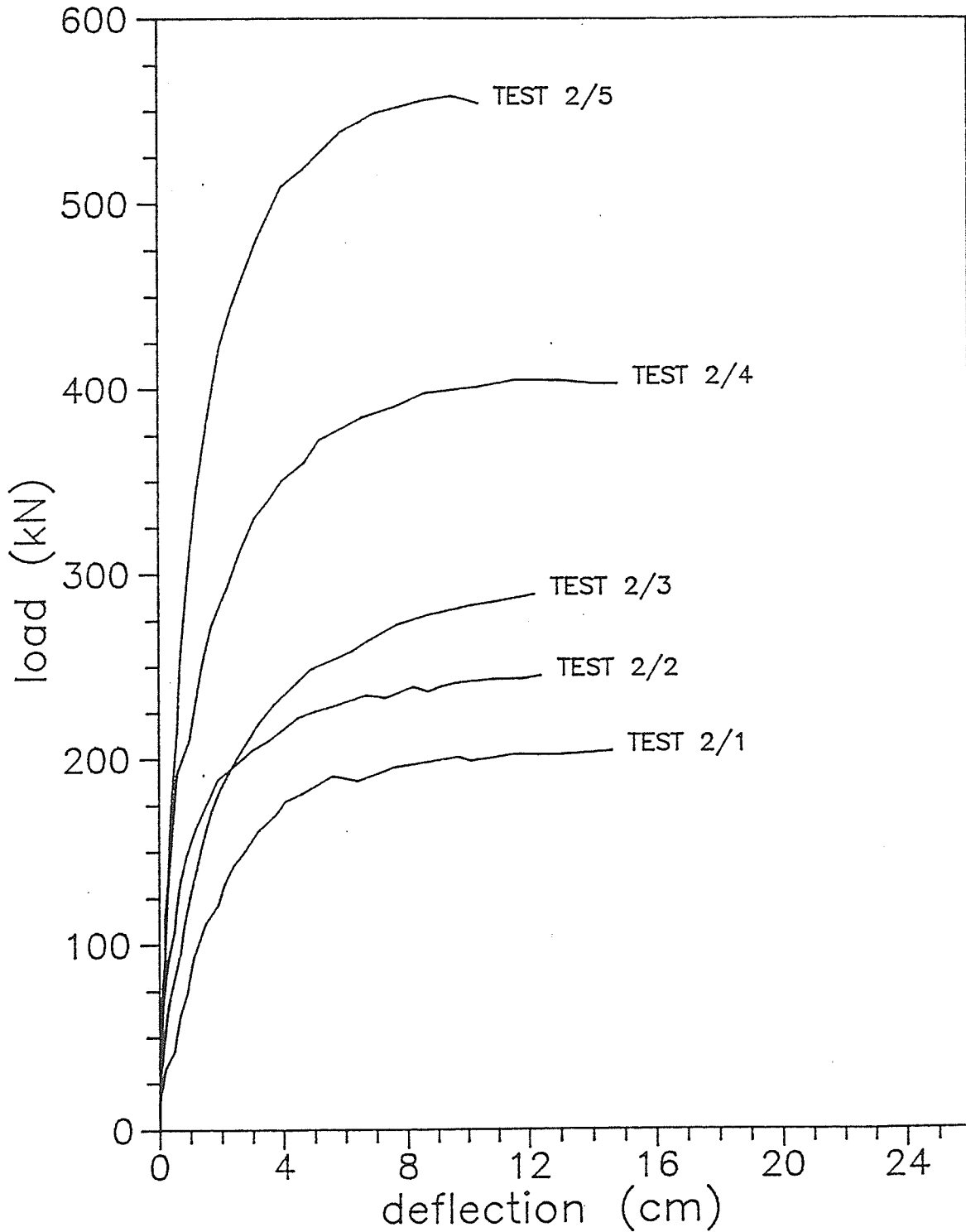


Figure A4.2. Load-relative deflection relationship of the test specimens originated from the same pole

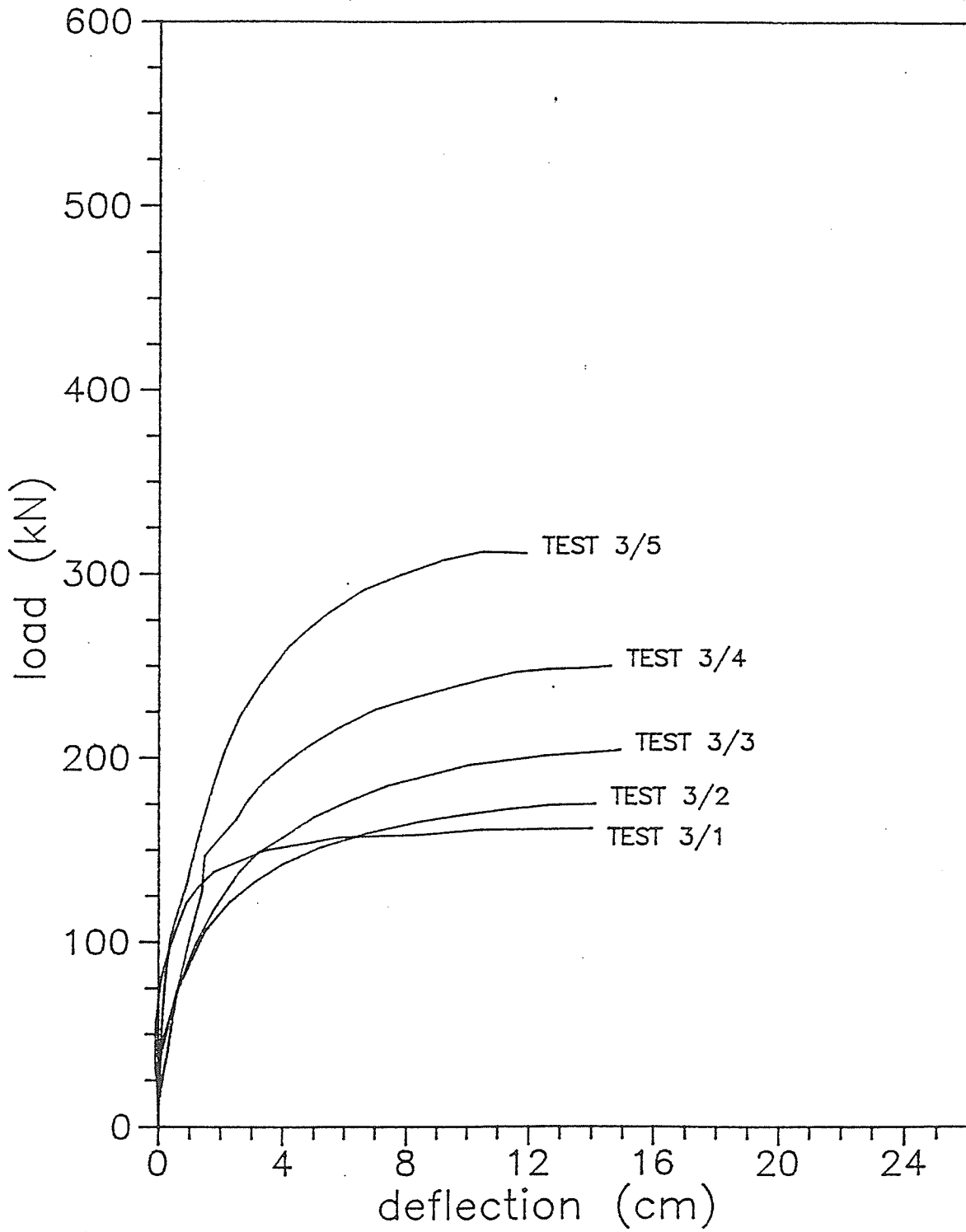


Figure A4.3. Load-relative deflection relationship of the test specimens originated from the same pole

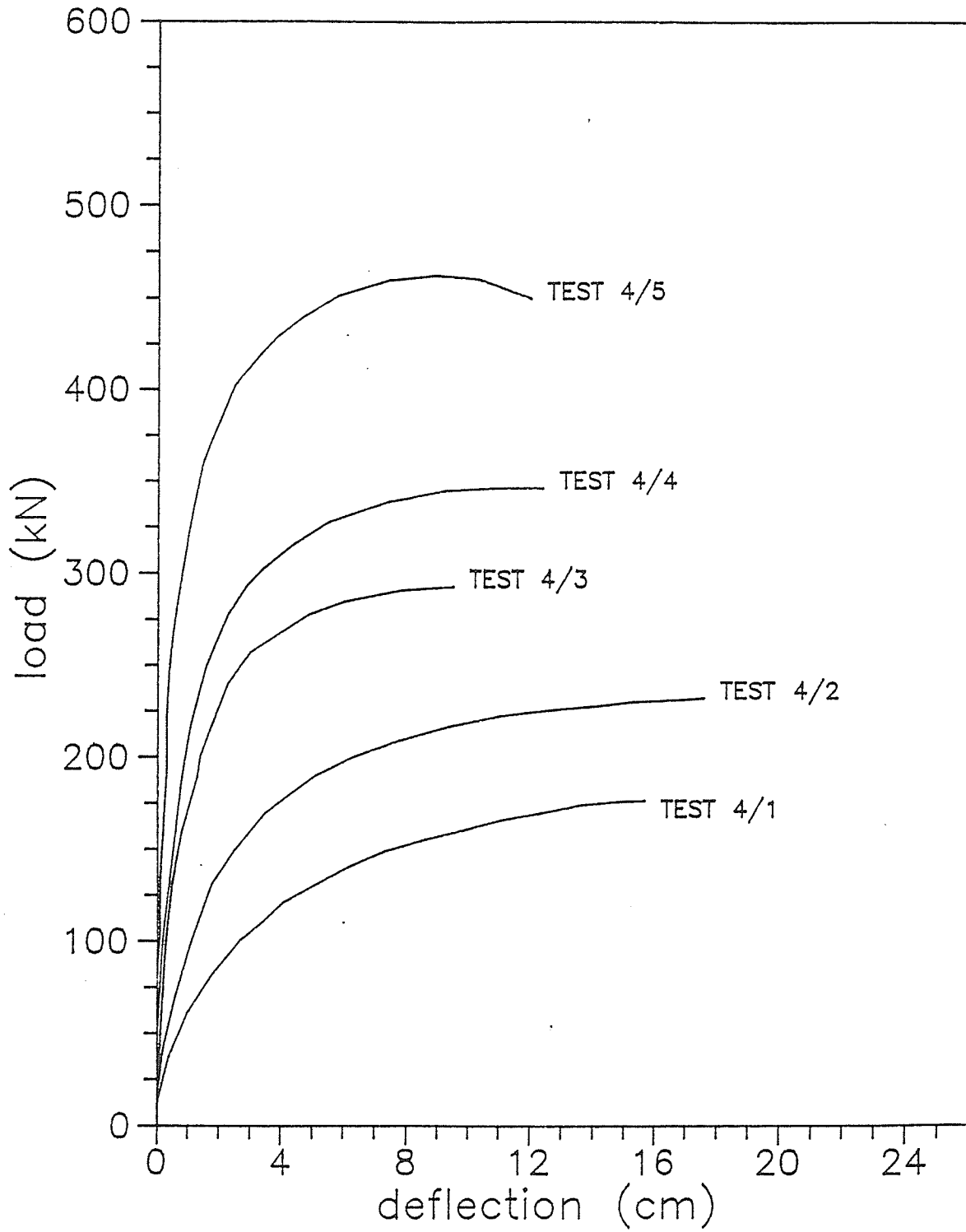


Figure A4.4. Load-relative deflection relationship of the test specimens originated from the same pole

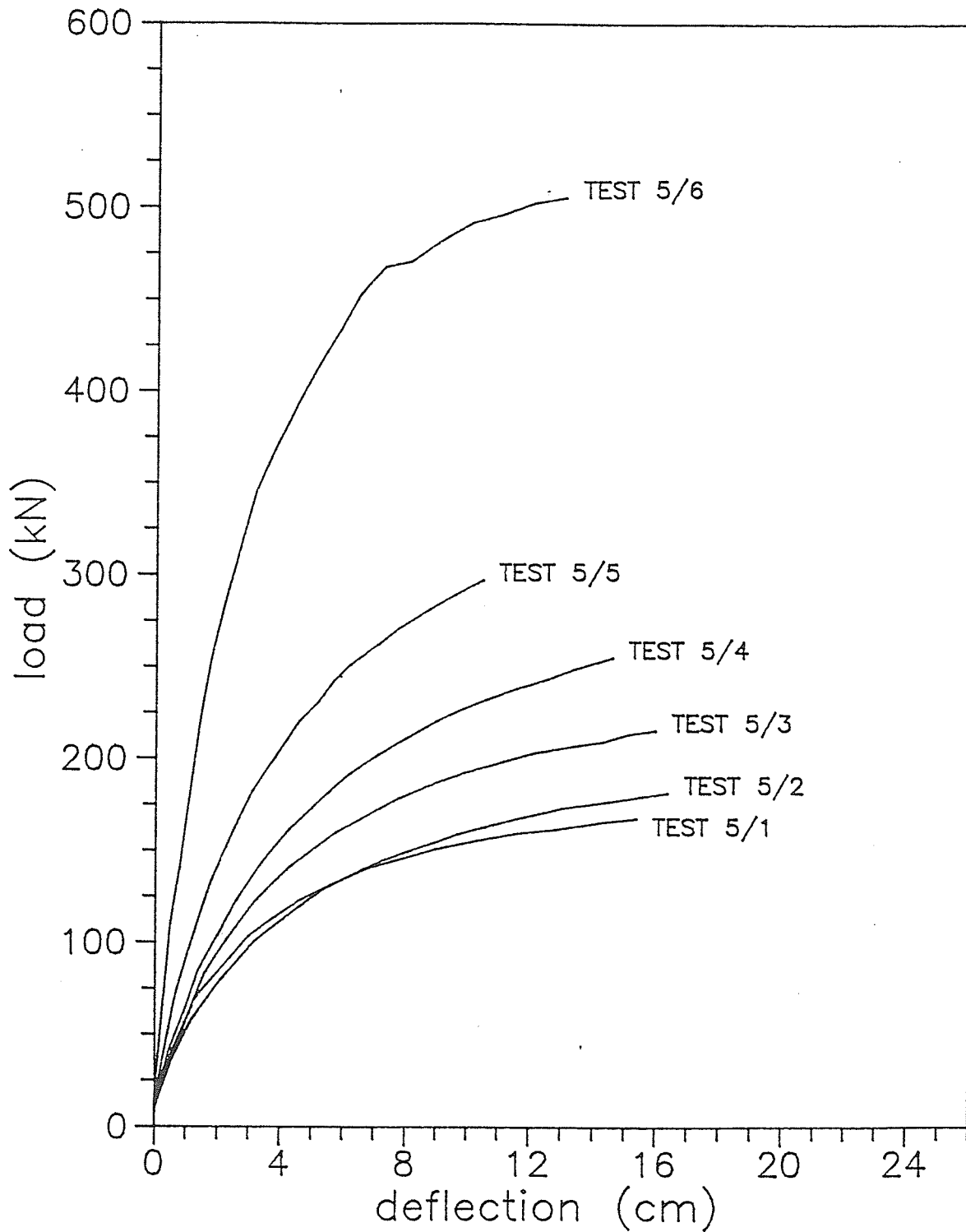


Figure A4.5. Load-relative deflection relationship of the test specimens originated from the same pole

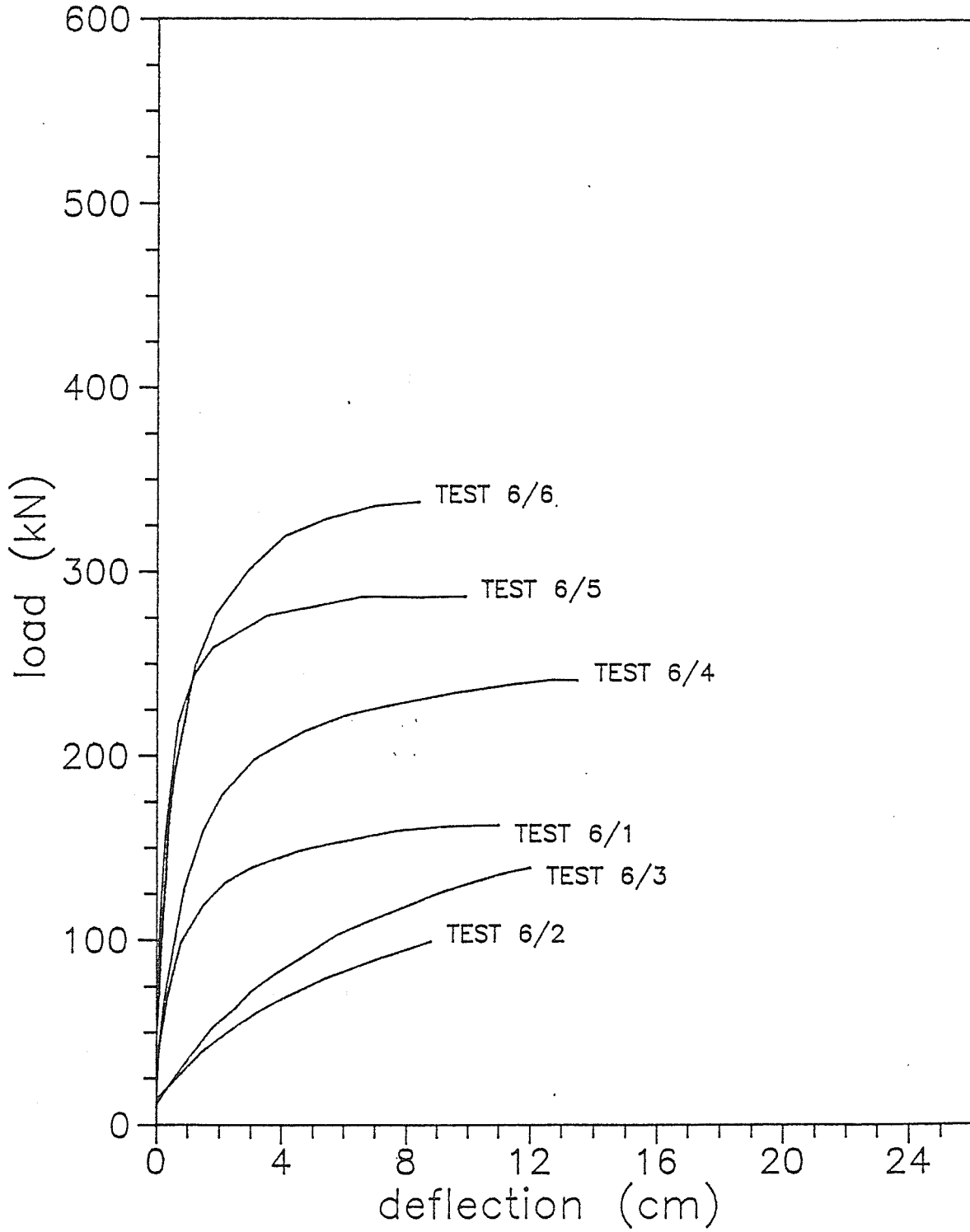


Figure A4.6. Load-relative deflection relationship of the test specimens originated from the same pole

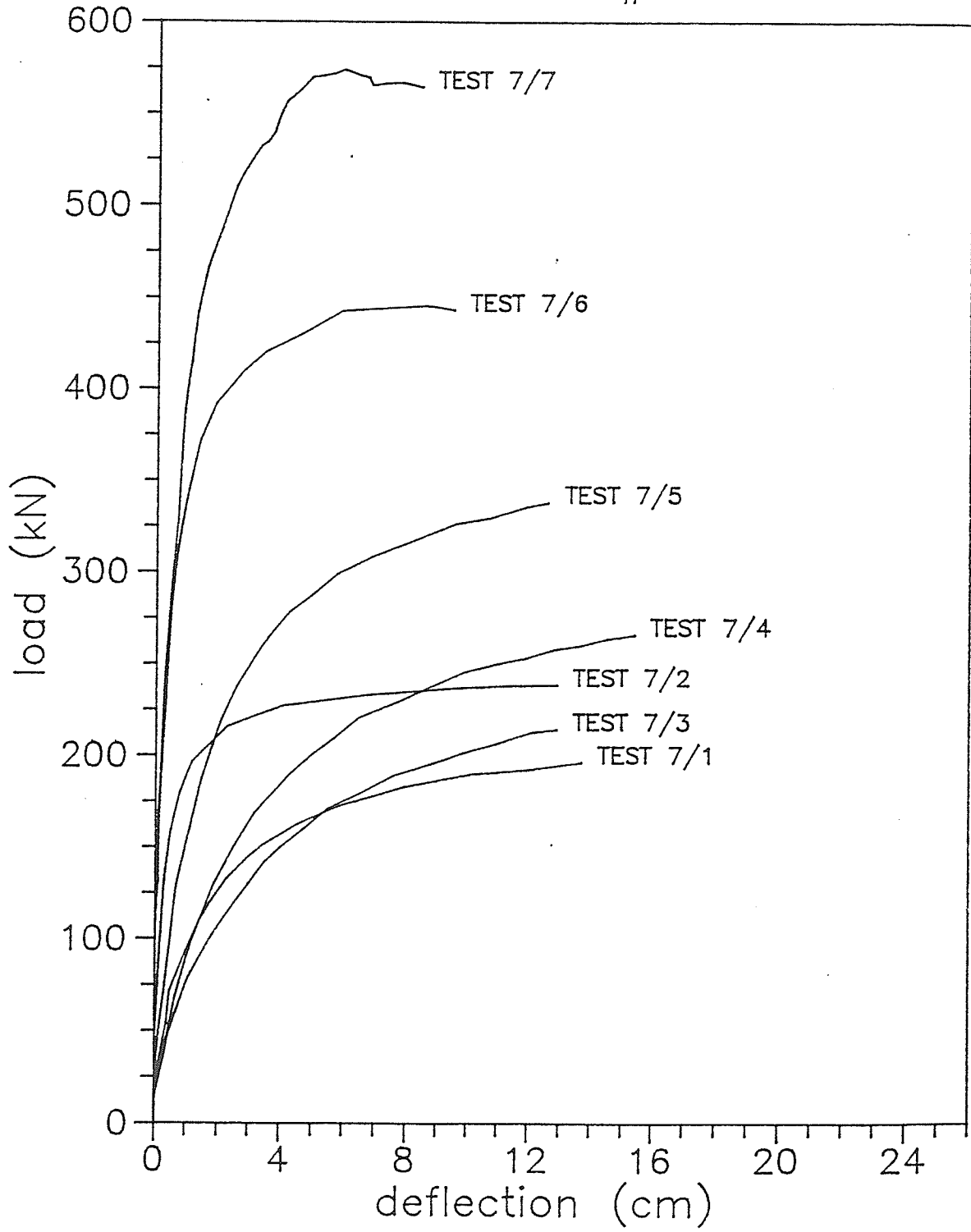


Figure A4.7. Load-relative deflection relationship of the test specimens originated from the same pole

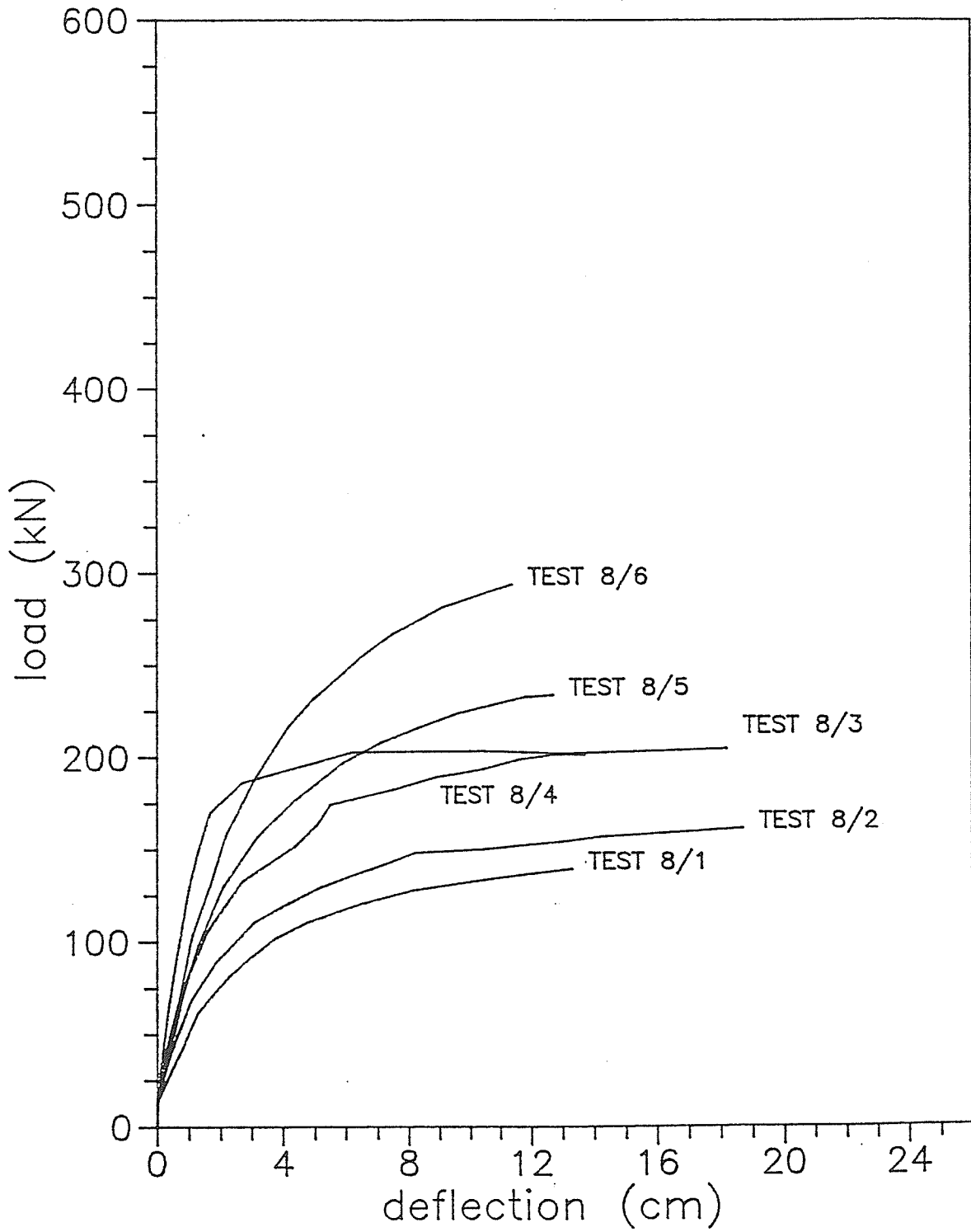


Figure A4.8. Load-relative deflection relationship of the test specimens originated from the same pole

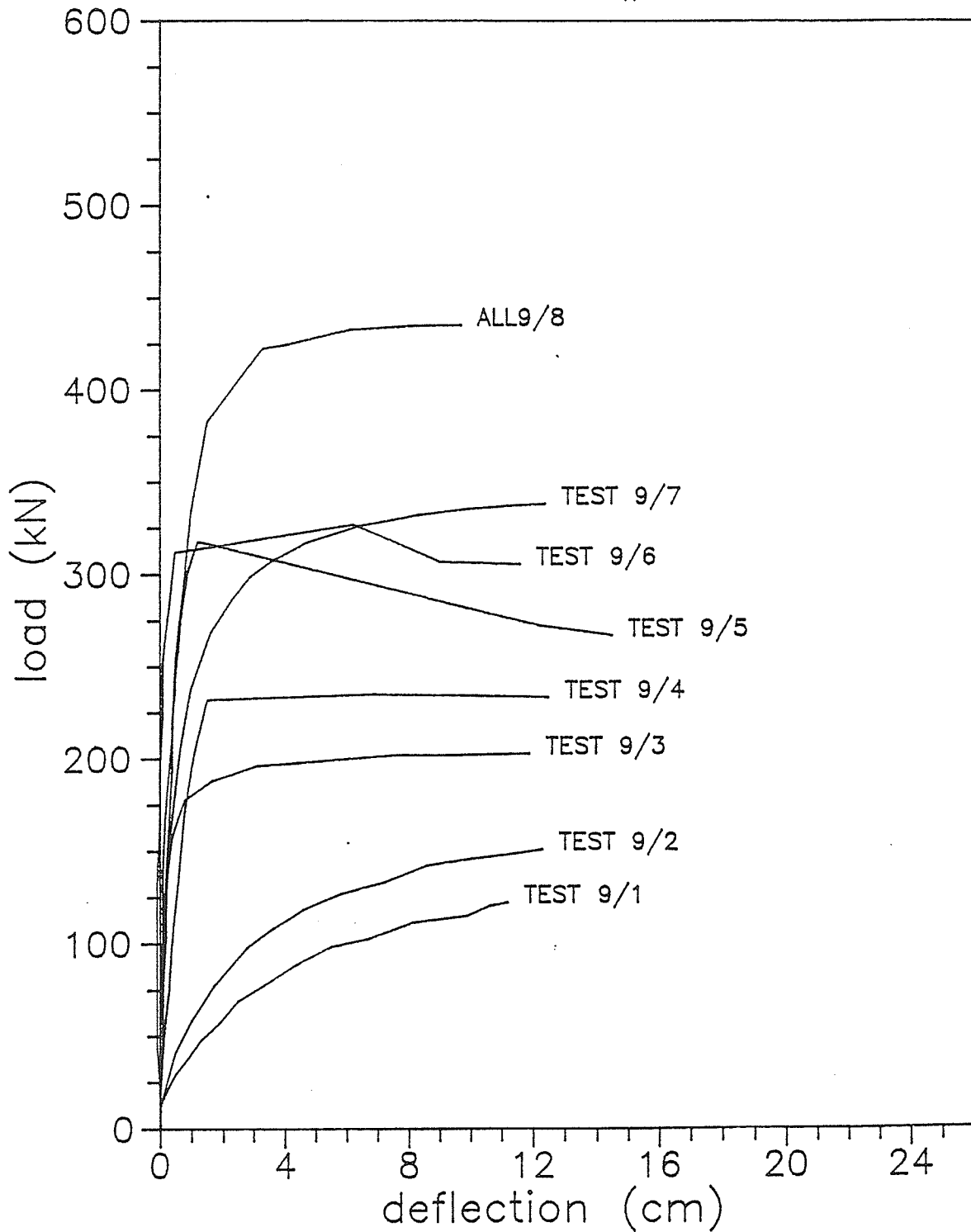


Figure A4.9. Load-relative deflection relationship of the test specimens originated from the same pole

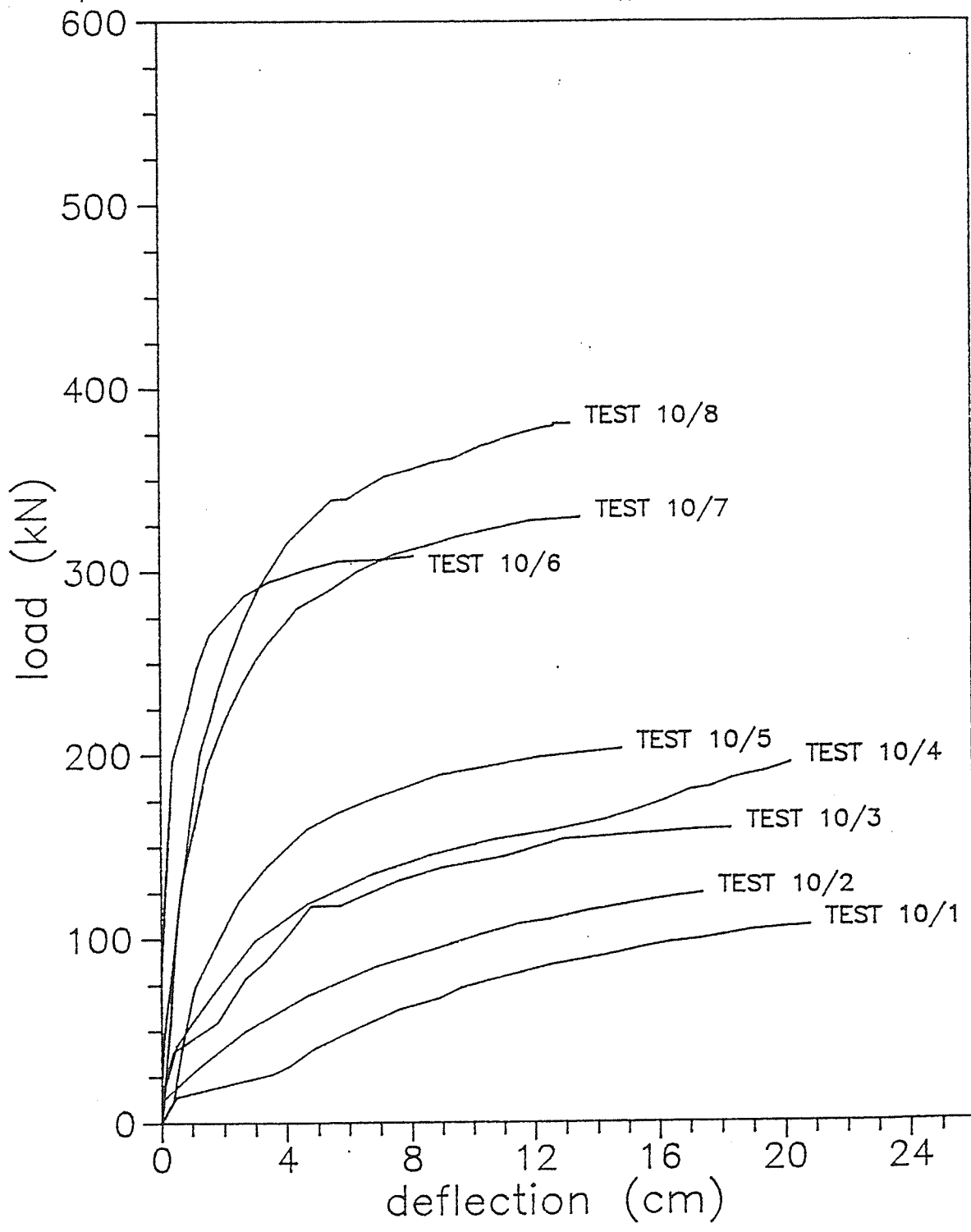


Figure A4.10. Load-relative deflection relationship of the test specimens originated from the same pole

## APPENDIX *B*

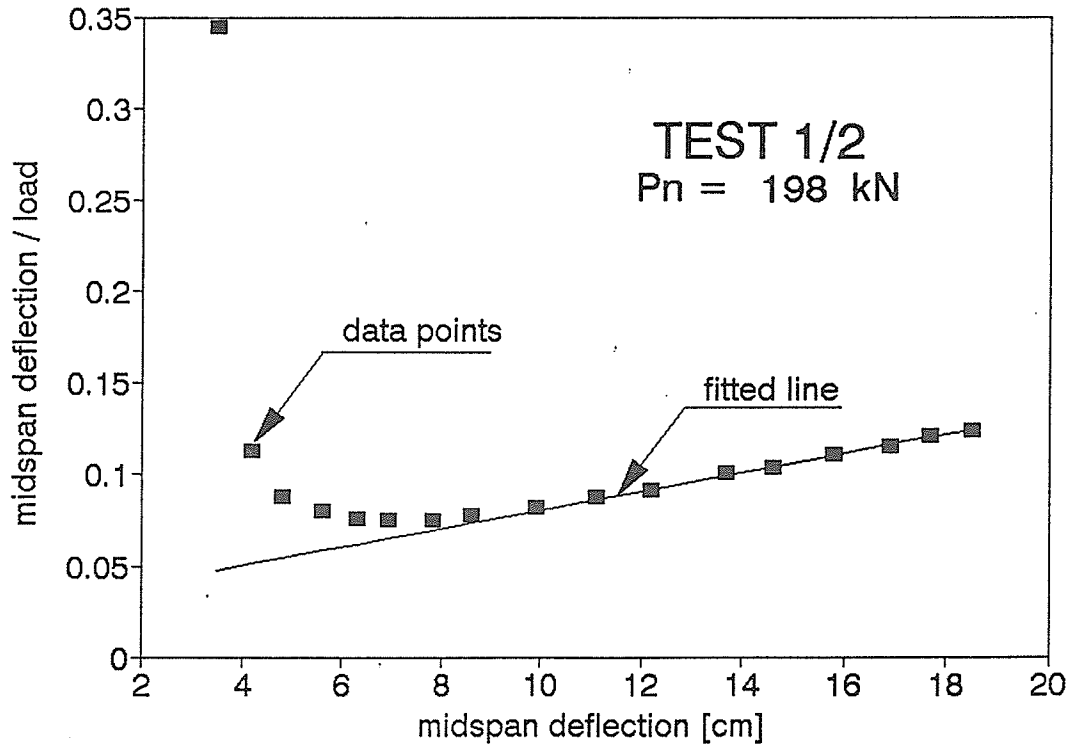
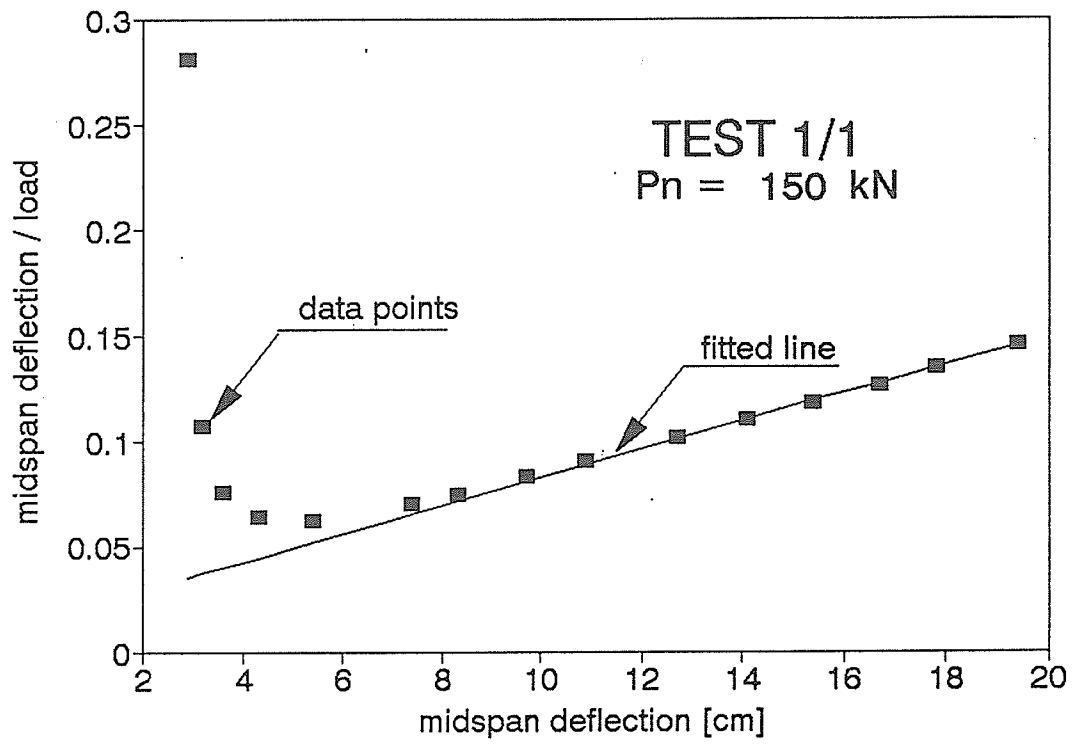


Figure B1.1. Southwell plot

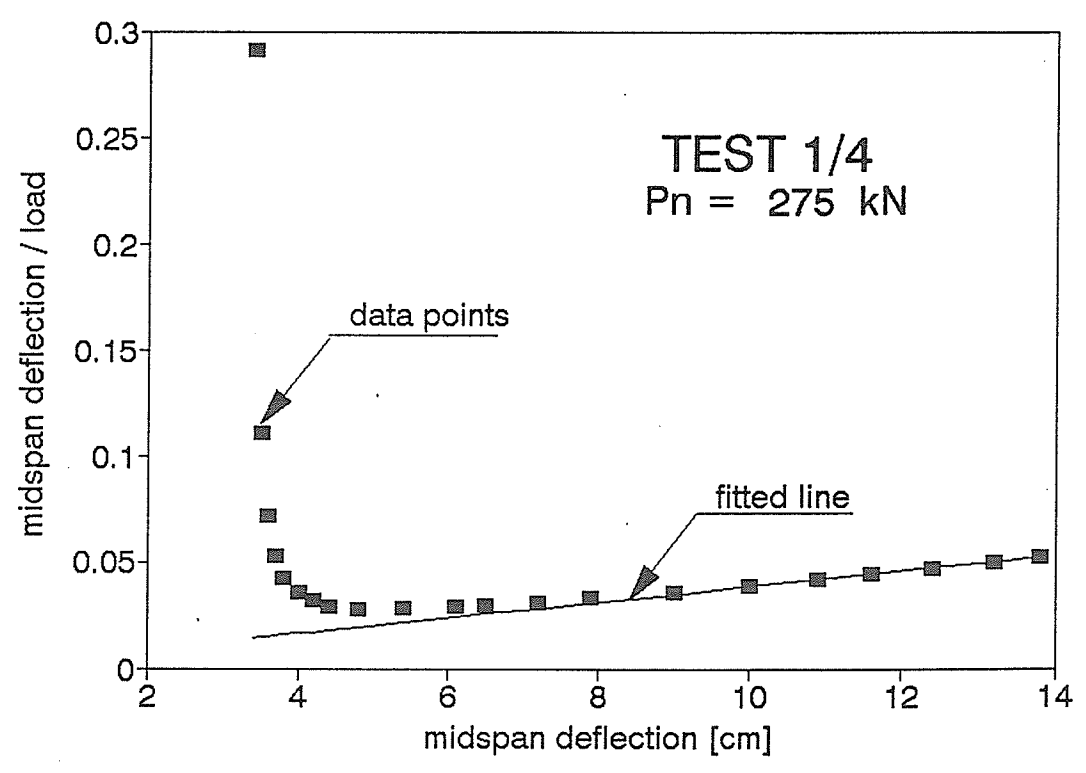
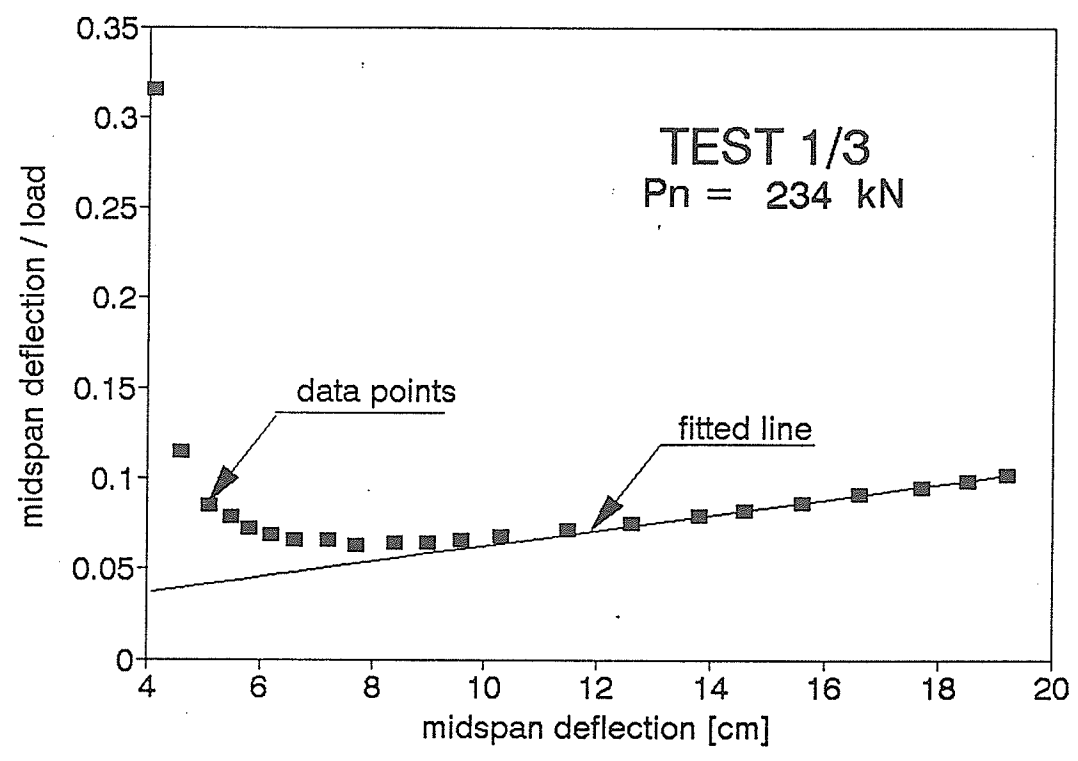


Figure B1.2. Southwell plot



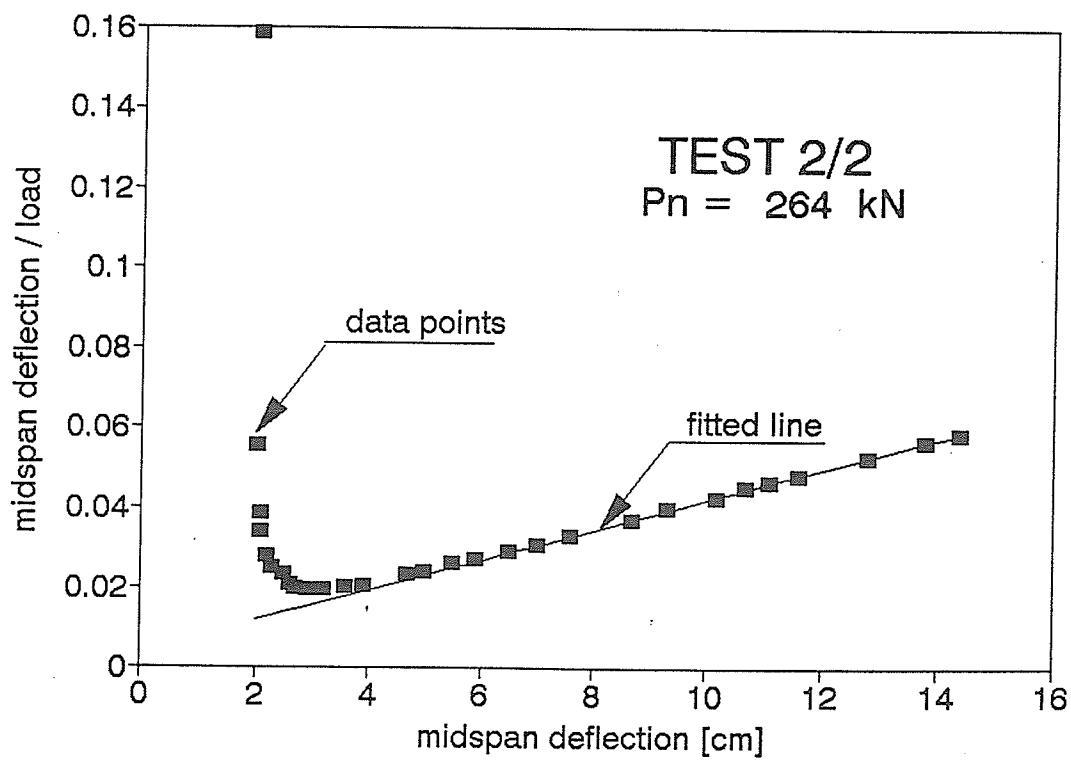
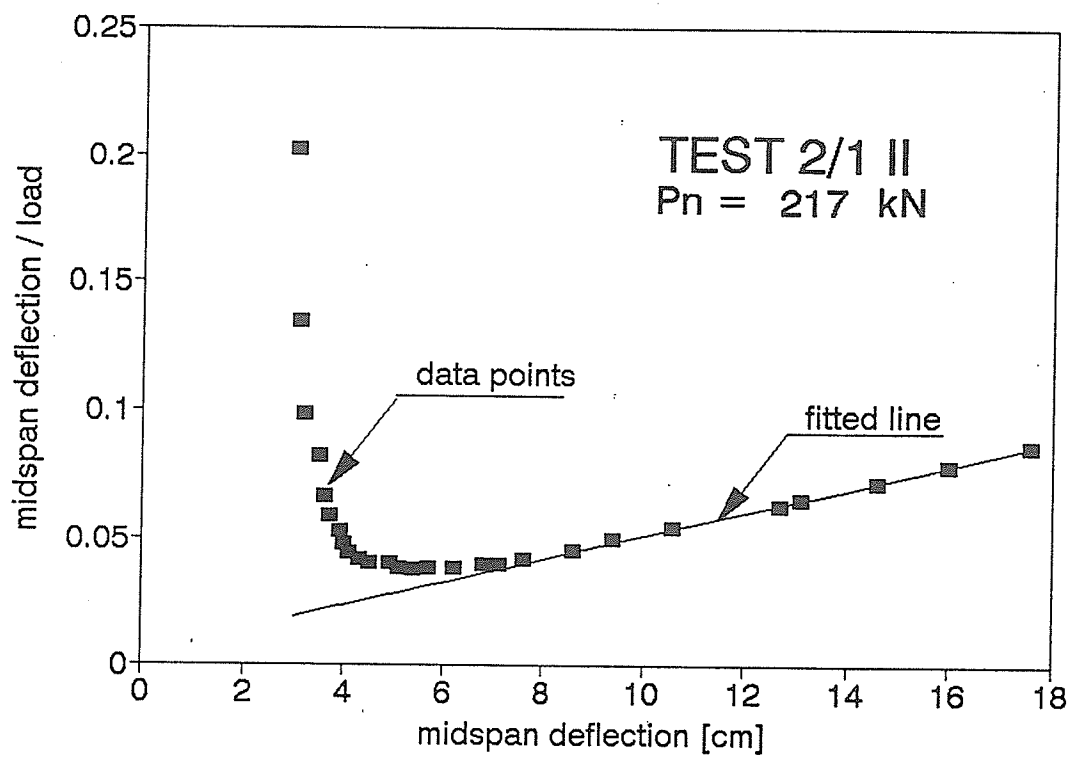


Figure B1.4. Southwell plot

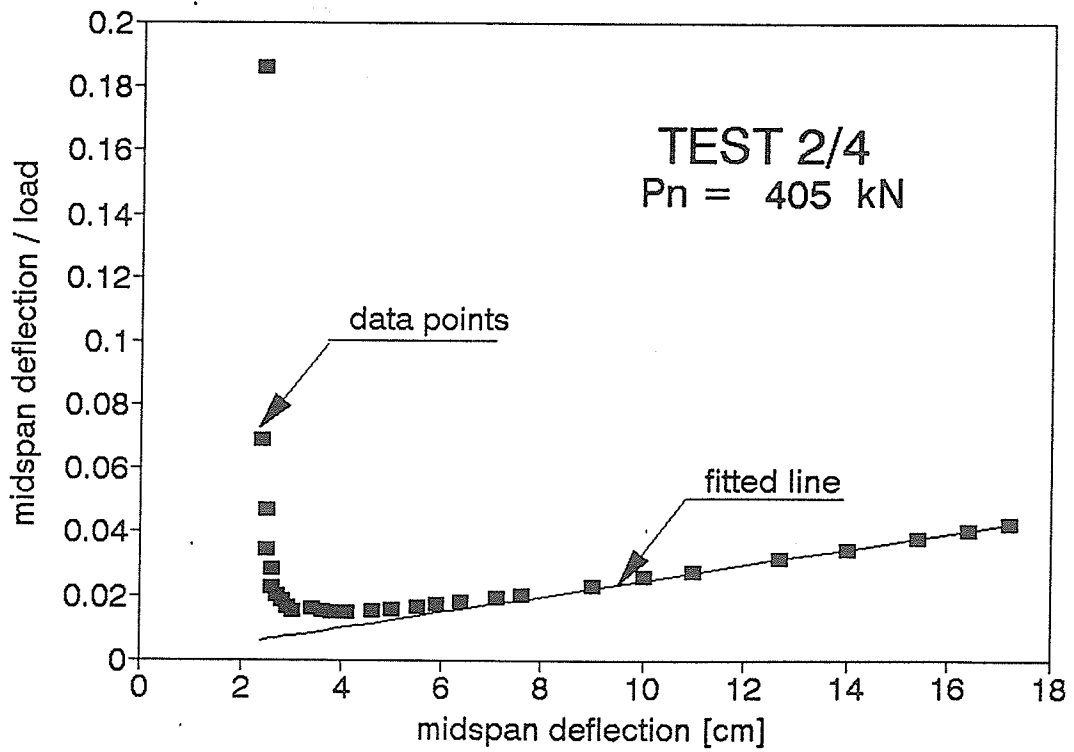
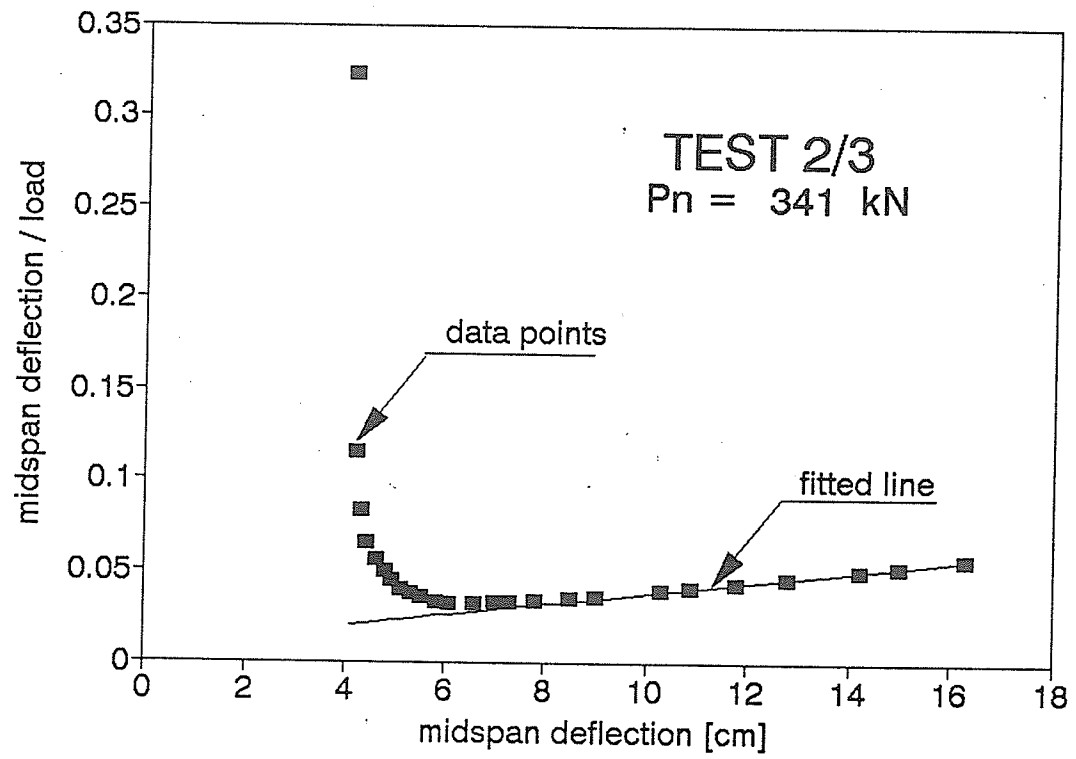


Figure B1.5. Southwell plot

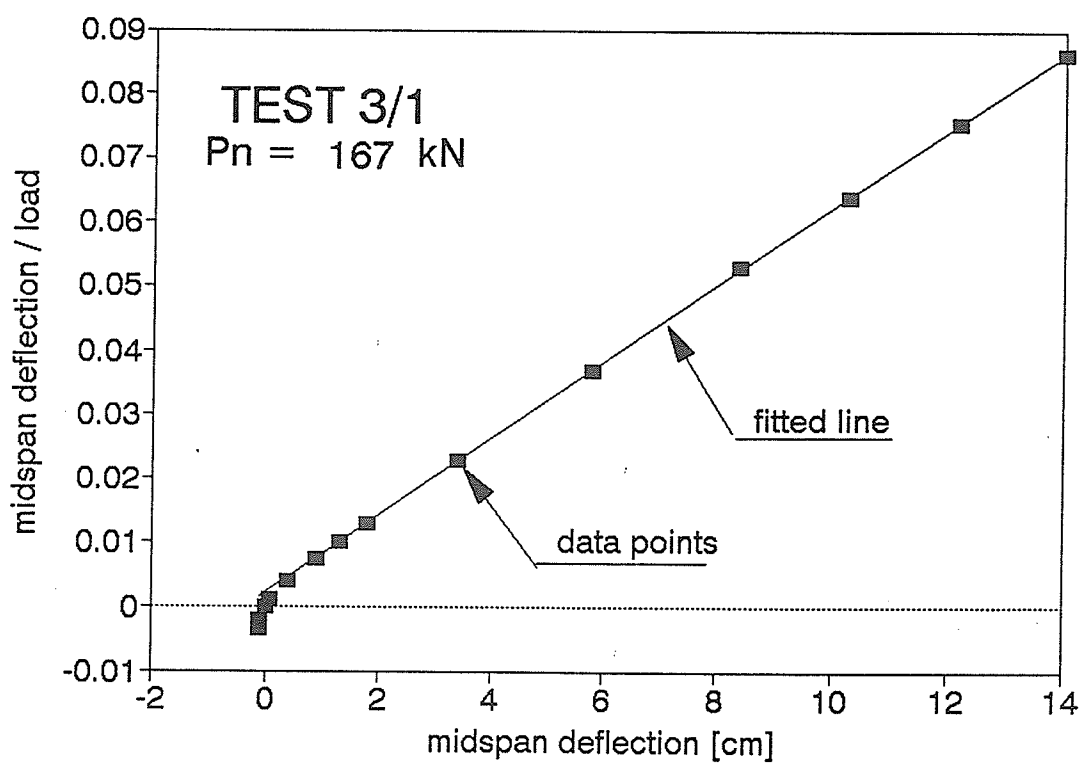
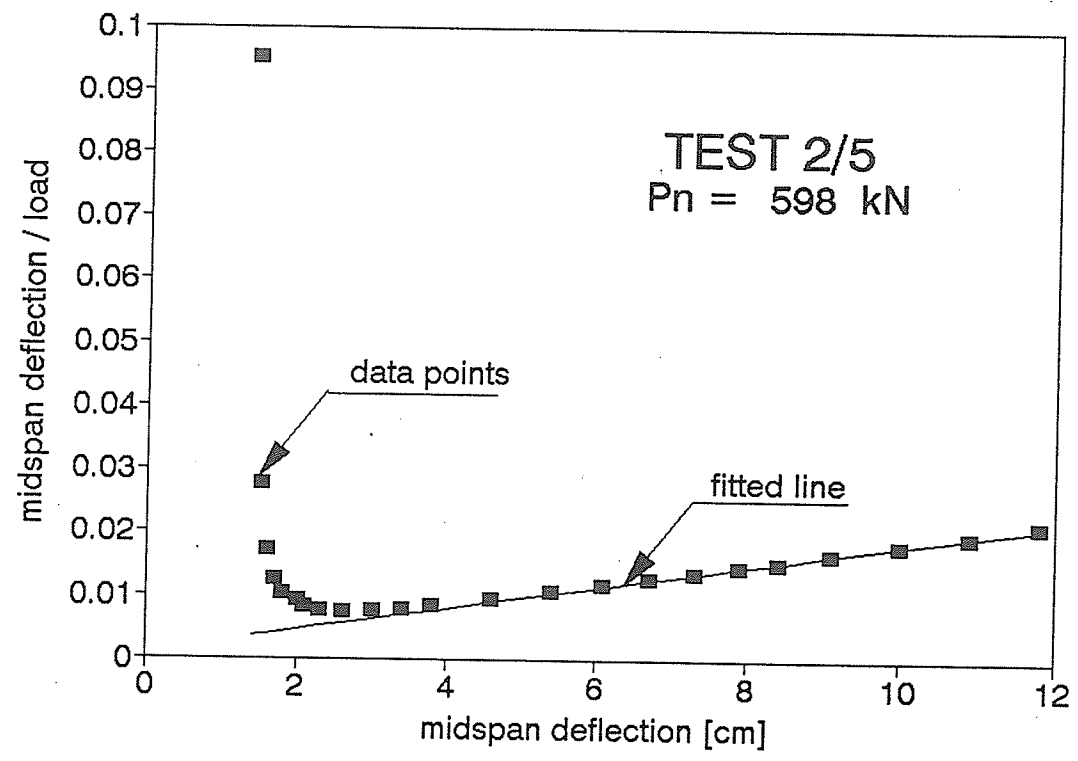


Figure B1.6. Southwell plot

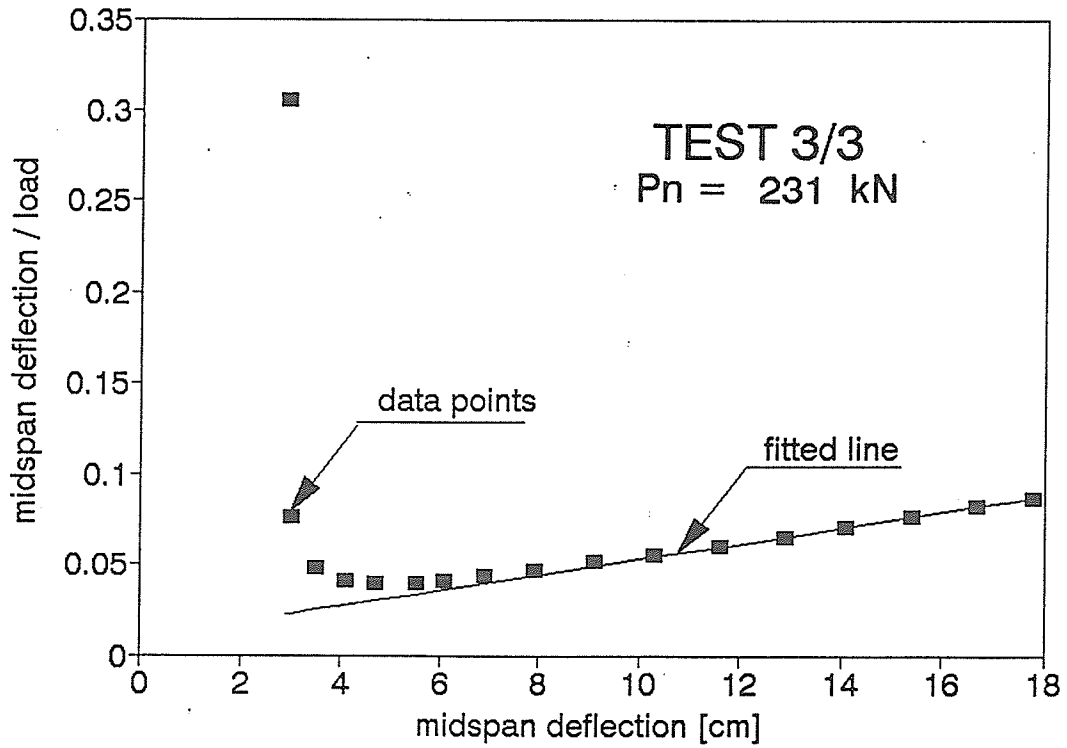
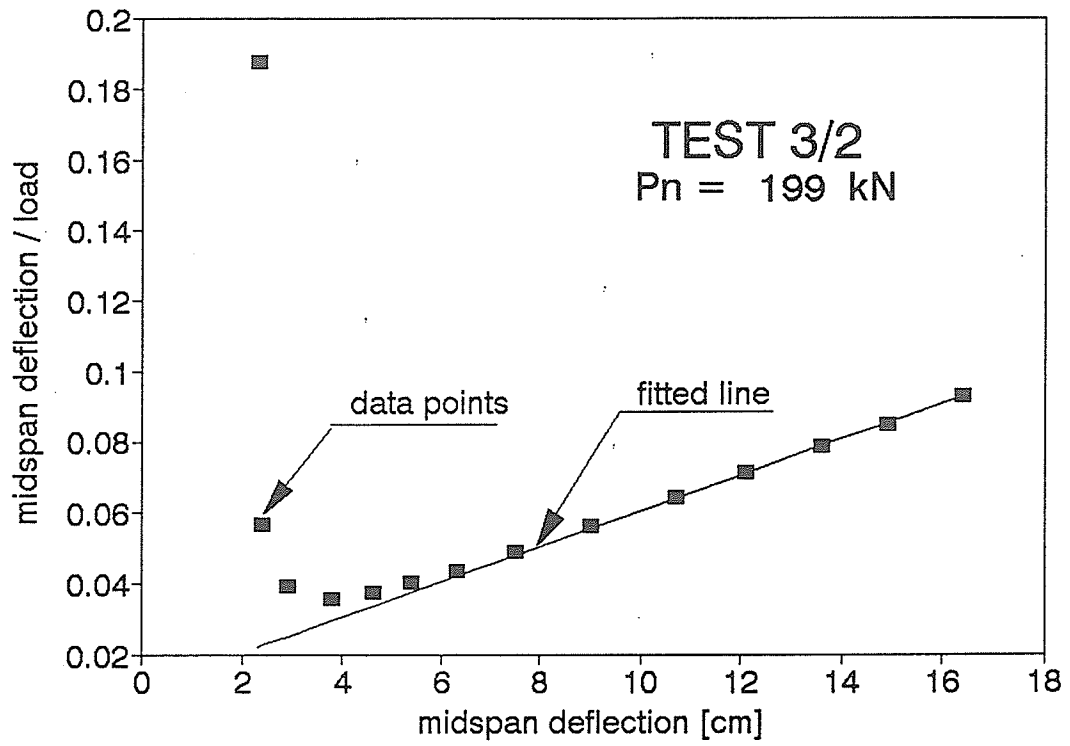


Figure B1.7. Southwell plot

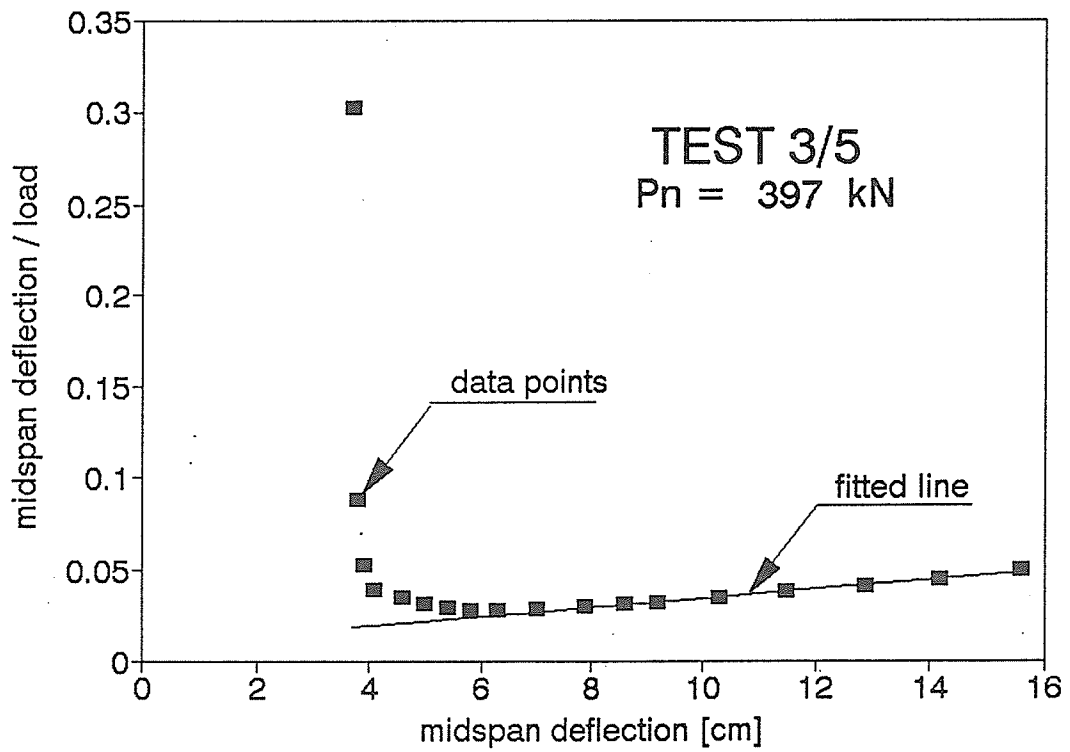
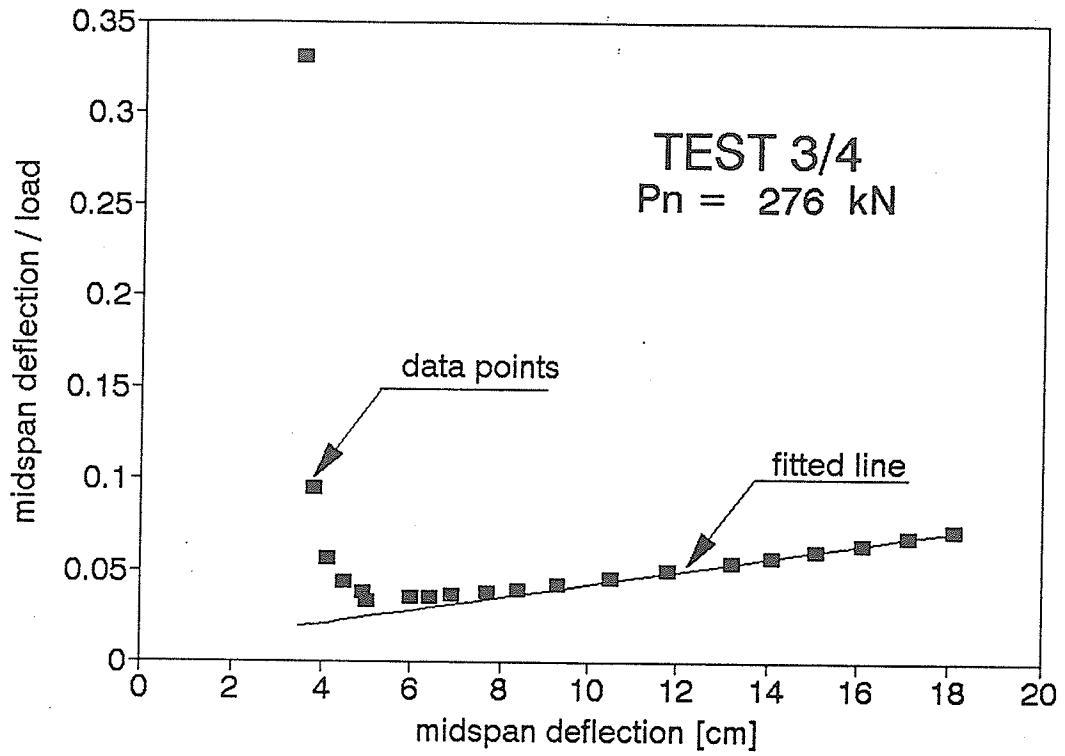


Figure B1.8. Southwell plot

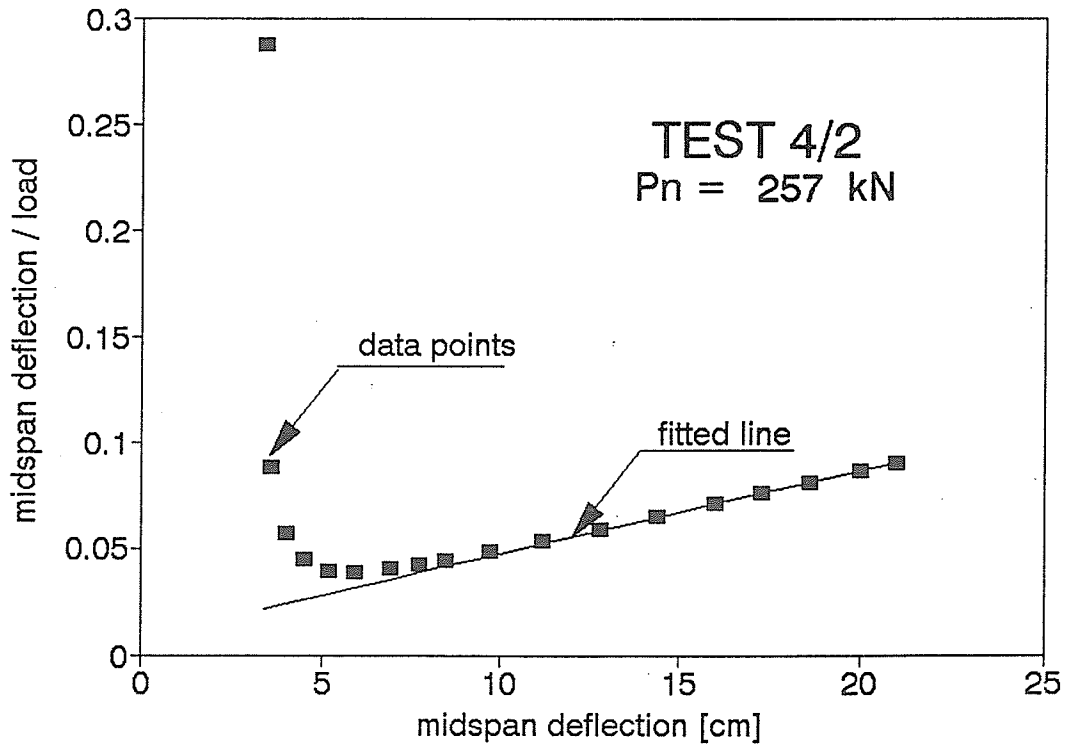
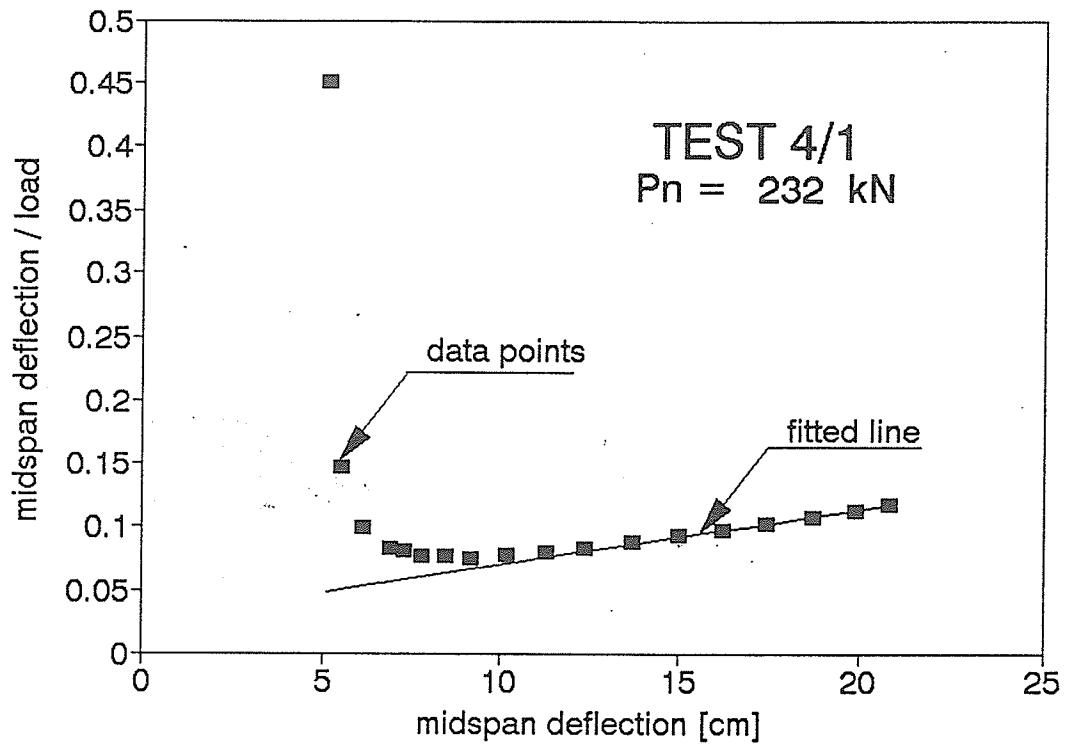


Figure B1.9. Southwell plot

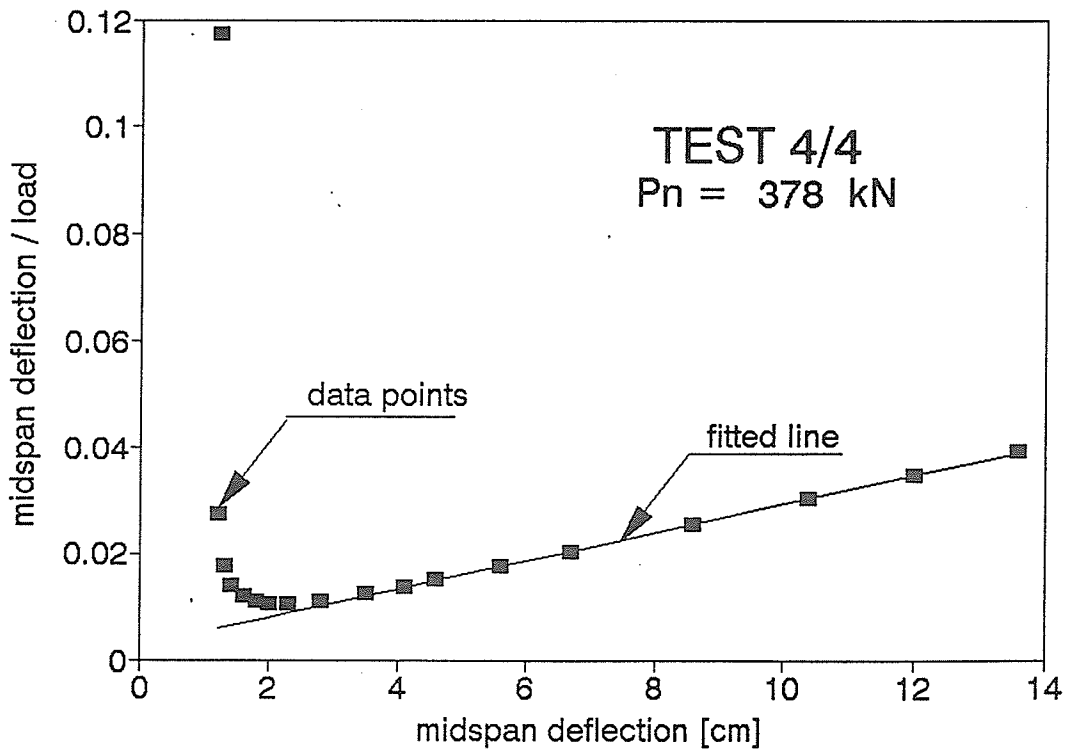
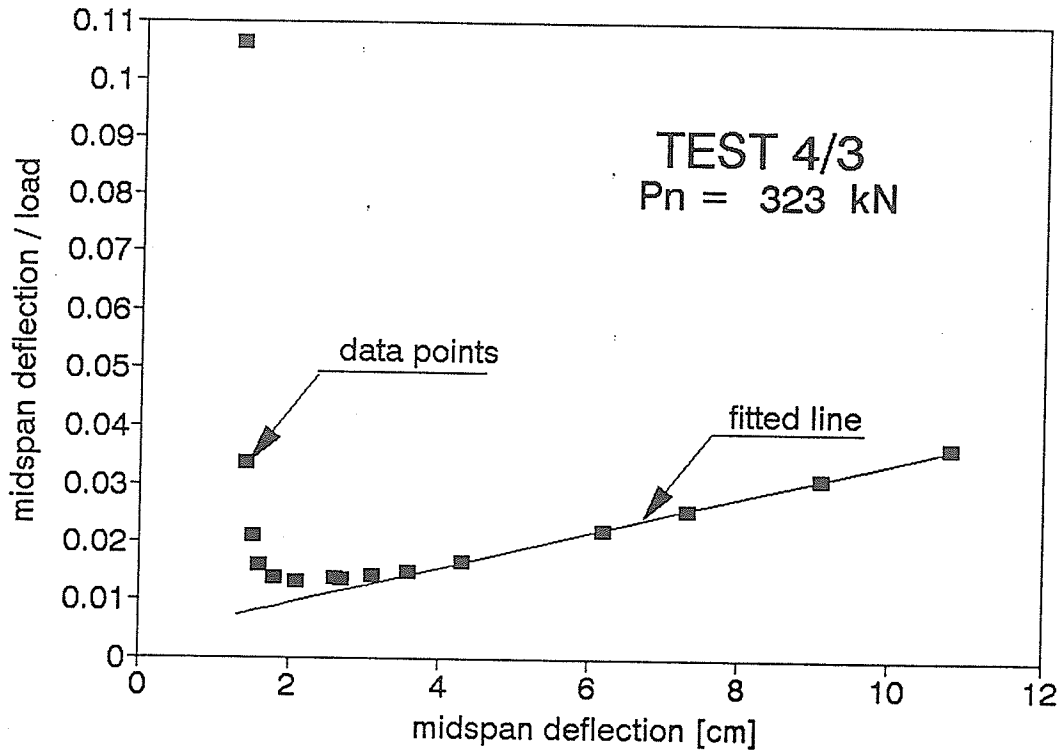


Figure B1.10. Southwell plot

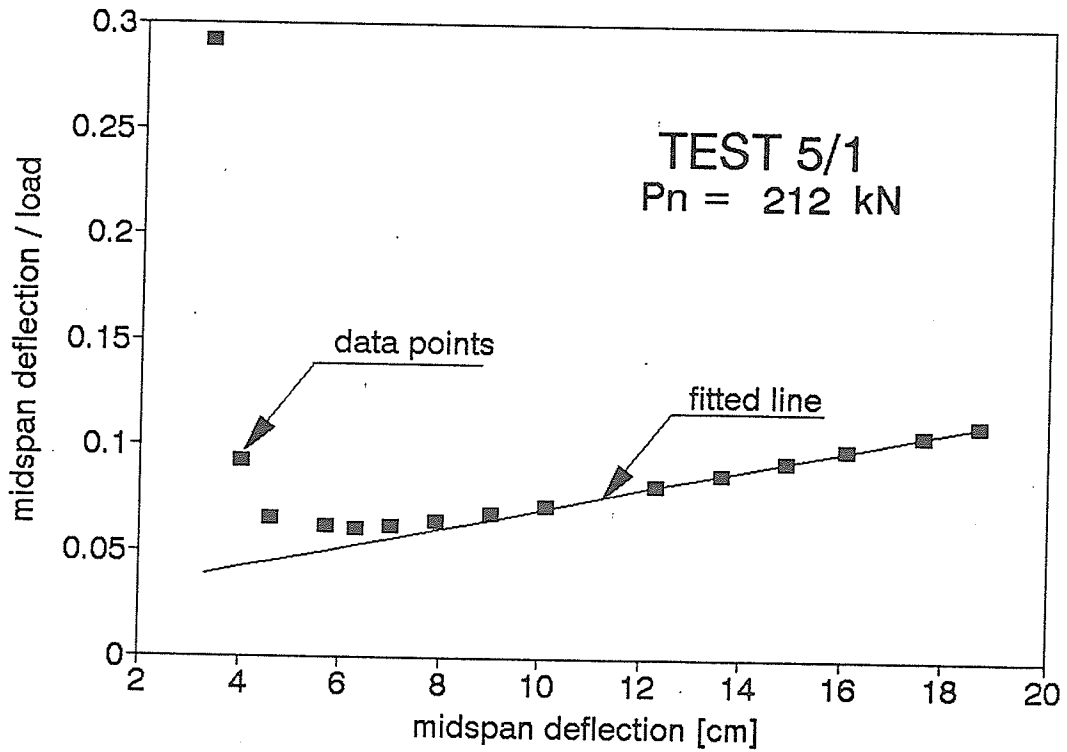
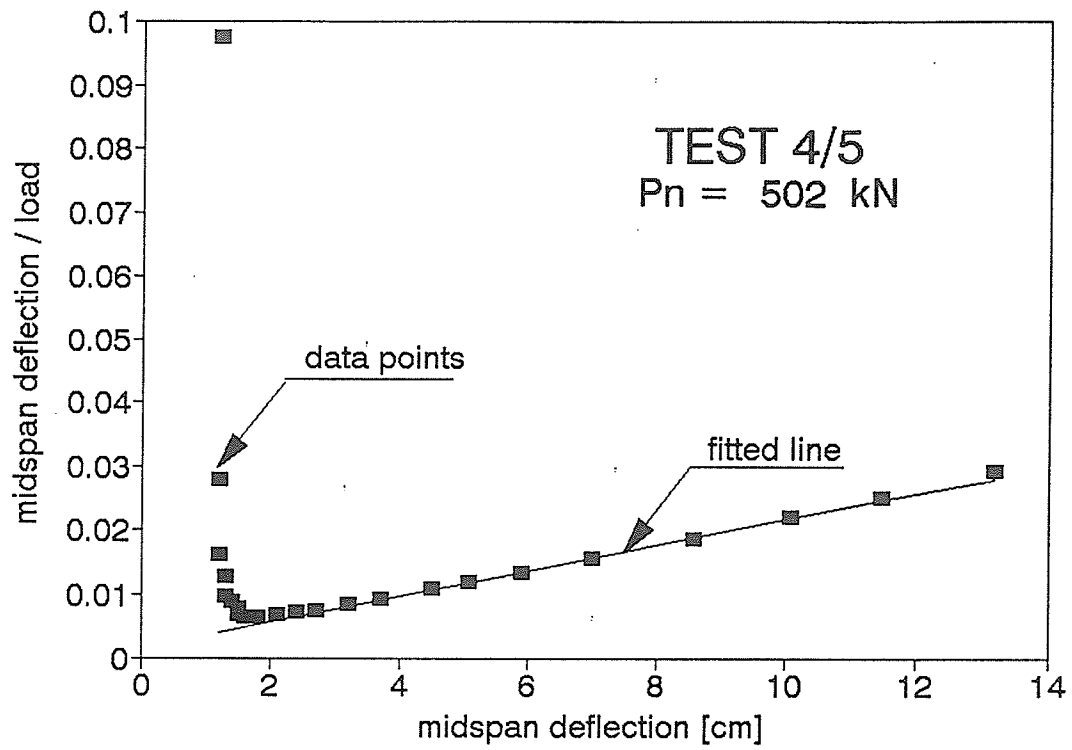


Figure B1.11. Southwell plot

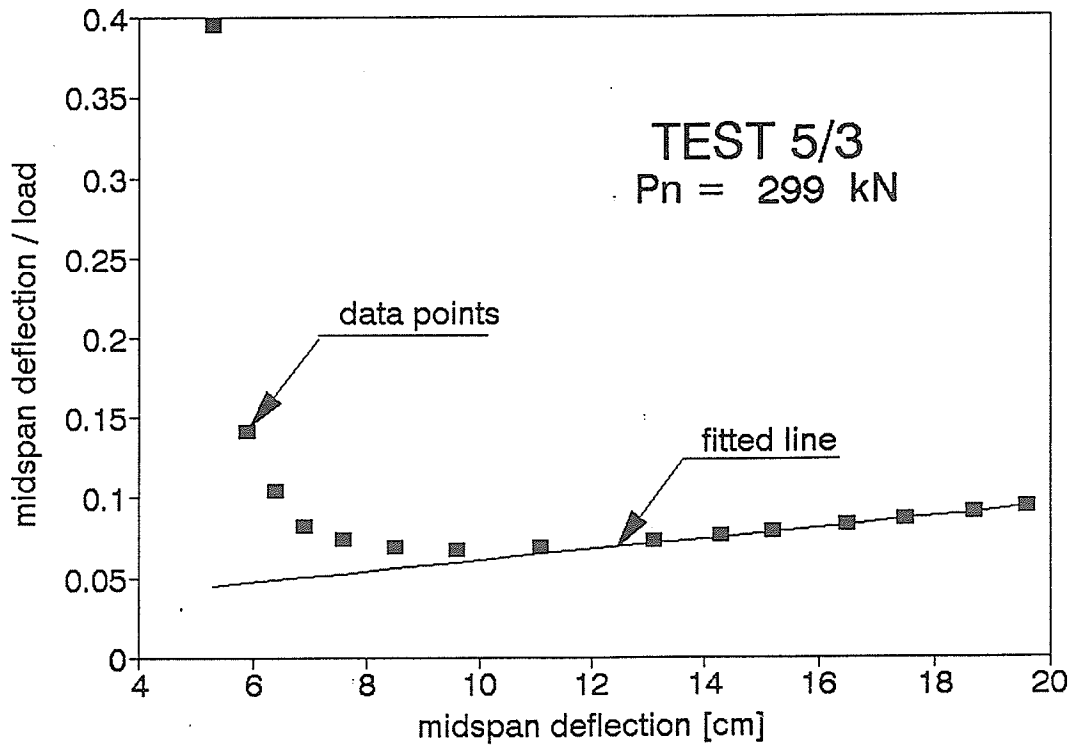
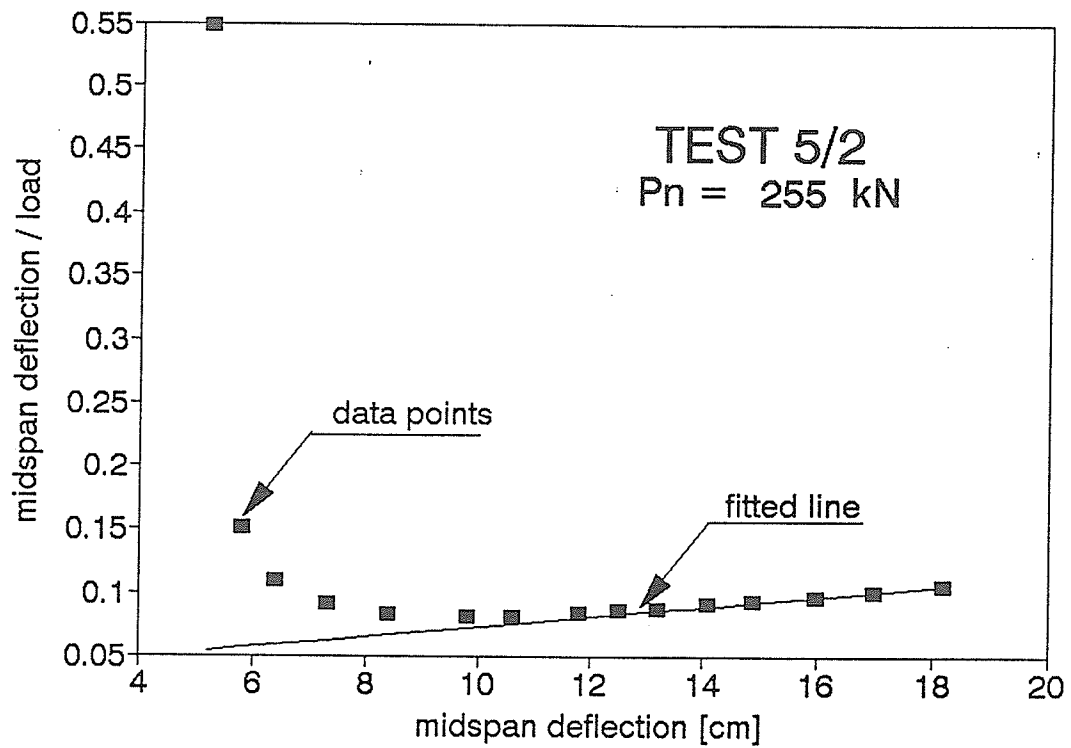


Figure B1.12. Southwell plot

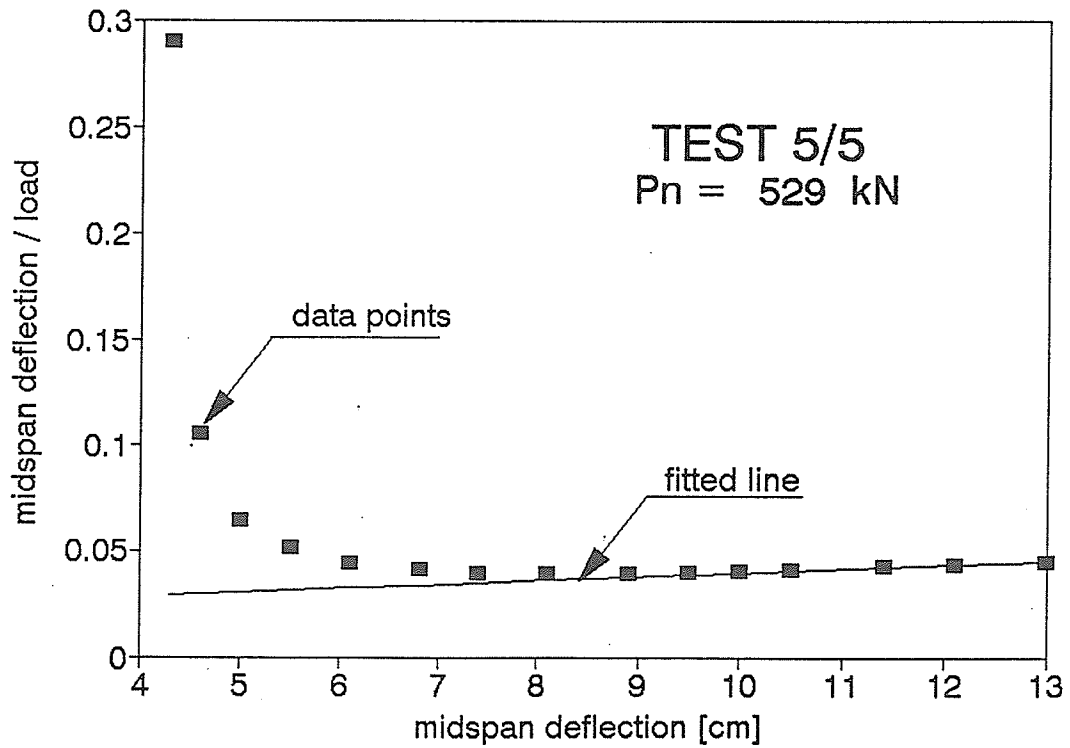
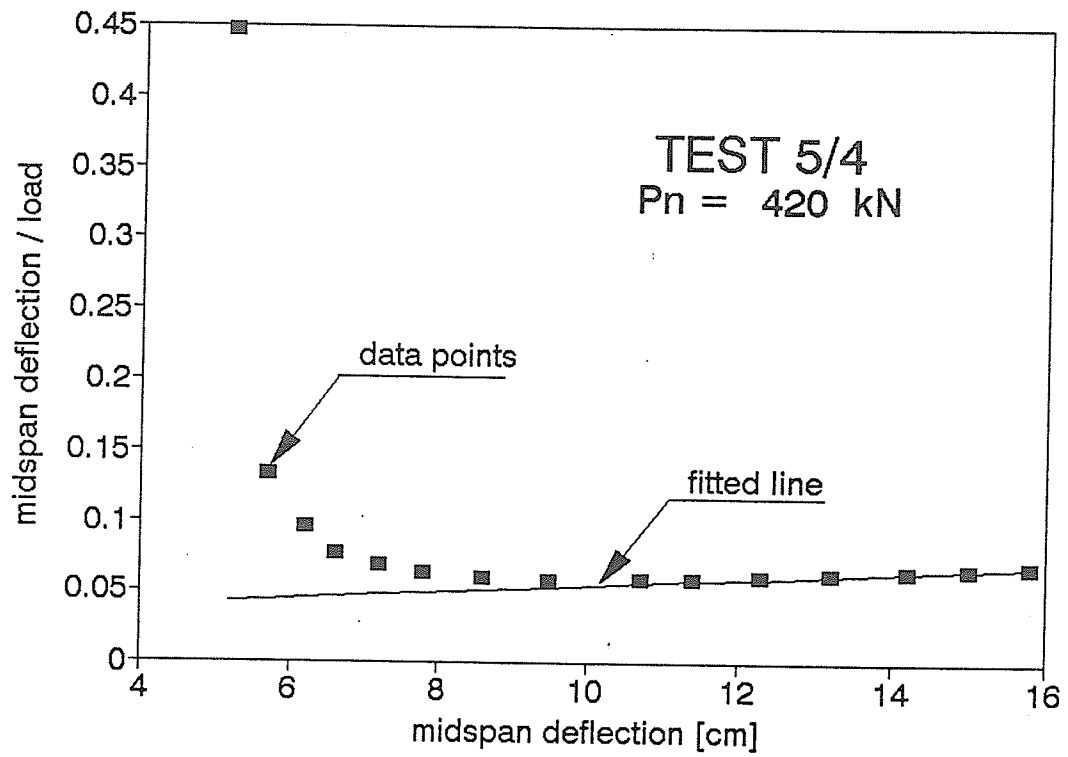


Figure B1.13. Southwell plot

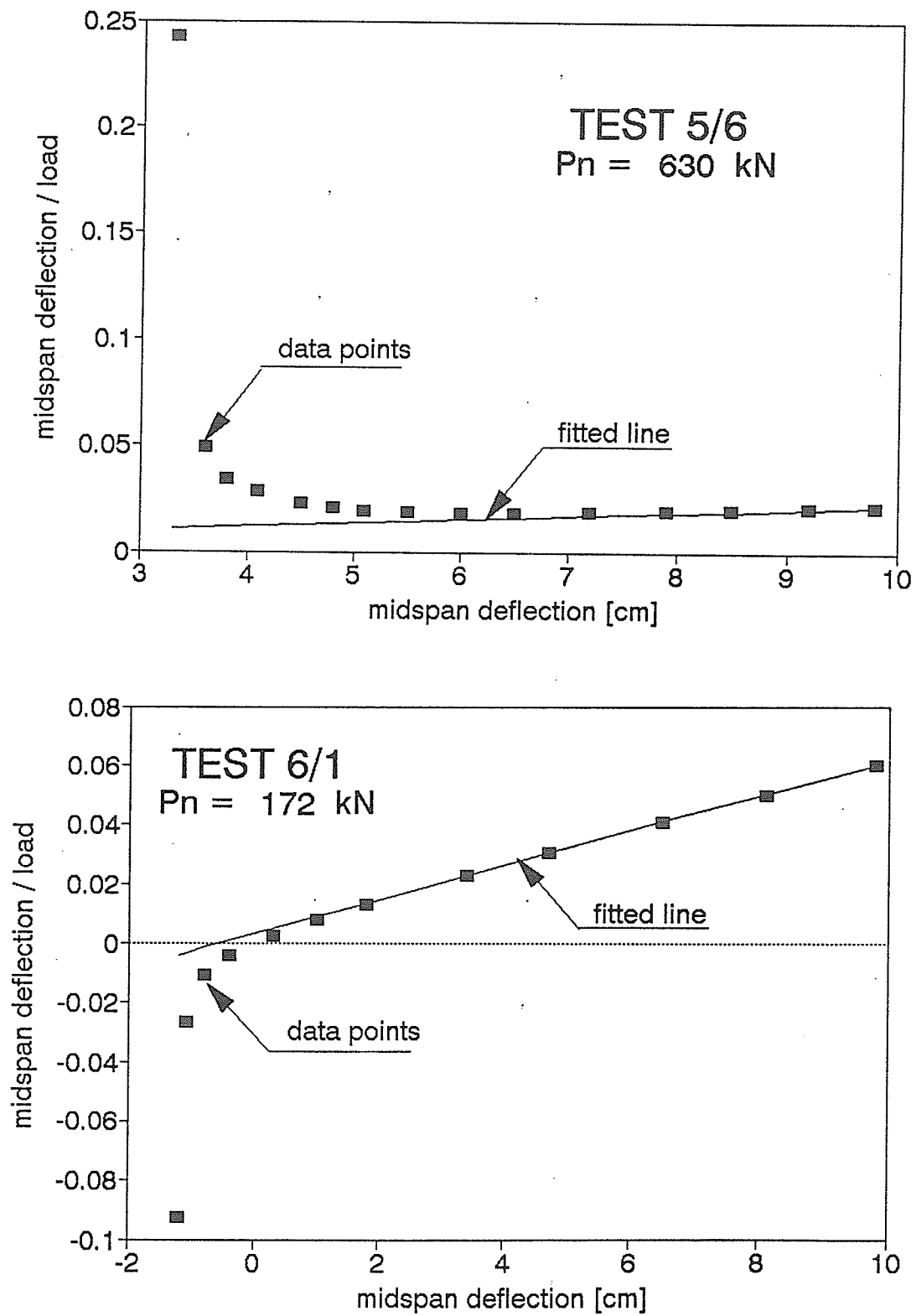


Figure B1.14. Southwell plot

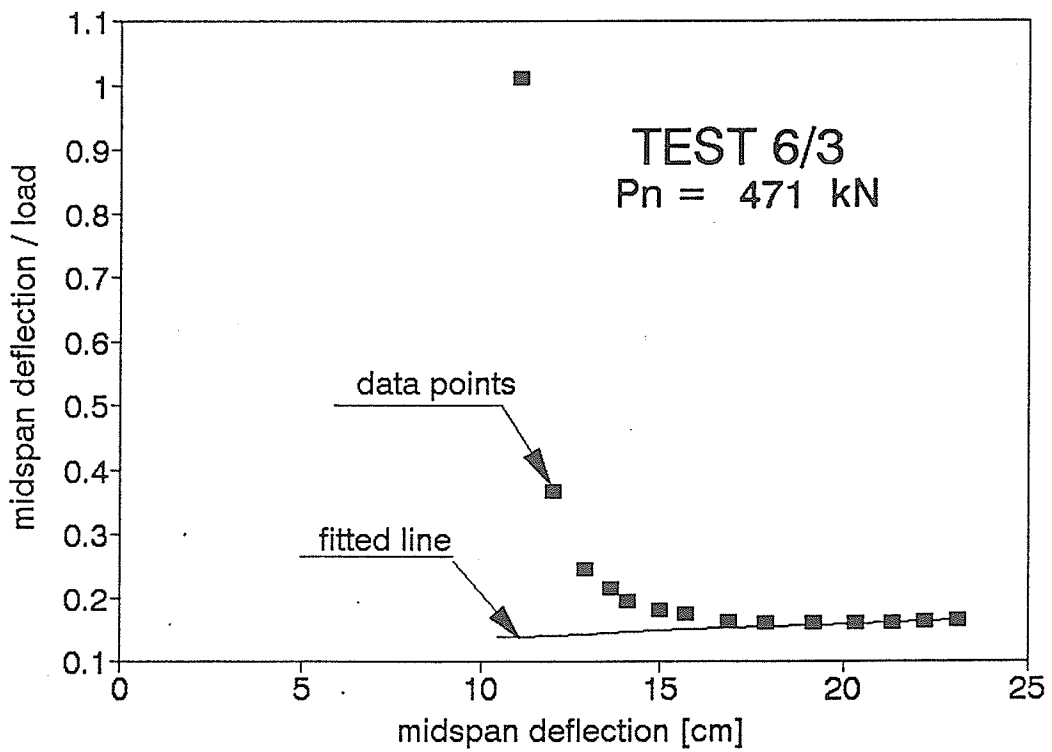
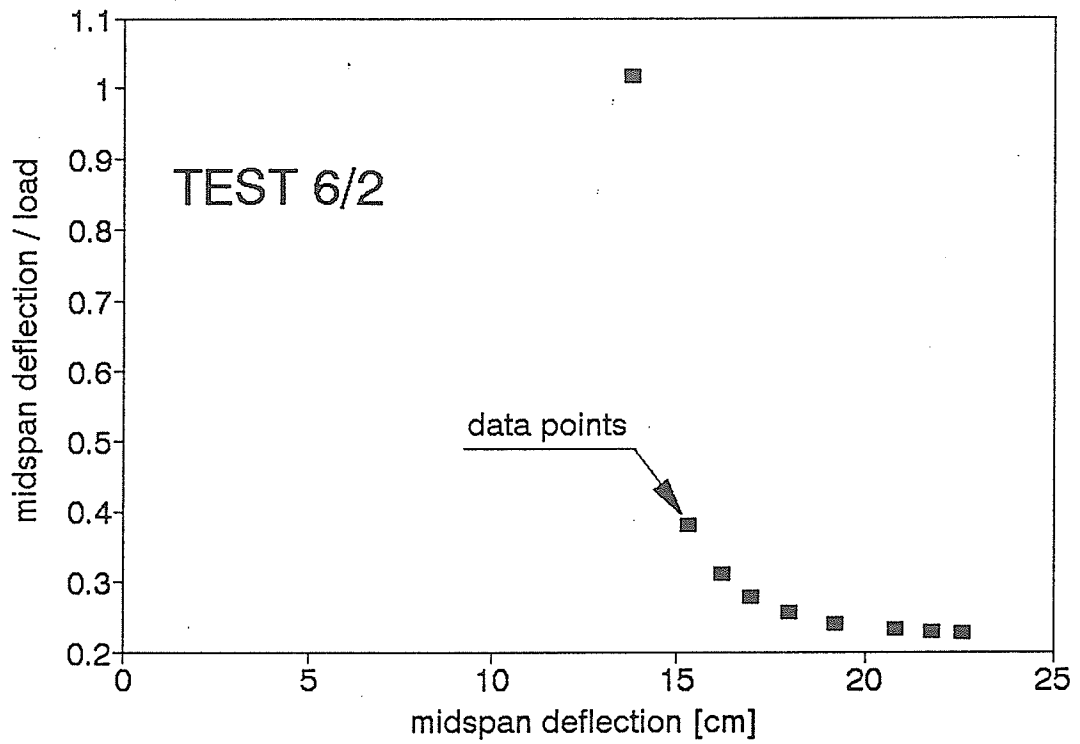


Figure B1.15. Southwell plot

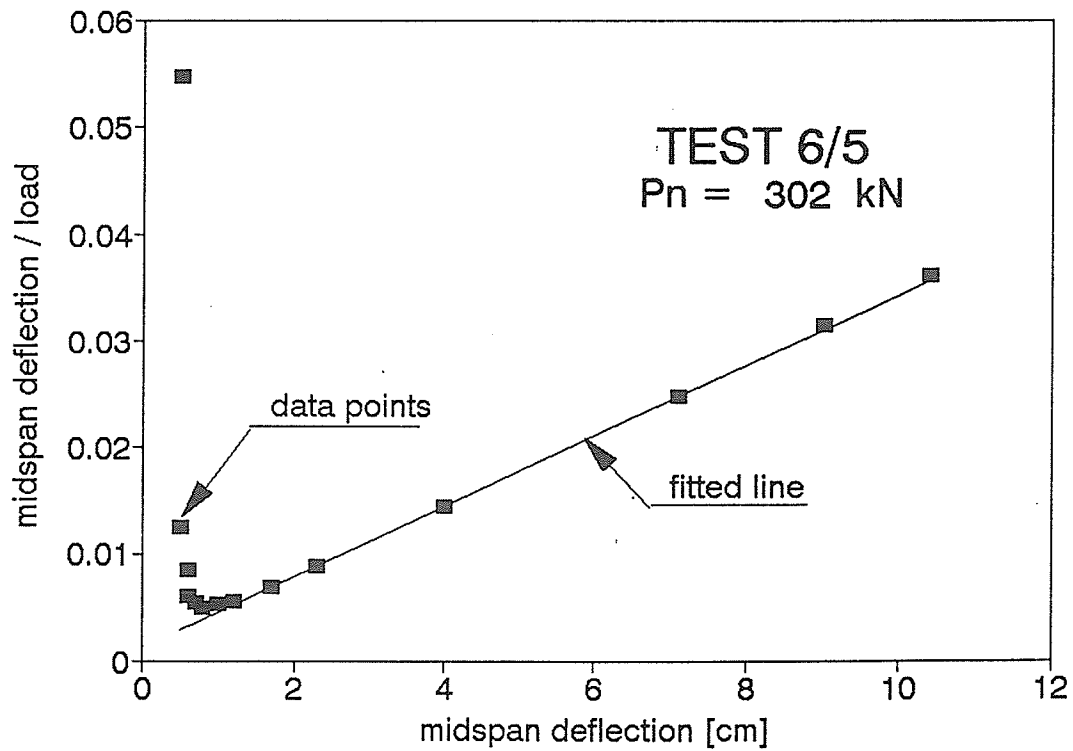
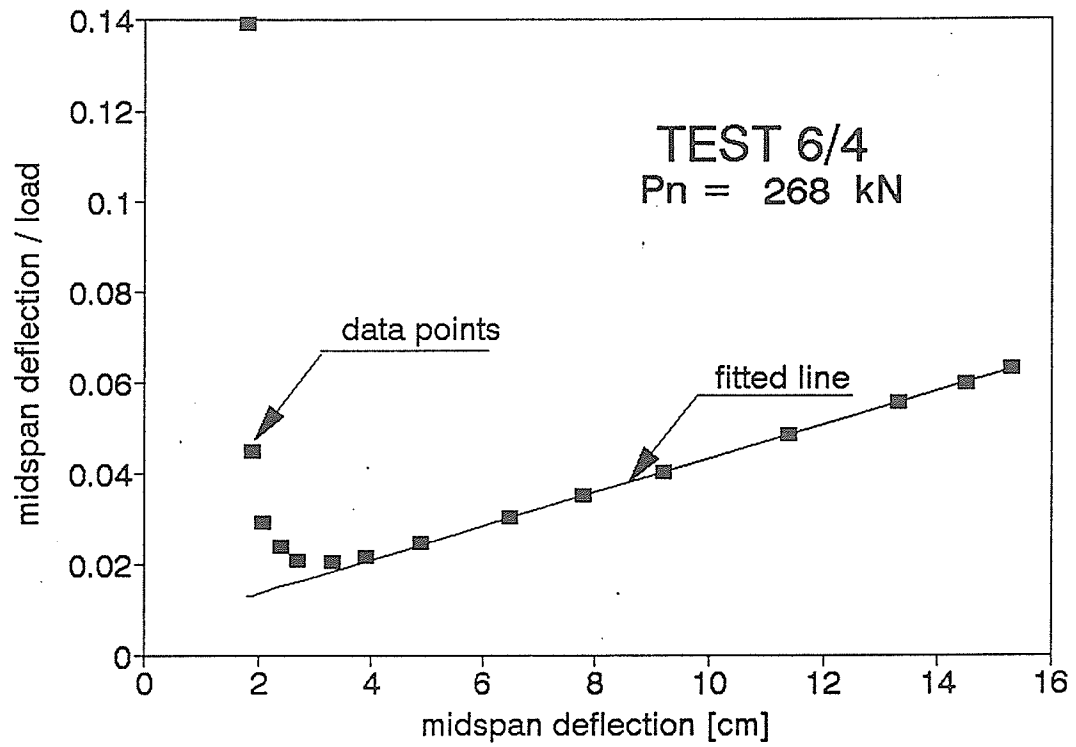


Figure B1.16. Southwell plot

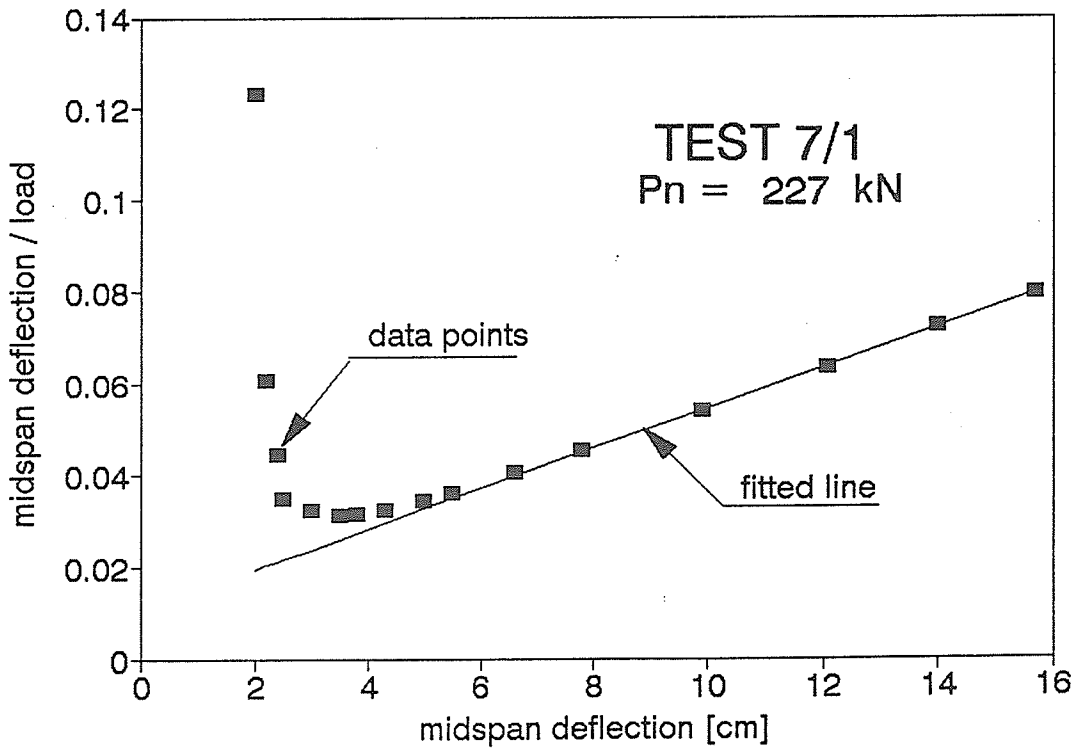
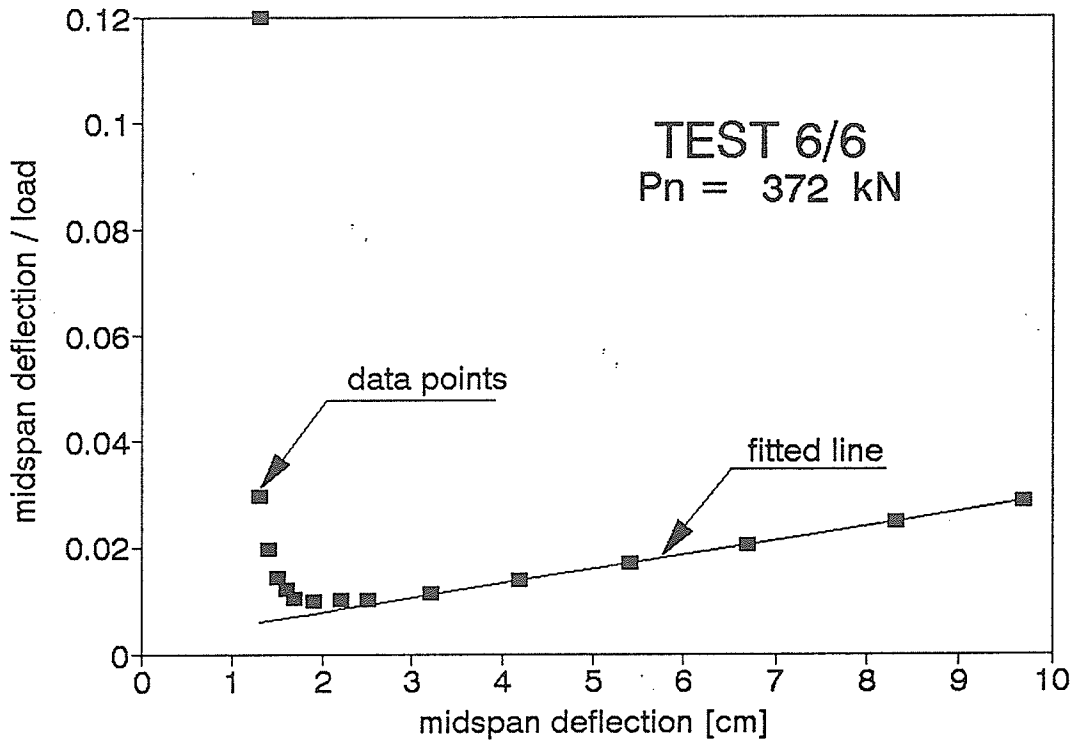


Figure B1.17. Southwell plot

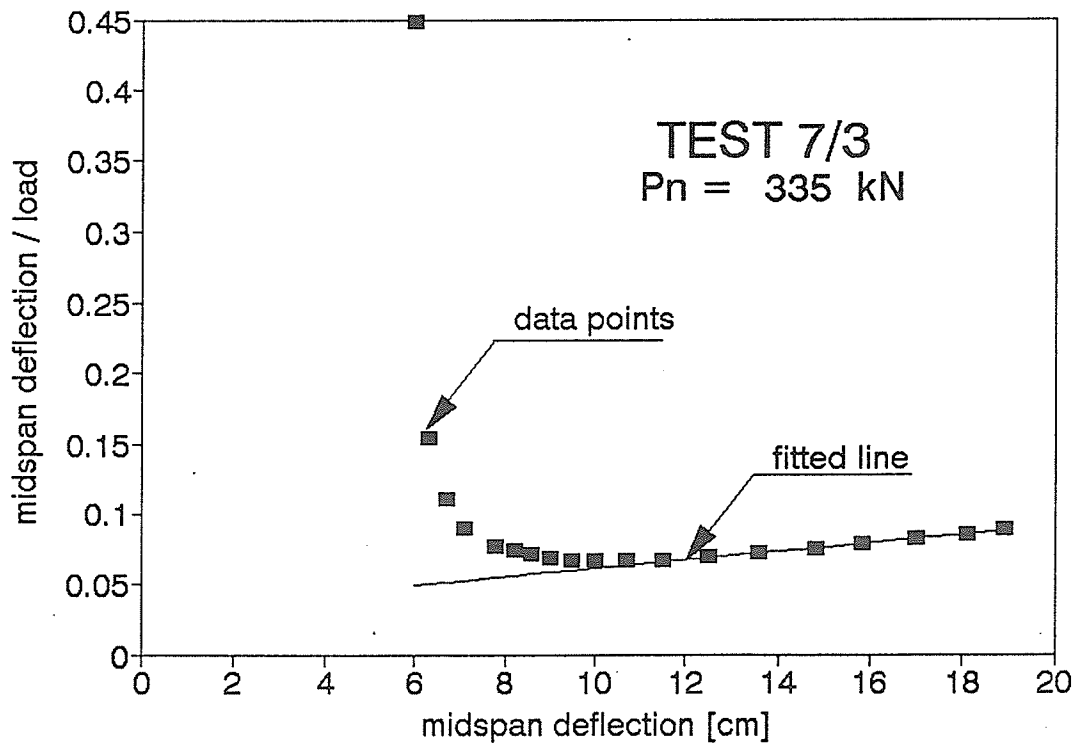
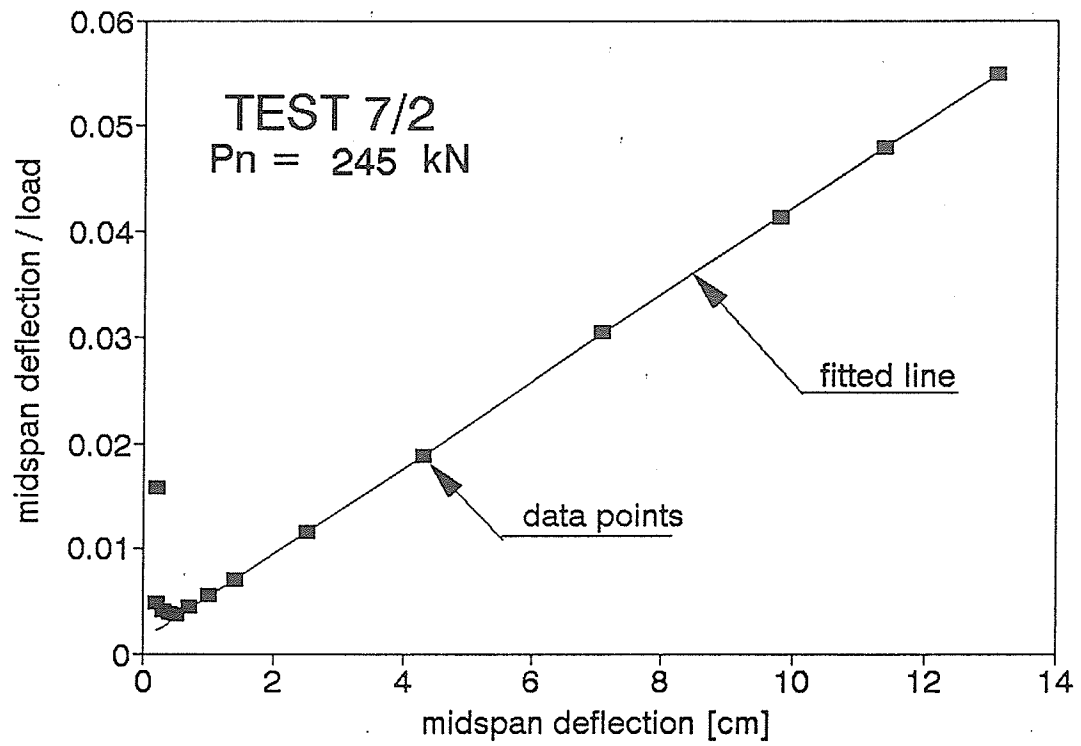


Figure B1.18. Southwell plot

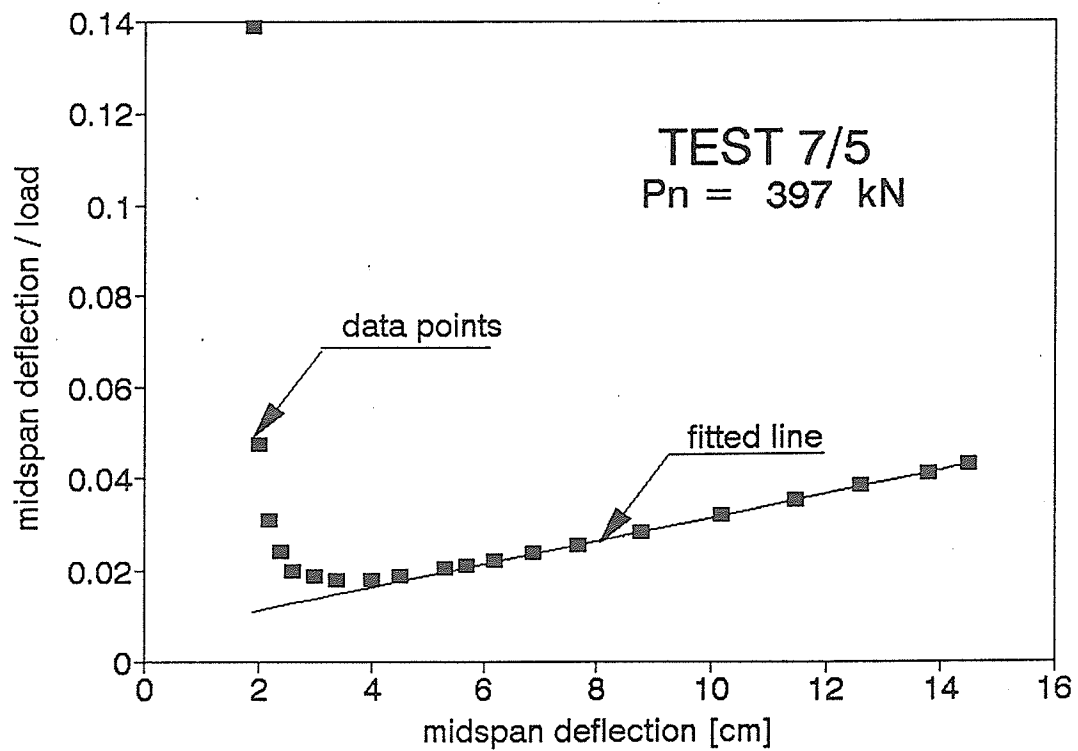
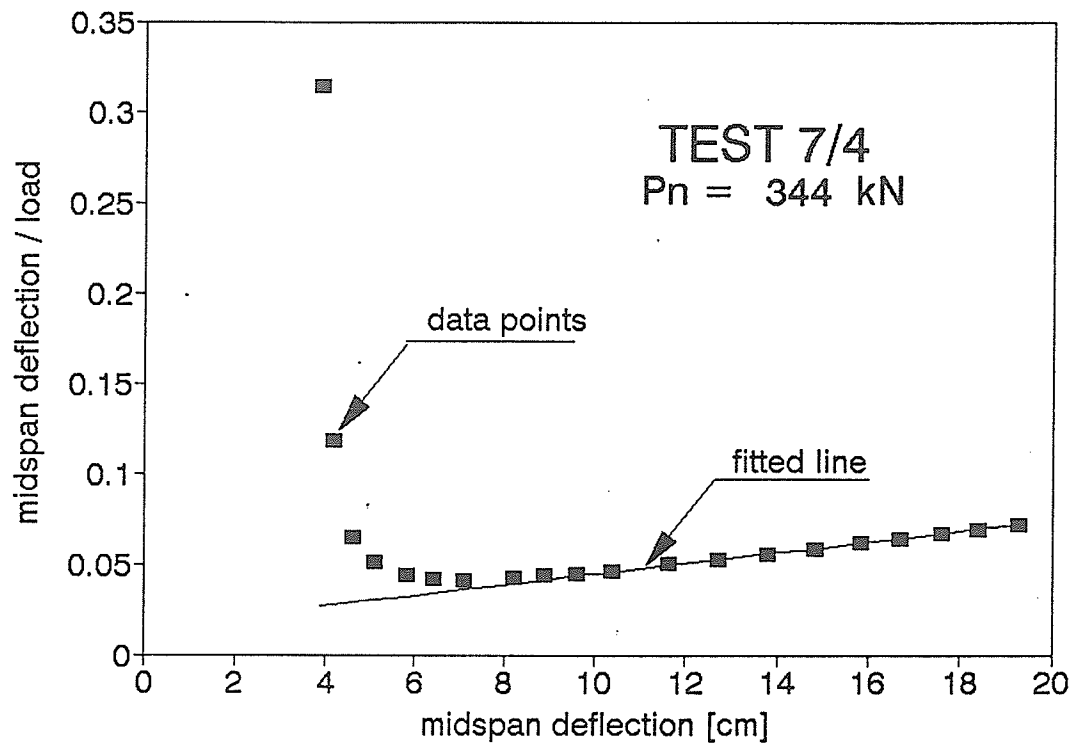


Figure B1.19. Southwell plot

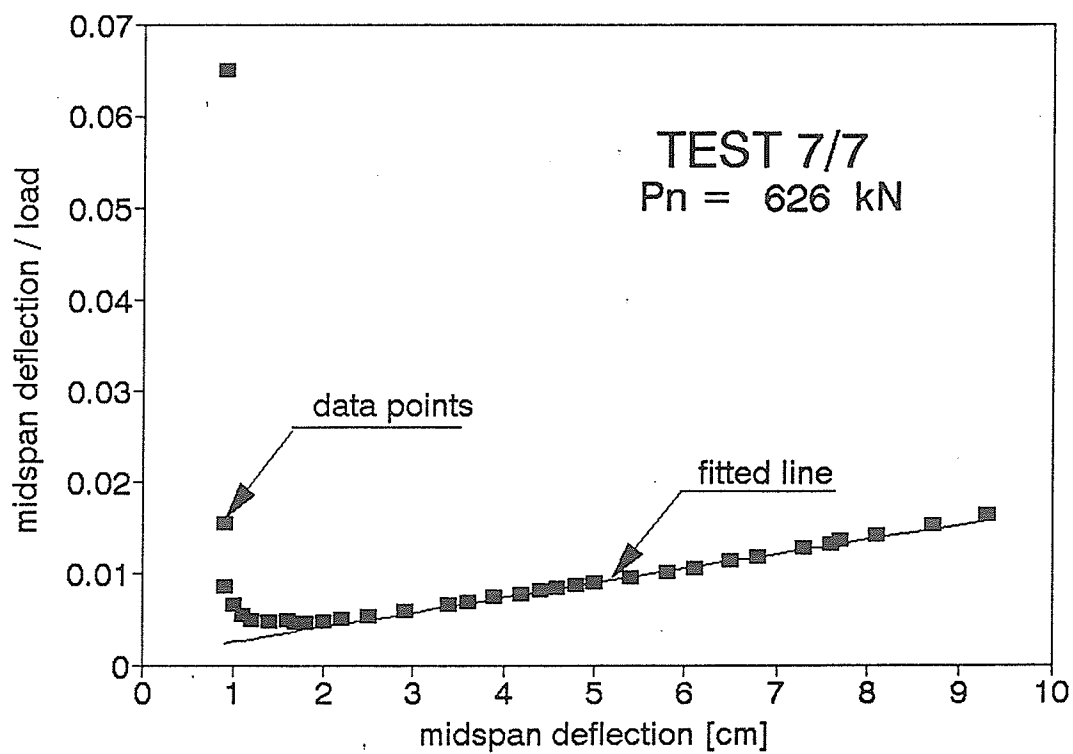
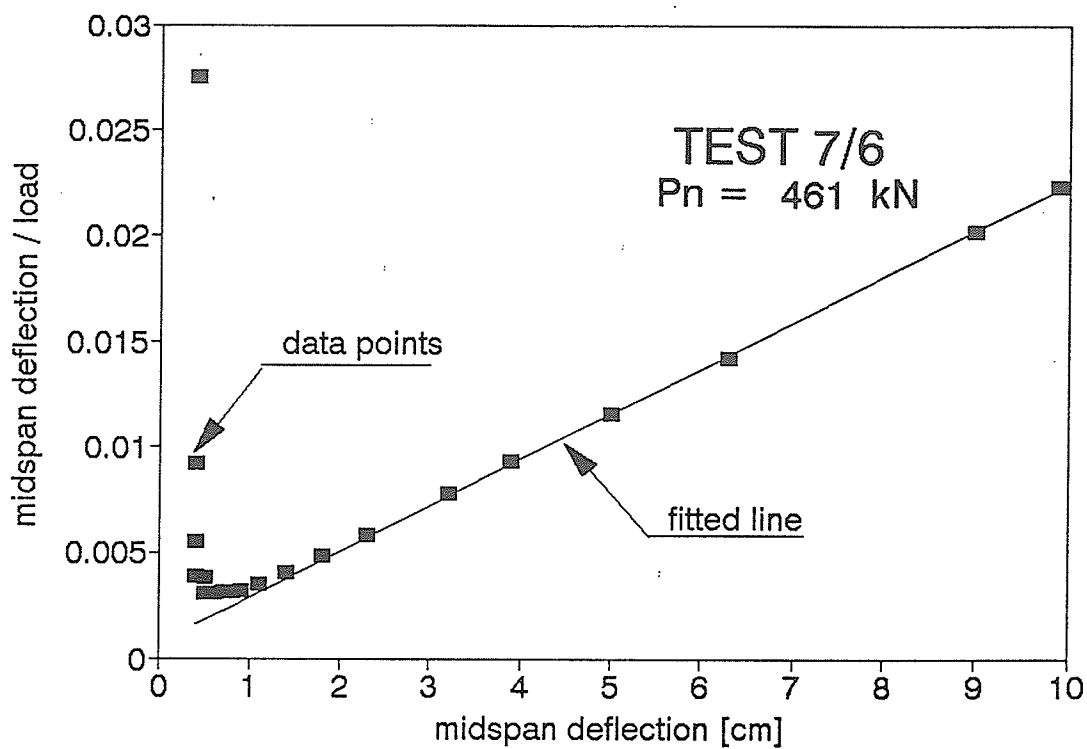


Figure B1.20. Southwell plot

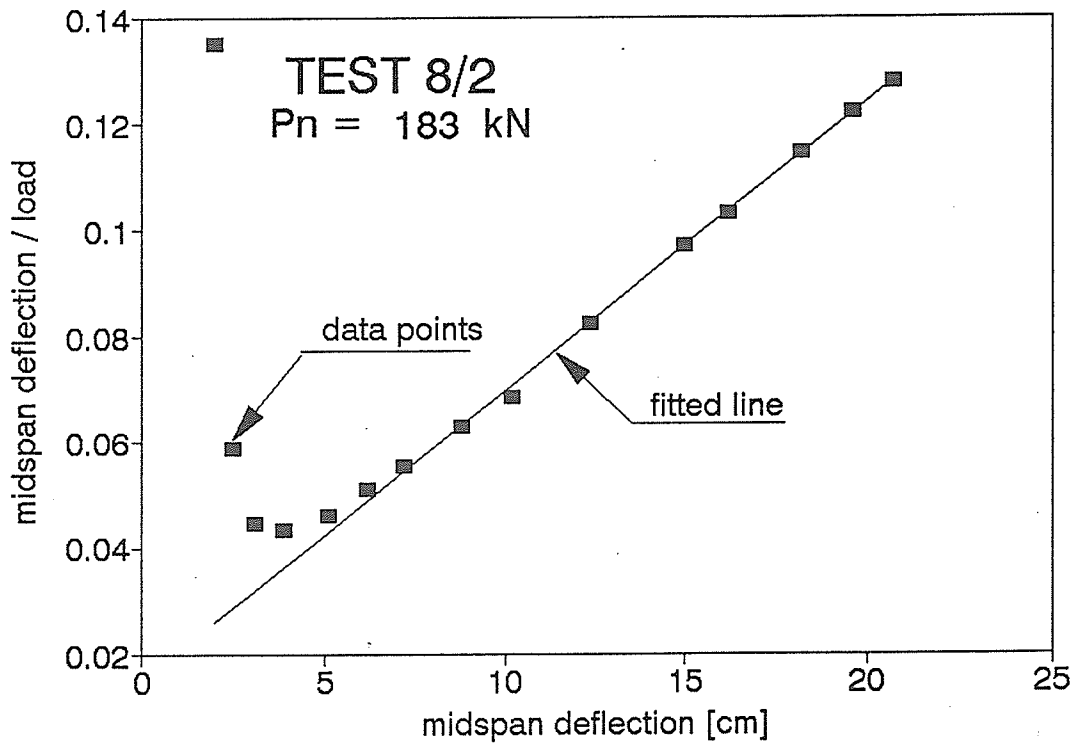
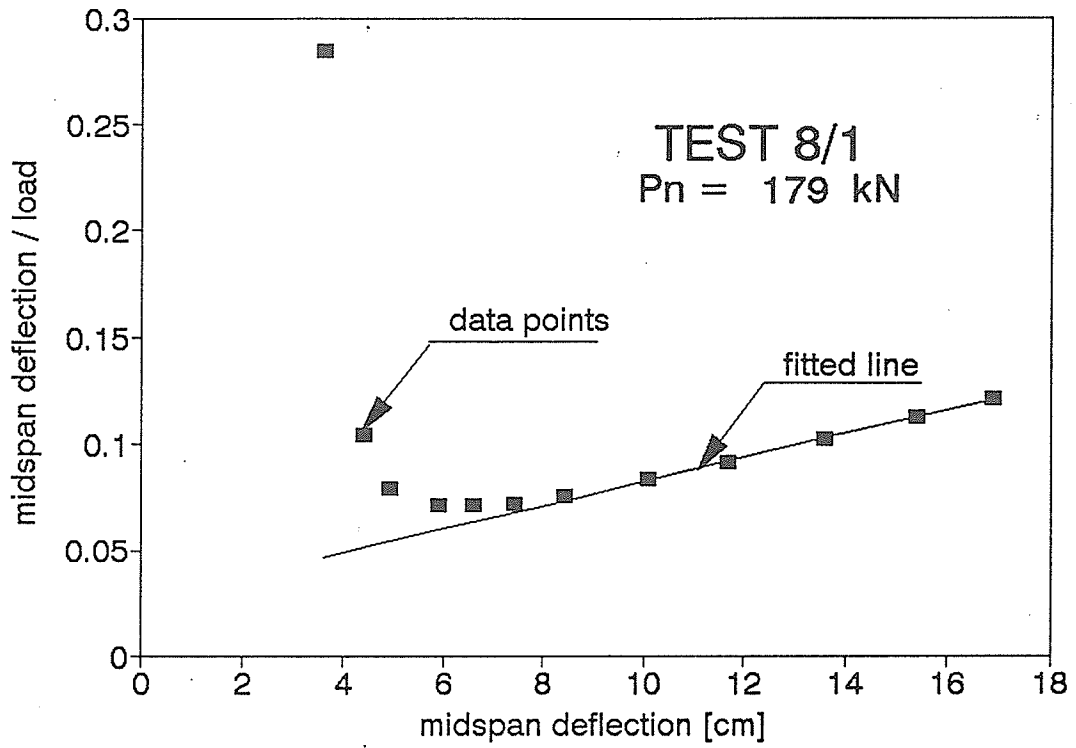


Figure B1.21. Southwell plot

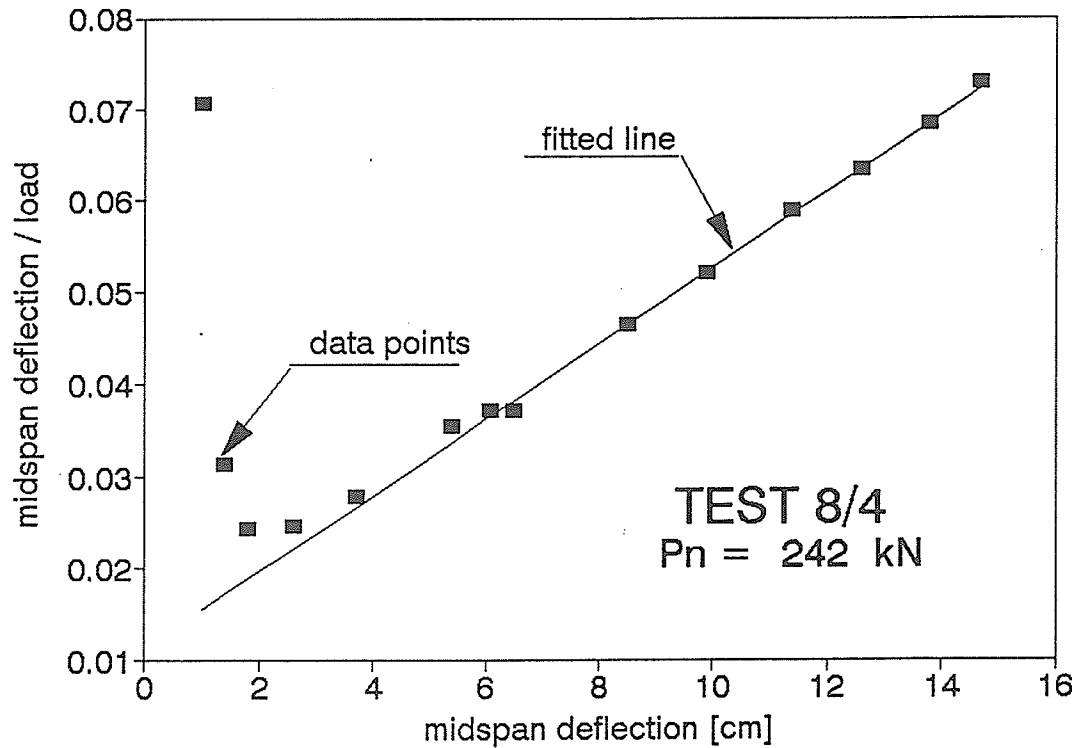
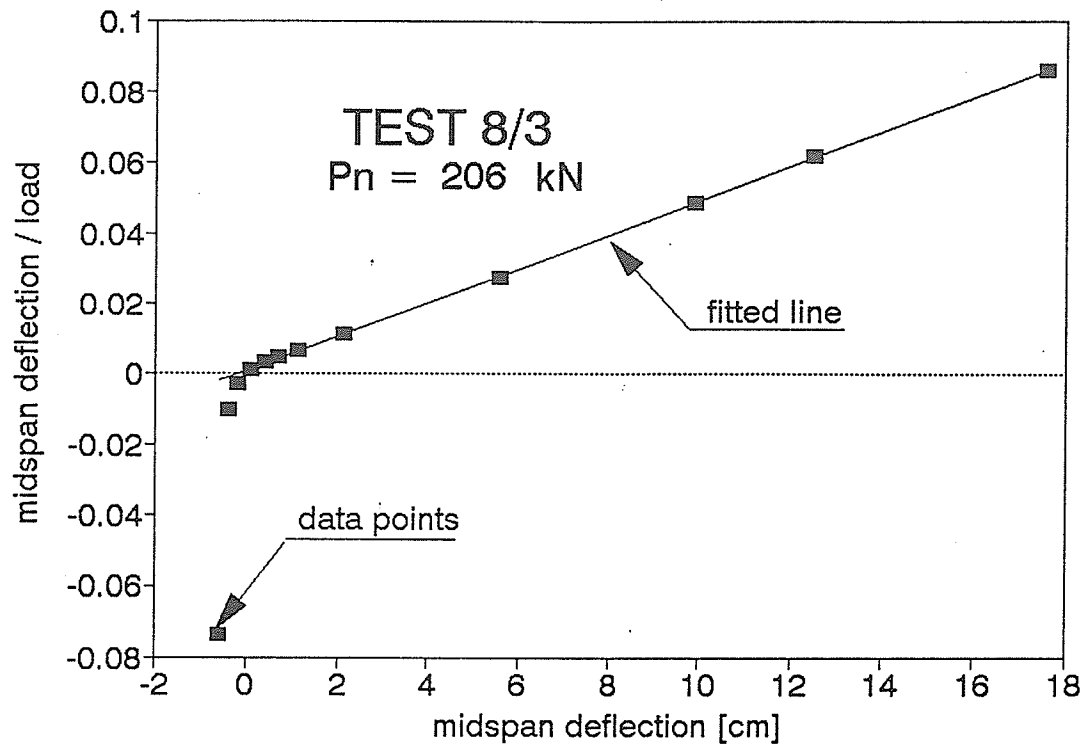


Figure B1.22. Southwell plot

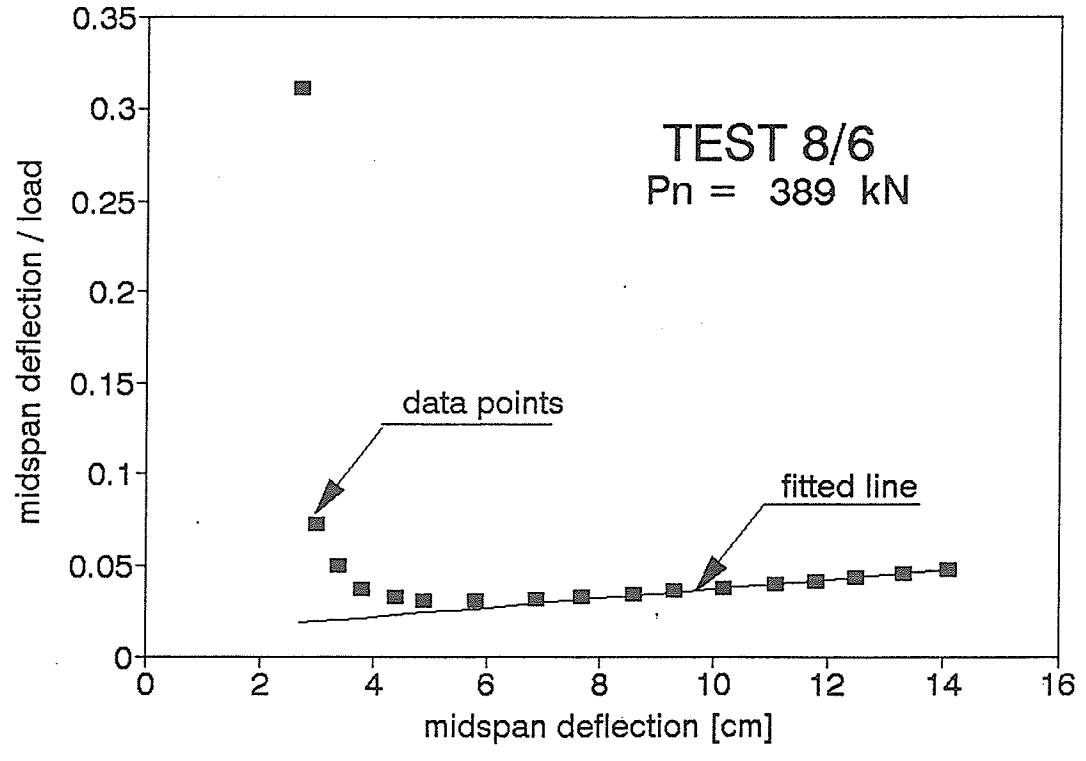
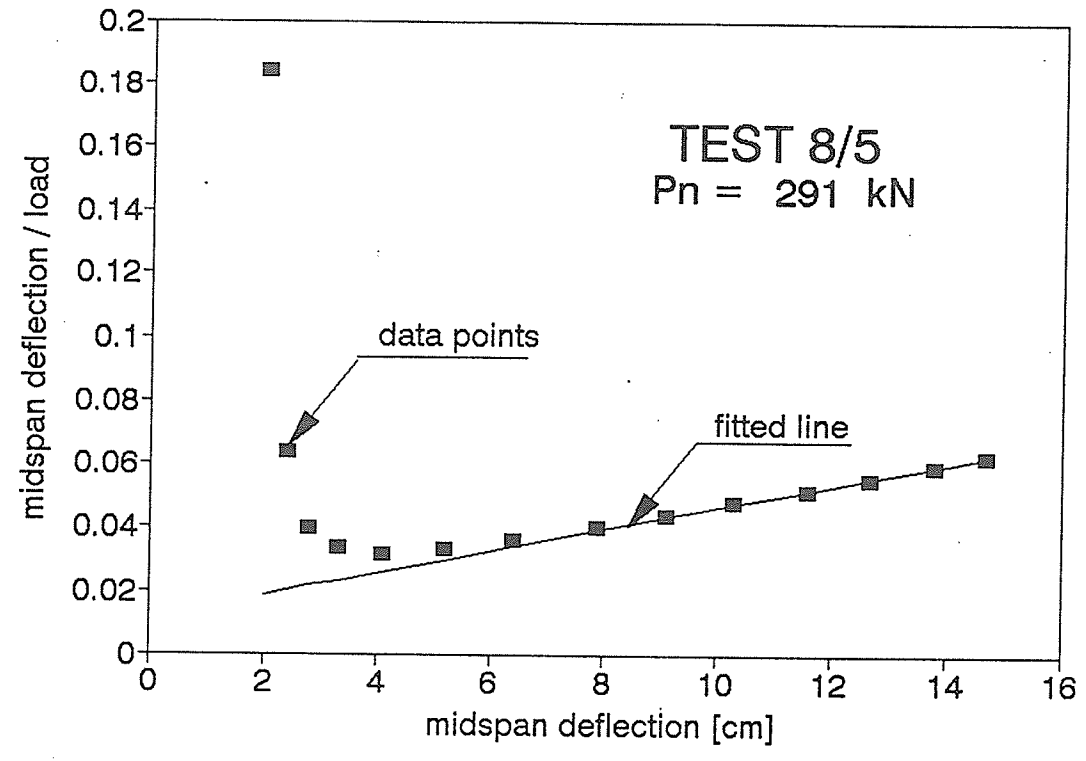


Figure B1.23. Southwell plot

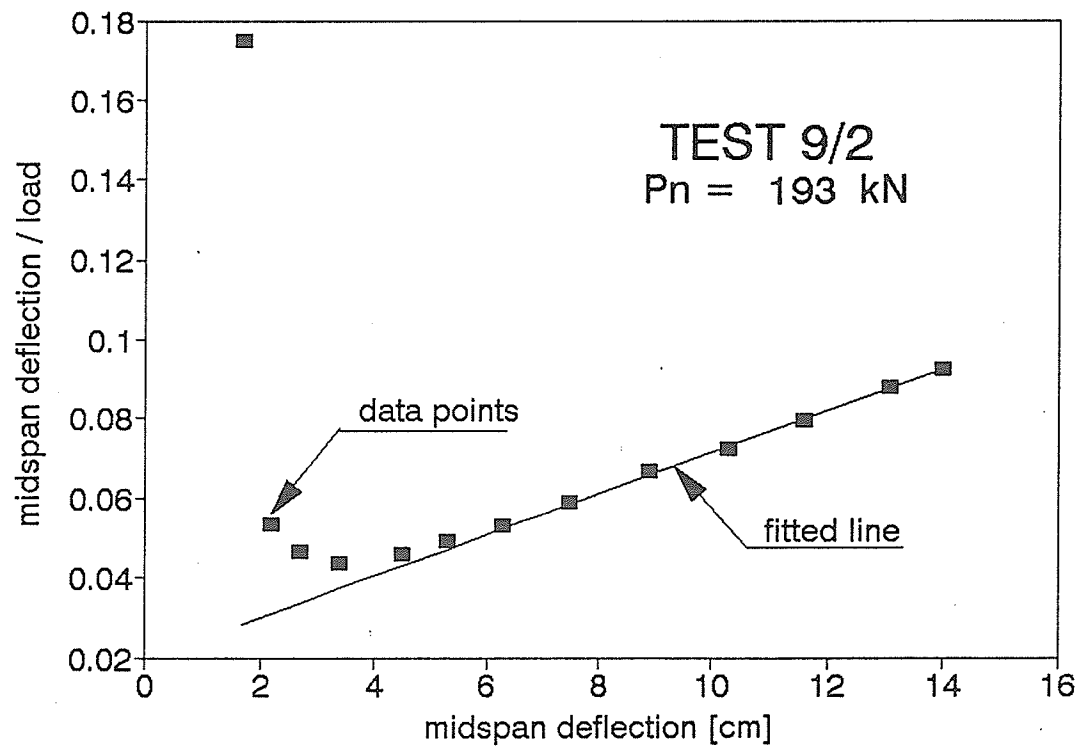
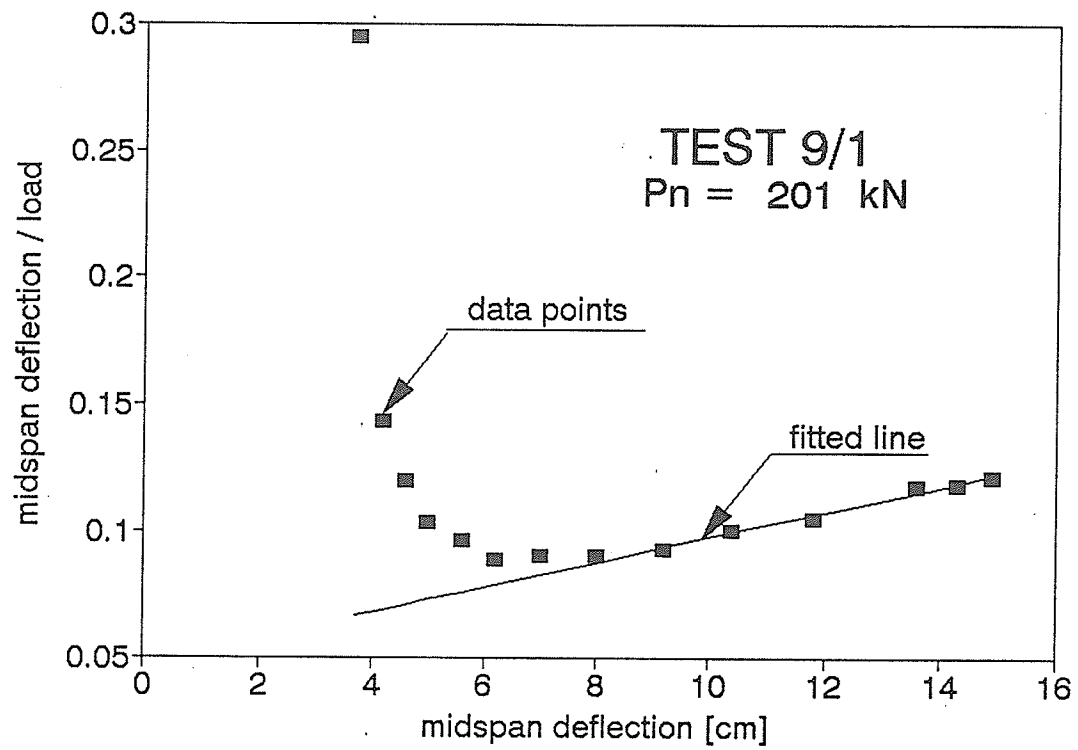


Figure B1.24. Southwell plot

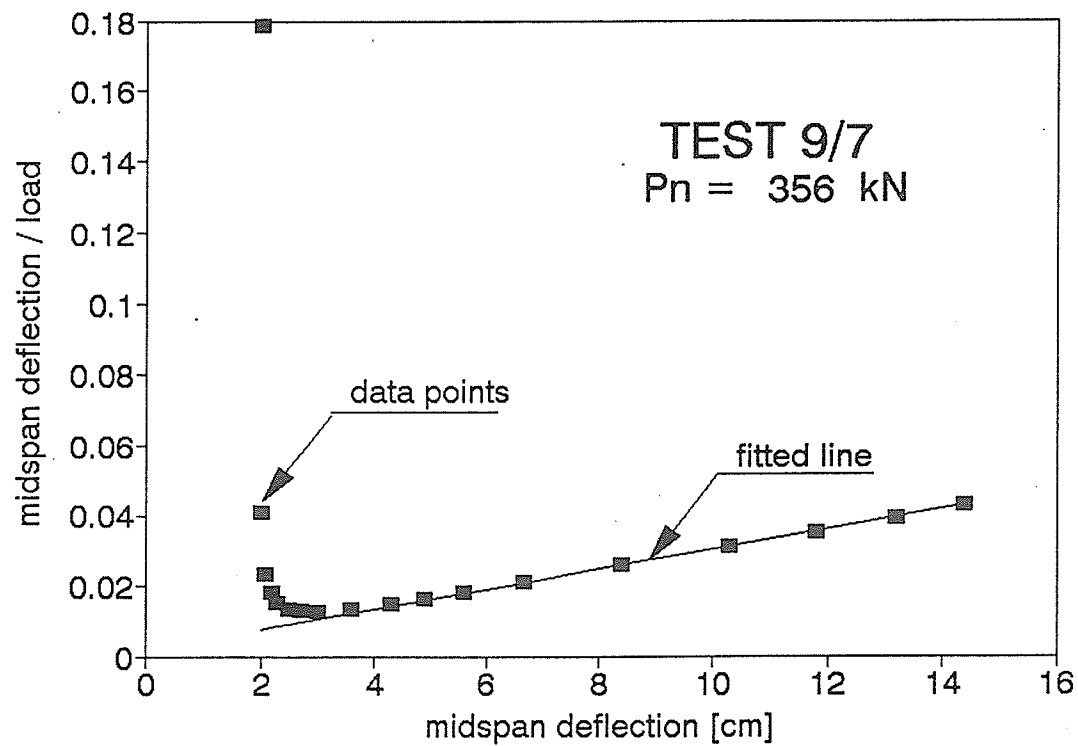
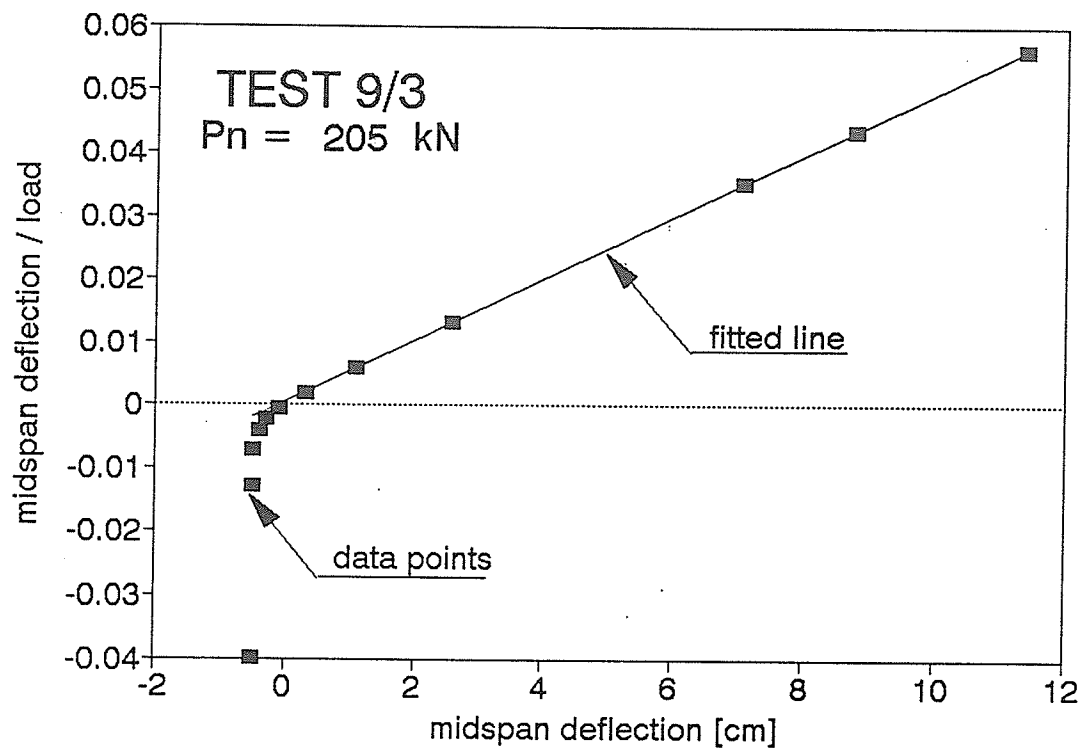


Figure B1.25. Southwell plot

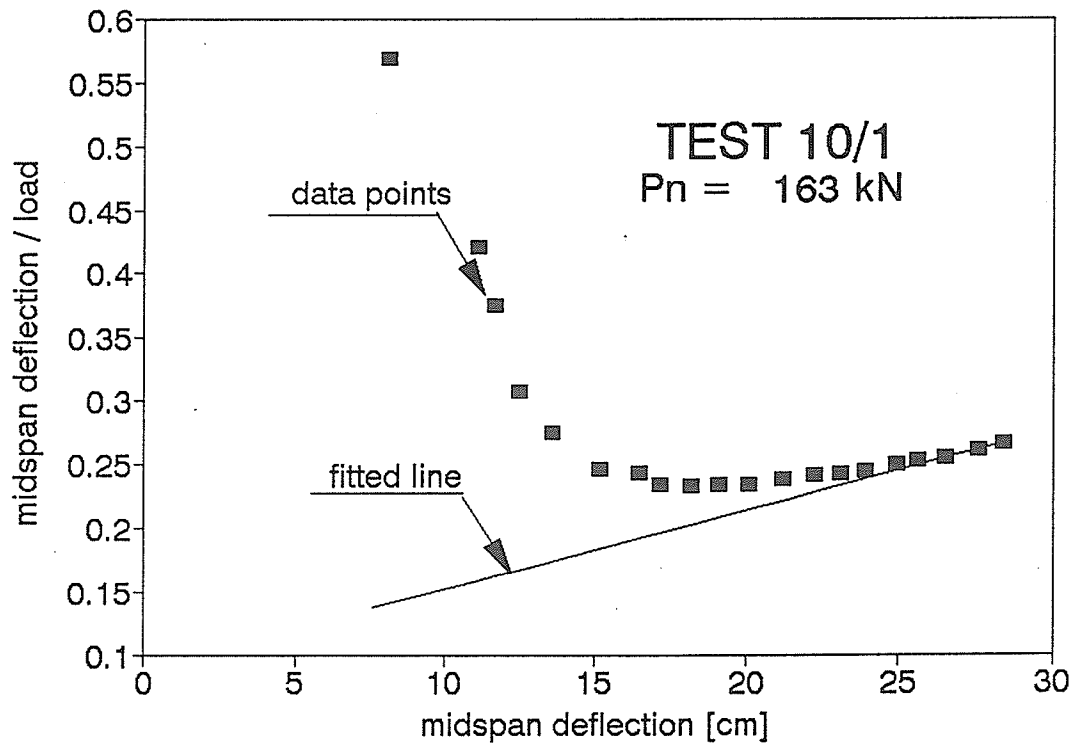
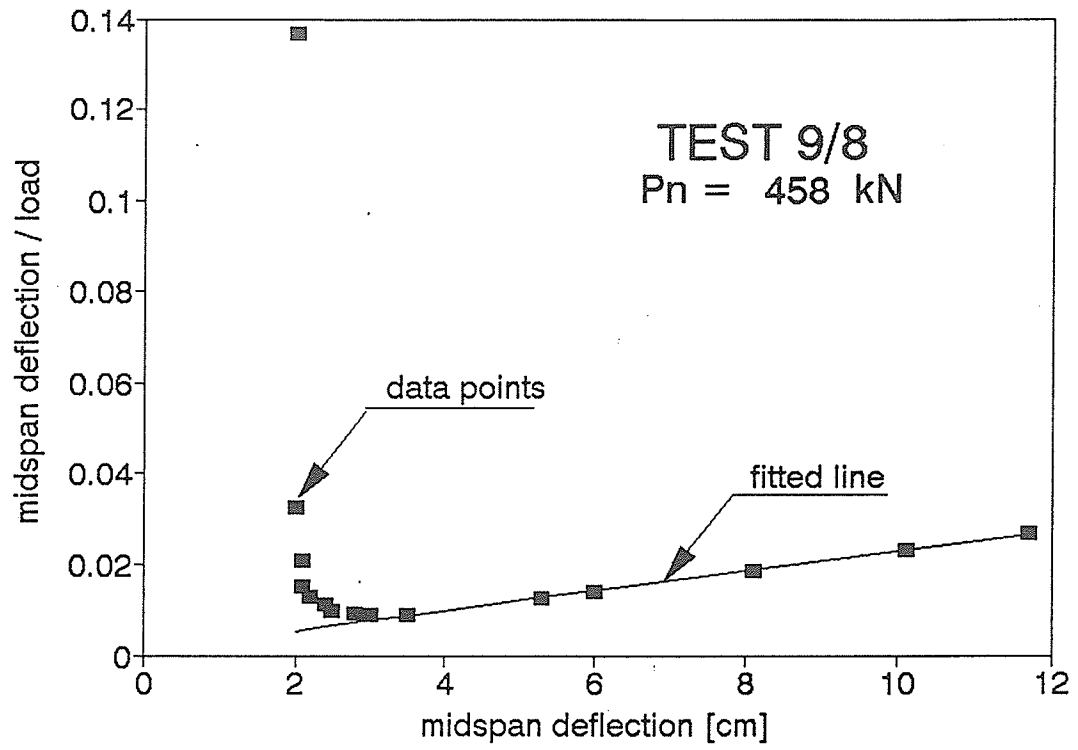


Figure B1.26. Southwell plot

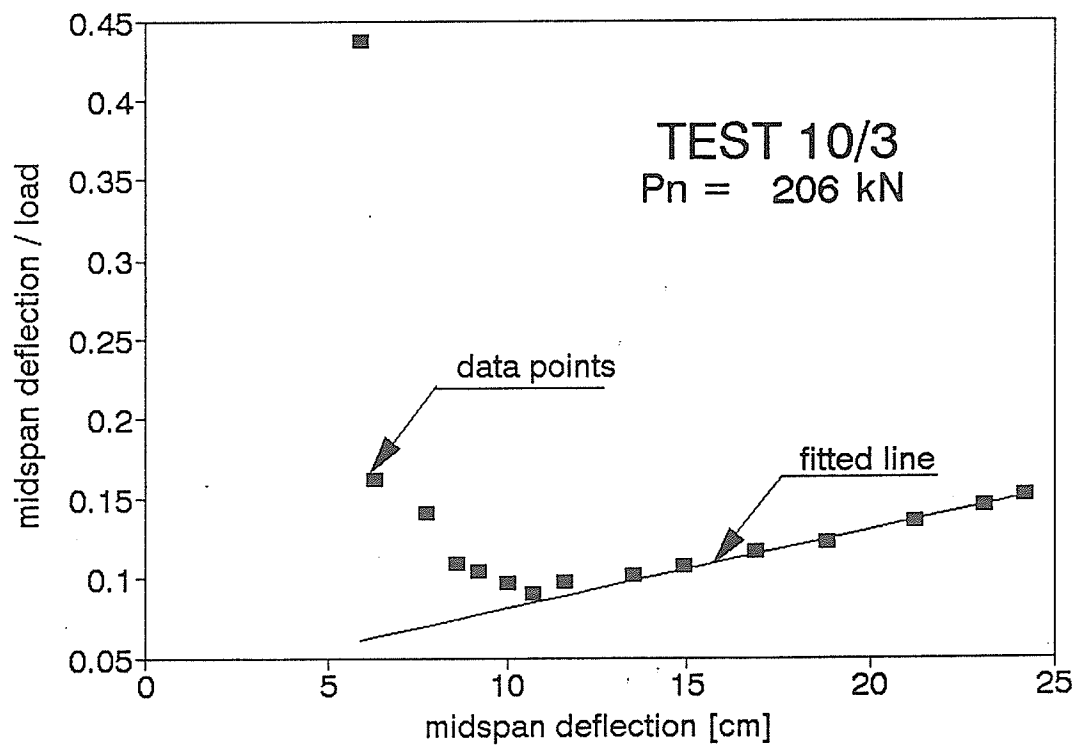
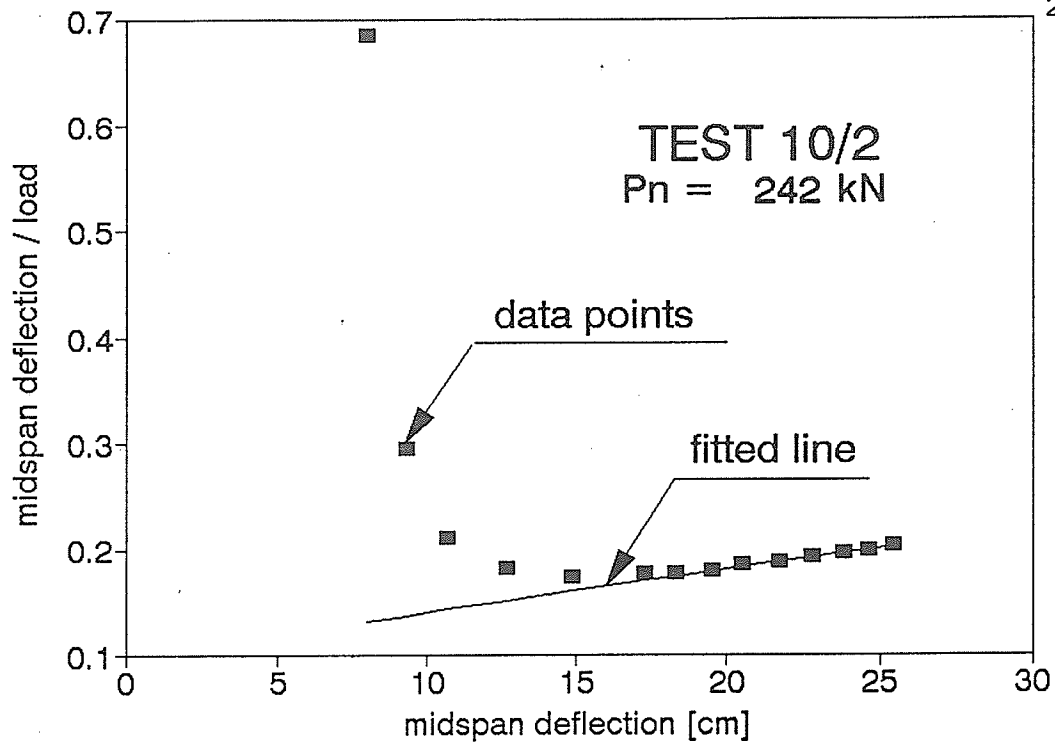


Figure B1.27. Southwell plot

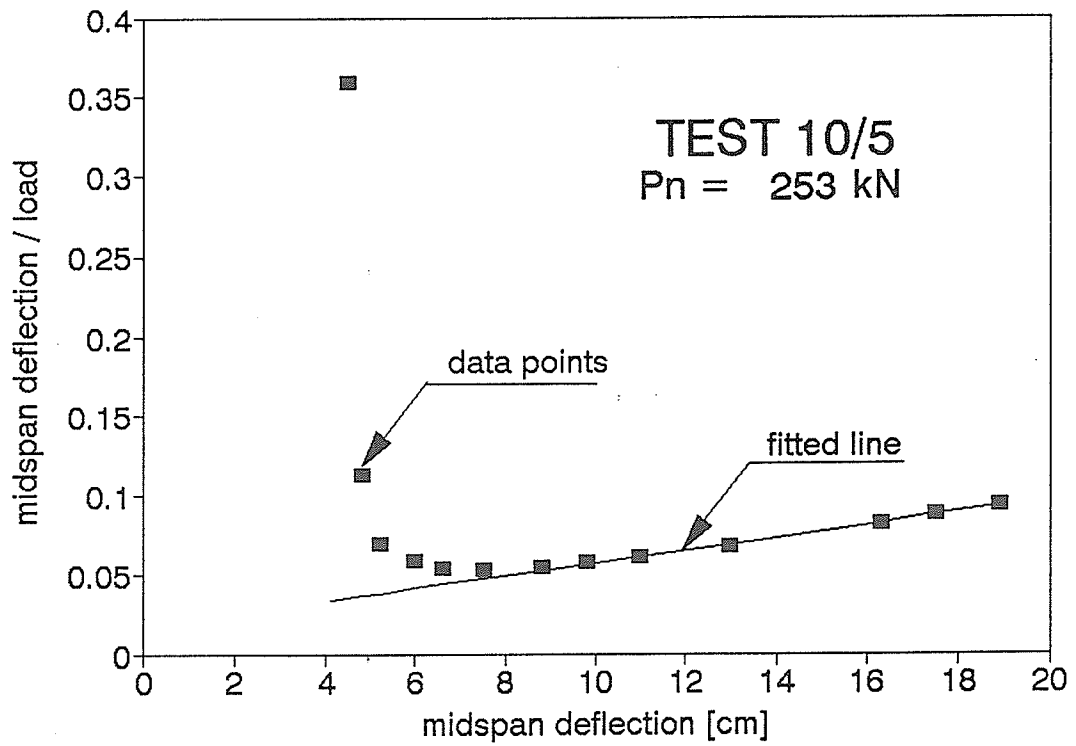
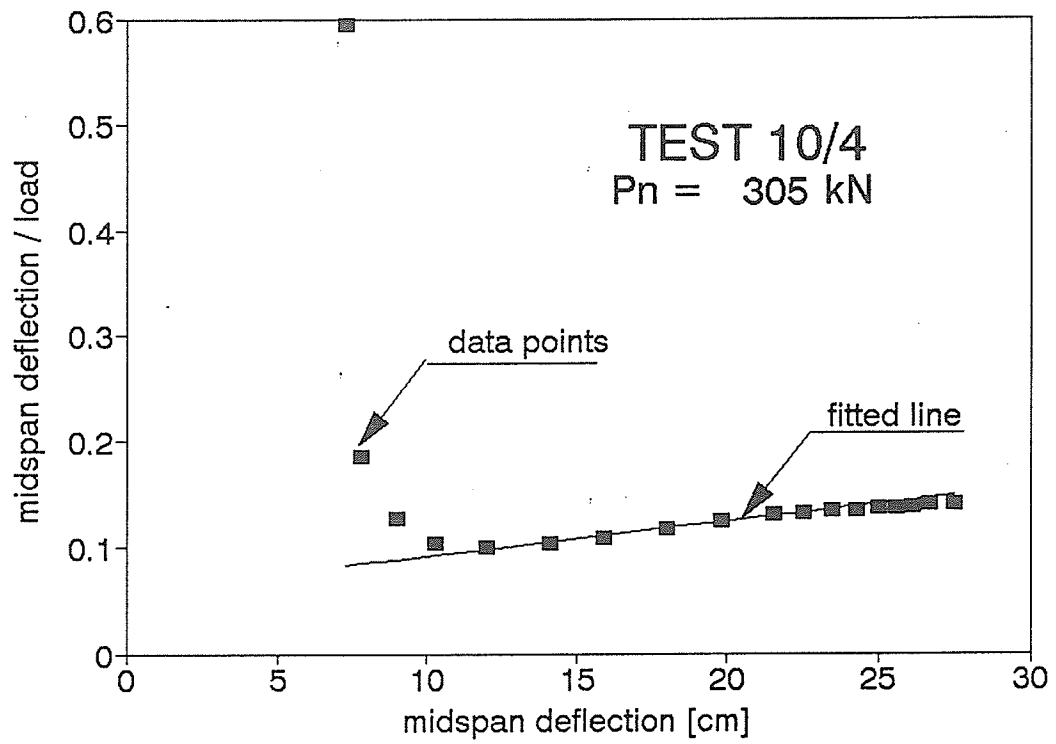


Figure B1.28. Southwell plot

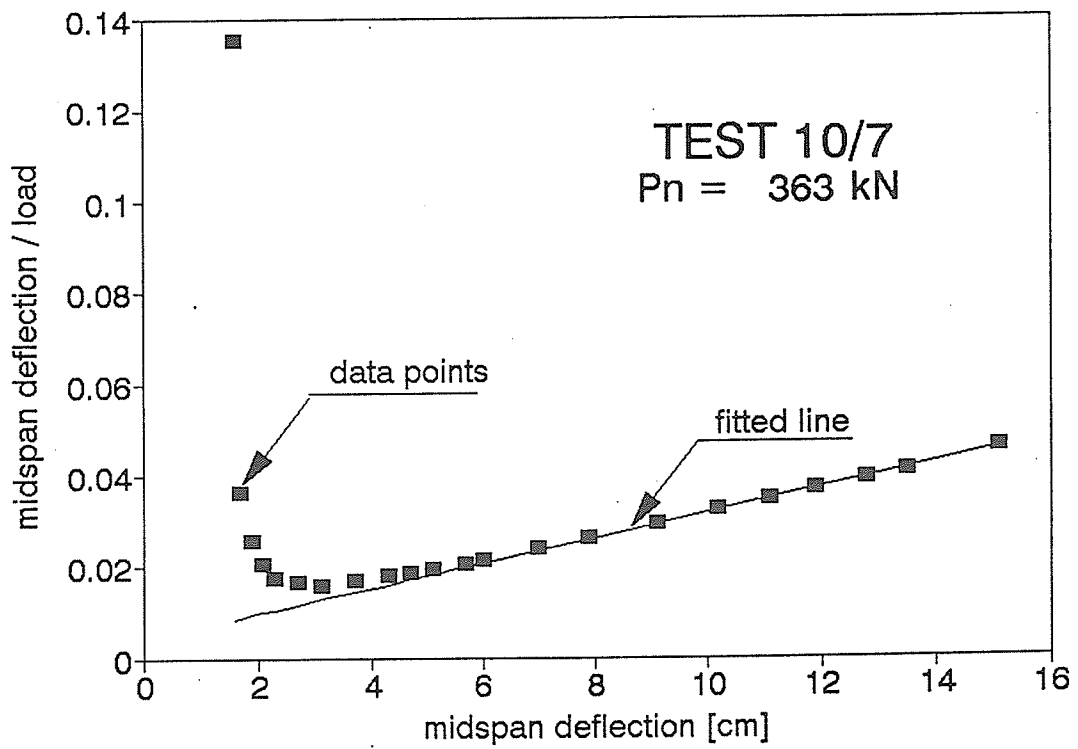
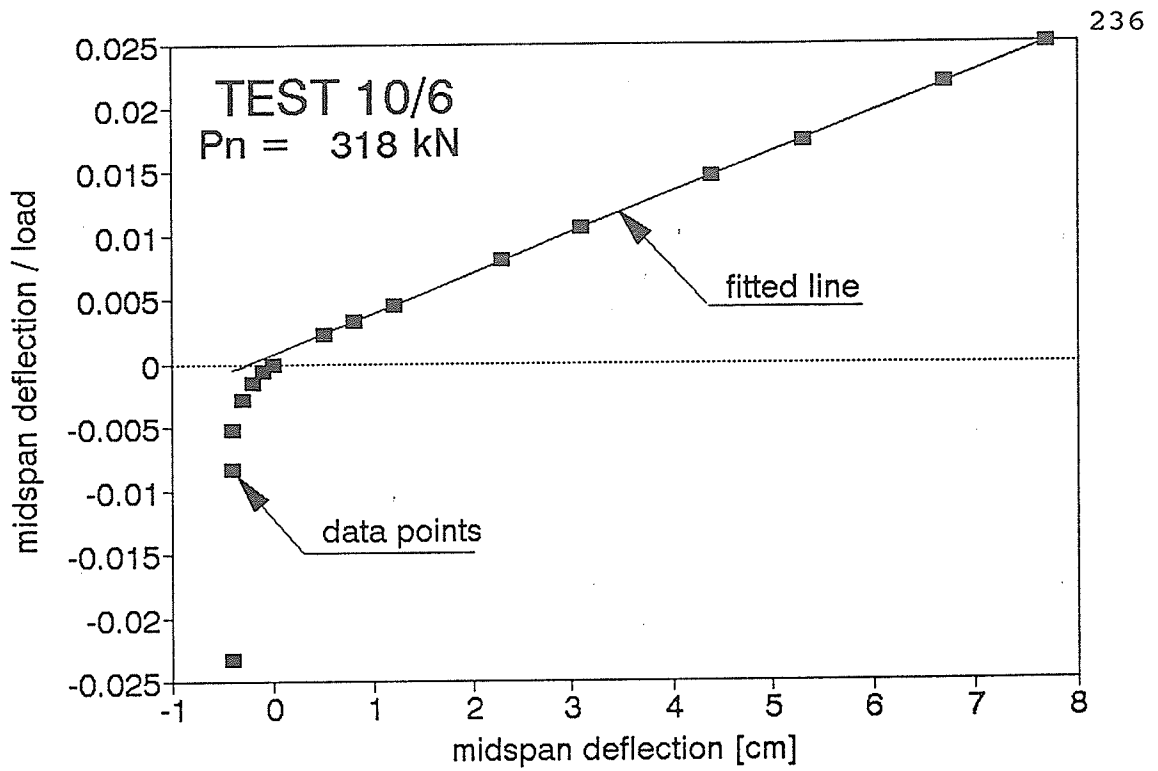


Figure B1.29. Southwell plot



APPENDIX C

APPENDIX CDESIGN EXAMPLE

C.1. Predicted buckling load using measured pole dimensions and material properties and equations given by the CAN/CSA086.1-M89

Measured pole dimensions:

$$d_{\min} = 246 \text{ mm}$$

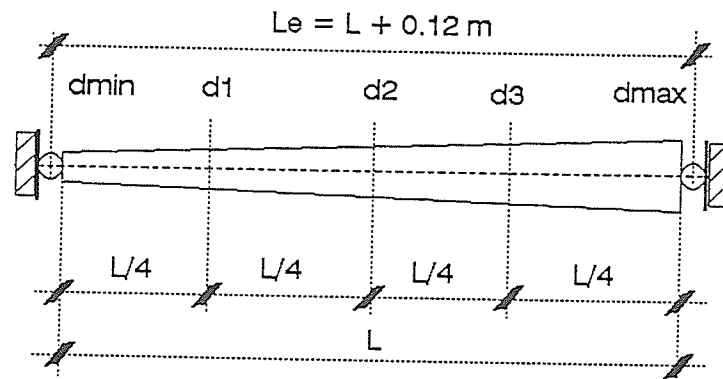
$$d_1 = 278 \text{ mm}$$

$$d_2 = 313 \text{ mm}$$

$$d_3 = 344 \text{ mm}$$

$$d_{\max} = 386 \text{ mm}$$

$$L = 12.116 \text{ m}$$



Measured material properties:

$$F_c = 24.88 \text{ MPa}$$

$$F_b = 39.69 \text{ MPa}$$

$$E = 9108 \text{ MPa}$$

$$\text{Specific gravity } g = 0.388 \text{ g/cm}^3$$

Effective diameter  $d_e$ :

$$d_e = d_{\min} + 0.45 (d_{\max} - d_{\min}) = 309 \text{ mm} \quad \dots \quad \text{Clause 12.5.2.5}$$

Cross-sectional area,  $A$ :

$$A = \frac{\pi \cdot d_e^2}{4} = 74,991 \text{ mm}^2$$

Moment of inertia:

$$I = \frac{\pi D_e^4}{64} = 447511105 \text{ mm}^4$$

Effective length is taken as distance between centres of the hinged connections as:

$$L_e = L + 0.12 = 12.236 \text{ m}$$

Axial compression strength of the columns cross-section,  $P_c$ :

$$P_c = F_c \cdot A = 1866 \text{ kN}$$

Nominal buckling load is determined by the Clauses 5.5.6.2.2. and 5.5.6.2.3. Since the measured material properties were used resistance factor and all modification factors for compression strength and modulus of elasticity are assumed to be unity. Consequently the nominal compression capacity is given as following:

$$P_n = \frac{P_c}{1 + \frac{F_c}{E} \frac{C_c^3}{35}} = 221 \text{ kN}$$

where  $C_c$  is the slenderness ratio given as:

$$C_c = \frac{L_e}{r\sqrt{12}} = \frac{2}{\sqrt{3}} \frac{L_e}{d_e} = 45.7 \quad \dots \quad \text{Clause 12.5.2.4.}$$

To predict the compression resistance,  $P_r$ , of the pole, existing moments were included in the evaluation by using interaction equation:

$$\frac{P_r}{P_n} + \frac{M_r}{M_n} \leq 1.0 \quad \dots \quad \text{Clause 5.5.10.}$$

Nominal bending moment resistance with the presence of the axial load was determined as:

$$M_r = F' \cdot M$$

where  $F'$  is commonly used magnification factor given as:

$$F' = \frac{1}{1 - \frac{P_r}{P_e}}$$

where  $P_e$  is the Euler's buckling load, given as:

$$P_e = \frac{\pi^2 EI}{L_e^2} = 269 \text{ kN}$$

Moment,  $M$ , determined by first order analyses, was taken as moment due to self-weight,  $M_d$ , and axial load,  $P_r$ , due to out-of-straightness,  $e$ , as:

$$M_r = M_d + e \cdot P_r$$

Since the pole was tested in the horizontal position, the deflection due to self-weight was deducted from the measured initial out-of-straightness. The deflected shape between the measured points was estimated as parabolic. Self-weight was estimated using measured specific gravity and assuming uniform taper shape between the measured diameters at the two ends and three quarter lengths measurements. Deflections due to self-weight were determined using conjugate beam method.

Nominal bending moment resistance,  $M_n$ , is given in the

Clause 5.5.4.1. Since the measured material properties were used all modification factors for bending strength and the resistance factor were taken to be one, yielding:

$$M_n = F_b \cdot S$$

where  $S$  is determined by the Clause 12.5.3. as section modulus of square cross-section having the same area as circular cross section:

$$S = \frac{a^3}{6}$$

where  $a$  is given as:

$$a = \sqrt{\frac{\pi \cdot d_e^2}{4}}$$

Uniform taper between the measured diameters was assumed in calculation of the section modulus. Measured eccentricity, moment due to self-weight,  $M_d$ , deflections due to self-weight, pole's out-of-straightness,  $e$ , and nominal bending capacity along the length of the pole are shown in Table C.1.

Buckling load was determined using iterative procedure. Ratio between buckling load resistance and nominal buckling load was assumed, and applied moment and magnification factor were calculated. Using interaction equation buckling load resistance was calculated and compared to the assumed value. Prediction of the buckling load of the pole is presented in

Table C.2.

Calculated ratio between buckling load resistance and nominal buckling load was determined as:

$$P_r/P_n = 0.794$$

thus predicting the ultimate compression resistance of the pole with existing moments as:

$$P_r = 0.793 \cdot 221 = 175 \text{ kN}$$

Measured buckling load for this pole was  $P_{\max} = 182 \text{ kN}$

Therefore the ratio of the measured and predicted buckling load is:

$$\frac{P_{\text{measured}}}{P_r} = \frac{182}{175} = 1.04$$

It can be concluded that proposed model gives conservative solution for the buckling load of the pole.

**C.2. Predicted buckling load using nominal pole dimensions, proposed out-of-straightness at the mid height, and measured material properties and equations given by the CAN/CSA086.1-M89**

Nominal pole dimensions:

$$d_{\max} = 201 \text{ mm}$$

$$d_{\max} = 382 \text{ mm}$$

$$L = 12.192 \text{ m}$$

Material properties were taken as average of the all Western Red Cedar poles tested in this research program:

$$F_c = 23.07 \text{ MPa}$$

$$F_b = 39.52 \text{ MPa}$$

$$E = 8784 \text{ MPa}$$

Effective diameter  $d_e$ :

$$d_e = d_{\min} + 0.45 (d_{\max} - d_{\min}) = 282 \text{ mm}$$

Cross-sectional area, A:

$$A = \frac{\pi \cdot d_e^2}{4} = 62,657$$

Axial compression strength of the columns cross-section,  $P_c$ :

$$P_c = F_c \cdot A = 1446 \text{ kN}$$

Nominal buckling load:

$$P_n = \frac{P_c}{1 + \frac{F_c}{E} \frac{C_c^3}{35}} = 140 \text{ kN}$$

To predict the compression resistance of the pole including the moments, the following interaction equation could be used:

$$\frac{P_r}{P_n} + \frac{F' \cdot M_r}{M_n} \leq 1.0$$

Initial moment,  $M_r$ , was taken as moment due to pole's out-of-straightness. It was assumed that the pole has parabolic shape with maximum value at the mid-height of the column of:

$$e = \frac{L}{200} = 61 \text{ mm}$$

Nominal bending moment resistance,  $M_n$ , was determined using measured material properties and assuming uniform taper between the minimum and maximum diameters as:

$$M_n = F_b \cdot S$$

where  $S$  is section modulus of square cross-section having the same area as circular cross section:

$$S = \frac{a^3}{6}$$

where  $a$  is given as:

$$a = \sqrt{\frac{\pi \cdot d_e^2}{4}}$$

Applied moments on the pole were calculated as:

$$M_r = e \cdot P_r$$

Buckling load was determined using iterative procedure.

Pole's out-of-straightness,  $e$ , nominal bending capacity along the length of the pole and prediction of the buckling load of the pole are shown in Table C.3. Calculated ratio between buckling load resistance and nominal buckling load was determined as:

$$P_r/P_n = 0.822$$

thus predicting the ultimate compression resistance of the pole with existing moments as:

$$P_r = 0.822 \cdot 140 = 115 \text{ kN}$$

### C.3. Predicted buckling load according to CAN/CSA-086.1

Nominal pole dimensions are represented in the section C.2.

Material properties given by the Clause 12.3 of the Code:

$$F_c = 5.76 \text{ MPa}$$

$$E = 5500 \text{ MPa}$$

Effective diameter,  $d_e$ , cross-sectional area,  $A$ , Slenderness ratio of the column are the same as presented in section C.2. Load duration factor,  $K_D$ , was taken as one according to Table 4.3.2.1. for standard term loading. System factor,  $K_H$ , is also taken as one, according to Clause 5.4.4. Service condition factors,  $K_S$ , were assumed to be one, for dry service conditions as given in Table 5.4.2. Treatment factor is given in Clause 5.4.3. as one.

Axial compression strength of the columns cross-section,  $P_c$ :

$$P_c = F_c \cdot A = 321 \text{ kN}$$

Size effect,  $K_{zb}$ , factor is given in Clause 5.5.6.2.2. as:

$$K_{zc} = 6.3 (d_e L_e)^{-0.13} = 0.890 \leq 1.3$$

Nominal buckling load:

$$P_n = \frac{P_c K_{zc}}{1 + \frac{F_c K_{zc}}{E} \frac{C_c^3}{35}} = 75 \text{ kN}$$

point	Distance from the top of the pole [m]	Measured eccentricity [mm]	Moment due to self-weight [kNm]	Deflections due to self-weight [mm]	Pole's out-of- -straightness [mm]	Nominal bending capacity [kNm]
0	0.000	0	0.00	0	0	68.55
1	0.765	-17	1.14	5	-22	75.46
2	1.530	-30	2.16	9	-40	82.82
3	2.294	-40	3.06	13	-53	90.64
4	3.059	-46	3.84	17	-63	98.93
5	3.824	-50	4.48	19	-69	108.57
6	4.589	-52	4.97	20	-73	118.82
7	5.353	-53	5.32	21	-74	129.69
8	6.118	-52	5.50	21	-73	141.20
9	6.883	-50	5.51	20	-70	151.95
10	7.647	-47	5.34	19	-66	163.24
11	8.412	-43	4.98	16	-60	175.06
12	9.177	-38	4.43	14	-52	187.45
13	9.942	-31	3.66	11	-42	205.14
14	10.707	-23	2.68	7	-30	223.92
15	11.471	-13	1.46	4	-17	243.80
16	12.236	0	0.00	0	0	264.83

Table C.1. Moments and deflections due to self-weight, out-of-straightness, and nominal buckling capacity of the pole

Assumed ratio between compression resistance of the pole  
and nominal compression resistance:

$$P_r/P_n = 0.794$$

Magnification factor:

$$F = 2.8685$$

point	Ratio between applied moment and nominal moment capacity	Ratio between predicted axial load and nominal compression capacity
0	0.000	1.000
1	-0.036	0.896
2	-0.058	0.835
3	-0.068	0.804
4	-0.072	0.794
5	-0.070	0.799
6	-0.065	0.813
7	-0.059	0.832
8	-0.052	0.852
9	-0.045	0.872
10	-0.038	0.892
11	-0.031	0.911
12	-0.025	0.929
13	-0.018	0.948
14	-0.012	0.966
15	-0.006	0.983
16	0.000	1.000

Table C.2. Predicted buckling load

Assumed ratio between compression resistance of the pole and nominal compression resistance:  $P_r/P_n = 0.822$   
Magnification factor:  $F = 2.7229$

point	Distance from the top of the pole [m]	Pole's out-of-straightness [mm]	Nominal bending capacity [kNm]	Ratio between applied moment and nominal moment capacity	Ratio between predicted axial load and nominal compression capacity
0	0.000	0	37.23	0.000	1.000
1	0.762	14	46.10	0.036	0.902
2	1.524	27	56.29	0.055	0.851
3	2.286	37	67.87	0.063	0.827
4	3.048	46	80.94	0.065	0.822
5	3.810	52	95.58	0.063	0.827
6	4.572	57	111.90	0.059	0.839
7	5.334	60	129.98	0.053	0.854
8	6.096	61	149.90	0.047	0.872
9	6.858	60	171.76	0.040	0.890
10	7.620	57	195.65	0.034	0.908
11	8.382	52	221.66	0.027	0.926
12	9.144	46	249.88	0.021	0.942
13	9.906	37	280.40	0.015	0.958
14	10.668	27	313.30	0.010	0.973
15	11.430	14	348.69	0.005	0.987
16	12.192	-0	386.64	0.000	1.000

Table C.3. Predicted buckling load